

**MADAGASCAR'S CLIMATE HISTORY
UNLOCKED BY GIANT CORALS**

The research reported in this thesis was carried out at the following institutions:

Department of Marine Geology, Royal Netherlands Institute for Sea Research (NIOZ). P.O. Box 59, 1790 AB Den Burg, The Netherlands.
Faculty of Earth and Life Sciences, VU University. De Boelelaan 1085, 1081 HV Amsterdam, The Netherlands.

This research was funded through the SINDOCOM project, under the NWO program 'Climate Variability', grant no. 854.00.034/035.

ISBN: 978-94-6203-032-9

Edited by: Julie Ogier

Cover design by: Sebastian Kasper

Cover photograph taken by: Charlotte Spliethoff

Figures by: Craig Grove, Jens Zinke, Tim Scheufen and Sebastian Kasper

Printed by: Wöhrmann Print Service, Zutphen

VRIJE UNIVERSITEIT

MADAGASCAR'S CLIMATE HISTORY UNLOCKED BY GIANT
CORALS

ACADEMISCH PROEFSCHRIFT

ter verkrijging van de graad Doctor aan
de Vrije Universiteit Amsterdam,
op gezag van de rector magnificus
prof. dr. L.M. Bouter,
in het openbaar te verdedigen
ten overstaan van de promotiecommissie
van de faculteit der Aard- en Levenswetenschappen
op maandag 4 juni om 13.45 uur
in de aula van de universiteit,
De Boelelaan 1105

door

Craig Alexander Grove
geboren te Irvine, Schotland

promotor:
prof. dr. G.J.A. Brummer

copromotor:
dr. J. Zinke

reading committee:
prof. dr. R.P.M. Bak
prof. dr. G.T. Davies
dr. T. Felis
prof. dr. D. Kroon
prof. dr. M.T. McCulloch
dr. M. Pfeiffer

“The organic forces separate the atoms of carbonate of lime, one by one, from the foaming breakers, and unite them into a symmetrical structure. Let the hurricane tear up its thousand huge fragments; yet what will that tell against the accumulated labour of myriads of architects at work night and day, month after month. Thus do we see the soft and gelatinous body of polypus, through the agency of the vital laws, conquering the great mechanical power of the waves of an ocean, which neither the art of man nor the inanimate works of nature could successfully resist.”

Charles Darwin, in: *Journal of researches into the natural history and geology of the countries visited during the voyage round the world of H.M.S. Beagle under command of Captain Fitz Roy* London, John Murray Eds, Albemarle Street, 1845.

CONTENTS

Summary	9
Samenvatting	15
Chapter 1	Introduction 21
Chapter 2	River runoff reconstructions from novel spectral luminescence scanning of massive coral skeletons 51
Chapter 3	Spatial linkages between coral proxies of terrestrial runoff across a large embayment in Madagascar 85
Chapter 4	Madagascar corals reveal Pacific multidecadal modulation of rainfall since 1708 125
Chapter 5	Opposing Sr/Ca response to reef scale sea surface temperature in Eastern Madagascar corals: implications for tropical paleothermometry 151
Chapter 6	Synthesis 185
Acknowledgements	209
Curriculum Vitae	217

Summary

Soil erosion resulting from land degradation and current climate change pose a mounting threat to coastal nations in the western Indian Ocean. However, vital long-term observational data are missing to properly assess and clarify the impact of a changing climate and land-use. Furthermore, environmental management strategies have been formulated on short-term instrumental records at best, as proper historical time-series data are rarely available, even for the most sensitive river catchments.

This thesis examines the spatial and temporal environmental changes that affect coral reef ecosystems in the western Indian Ocean using coral proxy archives combined with climate indices, as well as biological and ecological data. Coral archives offer continuous seasonally resolved data spanning multiple centuries, which faithfully record climate variability and the occurrence of events such as ENSO (El Niño Southern Oscillation) related floods, tropical cyclones and multidecadal precipitation and runoff changes.

This coral proxy based climate project (SINDOCOM) entailed the drilling of coral cores, with a diameter of 4 cm and more than 3 m in length, to reconstruct past environmental change for various reef complexes across northern and eastern Madagascar. Massive corals grow at an approximate rate of 1 cm per year, archiving specific climate signals in their skeleton. In order to read these climate signals a novel scanning technique was devised that quantifies luminescence intensities of coral skeletons by splitting the total luminescence spectrum into three spectral domains (RGB; Chapter 2). By applying such a method, the amount of terrestrial humic acids could be determined that have been flushed into marine catchments at the time of skeletal precipitation (Chapter 2). As humic acids (green) have a slightly longer emission wavelength than the skeletal aragonite (blue), taking a Green/Blue (G/B) ratio provided a quantitative estimate of terrestrial erosion related to river runoff. The unprecedented sampling resolution of the luminescence device enabled weekly reconstructions of soil erosion and river discharge in northeast Madagascar over several decennia that resulted from natural rainfall cycles, intense cyclones and deforestation.

Combining the novel spectral luminescence approach with a proxy for sediment runoff (Ba/Ca), salinity ($\delta^{18}\text{O}_{\text{sw}}$) and turbidity/DIC ($\delta^{13}\text{C}$) it was

possible to identify the impact of runoff on individual corals associated with separate rivers in and around Antongil bay, the wettest region of Madagascar (Chapter 3). Moreover, three coral colonies were drilled close to individual rivers mouths, and proxies were combined with modelled data to identify the river runoff dynamics of the bay system. By modelling discharge and sediment yield for individual river catchments it was possible to recognise the river that experienced the highest rates of both sediment runoff and discharge, and compare the results with proxy data (Chapter 3). We relate differences to the distance between the coral and the river mouth, local physiochemical conditions and proxy behaviour. Our results provide information which will assist in future marine and terrestrial management programs (Chapter 3).

Long-term runoff patterns were assessed by using a longer core from the same region. Decoupling Madagascar's 20th century human deforestation from rainfall induced soil erosion using luminescence and geochemistry in the coral archives revealed a far-field precipitation link to the Pacific Ocean on multidecadal time-scales (Chapter 4). Indeed, the corals provide the first evidence for Pacific decadal modulation of rainfall over the western Indian Ocean. Positive phases of the Pacific Decadal Oscillation (PDO) are associated with increased Indian Ocean temperatures and rainfall across eastern Madagascar, while precipitation in southern Africa and eastern Australia decline. Consequently, the negative PDO phase that started in 1998 should lead to reduced rainfall over northeast Madagascar and increased precipitation in southern Africa and eastern Australia (Chapter 4). These results have important implications for future multidecadal variability of rainfall in Africa where water resource management is increasingly important under the warming climate.

To test whether coastal eastern Madagascar had warmed significantly over the past 43 years, sea surface temperatures (SST) were reconstructed from two coral skeletal Sr/Ca records (Chapter 5). Unfortunately, significant growth related influences on the skeletal precipitation of Sr/Ca were identified, hampering SST reconstructions. These are often referred to as vital effects. In both corals a positive correlation was observed between extension rate and Sr/Ca. Increasing extension rates in one coral were coupled with increasing Sr/Ca ratios, while decreasing extension rates in a different coral

were coupled with decreasing Sr/Ca ratios. Further, during individual positive ENSO events, calcification rates in both corals were negatively correlated, causing a diverging Sr/Ca response. As both corals were of the same species (*Porites lutea*) and from the same environment (0.72 km apart), the reliability of Sr/Ca as a paleothermometer is compromised. Accounting for these coral vital effects we estimate SST to have risen by $0.75^{\circ}\text{C} - 1.07^{\circ}\text{C}$ in eastern Madagascar over the past 43 years. This value is significantly higher than the range of $0.09^{\circ}\text{C} - 0.44^{\circ}\text{C}$ as given by gridded satellite data, suggesting gridded data may seriously underestimate trends at the reef scale.

The link between SST and rainfall is complicated and not always consistent. Identifying the ENSO-related precipitation response over NE Madagascar by applying coral cores as natural monitoring stations provides a greater insight into this complex connection (Synthesis). During La Niña events, when the southwest Indian Ocean cools, coral luminescence records indicate that precipitation over NE Madagascar increased. This is unexpected, however, and is likely due to the onset of an anomalous SST-gradient rather than the absolute SST in the southwest Indian Ocean. As the south-central Indian Ocean cools more than the south-west during La Niña events, convection is shifted towards the region of anomalously higher SST. This creates increased moisture transport towards Madagascar from the south-central Indian Ocean, and therefore more rainfall (Synthesis). However, the relationship between La Niña and precipitation broke down post 1976 when climate shifted to a new base level due to anthropogenic warming. This was probably caused by weakening of the SST-gradient between the south-west and the south-central Indian Ocean, as anthropogenic warming in the south-west increased at a faster rate than the south-central region. If anthropogenic warming continues, a reversal of the ENSO related precipitation response may occur, whereby El Niño events may lead to increased precipitation over NE Madagascar.

Another time interval where cooler SST triggered increased rainfall in parts of southern Africa was the Little Ice Age (LIA), between the 15th and the mid-19th century. The long coral luminescence record from north-east Madagascar provides evidence that conditions were significantly wetter during this period (Synthesis). This is in agreement with eastern African lake records, yet in contrast to central and southern African records. A stronger

monsoonal system in the Indian Ocean, related to a southern shift in Inter Tropical Convergence Zone (ITCZ), is likely responsible for this precipitation response. Again, this is probably linked to associated changes in SST-gradients. Indeed, there is much scope for future research in the SW Indian Ocean region to define the rainfall-drought cycles experienced over eastern and southern Africa during the LIA. This will be achieved by increasing the spatial and temporal resolution of coral cores in the region (CLIMATCH).

Samenvatting

Bodemerosie, landuitputting en klimaatverandering vormen een groeiende bedreiging voor de kuststaten in de westelijke Indische Oceaan. Belangrijke lange-termijn gegevens ontbreken echter om de gevolgen van dergelijke veranderingen goed te kunnen bepalen. Bovendien zijn milieumanagement strategieën in het gunstigste geval gebaseerd op kortlopende meetseries die wel beschikbaar zijn, zoals van satellieten. Zelfs voor de kwetsbare stroomgebieden en kuststreken waar rivieren uitkomen in zee, ontbreekt het aan metingen die ver genoeg teruggaan in de tijd.

Dit proefschrift onderzoekt de veranderingen die invloed hebben op de koraalrifecosystemen in de westelijke Indische Oceaan. Dit is gedaan door te kijken naar zowel koraalarchieven als naar de beschikbare klimaatindices, milieumodellen en ecosysteemgegevens. De koraalarchieven blijken doorlopend klimaatgegevens en klimaatgebeurtenissen te registreren, zoals seizoensvariatie, overstromingen gerelateerd aan ENSO (El Niño Southern Oscillation), tropische cyclonen en lange-termijn veranderingen in neerslag en rivierafvoer.

Een onderdeel van het klimaatproject SINDOCOM was het boren van enkele koraalkernen -met een diameter van 4 cm en een lengte van meer dan 3 meter- om de veranderingen in het milieu te reconstrueren voor diverse rif-complexen. Deze koralen groeien met een gemiddelde snelheid van 1 cm per jaar, waarbij ze voortdurend specifieke, aan klimaat gerelateerde, signalen opslaan in hun kalkskeletten. Om deze klimaat-signalen te kunnen interpreteren, werd een nieuwe scantechniek ontwikkeld waarmee de intensiteit van luminescentie in koraalskeletten gemeten kan worden door het luminescentiespectrum op te splitsen in drie spectrale domeinen (Rood/Groen/Blauw; Hoofdstuk 2). De luminescentie wordt mede bepaald door de hoeveelheid humuszuren die door rivieren in zee is gespoeld op het moment van de opbouw van het koraalskelet (Hoofdstuk 2). Aangezien humuszuren een langere (groene) emissiegolflengte hebben dan het koraalskelet (blauw), levert de “groen/blauw” ratio een kwalitatieve maat op voor de aan bodemerosie gerelateerde rivierafvoer. De ongekeerde monster resolutie van de luminescentietechniek maakte wekelijkse reconstructies mogelijk van bodemerosie en rivierafvoer door de eeuwen heen in Noordoost-Madagaskar als gevolg van natuurlijke neerslagcycli, cyclonen en ontbossing.

Door de nieuwe spectrale luminescentietechniek te combineren met proxies voor de slibafvoer (Ba/Ca), het zoutgehalte ($\delta^{18}\text{O}_{\text{sw}}$) en de troebelheid ($\delta^{13}\text{C}$) in de koraalskeletten, kon de invloed van erosie op individuele koralen, beïnvloed door drie afzonderlijke rivieren in en nabij de Antongil baai (de natste regio van Madagaskar), worden onderscheiden (Hoofdstuk 3). Voor drie koraalkolonies dichtbij de riviermond werden de proxymetingen gecombineerd met modelresultaten om de karakteristieken van ieder stroomgebied te bepalen. Hierdoor bleek het mogelijk de rivier te herkennen aan de mate van afvoer van zowel slib als humuszuren in de baai. We relateren verschillen aan de afstand tussen koraal en riviermond, plaatselijke fysio-chemische factoren en de reacties van proxies op omgevingsomstandigheden. Deze informatie zal in de toekomst bijdragen aan een beter beheer van het mariene en het terrestrische milieu (Hoofdstuk 3).

Aan de hand van een langere koraalkern uit dezelfde regio konden ook de lange-termijn patronen in de rivierafvoer worden bepaald. De data verkregen uit de koraalarchieven voor de antropogene ontbossing in de 20^e eeuw in Madagaskar, werden ontkoppeld van door neerslag veroorzaakte bodemerrosie, door zowel de luminescentietechniek als geochemie te gebruiken. Daarmee kon er voor het eerst een verband worden aangetoond tussen de veranderende neerslag in Madagaskar en de temperatuur van het zeewateroppervlakte in de Stille Oceaan vele duizenden kilometers verderop (Hoofdstuk 4). Deze koraalarchieven leverden de eerste aanwijzingen voor een langzaam oscillerend patroon in de neerslag over de westelijke Indische Oceaan, dat bekend staat als de ‘Pacific Decadal Oscillation’ (PDO). De positieve fase van de PDO wordt geassocieerd met stijgende zeewatertemperaturen in de Indische Oceaan en toenemende neerslag in Oost-Madagaskar, terwijl het in Zuid-Afrika en Oost-Australië zorgt voor een afname van de neerslag. Hierdoor zou de negatieve PDO fase in 1998 moeten leiden tot een afname in neerslag in Noordoost-Madagaskar en een toename in neerslag in Zuid-Afrika en Oost-Australië (Hoofdstuk 4). Met deze resultaten kan ingespeeld worden op de lange-termijn verwachting van klimaatveranderingen in neerslag in Afrika, waar watermanagement van groeiend belang is.

Om te bepalen of het kustgebied van Oost-Madagaskar significant is opgewarmd over de afgelopen 43 jaar werd de temperatuur van het

zeewateroppervlakte bepaald door de Sr/Ca samenstelling te meten van twee koraalkernen (Hoofdstuk 5). Helaas werd hierbij een significant effect van groei op de neerslag van Sr/Ca in het koraalskelet gevonden, waardoor de reconstructie van de temperatuur van het zeewateroppervlakte belemmerd werd. In beide koralen werd een positieve correlatie gevonden tussen de groeisnelheid en Sr/Ca. Toenemende groei in één koraal bleek gekoppeld aan toenemende Sr/Ca waardes terwijl afnemende groei in een naburige koraal gekoppeld was aan afnemende Sr/Ca waardes. Bovendien waren de calcificatiesnelheden in beide koralen negatief gecorreleerd tijdens positieve ENSO periodes, wat resulteerde in een uiteenlopende Sr/Ca reactie. Aangezien beide koralen van dezelfde soort zijn (*Porites lutea*) en uit dezelfde omgeving komen (0.72 km van elkaar) wordt de betrouwbaarheid van Sr/Ca als paleo-thermometer hierdoor in twijfel gebracht. Rekening houdende met dit groei-effect op de koralen schatten we dat de temperatuur van de zeewateroppervlakte over de laatste 43 jaar in Oost-Madagaskar gestegen is met $0.75^{\circ}\text{C} - 1.07^{\circ}\text{C}$. Deze waarde is significant hoger dan de grenswaarden $0.09^{\circ}\text{C} - 0.44^{\circ}\text{C}$, bepaald door satellietgegevens. Dit suggereert dat deze gegevens de lange-termijn effecten op rif-schaal sterk onderschatten.

Het verband tussen de temperatuur van het zeewater (SST) en neerslag is gecompliceerd. Door met behulp van koraalkernen de reactie op de door ENSO veroorzaakte neerslag te bepalen, kan een beter inzicht verkregen worden van de gevolgen van een veranderend ENSO systeem (Synthese). In de La Niña fase, wanneer de zuidwestelijke Indische Oceaan afkoelt, neemt de neerslag in Noordoost-Madagaskar toe en niet af zoals blijkt uit de luminescentiemetingen. Dit wordt waarschijnlijk veroorzaakt door een veranderde SST-gradiënt, in plaats van de absolute SST in de zuidwestelijke Indische Oceaan. Aangezien de zuid centrale Indische Oceaan gedurende La Niña sterker afkoelt dan de zuidwestelijke Indische Oceaan, neemt het vochttransport toe richting Madagaskar en daaruit de neerslag (Synthese). Die relatie tussen La Niña en verhoogde neerslag werd echter verbroken na 1976 toen het klimaat door antropogene opwarming verschoof naar een nieuw basisniveau. Dit is waarschijnlijk veroorzaakt door het verzwakken van de SST-gradiënt tussen de zuidwestelijke en de zuid centrale Indische Oceaan, aangezien antropogene opwarming in het zuidwesten van de Indische Oceaan met een hogere snelheid toenam dan in de zuid centrale

regio. Verdere antropogene opwarming zal mogelijk een ommekeer in de ENSO gerelateerde neerslag veroorzaken, met een toename tijdens El Niño in Noordoost-Madagaskar.

Een ander voorbeeld van een regionale toename in neerslag door een afkoelende zee vond plaats tijdens de Kleine IJstijd in Zuid-Afrika vanaf de 15^e tot medio 19^e eeuw. De luminescentiemetingen aan de lange koraalkern uit Noordoost-Madagaskar geven een significant natter klimaat gedurende deze periode (Synthese). Dit komt overeen met gegevens van Oost-Afrikaanse meren, maar niet met die uit Centraal- en Zuid-Afrika. Een sterker moessonsysteem in de Indische Oceaan, gerelateerd aan een zuidelijke verschuiving van de 'Intertropische Convergentie Zone', is waarschijnlijk daarvoor verantwoordelijk en ook hier vermoedelijk gekoppeld aan SST-gradiënten. Nader onderzoek in het CLIMATCH-programma zal bepalen wat de lange-termijn veranderingen zijn in de 'nat-droog cycli' van Oost- en Zuid-Afrika.

Chapter 1

Introduction

Many characteristics of climate change have been identified and attributed to global warming. Changing rainfall patterns and an increase in the intensity and frequency of extreme climate events i.e. heat waves and cyclones, are just two examples of how weather patterns are thought to respond to anthropogenic warming. While some evidence exists for such changes, it is not enough, however, to compile conclusions solely based on data that does not extend past the last century (generated by satellites, weather stations and ships), and therefore a widespread need for spatiotemporally resolved geological records is required. Moreover, it is essential to recognise how climate has evolved naturally throughout different eras in order to comprehend the extent to which modern day climate is changing and at what rate. Substantial uncertainties still exist in determining the natural feedback mechanisms and teleconnections within the earth's climate system, which have been continuously evolving to reach equilibrium since the earth's genesis.

Global Warming and Climate Change

'Global warming' is the most important environmental threat our world currently faces (Forster et al., 2007). The last century has seen a rapidly growing global population and more intensive exploitation of resources, leading to greatly increased emissions of gases, such as carbon dioxide and methane. Such gases are commonly referred to as greenhouse gases, and result from the burning of fossil fuels (oil, gas and coal), agriculture, cement production and deforestation (Houghton, 2005). Greenhouse gases absorb infrared radiation emitted by the Earth's surface and act as blankets keeping it warmer than it would otherwise be. Most greenhouse gases are naturally occurring (CO_2 , CH_4 , N_2O), however, as human population levels have risen and the need to exploit resources has grown, the accelerated release of greenhouse gases has triggered global warming (Cox et al., 2000). Associated with this warming is climate change.

The basic science behind the 'greenhouse effect' that leads to warming is well understood (Lashof and Ahuja, 1990); yet, to comprehend how climate is changing in its response is less clear. A more detailed understanding therefore relies on numerical models of climate that integrate the basic dynamical and physical equations describing the complete climate system (Cox et al., 2000).

The Earth's climate currently appears out of balance and is warming at an unnatural rate (Forster et al., 2007; Meehl et al. 2004). Global average surface temperatures have increased on average by about 0.6°C over the period 1956–2006 (Meehl et al., 2005). Many components of the climate system, including atmospheric, land and ocean temperatures, sea ice and mountain glaciers, sea level, precipitation, and the length of seasons are now changing at rates and patterns out of range of what is thought to be the natural variation. These are best explained by the increased atmospheric concentrations of greenhouse gases and aerosols generated by human activity during the 20th century, yet the interaction with natural climate variability needs to be further addressed in order to fully comprehend the ‘change’ (Cane, 2010).

There is now widespread concern that the Earth's climate will warm further; not only because of the lingering effects of the added carbon already in the Earth's system, but also because of further carbon additions as the human population continues to grow (Forster et al., 2007; Meehl et al., 2005). In the next 50 years, even the lower limit of impending climate change (an additional global mean warming of 1°C above the last decade) is far beyond the range of climate variability experienced during the past thousand years (Meehl et al. 2005). Adaptation to a rapidly changing environment is therefore essential to sustain species survival, while mitigation to reduce its impacts seems inevitable to combat the abrupt rate of change. The extent to which global warming has shifted the natural climate state will be fundamental in determining how the human population will manage food security, natural resources and indeed, survive. This is particularly evident for regions across eastern and southern Africa, whereby a combination of increasing population size and more frequent and intense flooding and drought events have already had a severe impact. This thesis provides a stepping stone towards unravelling the Earth's complex climate system and the implications global warming will have on it. With the help of geological archives we can begin to scrape the surface of this synergy.

Climate across eastern and southern Africa is largely heterogeneous due to topographic regional differences, and strong (weak) coastal (inland) links to the Indian Ocean (Funk et al., 2008). Warming of the south-central Indian Ocean (0-15°S, 60-90°E) is thought to reduce the onshore moisture

flux towards southern Africa in austral summer and fall, facilitating drought-like conditions (Goddard and Graham, 1999; Hoerling et al., 2006; Richard et al., 2000). Eastern Africa rainfall trends are less clear as both increasing (Goddard and Graham, 1999; Hoerling et al., 2006) and decreasing (Funk et al., 2008) patterns have been reported in response to Indian Ocean warming. Madagascar rainfall appears anti-correlated with southern African rainfall on interannual to interdecadal time-scales due to the shifting tropical temperature troughs in response to large-scale changes in SST and sea level pressure (Fauchereau et al., 2008; Reason and Rouault, 2002).

Unfortunately, long-term climate trends or multidecadal oscillations are poorly understood as weather station data is scarce and satellite data are often incomplete or too short to make a proper assessment, particularly in Madagascar (Dewar and Richard, 2007; Dewar and Wallis, 1999). Nevertheless, Pacific decadal variability is known to affect Indian Ocean temperatures and African climate (Charles et al., 1997; Cole et al., 2000; Crueger et al., 2009; Damassa et al., 2006; Zinke et al., 2009), and suggested to influence Indian Ocean and continental rainfall as well (Deser et al., 2004; Zinke et al., 2008). Madagascar's geographical position makes it particularly susceptible to a high variability in temperature, precipitation and cyclone activity (Dewar and Richard, 2007; Jury et al., 1995; Kuleshov et al., 2008), all of which pose a severe threat to Madagascar's rich marine and terrestrial biodiversity.

The Indian Ocean and Madagascar

The Indian Ocean is land locked in the northern hemisphere by the Eurasian continent, preventing northward heat export and allowing only weak ventilation of the thermocline waters from the north. It is the third largest oceanic body covering approximately 20% of the Earth's surface (water volume of 292,131,000 km³), surrounded by the three continents Africa, Asia and Australasia. The Asian continent drives the strongest monsoon on Earth, and the monsoonal winds generate large seasonal variations in ocean currents, many of which display annual reversals. The switching trade winds have historically facilitated early trade, also allowing the settlement of Indonesians in Madagascar.

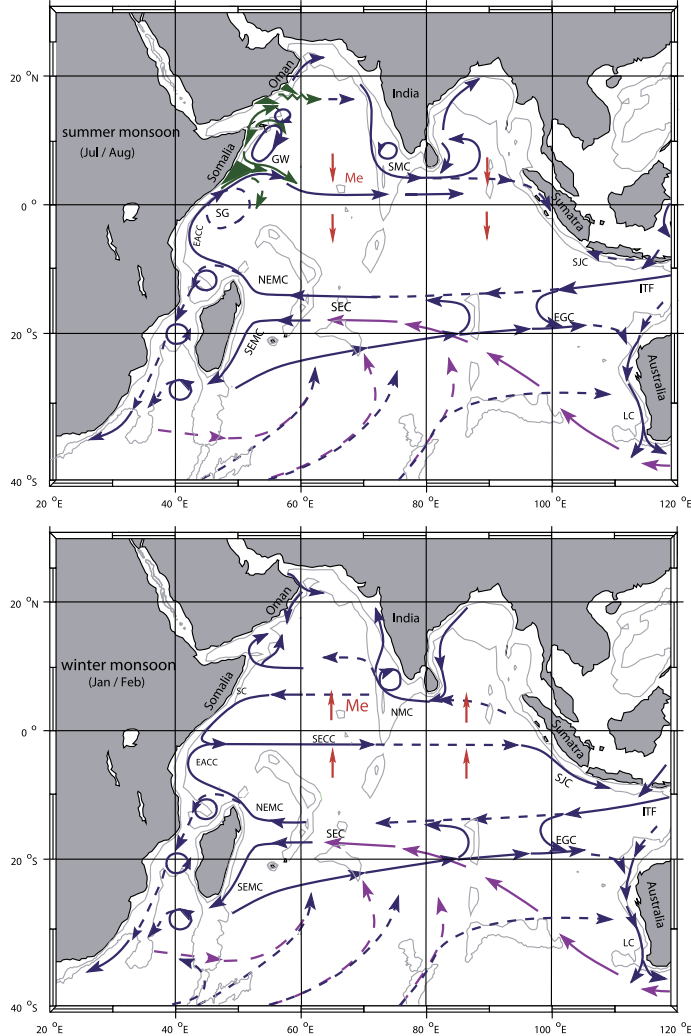


Figure 1.1. Schematic representation of current branches during the summer (southwest) monsoon (upper panel), and winter (northeast) monsoon (lower panel). Current branches indicated are the South Equatorial Current (SEC), South Equatorial Countercurrent (SECC), Northeast and Southeast Madagascar Current (NEMC and SEMC), East African Coastal Current (EACC), Somali Current (SC), Southern Gyre (SG) and Great Whirl (GW) and associated upwelling wedges (green shades), Southwest and Northeast Monsoon Currents (SMC and NMC), South Java Current (SJC), East Gyrar Current (EGC), and Leeuwin Current (LC). The subsurface return flow of the supergyre is shown in magenta. Depth contours shown are for 1000 m and 3000 m (grey). Red vectors (Me) show directions of meridional Ekman transports. ITF indicates Indonesian Throughflow (from Schott et al., 2009).

The Indonesian Throughflow, which feeds the Southern Equatorial Current (SEC), provides the Indian Ocean with a low-latitude exchange with the Pacific Ocean. The SEC runs from the eastern side of the Indian Ocean westwards, to form the western limb of two subtropical gyres (Schott et al., 2009). As it hits the eastern side of Madagascar (near 17°S) it forms a clockwise current flowing north (NEMC) and an anticlockwise current flowing south (SEMC) (Schott et al., 2009; Fig. 1.1). The positioning of these gyre limbs vary depending on the season as surface currents are primarily driven by the monsoonal trade winds. The easterly trade winds, which prevail over the equatorial Pacific and Atlantic, cause shoaling of the thermocline in the eastern equatorial ocean and hence promote upwelling of cool subsurface waters. In contrast, the annual mean winds over the equatorial Indian Ocean are weak and westerly, therefore the thermocline is flat, with little or no upwelling in the eastern equatorial Indian Ocean. Precipitation patterns of the Indian Ocean are remarkably similar to those for sea surface temperatures (SST), indicative of the strong coupling between these two fields (SST and precipitation).

SW Indian Ocean Natural Climate Variability

Seasonal Variability

The Asian monsoon is a major manifestation of the seasonal cycle in the tropical-subtropical regions, driven by the pressure gradients resulting from differential heating over the Eurasian continent and the Indian Ocean, modified by the rotation of the Earth (Wang et al., 2005; Webster et al., 1998). The inherent seasonality of the Asian monsoon circulation affects the Indian Ocean, leading to strong seasonal variability in atmospheric circulation, SST and salinity (Wang et al., 2005). The Intertropical Convergence Zone (ITCZ) is described as the maximum line of solar heating, marked by a belt of high cloud cover and precipitation around the Earth that shifts back and forth across the equator in response to the sun's zenith point. During austral summer (DJF) it is located as far south as 20°S, where it is positioned over northern Madagascar (Fig. 1.2). This region of convection is essentially the rising limb of the Hadley cell and is responsible for Madagascar's heavy rains (Hu et al., 2007). The trade winds connecting the descending limb are located

approximately 30° north and south of the ITCZ. The descending limb of the Hadley cell is associated with higher air pressure and responsible for dryer conditions in the southern hemisphere during austral winter.

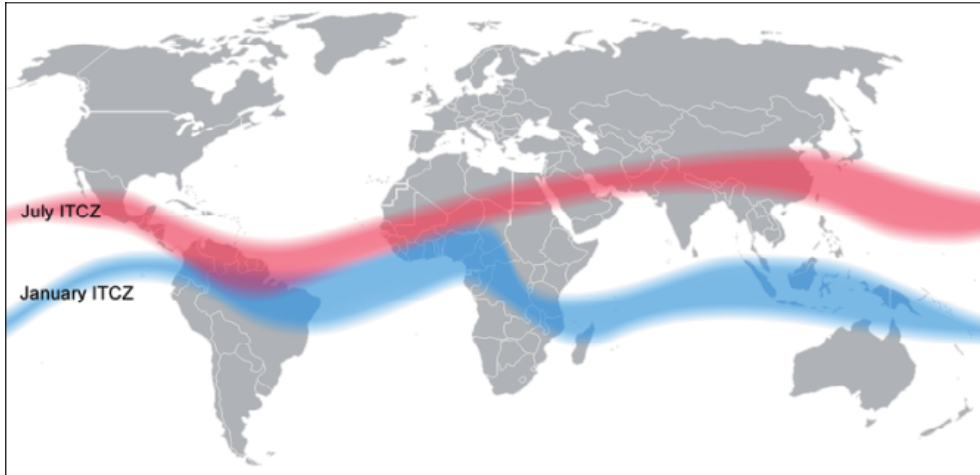


Figure 1.2. Location of the Inter Tropical Convergence Zone (ITCZ) in austral summer (blue) and austral winter (red).

North of 10°S the trade winds seasonally reverse with the monsoon. South of 10°S , the southeast trade winds, associated with Madagascar, differ as they are relatively steady in their direction. However, as the ITCZ moves north (south) during the boreal summer and fall (winter and spring) the trade winds strengthen (weaken) and their northern edge shifts northward (southward) (Schott et al., 2009). It is the strength of the trade winds feeding the ITCZ, coupled with the SW Indian Ocean SST, which determines the amount of regional precipitation Madagascar experiences. High regional SST and strong winds (strong SST-gradient with adjacent regions) drive maximum ITCZ convection, effectively drawing in air and moisture (Yasunari, 1998). In the Indian Ocean the ITCZ spawns on average ten tropical cyclones per year during austral summer through easterly waves and surges of the monsoon (Jury et al., 1994). The NE Madagascar region is vulnerable to these cyclones, which travel across the Indian Ocean in a westerly direction.

Interannual Variability

There are two prominent modes of interannual variability that impact the Indian Ocean; the El Niño Southern Oscillation (ENSO) (McPhaden et al., 2006) and the Indian Ocean Dipole (IOD) (Saji et al., 1999), which have frequencies of 2 - 7 years and 2 – 5 years, respectively. There are two other modes of variability that exist, namely the subtropical dipole (Behera and Yamagata, 2001; Reason, 2002) and the Tropical Biennial Oscillation (TBO) (Meehl and Alabaster, 2002); however, the impact of these on the Indian Ocean is much weaker than ENSO or the IOD.

The most dominant mode of natural climate variability in recent (instrumented) times is ENSO, characterised by recurrent warming (El Niño) and cooling (La Niña) of the eastern equatorial Pacific (McPhaden et al., 2006). These anomalies arise from changes in the Walker Circulation pattern. Normally, the tropical western Pacific is warm and wet under a low pressure system, and the cool and dry eastern Pacific lies under a high pressure system. This creates a pressure gradient from east to west and causes surface air to move in the same direction, from the high pressure in the eastern Pacific to the low pressure in the western Pacific. The ENSO induced SST anomalies of the eastern Pacific develop during boreal summer, peaking in boreal winter, and decaying in the following spring. There is an eastward (westward) shift in atmospheric convection over the Pacific during an El Niño (La Niña) event (see McPhaden et al., 2006). The convective currents then intensify over the central eastern (western) Pacific, resulting in slow anomalous subsidence over the western (eastern) Pacific and maritime continent (Fig. 1.3). These large-scale shifts in convection alter the atmospheric circulation remotely both in the tropics and extratropics via atmospheric wave adjustments (atmospheric bridge). These alterations have a global ‘knock on effect’ and are often referred to as global teleconnections. During a positive ENSO event (El Niño) there is a corresponding warming of the Indian Ocean, which peaks during the boreal spring (March – May). Maximum Indian Ocean SST therefore occurs approximately one season after the equatorial eastern Pacific (Klein et al., 1999; Nigam and Shen, 1993). Much of the basin wide Indian Ocean warming is caused by ENSO-induced surface changes in surface heat fluxes, particularly the wind-induced latent heat and cloud-induced solar radiation fluxes (Fig. 1.4; Klein et al., 1999).

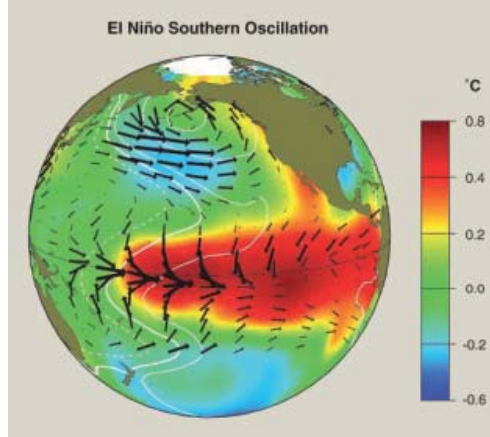


Figure 1.3. El Niño anomalies in SST (colour shading and scale in °C), surface atmospheric pressure (contours), and surface wind stress (vectors) in the Pacific basin. Pressure contour interval is 0.5 mb, with solid contours positive and dashed contours negative. Wind stress vectors indicate direction and intensity, with the longest vector equivalent to $\sim 1 \text{ N m}^{-2}$. The patterns in this graphic are derived from a linear regression against SST anomalies averaged over 6°N – 6°S , 90°W – 180° in the eastern and central equatorial Pacific. All quantities scale up or down with the intensity of anomalies in this index region, that is, higher for strong El Niños and lower for weak El Niños. Anomalies of opposite sign apply to La Niña events, although there are some differences in the spatial patterns of El Niño and La Niña. From McPhaden et al. (2006).

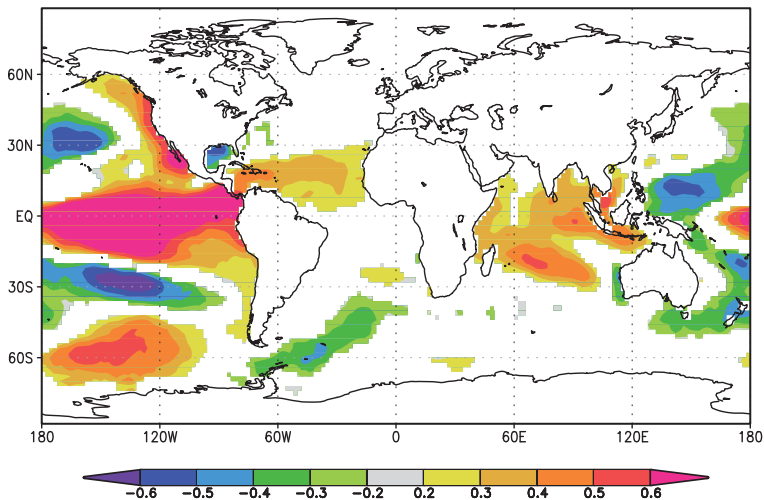


Figure 1.4. The spatial correlation of global SST (ERSSTv.3) with the Nino 3.4 index for Madagascar wet season (JFMA).

While it is evident that positive ENSO events are characterised by basin wide Indian Ocean warming (Fig. 1.4), the cause of warming in the SW Indian Ocean cannot solely be explained by surface fluxes (Klein et al., 1999). There is a thermocline ridge from 5°S to 10°S in the SW Indian Ocean where cool isotherms lie near the surface. It is here that thermocline variability strongly influences SST (Xie et al., 2002). During the mature phase of El Niño (December), anomalous anticyclonic wind stress forms in the tropical southeast Indian Ocean, caused by an atmospheric bridge from the Pacific, which is an anomaly of the Walker Circulation. This forces downwelling Rossby waves in the southeast Indian Ocean, which after they arrive in the SW Indian Ocean several months later, deepen the thermocline ridge and warm SST there (Fig. 1.5; Xie et al., 2002). SW Indian Ocean SST is therefore largely determined by remotely forced changes in the depth of this ridge.

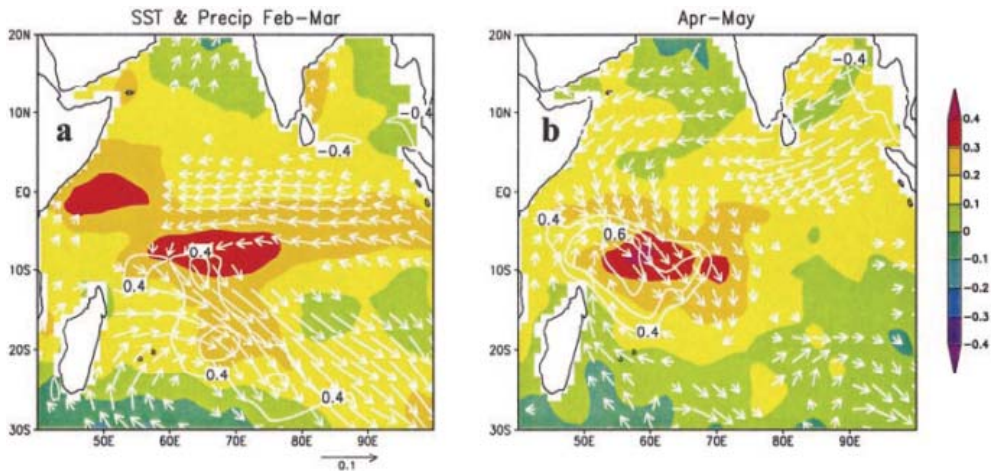


Figure 1.5. Regression coefficients of SST (colour shade in °C) and surface wind stress (vectors in 10^{-1} N m^{-2}) with the ENSO index in (a) Feb–Mar and (b) Apr–May. The precipitation correlation is plotted in contours. From Xie et al. (2002).

Local maximum SST forms over the thermocline ridge during boreal spring (April – July), where a mean standard deviation of 0.4°C - 0.5°C is reported (Xie et al., 2002). Moreover, embedded in the basin wide warming of the Indian Ocean that peaks between February – April following El Niño, SST anomalies display a positive core that co-propagates westward with the Rossby waves (Fig. 1.5; Xie et al., 2002). This core is the deepening

of the thermocline in the SW Indian Ocean, which together with SST and precipitation, shows positive correlations with ENSO (Fig. 1.5; Xie et al., 2002). As the ITCZ is displaced south of the equator during boreal winter, covering the 5°S to 10°S thermocline ridge, atmospheric convection and thus precipitation the SW Indian Ocean also increases in the region, with significant impacts on both local and remote climate (Fig. 1.5). Increased precipitation following positive ENSO events in the SW Indian Ocean is associated with an anomalous cyclonic circulation in the lower troposphere, as well as an increase in the number of tropical cyclones (Xie et al., 2002). Furthermore, the persistent SW Indian Ocean warming anchors convection south of the equator, delaying the onset of the south Asian monsoon in May (Joseph et al., 1994; Kawamura et al., 2001).

There is evidence to suggest that ENSO is correlated with the Indian Ocean Dipole, although from 1876 to 1999 about half of the IOD events occurred independently of ENSO (Meyers et al. 2007). Triggering of the IOD seems to therefore be by either ENSO, or by self-generation, provided the thermocline off Sumatra is shallow enough to support a type of feedback, namely Bjerknes feedback (Meyers et al., 2007). The IOD develops in June and peaks in October (Saji et al., 1999). Due to the strong seasonal variability of the monsoon winds, sometimes conditions prevail that allow a shoaling of the eastern equatorial thermocline, similar to La Niña-like ocean-atmosphere anomalies in the Pacific. This phenomenon is characteristic of an IOD event. South easterly winds, associated with the monsoon, form off the Sumatra coast, reaching a peak during the summer at which point the winds have an easterly component all along the equator. This forcing favours a shoaling of the thermocline and upwelling in the eastern equatorial Indian Ocean. Through the Bjerknes feedback mechanism, there is then a zonal gradient of tropical SST, with cooling off the coast of Sumatra and warming in the western ocean (Saji et al., 1999). As the IOD develops, an east–west dipole of anomalous rainfall is established over the tropical Indian Ocean, with precipitation increasing in the west because of the low-level convergence associated with the anomalous equatorial easterlies, and vice versa in the east (Saji et al., 1999; Schott et al., 2009). The intense winter monsoonal forcing eventually weakens the southeasterly winds off Sumatra, leading to the rapid termination of IOD events. The IOD is weak in most years, likely because the Sumatra

thermocline is too deep. It should be noted that the main impact region of the SW Indian Ocean is above 10°S, and therefore the impact on Madagascar is likely to be minimal.

Interdecadal and Multidecadal Variability

Both the IOD and ENSO display decadal variability. Further, the correlation between ENSO and the IOD varies on decadal timescales. As there is decadal variability in the depth of the eastern equatorial thermocline, the correlation between ENSO and the IOD increases when the thermocline is deep, as it takes a positive ENSO event to force an IOD event. It may well be that the decadal variability associated with the eastern equatorial thermocline is related to the Indonesian Throughflow (Santoso et al., 2011), which in turn might be related to another external decadal/multidecadal force. Indeed, IOD events occurred more independently from ENSO in the 1950's and 1960's, and then from the mid-1970's onwards became highly correlated (Schott et al., 2009). Interestingly, in 1976 the Pacific Decadal Oscillation (PDO) switched from a negative to a positive phase, and according to Williams and Grottolli (2010), the PDO can influence the depth of the thermocline, whereby a positive PDO phase (1976 – 1998) will deepen the thermocline in eastern equatorial Indian Ocean (Williams and Grottolli, 2010).

The PDO is a major internal mode of ocean-atmosphere variability (Mantua et al., 1997). Positive PDO phases are characterised by low SST in the central midlatitude Pacific and warm anomalies along the northern and eastern margins, and south of 30°N (Fig. 1.6). The PDO is remotely forced from the Tropics in part (Schneider and Cornuelle, 2005), and responsible for strong multidecadal (50 – 70 years; Minobe, 1997) and interdecadal Pacific oscillations in SST (IPO; 17 – 28 years) (Meehl and Hu, 2006). It is considered the leading mode of North Pacific SST defined by instrumental data for the past 120 years (Mantua et al., 1997). Mounting evidence indicates that the PDO has teleconnections extending over thousands of kilometers to the Indian Ocean (Cole et al., 2000; Crueger et al., 2009). The positive PDO phase corresponds to warm Indian Ocean SST anomalies (Deser et al., 2004), thought to exceed anomalies associated with ENSO (Krishnan and Sugi, 2003), particularly in the southwestern Indian Ocean (Fig. 1.6; Meehl and

Hu, 2006). While it is evident that changing rainfall patterns over Australia respond to the PDO (Arblaster et al., 2002; Lough, 2007), links to rainfall in southeastern Africa and the western Indian Ocean have also been suggested (Deser et al., 2004; Zinke et al., 2008).

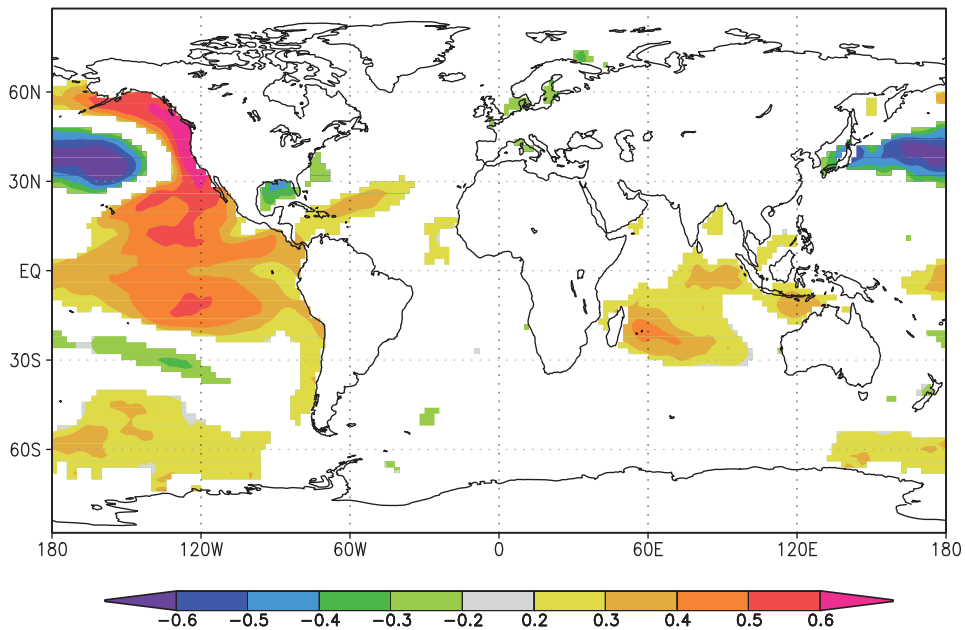


Figure 1.6. The spatial correlation of global SST (ERSSTv3;) with the PDO index for Madagascar wet season (JFMA).

Coral Reefs

“The organic forces separate the atoms of carbonate of lime, one by one, from the foaming breakers, and unite them into a symmetrical structure. Let the hurricane tear up its thousand huge fragments; yet what will that tell against the accumulated labour of myriads of architects at work night and day, month after month. Thus do we see the soft and gelatinous body of polypus, through the agency of the vital laws, conquering the great mechanical power of the waves of an ocean, which neither the art of man nor the inanimate works of nature could successfully resist.” Charles Darwin, in: *Journal of researches into the natural history and geology of the countries visited during*

the voyage round the world of H.M.S. Beagle under command of Captain Fitz Roy London, John Murray Eds, Albemarle Street, 1845.

Coral reef ecosystems are among the most biologically diverse ecosystems on the planet (Hallock, 2001). Corals have evolved to dominate well lit, shallow tropical waters, producing a diverse assortment of colourful colonies and morphologies. It is their ability to secrete an aragonite skeleton through extracting calcium (Ca^{2+}), carbonate (CO_3^{2-}) and bicarbonate (HCO_3^-) ions from seawater that allows symbiotic corals to construct giant reef frameworks upon which coral reef ecosystems thrive (Stanley and Schootbrugge, 2009). These living carbonate structures provide habitats for over a million species of plant, animal, fungi and bacteria, of which as much as 90% are yet to be discovered (Reaka-Kudla, 1996). In addition to the significant biodiversity, coral reefs provide food and resources for over 500 million people (Hoegh-Guldberg, 2011). Ecosystem services provided by coral reefs include food generated by small-scale fisheries, income from commercial fishing and tourism, and coastal protection against storms and hurricanes. Altogether, coral reefs play pivotal roles, bringing social, economic and cultural benefits which are crucially important to tropical island societies and nations (Spalding et al., 2001).

Symbiotic relationship

Scleractinian (stony) corals are the result of mutualistic symbiotic associations between cnidarian invertebrates and intracellular dinoflagellate algae of the genus *Symbiodinium*. This symbiosis underpins the success of coral reef ecosystems. Physiologically, the endosymbiont algae play a crucial role in host sustenance and survival in nutrient-poor tropical waters (Muscatine and Porter, 1977). The photosynthetically fixed carbon translocated from the algae can cover most or the entire energetic demands of the host (Muscatine et al., 1984) and powers the metabolically expensive process of calcification, allowing corals to deposit huge amounts of calcium carbonate (Hoegh-Guldberg, 1999). In return for the energy given to the coral host, the symbiotic algae receive access to inorganic nutrients resulting from animal metabolism, and are sheltered from threats such as ultraviolet (UV) radiation damage (Muller-Parker and D'Elia, 1997; Yellowlees et al., 2008). The close proximity of the autotrophic and heterotrophic components

facilitates molecular exchange and prevents nutrient losses (Tanaka et al., 2006), another adaptation to the oligotrophic conditions. Due to its crucial nutritional function, the phototrophic component of the association plays a major role in coral niche occupation. Specifically, algal symbiont functional diversity has been hypothesised to regulate the vertical distribution of corals (Iglesias-Prieto et al., 2004). Divergent genetic lineages of these algal symbionts appear to be adapted to particular environmental niches (Frade et al., 2008a; Frade et al., 2008b) and to confer varying levels of tolerance to increased seawater temperatures (Sampayo et al., 2008). The close relationship between corals and symbiotic dinoflagellates has been in existence for at least 220 million years (Muscatine et al., 2005), and is largely responsible for the huge reserves of limestone found in the upper layers of the earth's crust. The oldest fossil records of scleractinian corals date back 245 million year ago (Hoegh-Guldberg, 2011).

Threats

The current global distribution of coral reefs provides insight into the environmental conditions needed for maintaining corals and the reefs that they build. Because corals need abundant light for their photosynthetic symbionts, their distribution is limited to shallow seas (not deeper than 100 m) in regions within 30° north and 30° south of the equator. Coral reefs are also dependent on warm and thermally stable oceans, where temperatures do not fall below 18°C in the winter (Kleypas et al., 1999). However, one of the major contemporary threats to coral reefs comes in the form of widespread temperature rises associated with both ENSO and anthropogenic warming. These have been shown to cause coral bleaching; a loss or reduction of the symbiont populations or their photosynthetic pigments which often results in host mortality (Carpenter et al., 2008; Lesser, 2007). Bleaching most often results from physiological stresses on the algal symbionts caused by the synergistic effect of elevated seawater temperature and high light intensity (Douglas, 2003). Intact symbioses vary in their bleaching susceptibility and much of this variation has been attributed to differences in the tolerance of symbiont types towards temperature (Sampayo et al., 2008; Thornhill et al., 2008). Their narrow range of temperature tolerance puts coral reefs among the most threatened ecosystems on the planet (Carpenter et al., 2008; Lesser, 2007).

Coral bleaching is one of the most important causes for coral reef decline worldwide. This phenomenon has occurred with increasing frequency over the last twenty years, primarily due to the more frequent occurrence of strong ENSO events (Hoegh-Guldberg, 2004). Regional patterns in coral cover distribution in the Indian Ocean are driven mainly by episodic and acute environmental stress (Ateweberhan et al., 2011). In fact, coral reefs face widespread degradation, seen for instance in major losses of coral cover worldwide (Bak et al., 2005; Wilkinson 2008). In the Western Pacific the abundance of coral reefs has declined by as much as 50% and is continuing to decline at the rate of 1-2% per year (Bruno and Selig, 2007). At the local level, coral reefs are affected by declining water quality (resulting from increasing nutrient and sediment load from disturbed coastlines), over-exploitation of key marine species, destructive fishing practices and pollution from expanding urban areas (Hughes et al., 2003). Climate change is dramatically altering the circumstances under which corals have prospered for many millions of years, therefore exacerbating changes caused by local anthropogenic influence. Rapidly changing global climate is predicted to be shifting the face of coral reefs as we know them, carrying along important ecological and socioeconomic alterations (Hoegh-Guldberg, 2011).

Coral paleoclimatology

Massive tropical corals

Massive tropical corals continuously secrete a carbonate skeleton that may accumulate for centuries, creating giant structures. The most common genus of these scleractinian corals in the Indo-Pacific region is *Porites* spp. (Fig. 1.7). In the southwest Indian Ocean particularly, the primary reef-building species of *Porites* are *P. solida*, *P. lutea* and *P. lobata*. Massive colonies are spherical or hemispherical when small, and helmet or dome-shaped when large, which may be over 5 meters across (Fig. 1.7). Their corallites are small, immersed, and filled with septa, and the tentacles of most, but not all species, are extended only at night when they feed on zooplankton. Colours of the colonies mainly consist of cream, yellow or pale brown, however, brighter colours such as greens, blues and purples are found in shallower waters (Fig. 1.7). Differences in colours are largely related to the coral symbiont type.



Figure 1.7. A large *Porites* species photographed in eastern Madagascar. Photograph taken by Dr. Jens Zinke.

Calcification Processes

The coral skeleton is extracellular, located at the base of coral tissue, like a finger covered by a glove. Composition of the biomineral aragonite includes two fractions, one mineral and one organic, called the organic matrix. This organic framework is secreted by the coral periodically, on which mineral ions fix onto (Allemand et al., 2004; Cuif and Dauphin, 2005; Ingalls et al., 2003). Epithelial transport of molecules from seawater to the calcification site can be achieved by two mechanisms: a paracellular pathway, between cells (in this case, transport of the molecule is only driven by its chemical gradient, transport is diffusional and passive), or a transcellular pathway through cells (Allemand et al., 2004). In this last case, the molecule needs to enter the cell, cross the cell and then exit. Thus the transport is active, against a gradient with energy supply (Fig. 1.8). Transport of charged species across the hydrophobic

cell membrane requires specific carrier proteins (Allemand et al., 2004; Furla et al., 2000; Ingalls et al., 2003).

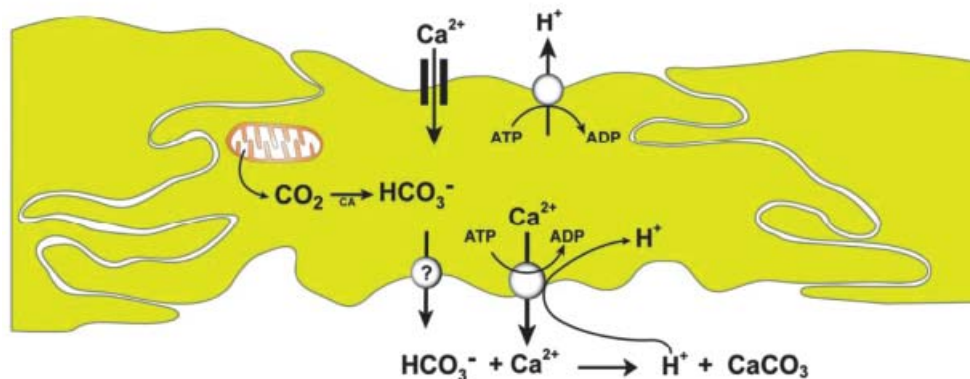


Figure 1.8. Schematic diagram showing the pathway of entry and exit of calcium through the calcicoblastic cells during calcification in hermatypic corals. From Allemand et al., 2004.

The accretion of calcium carbonate by reef building corals depends on a number of environmental factors, such as sun hour, light transparency, nutrient exposure, partial pressures and temperature. These environmental factors affect the accretion of high and low density bands within the skeletal matrix of coral colonies. The high density and low density bands are revealed by X-ray radiographic techniques (Carricart-Ganivet and Barnes, 2007; Chalker and Barnes, 1990). Generally one year of growth consist of two density bands, one high density band and the other low density band, providing a means to age the coral by counting the paired bands. The precipitation of these bands is mostly related to seasonal variability. Coral colony growth rates of *Porites* spp. can vary between 5 and 20 mm per year depending on environmental conditions (see above).

Calcification is a product of both coral extension rates and density (Cantin et al., 2010; De'ath et al., 2009; Lough and Barnes, 2000). By assessing changes in calcification over time there is great potential to link growth variability to environmental conditions (Cantin et al., 2010; De'ath et al., 2009; Scoffin et al., 1992). Physical characteristics of coral bands, such as their skeletal density, linear extension rate, tissue thickness and calcification rate, provide time-series data on the environmental conditions controlling coral growth, such as sea surface temperature (SST) (Cantin et

al., 2010; Lough and Barnes, 2000). As coral reefs around the world are becoming increasingly threatened by bleaching, pollution, ocean acidification and sedimentation, the coral skeleton itself therefore provides an indicator of a changing environment (Helmle et al., 2011). Furthermore, locked within the coral skeleton, geochemical proxies can identify and record these past environmental conditions, providing important information on both the coral reefs environmental response and global climate itself (Felis and Paetzold, 2003; Lough, 2004).

Coral Proxies

Massive corals growing in shallow tropical and sub-tropical oceans have micro-laminations (density banding) that contain physical, isotopic and geochemical evidence of past environments at annual and sub-annual resolution (Gagan et al., 2000; Lough, 2004). The stable oxygen isotope ratios ($\delta^{18}\text{O}$) of coral carbonate provide information on past SST, sea surface salinity and the hydrological balance of oceans (Guilderson and Schrag, 1999; McConnaughey, 1989; McConnaughey, 2003; Zinke et al., 2004). When the $\delta^{18}\text{O}$ composition of seawater is more strongly governed by the interaction of precipitation, evaporation and water advection, the coral carbonate provides a record of changes in the hydrologic balance (Pfeiffer et al., 2004). However, the $\delta^{18}\text{O}$ composition of seawater may or may not correlate with precipitation, depending on SST variability (Charles et al., 1997). Moreover, if the coral records are positively correlated with precipitation, $\delta^{18}\text{O}$ can be used to reconstruct past rainfall (see Gagan et al. 2000 for a review). Alternatively, pairing $\delta^{18}\text{O}$ with geochemical SST proxies (e.g. Sr/Ca) gives a more accurate indication of past hydrological changes (Pfeiffer et al., 2006; Zinke et al., 2004).

In addition to $\delta^{18}\text{O}$, the stable carbon isotope ratios ($\delta^{13}\text{C}$) of the coral skeleton may show strong seasonal annual cycles. However, the $\delta^{13}\text{C}$ of coral carbonate is confounded by many effects, other than the $\delta^{13}\text{C}$ of seawater (Omata et al., 2008; Reynaud et al., 2007; Reynaud et al., 2002; Rodrigues and Grottoli, 2006; Suzuki et al., 2005), meaning surface productivity reconstructions are severely constrained. Coral autotrophy (Omata et al., 2008; Reynaud et al., 2007), heterotrophy (Reynaud et al., 2002), riverine

DIC (Moyer and Grottoli, 2011) and productivity of the water column all influence the skeletal $\delta^{13}\text{C}$ signal, complicating the signal.

The geochemistry of coral bands have also been used to reconstruct past SSTs, with the most robust being the strontium-calcium ratio (Sr/Ca) (Alibert and McCulloch, 1997; Gagan et al., 1998). A negative relationship exists with SST, whereby as temperatures increase, less Sr is incorporated into the aragonite lattice relative to Ca. Since Sr has a long oceanic residence time, heterogeneity in skeletal Sr/Ca is assumed to mainly reflect SST variability, therefore down-core sampling of massive corals yields an *in situ* SST time-series in which the resolution is only limited by the coral growth rate (Sun et al., 2005). However, recent studies suggest that the Sr/Ca signal is also confounded by vital effects, meaning coral growth parameters play an important role in determining skeletal Sr/Ca ratios (Cohen and Gaetani, 2010; Gaetani et al., 2011). A compilation of recent coral Sr/Ca-SST calibrations revealed that the mean Sr/Ca response to a 1°C increases in SST is -0.061 mmol/mol, with a range of -0.04 mmol/mol and -0.08 mmol/mol (Correge, 2006). Other coralline geochemical proxies for temperature have been explored (Fallon et al., 2003), including magnesium-calcium ratios (Mg/Ca), uranium-calcium ratios (U/Ca), boron (B) and fluorine (F) (Hart and Cohen, 1996; Min et al., 1995; Mitsuguchi et al., 1996). Nevertheless, the Sr/Ca ratio remains to this date the most robust.

As well as assessing the stable isotope $\delta^{18}\text{O}$ signal in coral skeletons to reconstruct rainfall, other proxies exist that are related to terrestrial erosion products, indirectly linked to river runoff and precipitation. Luminescent banding found in coral skeletons has been used to improve dating of coral records as well as provide a proxy for precipitation and river runoff from adjacent land masses (e.g. Hendy et al. 2003). Although the exact nature and cause of luminescent banding is still debated, there are positive correlations with river runoff variability (Isdale et al., 1998; Lough, 2011; Lough, 2007). The incorporation of terrestrial humic acids was first proposed as the likely cause of luminescence, meaning increasing runoff would increase humic acid erosion and therefore the incorporation of the fluorescent compound into the skeleton (Isdale, 1984). However, coral skeletal density was later proposed as the likely source, as aragonite itself is fluorescent, and banding was observed in corals far from terrestrial influence (Barnes and Taylor, 2001, 2005). A

detailed assessment of luminescent banding in corals can be found in Chapter 2 (Grove et al., 2010).

The barium-calcium ratio (Ba/Ca) is used to reconstruct sediment runoff (McCulloch et al., 2003; Prouty et al., 2010; Sinclair and McCulloch, 2004). Ba is desorbed from sediment particles in the low-salinity range, mixed into the water column and incorporated into the coral skeleton (Coffey et al., 1997). Elevated skeletal Ba/Ca concentrations therefore indicate increased sediment runoff conditions. Other coralline geochemical proxies applied to reconstruct runoff include yttrium (Y) and manganese (Mn), both of which are associated with the erosion of bedrock (Lewis et al., 2007).

Similar to all other palaeoclimate proxy records, corals are biased by factors unrelated to climate. For example, the upward growth of a coral can lead to the exposure of its surface to shallower water depths, and in turn slightly different temperature, salinity and light intensity levels. This has potential ramifications for the isotopic and geochemical records obtained (Felis et al., 2003; Gagan et al., 2000; Inoue et al., 2007; Omata et al., 2008; Reynaud et al., 2007; Suzuki et al., 2005). One way to identify and adequately take such effects into account is to cross match coral records and/or create composite records (Cahyarini et al., 2008; Pfeiffer et al., 2009). Indeed, some studies have done this, attempting to quantify the reliability of climate proxies contained within coral records through local, regional and global cross matching as well as comparing single and composite records with instrumental records (Cahyarini et al., 2008; Evans et al., 2002; Guilderson and Schrag, 1999; Hendy and Gagan, 2003; Pfeiffer et al., 2009). However, many studies continue to rely on the implicit assumption that variations identified in a single coral record are attributable to one or more climatic variables (Lough, 2004). Some caution therefore needs to be applied in utilising coral records. If the various potential influences on proxies contained within corals are well understood, and the coral records obtained are well calibrated and validated, they provide an extremely powerful tool for understanding climate change and variability from seasonal through to millennial time scales. However, it is important to remember that a coral is an animal, not a piece of equipment.

References

- Alibert, C., McCulloch, M.T., 1997. Strontium/calcium ratios in modern *Porites* corals from the Great Barrier Reef as a proxy for sea surface temperature: calibration of the thermometer and monitoring of ENSO. *Paleoceanography* 12, 345-363.
- Allemand, D., Ferrier-Pages, C., Furla, P., Houlbreque, F., Puverel, S., Reynaud, S., Tambutte, E., Tambutte, S., Zoccola, D., 2004. Biomineralisation in reef-building corals: from molecular mechanisms to environmental control. *Comptes Rendus Palevol* 3, 453-467.
- Arblaster, J.M., Meehl, G.A., Moore, A.M., 2002. Interdecadal modulation of Australian rainfall. *Climate Dynamics* 18, 519-531.
- Ateweberhan, M., McClanahan, T., Graham, N., Sheppard, C., 2011. Episodic heterogeneous decline and recovery of coral cover in the Indian Ocean. *Coral Reefs*, 1-14, doi:10.1007/s00338-011-0775-x.
- Bak, R.P., Nieuwland, G., Meesters, E.H., 2005. Coral reef crisis in deep and shallow reefs: 30 years of constancy and change in reefs of Curacao and Bonaire. *Coral Reefs* 24, 475-479.
- Barnes, D.J., Taylor, R.B., 2001. On the nature and causes of luminescent lines and bands in coral skeletons. *Coral Reefs* 19, 221-230.
- Barnes, D.J., Taylor, R.B., 2005. On the nature and causes of luminescence lines and bands in coral skeletons: II. contribution of skeletal crystals. *Journal of Experimental Marine Biology and Ecology* 322, 135-142.
- Behera, S.K., Yamagata, T., 2001. Subtropical SST dipole events in the southern Indian Ocean. *Geophysical Research Letters* 28, 327-330.
- Cahyarini, S.Y., Pfeiffer, M., Dullo, W.-C., 2008. Improving SST reconstructions from coral Sr/Ca records: multiple coreals rom Tahiti (French Polynesia). *International Journal of Earth Sciences*, doi:10.007/s00531-00008-00302-00532.
- Cane, M.A., 2010. Decadal predictions in demand. *Nature Geoscience* 3, 231-232.
- Cantin, N.E., Cohen, A.L., Karnauskas, K.B., Tarrant, A.M., McCorkle, D.C., 2010. Ocean Warming Slows Coral Growth in the Central Red Sea. *Science* 329, 322-325.
- Carpenter, K.E., Abrar, M., Aeby, G., Aronson, R.B., Banks, S., Bruckner, A., Chiriboga, A., Cortes, J., Delbeek, J.C., DeVantier, L., Edgar, G.J., Edwards, A.J., Fenner, D., Guzman, H.M., Hoeksema, B.W., Hodgson, G., Johan, O., Licuanan, W.Y., Livingstone, S.R., Lovell, E.R., Moore, J.A., Obura, D.O., Ochavillo, D., Polidoro, B.A., Precht, W.F., Quibilan, M.C., Reboton, C., Richards, Z.T., Rogers, A.D., Sanciangco, J., Sheppard, A., Sheppard, C., Smith, J., Stuart, S., Turak, E., Veron, J.E.N., Wallace, C., Weil, E., Wood, E., 2008. One-third of reef-building corals face elevated extinction risk from climate change and local impacts. *Science* 321, 560-563.
- Carricart-Ganivet, J.P., Barnes, D.J., 2007. Densitometry from digitized images of X-radiographs: methodology for measurement of coral skeletal density. *Journal of Experimental Marine Biology and Ecology* 344, 67-72.
- Chalker, B.E., Barnes, D.J., 1990. Gamma-densitometry for the measurement of skeletal density. *Coral Reefs* 9, 11-23.

- Charles, C.D., Hunter, D.E., Fairbanks, R.G., 1997. Interaction between the ENSO and the Asian Monsoon in a coral record of tropical climate. *Science* 277, 925-928.
- Coffey, M., Dehairs, F., Collette, O., Luther, G., Church, T., Jickells, T., 1997. The behaviour of dissolved barium in estuaries. *Estuarine Coastal and Shelf Science* 45, 113-121.
- Cohen, A.L., Gaetani, G.A., 2010. Ion partitioning and the geochemistry of coral skeletons: solving the mystery of the vital effect. *EMU Notes in Mineralogy* 11, 377-397.
- Cole, J.E., Dunbar, R.B., McClanahan, T.R., Muthiga, N.A., 2000. Tropical Pacific forcing of decadal SST variability in the Western Indian Ocean over the past two centuries. *Science* 287, 617-619.
- Correge, T., 2006. Sea surface temperature and salinity reconstructions from coral geochemical tracers. *Palaeogeography, Palaeoclimatology, Palaeoecology* 232, 408-428.
- Cox, P.M., Betts, R.A., Jones, C.D., Spall, S.A., Totterdell, I.J., 2000. Acceleration of global warming due to carbon-cycle feedbacks in a coupled climate model. *Nature* 408, 184-187.
- Crueger, T., Zinke, J., Pfeiffer, M., 2009. Patterns of Pacific decadal variability recorded by Indian Ocean corals. *International Journal of Earth Sciences* 98, doi:10.007/s00531-00008-00324-00531.
- Cuif, J.P., Dauphin, Y., 2005. The environment recording unit in coral skeletons- a synthesis of structural and chemical evidences for a biochemically driven, stepping-growth process in fibres. *Biogeosciences* 2.
- Damassa, T.D., Cole, J.E., Barnett, H.R., Ault, T.R., McClanahan, T.R., 2006. Enhanced multidecadal climate variability in the seventeenth century from coral isotope records in the western Indian Ocean. *Paleoceanography* 21, doi:10.1029/2005PA001217.
- De'ath, G., Lough, J.M., Fabricius, K.E., 2009. Declining coral calcification on the Great Barrier Reef. *Science* 323, 116-119.
- Deser, C., Phillips, A.S., Hurrell, J.W., 2004. Pacific Interdecadal climate variability: linkages between the tropics and the North Pacific during boreal winter since 1900. *J. Clim.* 17, 3109-3124.
- Dewar, R.E., Richard, A.F., 2007. Evolution in the hypervariable environment of Madagascar. *Proceedings of the National Academy of Sciences of the United States of America* 104, 13723-13727.
- Dewar, R.E., Wallis, J.R., 1999. Geographical patterning of interannual rainfall variability in the tropics and near tropics: An L-moments approach. *J. Clim.* 12, 3457-3466.
- Douglas, A.E., 2003. Coral bleaching - how and why? *Marine Pollution Bulletin* 46, 385-392.
- Evans, M.N., Kaplan, A., Cane, M.A., 2002. Pacific sea surface temperature field reconstruction from coral delta O-18 data using reduced space objective analysis. *Paleoceanography* 17.
- Fallon, S.J., McCulloch, M.T., Alibert, C., 2003. Examining water temperature proxies in Porites corals from the Great Barrier reef: a cross-shelf comparison. *Coral Reefs* 22, 389-404.
- Fauchereau, N., Pohl, B., Reason, C.J.C., Rouault, M., Richard, Y., 2008. Recurrent daily OLR patterns in the Southern Africa/Southwest Indian Ocean region, implications for South African rainfall and teleconnections. *Climate Dynamics*, doi:10.007/s00382-

- 00008-00426-00382.
- Felis, T., Paetzold, J., 2003. Climate records from corals, in: Wefer, G., et al. (Eds.), *Marine Science Frontiers for Europe*. Springer, Berlin, Heidelberg, New York, Tokyo, pp. 11-27.
- Felis, T., Paetzold, J., Loya, Y., 2003. Mean oxygen-isotope signatures in *Porites* spp. corals: inter-colony variability and correction for extension-rate effects. *Coral Reefs* 22, 328-336.
- Forster, P. et al. 2007. Changes in Atmospheric Constituents and in Radiative Forcing, Ch. 2 *Climate Change 2007: The Physical Science Basis*. Contribution of Working Group I to the Fourth Assessment Report of the Intergovernmental Panel on Climate Change, eds. Solomon, S. et al. Cambridge Univ. Press, Cambridge, UK.
- Frade, P.R., Bongaerts, P., Winkelhagen, A.J.S., Tonk, L., Bak, R.P.M., 2008a. In situ photobiology of corals over large depth ranges: A multivariate analysis on the roles of environment, host, and algal symbiont. *Limnology and Oceanography* 53, 2711-2723.
- Frade, P.R., De Jongh, F., Vermeulen, F., Van Bleijswijk, J., Bak, R.P.M., 2008b. Variation in symbiont distribution between closely related coral species over large depth ranges. *Molecular Ecology* 17, 691-703.
- Funk, C., Dettinger, M.D., Michaelsen, J.C., Verdin, J.P., Brown, M.E., Barlow, M., Hoell, A., 2008. Warming of the Indian Ocean threatens eastern and southern African food security but could be mitigated by agricultural development. *Proceedings of the National Academy of Sciences of the United States of America* 105, 11081-11086.
- Furla, P., Galgani, I., Durand, I., Allemand, D., 2000. Sources and mechanisms of inorganic carbon transport for coral calcification and photosynthesis. *Journal of Experimental Biology* 203, 3445-3457.
- Gaetani, G.A., Cohen, A.L., Wang, Z., Crusius, J., 2011. Rayleigh-based, multi-element coral thermometry: a biomineralization approach to developing climate proxies. *Geochimica et Cosmochimica Acta* 75, 1920-1932.
- Gagan, M.K., Ayliffe, L.K., Beck, J.W., Cole, J.E., Druffel, E.R.M., Dunbar, R.B., Schrag, D.P., 2000. New views of tropical paleoclimates from corals. *Quaternary Science Reviews* 19, 45-64.
- Gagan, M.K., Ayliffe, L.K., Hopley, D., Cali, J.A., Mortimer, G.E., Chappell, J., McCulloch, M.T., Head, M.J., 1998. Temperature and surface-ocean water balance of the mid-Holocene tropical western Pacific. *Science* 279, 1014-1018.
- Goddard, L., Graham, N.E., 1999. Importance of the Indian Ocean for simulating rainfall anomalies over eastern and southern Africa. *Journal of Geophysical Research* 104, 19099-19116.
- Grove, C.A., Nagtegaal, R., Zinke, J., Scheufen, T., Koster, B., Kasper, S., McCulloch, M.T., Bergh, G.v.d., Brummer, G.J.A., 2010. River runoff reconstructions from novel spectral luminescence scanning of massive coral skeletons. *Coral Reefs* 29, 579-591.
- Guilderson, T.P., Schrag, D.P., 1999. Releability of coral isotope records from the western Pacific warm pool: a comparison using age-optimized records. *Paleoceanography* 14, 457-464.
- Hallock, P. 2001. Coral reefs, carbonate sediments, nutrients and global change. In: Stanley

- Jr., G.D. (Ed.), *The History and Sedimentology of Ancient Reef Systems*. Kluwer Academic Publishing/Plenum, New York, 387-427.
- Hart, S.R., Cohen, A.L., 1996. An ion probe study of annual cycles of Sr/Ca and other trace elements in corals. *Geochimica et Cosmochimica Acta* 60, 3075-3084.
- Helmle, K.P., Dodge, R.E., Swart, P.K., Gledhill, D.K., Eakin, C.M., 2011. Growth rates of Florida corals from 1937 to 1996 and their response to climate change. *Nature Communications* 2:215, doi:10.1038/ncomms1222.
- Hendy, E.J., Gagan, M.K., 2003. Chronological control of coral records using luminescent lines and evidence for non-stationary ENSO teleconnections in northeast Australia. *The Holocene* 13, 187-199.
- Hoegh-Guldberg, O., 1999. Climate change, coral bleaching and the future of the world's coral reefs. *Marine and Freshwater Research* 50, 839-866.
- Hoegh-Guldberg, O., 2004. Coral reefs in a century of rapid environmental change. *Symbiosis* 37, 1-31.
- Hoegh-Guldberg, O., 2011. Coral reef ecosystems and anthropogenic climate change. *Regional Environmental Change* 11, S215-S227.
- Hoerling, M., Hurrell, J., Eischeid, J., Phillips, A., 2006. Detection and attribution of 20th century northern and southern African rainfall change. *Journal of Climate* 19, 3989-4008.
- Houghton, J., 2005. Global Warming. *Reports on Progress in Physics* 68, 1343.
- Hu, Y., Li, D., Liu, J., 2007. Abrupt seasonal variation of the ITCZ and the Hadley circulation. *Geophysical Research Letters* 34, doi:10.1029/2007GL030950.
- Hughes, T.P., Baird, A.H., Bellwood, D.R., Card, M., Connolly, S.R., Folke, C., Grosberg, R., Hoegh-Guldberg, O., Jackson, J.B.C., Kleypas, J., Lough, J.M., Marshall, P., Nystrom, M., Palumbi, S.R., Pandolfi, J.M., Rosen, B., Roughgarden, J., 2003. Climate change, human impacts, and the resilience of coral reefs. *Science* 301, 929-933.
- Iglesias-Prieto, R., Beltran, V.H., LaJeunesse, T.C., Reyes-Bonilla, H., Thome, P.E., 2004. Different algal symbionts explain the vertical distribution of dominant reef corals in the eastern Pacific. *Proceedings of the Royal Society of London Series B-Biological Sciences* 271, 1757-1763.
- Ingalls, A.E., Lee, C., Druffel, E.R.M., 2003. Preservation of organic matter in mound-forming coral skeletons. *Geochimica et Cosmochimica Acta* 67, 2827-2841.
- Inoue, M., Suzuki, A., Nohara, M., Hibino, K., Kawahata, H., 2007. Empirical assessment of coral Sr/Ca and Mg/Ca ratios as climate proxies using colonies grown at different temperatures. *Geophysical Research Letters* 34.
- Isdale, P.J., 1984. Fluorescent bands in massive corals record centuries of coastal rainfall. *Nature* 310, 578-579.
- Isdale, P.J., Stewart, B.J., Tickle, K.S., Lough, J.M., 1998. Palaeohydrological variations in a tropical river catchment: a reconstruction using fluorescent bands in corals of the Great Barrier Reef, Australia. *The Holocene* 8, 1-8.
- Joseph, P.V., Eischeid, J.K., Pyle, R.J., 1994. International variability of the onset of the Indian-summer monsoon and its association with atmospheric features, El Niño, and sea surface temperature anomalies. *J. Clim.* 7, 81-105.
- Jury, M.R., Parker, B., Waliser, D., 1994. Evolution and variability of the ITCZ in the SW

- Indian Ocean: 1988–90. *Theoretical and Applied Climatology* 48, 187-194.
- Jury, M.R., Parker, B.A., Raholijao, N., Nassor, A., 1995. Variability of summer rainfall over Madagascar: Climate determinants at interannual scales. *International Journal of Climatology* 15, 1323-1332.
- Klein, S.A., Soden, B.J., Lau, N.C., 1999. Remote sea surface temperature variations during ENSO: Evidence for a tropical atmospheric bridge. *Journal of Climate* 12, 917-932.
- Kawamura, R., Matsuura, T., Iizuka, S., 2001. Role of equatorially asymmetric sea surface temperature anomalies in the Indian Ocean in the Asian summer monsoon and El Niño-Southern Oscillation coupling. *Journal of Geophysical Research-Atmospheres* 106, 4681-4693.
- Kleypas, J.A., Buddemeier, R.W., Archer, D., Gattuso, J.P., Langdon, C., Opdyke, B.N., 1999. Geochemical consequences of increased atmospheric carbon dioxide on coral reefs. *Science* 284, 118-120.
- Krishnan, P., Sugi, M., 2003. Pacific decadal Oscillation and variability of the Indian summer monsoon rainfall. *Climate Dynamics* 21, 233-242.
- Kuleshov, Y., Qi, L., Fawcett, R., Jones, D., 2008. On tropical cyclone activity in the southern hemisphere: trends and the ENSO connection. *Geophysical Research Letters* 35, doi:10.1029/2008GL032983.
- Lashof, D.A., Ahuja, D.R., 1990. Relative contributions of greenhouse gas emissions to global warming. *Nature* 344, 529-531.
- Lesser, M.P., 2007. Coral reef bleaching and global climate change: Can corals survive the next century? *Proceedings of the National Academy of Sciences of the United States of America* 104, 5259-5260.
- Lewis, S.L., Shields, G.A., Kamber, B.S., Lough, J.M., 2007. A multi-trace element coral record of land-use changes in the Burdekin River catchment, NE Australia. *Palaeogeography, Palaeoclimatology, Palaeoecology* 246, 471-487.
- Lough, J., 2011. Great Barrier Reef coral luminescence reveals rainfall variability over northeastern Australia since the 17th century. *Paleoceanography* 26, doi:10.1029/2010PA002050.
- Lough, J.M., 2004. A strategy to improve the contribution of coral data to high-resolution paleoclimatology. *Palaeogeography, Palaeoclimatology, Palaeoecology* 204, 115-143.
- Lough, J.M., 2007. Tropical river flow and rainfall reconstructions from coral luminescence: Great Barrier Reef. *Paleoceanography* 22, doi:10.1029/2006PA001377.
- Lough, J.M., Barnes, D.J., 2000. Environmental controls on growth of the massive coral *Porites*. *Journal of Experimental Marine Biology and Ecology* 245, 225-243.
- Mantua, N., Hare, S., Zhang, Y., Wallace, J., Francis, R., 1997. A Pacific interdecadal oscillation with impacts on salmon production. *Bulletin Am. Meteorol. Soc.* 78, 1069-1079.
- McConnaughey, T., 1989. ^{13}C and ^{18}O isotopic disequilibrium in biological carbonates: I. Patterns. *Geochimica et Cosmochimica Acta* 53, 151-162.
- McConnaughey, T.A., 2003. Sub-equilibrium oxygen-18 and carbon-13 levels in biological carbonates: carbonate and kinetic models. *Coral Reefs* 22, 316-327.
- McCulloch, M., Fallon, S., Wyndham, T., Hendy, E., Lough, J., Barnes, D., 2003. Coral

- record of increased sediment flux to the inner Great Barrier Reef since European settlement. *Nature* 421, 727-730.
- McPhaden, M.J., Zebiak, S.E., Glantz, M.G., 2006. ENSO as an integrating concept in Earth Science. *Science* 314, 1740-1745.
- Meehl, G.A., Alabaster, J.M., 2002. GCM sensitivity experiments for the Indian Monsoon and tropospheric biennial oscillation transition conditions. *Journal of Climate* 15, 923-944.
- Meehl et al., 2004, Combinations of natural and anthropogenic forcings in twentieth-century climate: *Journal of Climate* 17, 3721-3727.
- Meehl, G.A., Washington, W.M., Collins, W.D., Arblaster, J.M., Hu, A., Buja, L.E., Strand, W.G., Teng, H., 2005. How much more global warming and sea level rise? *Science* 307(5716), 1769-1772.
- Meehl, G.A., Hu, A., 2006. Megadroughts in the Indian Monsoon Region and Southwest North America and a mechanism for associated multidecadal Pacific sea surface temperature anomalies. *Journal of Climate* 19, 1605-1623.
- Meyers, G., McIntosh, P., Pigot, L., Pook, M., 2007. The years of El Niño, La Niña, and interactions with the tropical Indian ocean. *Journal of Climate* 20, 2872-2880.
- Min, G.R., Edwards, R.L., Taylor, F.W., Recy, J., Gallup, C.D., Beck, J.W., 1995. Annual cycles of U/Ca in coral skeletons and U/Ca thermometry. *Geochimica et Cosmochimica Acta* 59, 2025-2042.
- Mitsuguchi, T., Matsumoto, E., Abe, O., Uchida, T., Isdale, P.J., 1996. Mg/Ca thermometry in coral skeletons. *Science* 274, 961-963.
- Moyer, R.P., Grottoli, A.G., 2011. Coral skeletal carbon isotopes $\delta^{13}\text{C}$ and $\Delta^{14}\text{C}$ record the delivery of terrestrial carbon to the coastal waters of Puerto Rico. *Coral Reefs* 30(3), 791-802.
- Muller-Parker, G., D'Elia, C.F., 1997. Interactions between corals and their symbiotic algae. In: Birkeland, C. (Ed) *Life and death of coral reefs*. Chapman & Hall, New York, 96-133.
- Muscatine, L., Falkowski, P.G., Porter, J.W., Dubinsky, Z., 1984. Fate of photosynthetically fixed carbon in light-adapted and shade-adapted colonies of the symbiotic coral *Stylophora pistillata*. *Proceedings of the Royal Society of London Series B-Biological Sciences* 222, 181-202.
- Muscatine, L., Goiran, C., Land, L., Jaubert, J., Cuif, J.P., Allemand, D., 2005. Stable isotopes ($\delta^{13}\text{C}$ and $\delta^{15}\text{N}$) of organic matrix from coral skeleton. *Proceedings of the National Academy of Sciences of the United States of America* 102, 1525-1530.
- Muscatine, L., Porter, J.W., 1977. Reef Corals – Mutualistic symbioses adapted to nutrient-poor environments. *Bioscience* 27, 454-460.
- Nigam, S., Shen, H.-S., 1993. Structure of oceanic and atmospheric low-frequency variability over the tropical Pacific and Indian Oceans. Part I: COADS observations. *J. Clim.* 6, 657-676.
- Omata, T., Suzuki, A., Sato, T., Minoshima, K., Nomaru, E., Murakami, A., Murayama, S., Kawahata, H., Maruyama, T., 2008. Effect of photosynthetic light dosage on carbon isotope composition in the coral skeleton: Long-term culture of *Porites* spp. *Journal of Geophysical Research-Biogeosciences* 113.

- Pfeiffer, M., Dullo, W.-C., Zinke, J., Garbe-Schoenberg, D., 2009. Three monthly coral Sr/Ca records from the Chagos Archipelago covering the period of 1950-1995 A.D.: reproducibility and implications for quantitative reconstructions of sea surface temperature variations. *International Journal of Earth Sciences* 98, doi:10.007/s00531-00008-00326-z.
- Pfeiffer, M., Timm, O., Dullo, W.-C., 2004. Oceanic forcing of interannual and multidecadal climate variability in the southwestern Indian Ocean: Evidence from a 160 year coral isotopic record (La Reunion, 50E, 21S). *Paleoceanography* 19, doi:10.1029/2003PA000964.
- Pfeiffer, M., Timm, O., Dullo, W.-C., Garbe-Schoenberg, D., 2006. Paired coral Sr/Ca and $\delta^{18}\text{O}$ records from the Chagos Archipelago: Late twentieth century warming affects rainfall variability in the tropical Indian Ocean. *Geology* 34, 1069-1072.
- Prouty, N.G., Field, M.E., Stock, J.D., Jupiter, S.D., McCulloch, M., 2010. Coral Ba/Ca records of sediment input to the fringing reef of the southshore of Moloka'i, Hawai'i over the last several decades *Marine Pollution Bulletin*.
- Reaka-Kudla, M.L. 1996, The global biodiversity of coral reefs: a comparison with rain forests. In: Reaka-Kudla, M.L., Wilson, D.E., Wilson, E.O. (Eds) *Biodiversity II: Understanding and Protecting our Biological Resources*. National Academy Press, Washington, DC, 83-108.
- Reason, C.J.C., 2002. Sensitivity of the southern African circulation to dipole sea-surface temperature patterns in the south Indian Ocean. *International Journal of Climatology* 22, 377-393.
- Reason, C.J.C., Rouault, M., 2002. ENSO-like decadal variability and South African rainfall. *Geophysical Research Letters* 29, 10.1029.
- Reynaud, S., Ferrier-Pages, C., Meibom, A., Mostefaoui, S., Mortlock, R., Fairbanks, R., Allemand, D., 2007. Light and temperature effects on Sr/Ca and Mg/Ca ratios in the scleractinian corals *Acropora* sp. *Geochimica et Cosmochimica Acta* 71, 354-362.
- Reynaud, S., Ferrier-Pages, C., Sambrotto, R., Juillet-Leclerc, A., Jaubert, J., Gattuso, J.P., 2002. Effect of feeding on the carbon and oxygen isotopic composition in the tissues and skeleton of the zooxanthellate coral *Stylophora pistillata*. *Marine Ecology-Progress Series* 238, 81-89.
- Richard, Y., Trzaska, S., Roucou, P., Rouault, M., 2000. Modification of the southern African rainfall variability/ENSO relationship since the late 1960's. *Climate Dynamics* 16, 883-895.
- Rodrigues, L.J., Grottoli, A.G., 2006. Calcification rate and the stable carbon, oxygen, and nitrogen isotopes in the skeleton, host tissue, and zooxanthellae of bleached and recovering Hawaiian corals. *Geochimica et Cosmochimica Acta* 70, 2781-2789.
- Saji, H.H., Goswami, B.N., Vinayachandran, P.N., Yamagata, T., 1999. A dipole mode in the tropical Indian Ocean. *Nature* 401, 360-363.
- Sampayo, E.M., Ridgway, T., Bongaerts, P., Hoegh-Guldberg, O., 2008. Bleaching susceptibility and mortality of corals are determined by fine-scale differences in symbiont type. *Proceedings of the National Academy of Sciences of the United States of America* 105, 10444-10449.
- Santoso, A., Cai, W., England, M.H., Phipps, S.J., 2011. The Role of the Indonesian

- Throughflow on ENSO Dynamics in a Coupled Climate Model. *J. Clim.* 24, 585-601.
- Schneider, N., Cornuelle, B.D., 2005. The forcing of the Pacific decadal oscillation. *J. Clim.* 18, 4355-4373.
- Schott, F.A., Xie, S.-P., McCreary, J.P. Jr., 2009. Indian Ocean circulation and climate variability. *Rev. Geophys.* 47, RG1002.
- Scoffin, T.P., Tudhope, A.W., Brown, B.E., Chansang, H., Cheeney, R.F., 1992. Patterns and possible environmental controls of skeletogenesis of *Porites lutea*, South Thailand. *Coral Reefs* 11, 1-11.
- Sinclair, D.J., McCulloch, M.T., 2004. Corals record low mobile barium concentrations in the Burdekin River during 1974 flood: evidence for limited Ba supply to rivers? *Palaeogeography, Palaeoclimatology, Palaeoecology* 214, 155-174.
- Spalding, M.D., Ravilious, C., Green, E.P., 2001. World atlas of coral reefs. Prepared at the UNEP world conservation monitoring centre. University of California Press, Berkeley, CA, USA.
- Stanley, G.D., Schootbrugge, B., 2009. The Evolution of the Coral–Algal Symbiosis, in: Oppen, M.J.H., Lough, J.M. (Eds.), *Coral Bleaching*. Springer Berlin Heidelberg, pp. 7-19.
- Sun, Y., Sun, M., Lee, T., Nie, B., 2005. Influence of seawater Sr content on coral Sr/Ca and Sr thermometry. *Coral Reefs* 24, 23-29.
- Suzuki, A., Hibino, K., Iwase, A., Kawahata, H., 2005. Intercolony variability of skeletal oxygen and carbon isotope signatures of cultured *Porites* corals: Temperature-controlled experiments. *Geochimica et Cosmochimica Acta* 69, 4453-4462.
- Tanaka, Y., Miyajima, T., Koike, I., Hayashibara, T., Ogawa, H., 2006. Translocation and conservation of organic nitrogen within the coral-zooxanthella symbiotic system of *Acropora pulchra*, as demonstrated by dual isotope-labeling techniques. *Journal of Experimental Marine Biology and Ecology* 336, 110-119.
- Thornhill, D.J., Kemp, D.W., Bruns, B.U., Fitt, W.K., Schmidt, G.W., 2008. Correspondence between cold tolerance and temperate biogeography in a western atlantic Symbiodinium (*Dinophyta*) lineage. *Journal of Phycology* 44, 1126-1135.
- Wang, P., Clemens, S., Beaufort, L., Braconnot, P., Ganssen, G., Jian, Z., Kershaw, P., Sarnthein, M., 2005. Evolution and variability of the Asian monsoon system: state of the art and outstanding issues. *Quaternary Science Reviews* 24, 595-629.
- Webster, P.J., Magana, V.O., et al., 1998. Monsoons: processes, predictability, and the prospects for prediction. *Journal of Geophysical Research* 103(C7), 14,451-14,510.
- Wilkinson, C., 2008. Status of coral reefs of the world: 2008. Global coral reef monitoring network. Australian Institute of Marine Science, Townsville.
- Williams, B., Grottoli, A.G., 2010. Recent shoaling of the nutricline and thermocline in the western tropical Pacific. *Geophysical Research Letters* 37.
- Xie, S.P., Annamalai, H., Schott, F.A., McCreary, J.P., 2002. Structure and mechanisms of South Indian Ocean climate variability. *J. Clim.* 15, 864-878.
- Yasunari, T., 1998. Monsoons: processes, predictability, and the prospects for prediction. *Journal of Geophysical Research* 103, 14,451-14,510.
- Yellowlees, D., Rees, T.A.V., Leggat, W., 2008. Metabolic interactions between algal

- symbionts and invertebrate hosts. *Plant Cell and Environment* 31, 679-694.
- Zinke, J., Dullo, W.-C., Heiss, G.A., Eisenhauer, A., 2004. ENSO and Indian Ocean subtropical dipole variability is recorded in a coral record off southwest Madagascar for the period 1659-1995. *Earth and Planetary Science Letters* 228, 177-194.
- Zinke, J., Pfeiffer, M., Timm, O., Dullo, W.-C., Brummer, G.J.A., 2009. Western Indian Ocean marine and terrestrial records of climate variability: a review and new concepts on land-ocean interactions since AD 1660. *International Journal of Earth Sciences* 98, doi:10.1007/s00531-00008-00365-00535.
- Zinke, J., Pfeiffer, M., Timm, O., Dullo, W.C., Kroon, D., Thomassin, B.A., 2008. Mayotte coral reveals hydrological changes in the western Indian Ocean between 1881 and 1994. *Geophysical Research Letters* 35, doi:10.1029/2008GL035634.

Chapter 2

River runoff reconstructions from novel spectral luminescence scanning of massive coral skeletons

Craig A. Grove, Roel Nagtegaal, Jens Zinke, Tim Scheufen,
Bob Koster, Sebastian Kasper, Malcolm T. McCulloch,
Gert van den Bergh and Geert-Jan A. Brummer

Based on the publication in Coral Reefs 29(3):579-591 (2010)

Abstract

Inshore massive corals often display bright luminescent lines that have been linked to river flood plumes into coastal catchments and hence have the potential to provide a long-term record of hinterland precipitation. Coral luminescence is thought to result from the incorporation of soil-derived humic acids transported to the reef during major flood events. Corals far from terrestrial sources generally only exhibit dull relatively broad luminescence bands, which are attributed to seasonal changes in coral density. We therefore tested the hypothesis that spectral ratios rather than conventional luminescence intensity provides a quantitative proxy record of river runoff without the confounding effects of seasonal density changes. For this purpose we have developed a new, rapid spectral luminescence scanning (SLS) technique that splits emission intensities into Red, Green and Blue domains (RGB) for entire cores with an unprecedented linear resolution of 71.4 μm . Since humic acids have longer emission wavelength than the coral aragonite, normalisation of spectral emissions should yield a sensitive optical humic acid/aragonite ratio for humic acid runoff, i.e. G/B ratio. Indeed, G/B-ratios rather than intensities are well correlated with Ba/Ca, a geochemical coral proxy for sediment runoff, and with rainfall data, as exemplified for coral records from Madagascar. Coral cores also display recent declining trends in luminescence intensity, which are also reported in corals elsewhere. Such trends appear to be associated with a modern decline in skeletal densities. By contrast, G/B spectral ratios not only mark the impact of individual cyclones but also imply that humic acid runoff increased in Madagascar over the past few decades while coral skeletal densities decreased. Consequently, the SLS technique deconvolves the long-term interplay between humic acid incorporation and coral density that have confounded earlier attempts to use luminescence intensities as a proxy for river runoff.

Introduction

Understanding the impact of global warming on present-day rainfall patterns and river discharge requires constraints on long-term ‘natural’ climate variability and hence the need for climate records extending back for at least several hundred of years. Unfortunately such records are rare and in

some locations such as Madagascar, even present day weather data remains scarce (Dewar and Richard, 2007; Dewar and Wallis, 1999). This lack of continuous long-term instrumental data highlights the importance of climate proxy records such as those preserved in the massive annually banded coral *Porites* sp. (Felis and Pätzold, 2003; Grottoli and Eakin, 2007 and ref. therein; Lough, 2004; McCulloch et al., 1994). Various skeletal properties have been employed to trace past climate change using coral records, yet their ability to be used as environmental proxies is compromised by our limited mechanistic understanding of their origin (Corrège, 2006; Jones et al., 2009 and ref. therein; Lough, 2004).

When placed under ultra-violet (UV) light, some coral cores show bright luminescence patterns that are related to freshwater flood events and thus past river flow and rainfall dynamics in tropical environments (Boto and Isdale, 1985; Isdale, 1984; Lough et al., 2002). Pioneered by Isdale (1984), a number of techniques have been developed to measure the varying intensity of luminescence in coral skeletons (Barnes et al., 2003 and references therein; Supplementary Information). Variability in emission intensities were first thought to be caused by the incorporation of luminescent humic acids, soil derived organic compounds introduced by seasonal river runoff (Isdale, 1984; Isdale et al., 1998; Matthews et al., 1996; Susic et al., 1991; Susic and Boto, 1989; Wild et al., 2000). Changing coral density and architecture have been proposed as another cause since massive corals form a skeleton of luminescent aragonite (MacRae and Wilson, 2008), and banded luminescence is also found in corals in oceanic environments devoid of terrestrial inputs (Barnes and Taylor, 2001a; Barnes and Taylor, 2001b). Barnes and Taylor (2005) introduced a classification of skeletal luminescence patterns discriminating between faint bands and bright lines. Faint luminescent banding is attributed to the annual skeletal density banding, while the brighter narrow luminescent lines (linked to runoff) are considered to be associated with another component, e.g. humic acids, relating to skeletal chemistry (Barnes and Taylor, 2005). Therefore, the hypotheses formulated for this research paper are (1) both humic acids and aragonite density determine luminescence intensities in corals; and (2) that their deconvolution is required in order to reconstruct river runoff accurately.

This study introduces a novel scanning technique that quantifies luminescence intensities by splitting the total emission spectrum into different spectral domains. Measured luminescence intensities and calculated spectral luminescence ratios are analysed from coral cores drilled in Madagascar to investigate the potential for normalising the episodic bright (humic acid) emission bands to the overall aragonite skeleton emission, thus generating normalised luminescence data using spectral luminescence ratios. Recently, Cobb et al. (2008) addressed various sources of uncertainties in coral luminescence based paleo-records. Firstly, the cause of luminescence in corals is not fully understood (Barnes and Taylor, 2001a; Barnes and Taylor, 2005; Jones et al., 2009), and secondly there is some evidence that luminescence intensities show an unexplained long-term declining trend that could compromise runoff reconstructions (Isdale et al., 1998; Lough, 2010). The aim of this research is to improve the robustness of luminescence as a proxy for humic acid runoff, while resolving the uncertainties addressed by Cobb et al. (2008).

While banded luminescence seems to reflect the organic flux carried by seasonal variability in river runoff (Isdale, 1984), coral Ba/Ca also provides a highly sensitive tracer of suspended sediment fluxes (Alibert et al., 2003, McCulloch et al., 2003) and in some regions, upwelling (Fallon et al., 1999). Suspended sediments (clays) carry adsorbed barium and other river-born trace elements that are desorbed in the low-salinity estuarine mixing zone and subsequently behave as conservative dissolved constituents of the ambient seawater in which the corals thrive (Sinclair and McCulloch, 2004). Consequently, Ba/Ca and luminescence are used to reconstruct sediment and humic acid runoff respectively in tropical catchments, where both have been shown to co-vary with the changing magnitude of precipitation and river flow (Fleitman et al., 2007). As Madagascar weather data are scarce (Dewar and Richard, 2007; Dewar and Wallis, 1999), novel spectral luminescence ratios and conventional luminescence intensities are paired with Ba/Ca to validate the method, supported by rainfall data from a nearby weather station. Finally, differences in luminescence between corals from reef environments near and distant from terrestrial inputs will be evaluated.

Materials and Methods

Spectral luminescence scanning (SLS) was developed to quantify skeletal emissions in different spectral domains from coral cores (Grove et al., 2009). Below we describe how spectral emission intensities are quantified for entire core slabs and the modifications undertaken of the Avaatech core-scanner, conventionally used for analysing the changing element composition of entire sediment cores by X-ray fluorescence (Jansen et al., 1998; Richter et al., 2006). The Avaatech XRF core-scanner is equipped with a line-scan camera that yields high resolution images using visible light to establish digital core archives and to assist in interpreting element stratigraphy data. It is the line-scan camera in combination with the core-scanning technology that makes this technique unique. A summary of the techniques advantages can be found in the electronic supplementary information together with a detailed description of the method (Supplementary Information).

Method summary

The standard light source of the Avaatech core-scanner was replaced by two long-wave UV-A tubes in the 350 – 450 nm range (Fig. 2.1). The light source and camera progress down the sample slab as a single unit when the scan is initiated, constantly scanning multiple lines, resulting in a continuous core image. A 450 nm light cut-off filter is optionally placed beneath the camera lens to eliminate reflected light from the UV source and record luminescence intensities in the blue domain (Fig. 2.1). Luminescence emission is recorded by a Line Scan Camera. Incoming light passing through the lens is split into three wavelength ranges (Red, Green and Blue) by a Dichroic RGB beam splitter prism, and recorded by separate sensors (Fig. 2.1). As the camera moves over the slab it continuously collects a single cross-core line image of 2048×1 pixels for each spectral range. The current setup gives a spatial resolution of 140 pixels per cm, each pixel therefore yielding a linear resolution of 71.4 μm . Three data points are produced for each individual pixel in the R, G and B range.

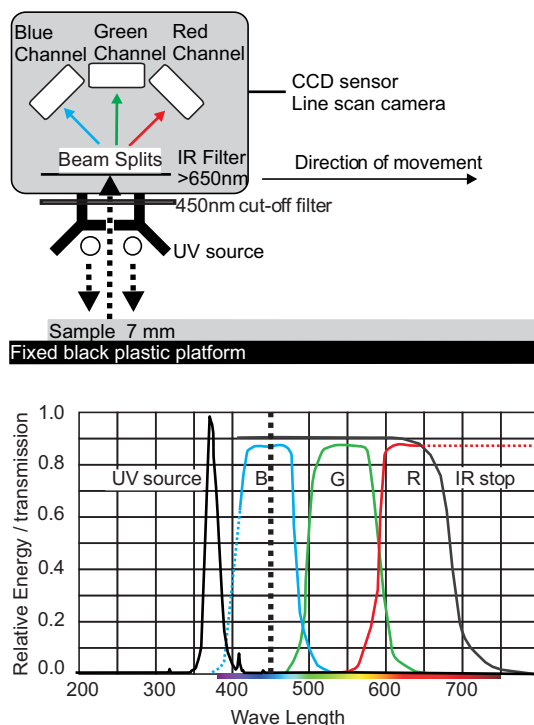


Figure 2.1. Schematic diagram of the modified Avaatech core-scanner used for spectral luminescence imaging (upper panel), and the spectral distribution and sensitivity of the light source and camera sensors (lower panel). The UV light source efficiently emits in the range of 315 nm to 450 nm. The 450 nm cut-off filter (black dotted line) removes all UV source emissions (reflected light) before splitting into red, green and blue fractions by a dichroic RGB beam splitter. A 650 nm infrared cut-off filter prevents light of greater wavelengths from entering the three separate CCD sensors.

The specifically designed software (Avaatech) enables linear transects to be manually drawn from the luminescence image to retrieve intensity profiles for any specified area and direction (Fig. 2.2). Once the areas of interest are identified, transects are created up to 150 cm in length and 15 cm in width, however usually limited to shorter transects depending on sample size, changes in the direction of growth axes or breaks and/or visual discrepancies in the sample. Connecting transects is achieved by transferring quantified intensity data into a separate program used for data management. Multiple transects can be created for any length, in any direction, at any required width from just a single scan taking up to one hour. Uranyl glass with homogenous

luminescent properties is mounted on the platform and used as a standard reference for all intensity measurements. Line transects drawn through the entire length of the standard material using the image and software are used to correct for any drift in either the light source intensity or camera recording sensitivity. Subsequently the resulting sample intensities are corrected for any drift to allow direct inter-comparisons between cores to be made over time. Importantly, SLS provides fast, non-destructive quantified data that allows for matching and comparing coral carbonate skeletons with little sampling effort.

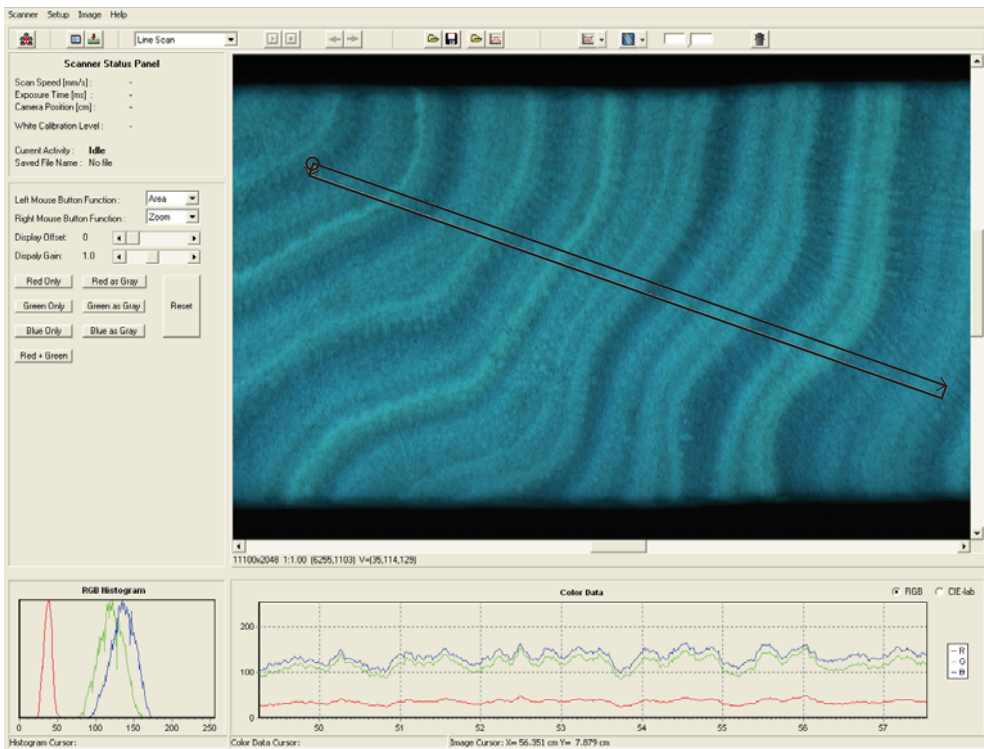


Figure 2.2. Screen shot of the software used to analyse UV luminescence imaging. The image shows a section of the coral core ANDRA, with a black transect drawn onto the image parallel to the growth axis. Multiple transects can be manually selected on the digital image in any direction for any width after a single scan.

Core collection and sample preparation

A total of five coral cores drilled from *Porites* sp. colonies; four from Antongil Bay (E 49°, S 15°) and one off St Marie island (E 49°, S 17°), Northeast Madagascar (Fig. 2.3), were used to test this new technique, with a more detailed coral climate analysis being given elsewhere. The four cores from Antongil Bay are all influenced by seasonal river plumes occurring in the wet season between December and April. The other core from St. Marie is not influenced by any river. All cores were collected in March and April 2007 between a depth range of 4 - 6m, and are dated between 27 and 129 years old (Table 2.1). A detailed description of the research area and climate setting is provided in the Supplementary Information. Coral chronologies were developed by counting density bands using digitalised X-Rays, complemented by counting luminescence intensity bands (Hendy et al., 2003).

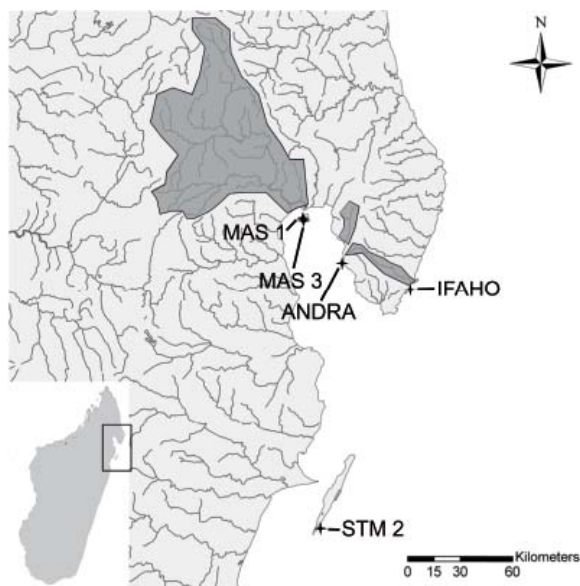


Figure 2.3. Map of the region where cores MAS1, MAS3, ANDRA, IFAHO and STM2 were drilled. Coral locations (stars) and their corresponding rivers and watersheds (grey shaded areas) are marked accordingly in and around Antongil Bay. The largest river is the Antainambalana, influencing MAS1 and MAS3; the river influencing ANDRA is the Ambanizana, flowing south westward into the bay; and the river influencing IFAHO is the Anaovandran flowing eastward outside the bay. The coral core STM2 is not influenced by any river and is located to the south east of the island St Marie.

Coral skeletal luminescence

Coral Name	Location	Length (cm)	Age (years)	Distance to closest river source (km)	Average Growth Rate (cm yr ⁻¹)
MAS1 (Antongil Bay)	S 15°30,566 E 49°45,437	120.78	102	7	1.18
MAS3 (Antongil Bay)	S 15°30,578 E 49°45,456	142.97	129	7	1.11
ANDRA (Antongil Bay)	S 15°41,17 E 49°57,419	119.82	94	7	1.27
IFAHO (Antongil Bay)	S 15°51,968 E 50°18,73	37.95	27	4.5	1.41
STM2 (St Marie)	S 17°05,685 E 49°51,483	168	115	40	1.45

Table 2.1. A summary of the five coral cores drilled in Madagascar, applied in a manner that demonstrates the potential of the SLS technique and the application of spectral luminescence ratios. In some cases only sections of cores were used for this study.

All coral cores were cut into 7mm thick slabs and ultrasoniced three times in ultrapure 17 Ω water for 10 minute periods, removing all surficial particles. For luminescence measurements coral slabs must have a smooth surface and be of uniform thickness. The slabs were also cleaned with compressed filtered air between ultrasonicing to remove all remaining loose particles, and dried for 24 hours in a laminar flow hood. It is essential to clean cores identically in order to prevent changes in emissions through the addition or removal of luminescent substances between cores (Carricart-Ganivet et al., 2007). Particularly for the most recent years, intensities decrease due to the quenching signal by residual organic matter associated with the coral tissue layer and/or endolithic algae. Oxidative cleaning for 24 hours with sodium hypochlorite (NaOCl, 10 - 13% reactive chloride; Sigma-Aldrich Company, St. Louis, MO) removes these contaminating organics, yet may also affect the chemistry of the skeletal lattice compromising climate reconstruction (Boiseau and Juillet-Leclerc, 1997; Grottoli et al., 2005; Watanabe et al., 2001). Therefore, cores were first sampled for geochemical analysis and then scanned for spectral luminescence before and after treatment with NaOCl.

Luminescence intensities generated by the SLS technique were also compared to the emission produced using an argon-ion laser-beam as an

excitation source and an Ocean-Optics linear diode array detector via an optical fibre at the VU University, Amsterdam. Laser-Ablation ICP-MS profiles were undertaken to determine Ba/Ca ratios at a sub-weekly resolution on the coral core MAS1 at ANU Canberra following the method of Sinclair et al. (1998) and Fallon et al. (2002). Geochemical analysis yielded Ba/Ca ratios, a well established proxy for sediment runoff, used here to cross-validate the luminescence results (McCulloch et al., 2003). Density profiles were measured using the CoralXDS program, where X-Ray images were digitalised, uploaded and calibrated using an aragonite wedge (Carricart-Ganivet et al., 2007; Helmle et al., 2002).

Rainfall and river discharge time series are not available for Antongil Bay and are generally scarce across Madagascar (Kremen, 2003). However, for calibration of coral luminescence data we use Tamatave (WMO code 67095), the nearest weather station with rainfall data from (18.15°S, 49.37°E), 293 km south of Antongil Bay, which also provides the most continuous time series for northeast Madagascar covering the period 1889 to 1985 (data available at <http://www.ncdc.noaa.gov/oa/climate/ghcn-monthly/>).

Results

Technique and resolution

Line-scanning achieves a linear resolution of 71.4 μm , generating detailed luminescence intensity profiles of coral skeletons. This equates to a temporal resolution of 2.6 days for corals growing at a rate of 1 cm yr^{-1} . The resolutions achieved by SLS are among the highest found in coral proxy analysis and comparable to Laser-Ablation ICP-MS, used for element composition in paleo-reconstructions (Fallon et al., 2002; Sinclair et al., 1998). The performance of the new SLS technique was also compared to that obtained from an argon laser excitation, coupled to a linear diode array detector via an optical fibre (Milne and Swart, 1994). Intensity profiles appear very similar for both methods, considering the lower linear resolution of 0.1 mm achieved with the laser method (Fig. S2.1).

Coral luminescence intensities

Digital images generated using visual and UV light are displayed for the top section of the MAS1 coral core, a 15.8 cm slab covering the years 1991 - 2006 (Fig. 2.4). Luminescence scanning displayed seasonal variability in relative intensities, with a gradual decline observed since 2003 (Fig. 2.4). Treated with NaOCl, the intensity of luminescence for the most recent bands increases (Fig. S2.2). MAS1 shows periodic yellow bands within the skeleton under visual light that correlate temporally with increased luminescence intensities (Fig. 2.4). As illustrated for the years 1996 and 1997, high magnification of the digital image improves the ability to identify and avoid physical discrepancies within cores and enables the precise selection of sampling tracks (Fig. 2.4).

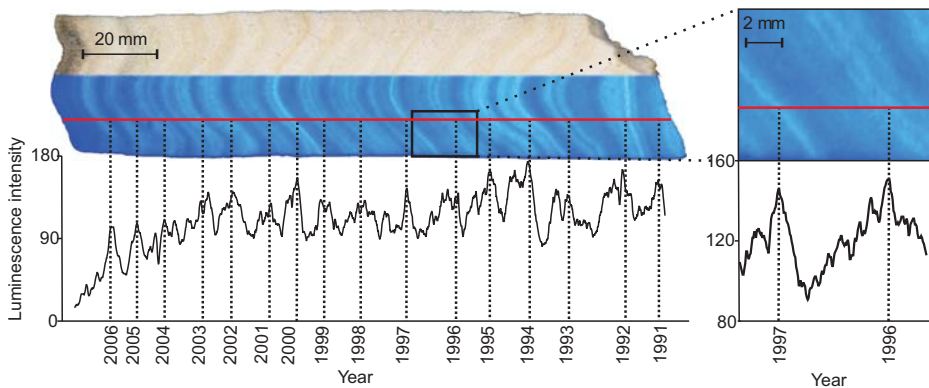


Figure 2.4. An example of the digital images generated by the line-scan camera using the top section of the coral core MAS1, scanned under visible light (top half) and UV light (bottom half). The red transect line marks the area of which green luminescence intensity (G) is measured, with annual cycles assigned to the raw data by designating peak values from 1991 to 2006. The black box marks an enlarged section of relative photoluminescent intensities (G) for the years 1996 and 1997 (right). A separate transect of a smaller size was created on the zoomed image (red), identifying fine-scaled fluctuations in intensities.

Luminescence assists with the construction of age models by analysing the green luminescence intensity profiles, exemplified for a nine year section of each core drilled within Antongil Bay (Fig. 2.4). In addition to counting annual bands down-core, there are singular sections within the profiles that each display a distinct pattern shared by all corals (Fig. 2.5). These provide

reference points independent of the annual banding leading to robust age models. As expected, the most similar intensity profiles were found for the two nearby cores influenced by the same watershed (MAS1 and MAS3; Fig. 2.3 and 2.5). For the complete monthly intensity time series, correlations of MAS1 with MAS3 ($R = 0.65$, $p < 0.001$, $n = 1234$) are higher than with ANDRA ($R = 0.63$, $p < 0.001$, $n = 1112$) and IFAHO ($R = 0.52$, $p < 0.001$, $n = 305$).

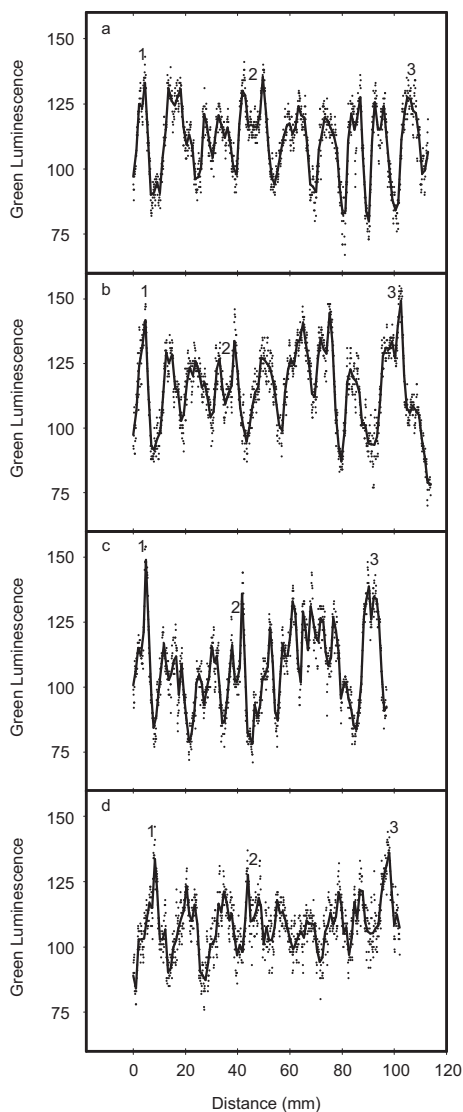


Figure 2.5. 14-point moving average (solid) applied to the raw (dots) luminescence intensity profile data in the green spectral domain (G) for nine year sections of the Antongil Bay cores MAS1 (a), MAS3 (b), ANDRA (c), and IFAHO (d). Points 1 and 3 mark exceptionally high luminescence intensities, and point 2 a clear double spike within a yearly cycle. MAS1 (a) and MAS3 (b) are located closest to each other (<1 km) and show the most observed similarities. ANDRA (c) is 30 km from both MAS1 and MAS3, and IFAHO (d) is a further 40 km away.

Application of spectral luminescence ratios

In all cores from Antongil Bay, intensity values in the green domain (G) were higher than in the red (R), whereas the green and blue (B) intensities were similar with the 450 nm filter fixed below the camera (Fig. S2.3). To validate luminescence as a proxy for river runoff we first correlated luminescence intensity (hereafter G) with Ba/Ca ratios, an established proxy for sediment runoff (McCulloch et al., 2003). Although temporally aligned, there is little agreement between G and Ba/Ca in terms of seasonal amplitudes and the long-term trend (Fig. 2.6). Spectral ratios are applied to optically remove the assumed density and architectural effect and to retrieve the luminescence signal emitted by the humic acids incorporated from soil runoff (Fig. 2.6b). As the spectral emissions of humic acids and aragonite cluster at similar wavelengths it is difficult to separate the two using traditional fluorescence spectroscopy (Matthews et al., 1996; Wild et al., 2000). Although both are within the green-blue range, humic acid emission wavelengths are slightly longer towards the green end of the spectrum (Ramseyer et al., 1997). Hence the green/blue (G/B) spectral ratio is a measure of the humic acid concentration relative to the aragonite density of the coral.

Correlations of Ba/Ca with the spectral G/B ratio improve compared to G, exemplified by core MAS1 (Fig. 2.6b). A marked peak in G/B ratios not observed in G now appears, matching a significant spike in Ba/Ca for the year 2000 (Fig. 2.6b). Indeed, for the total length of the MAS1 core, correlations of G/B ratios with Ba/Ca are higher and statistically significant ($R = 0.60$, $p < 0.001$, $n = 1234$) compared to G alone ($R = 0.09$, $p < 0.005$, $n = 1234$). For yearly averages, correlations between G/B ratios and Ba/Ca remain robust ($R = 0.61$, $p < 0.001$, $n = 102$), whereas G and Ba/Ca are negatively correlated ($R = -0.42$, $p < 0.001$, $n = 102$; Fig. 2.7). Correlations of monthly MAS1 G/B with MAS3 ($R = 0.69$, $p < 0.001$, $n = 1234$) are higher than with ANDRA ($R = 0.67$, $p < 0.001$, $n = 1112$) and IFAHO ($R = 0.64$, $p < 0.001$, $n = 305$). Indeed, correlations of G/B between all cores relative to MAS1 are now similar in contrast to G, testifying that G/B identifies an environmental signal of regional significance.

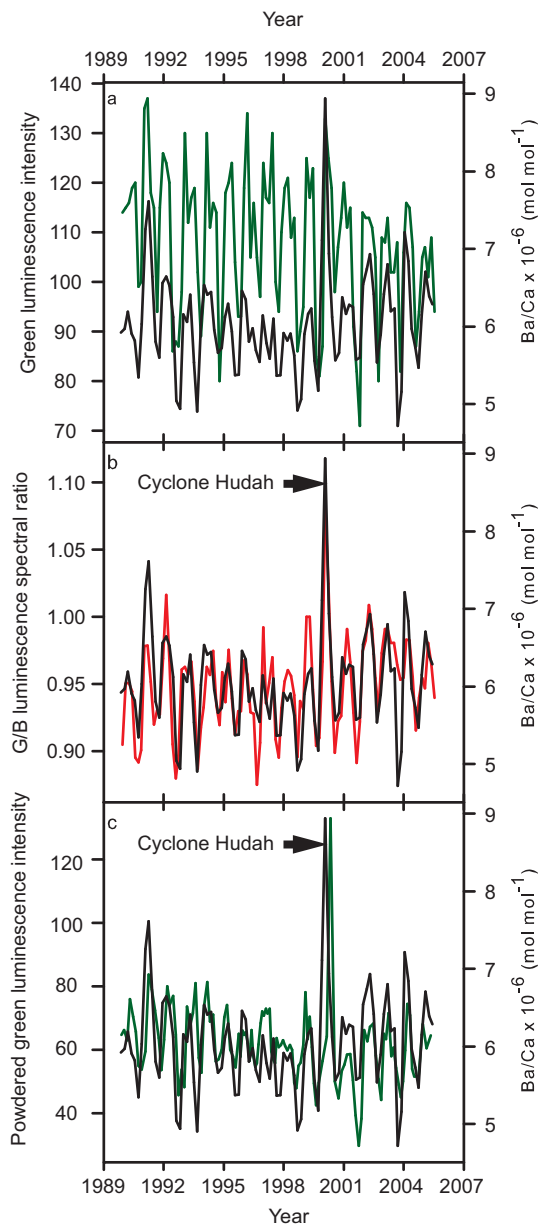


Figure 2.6. MAS1 monthly resolved Ba/Ca (black) compared with (a), the monthly averaged G (green) and (b), the G/B ratio (red). While the variability in green luminescence and Ba/Ca-runoff (a) is aligned, seasonal amplitudes and long-term trends are in poor agreement with each other. The correlation coefficient of G/B improves with Ba/Ca ($R = 0.69$, $p < 0.001$, $n = 185$; b) compared to G ($R = 0.5$, $p < 0.001$, $n = 185$; a), revealing a significant spike in the year 2000 corresponding to cyclone Hudah. To physically remove architectural effects, monthly sections of the coral sampling transect were powdered and compressed into micro-pellets (c). Green luminescence intensities (green) of micro-pellets also show an observed coherence with Ba/Ca (black), including the 2000 spike, testifying to the effect of skeletal architecture on absolute luminescence.

In order to further assess the effect of density and architecture on luminescence, samples were manually crushed from the same section of the MAS1 core. Crushing removed the large-scale architecture and was achieved by drilling sub-samples along the coral growth axis parallel to the optical

measurement track, homogenizing the extracted powder and pressing them into pellets. Each pellet approximately represented one month and was measured using the same SLS technique. Difference in resolution between the crushed samples and scanned cores hinders the perfect alignment of the two time series (Fig. 2.6c). Nevertheless, crushed sample luminescence intensities show a much improved coherence with Ba/Ca (Fig. 2.6c), as e.g. the marked peak of 2000 becomes apparent. Consequently, manual crushing confirms that G/B spectral ratios effectively normalises the humic acid signal to the aragonite signal in a manner conceptually similar to normalising elemental proxy concentrations against aragonite i.e. Ba/Ca, Sr/Ca. This provides the opportunity for tracing humic acid runoff in coral records without interference from density and architectural effects.

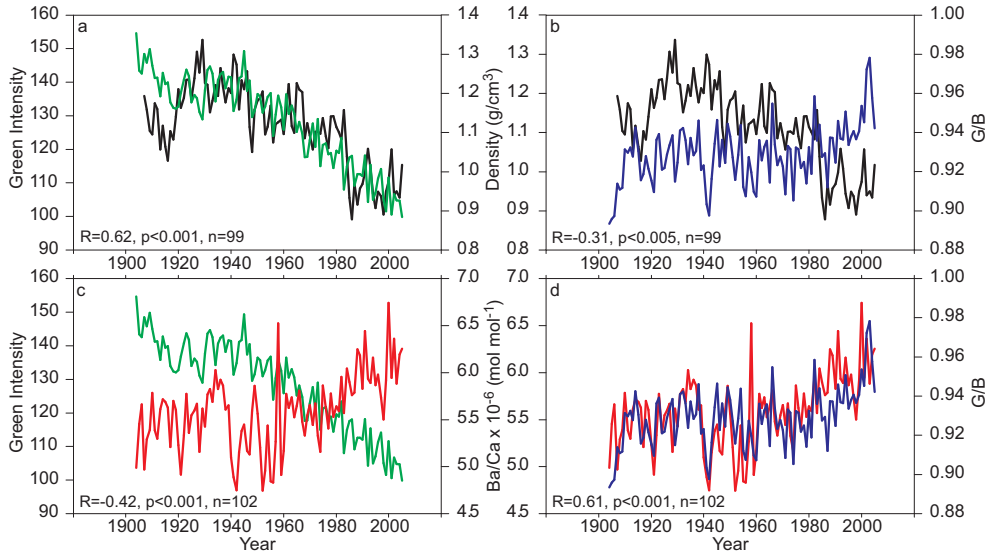


Figure 2.7. Time series plots for the annual means of MAS1 G (green), density (black), Ba/Ca (Red) and G/B (Blue). The last three years of the X-Ray image were distorted and were not used, therefore $n = 99$. All parameters were scaled by calculating yearly averages. Correlation coefficients and significance levels are shown at the bottom of each graph; luminescence intensity vs density (a), density vs. G/B (b), luminescence intensity vs. Ba/Ca (c), and Ba/Ca vs. G/B (d). Note the highly significant annual mean correlation of G/B with Ba/Ca and G with density, while negative correlations exist for G/B with density and G with Ba/Ca.

Coral STM2, from a reef devoid of terrestrial influences, typically shows very low luminescence intensities in the green domain, as exemplified for a 7 year section (Fig. 2.8). Both skeletal and powder intensities are considerably lower than MAS1, a core strongly affected by soil runoff (Fig. 2.6). Crushed samples from STM2 show no annual cycles and little variance, unlike the intensities in the intact core (Fig. 2.8). Removal of the density and architecture by crushing yields a low and stable intensity signal in the green domain without any trend, as opposed to the intact core which shows a declining luminescence intensity trend towards the core top.

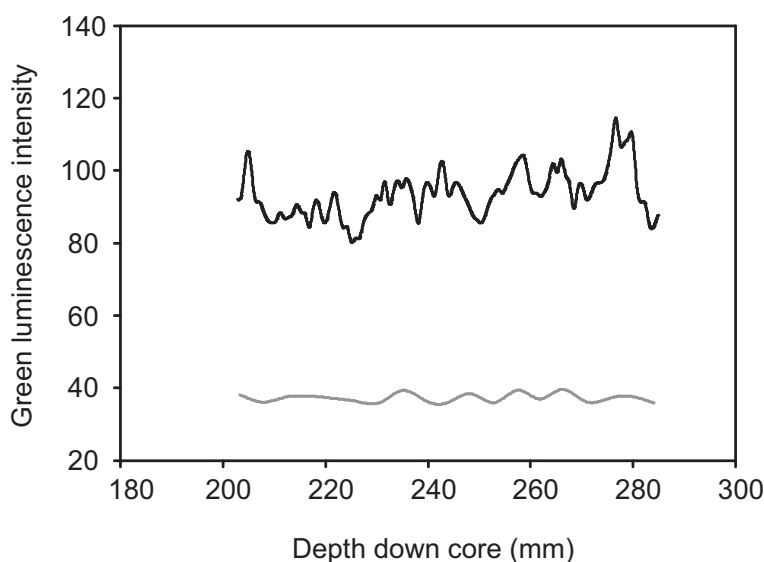


Figure 2.8. A 14-point moving average applied to G data (black), corresponding to a 7 year section (measuring 80 mm) from the coral core STM2. The core shows weak annual banding with relatively low amplitudes. By powdering and compressing monthly sections of the coral we physically removed the architecture. Pellets were then scanned to analyse luminescence intensities (grey), showing little variance and low relative intensities.

Declining luminescence intensities were observed for all three long corals from the Antongil Bay region (Fig. 2.9a), in concert with declining density (e.g. MAS1; Fig. 2.7). The decreasing trends over the period 1905 to 2006 in both luminescence intensities ($-40.92/100$ years; $r^2 = 0.42$, $p < 0.001$) and density ($-0.24\text{g/cm}^3/100$ years; $r^2 = 0.30$, $p < 0.001$) are statistically significant. Both show an accelerated decline since the 1950's. The decreasing trend over the period 1950 to 2006 in luminescence intensity and density is -33.77 ($r^2 = 0.37$,

$p < 0.001$) and -0.26 g/cm^3 ($r^2 = 0.37$, $p < 0.001$), respectively. Thus, the declining trends are most apparent after the 1950's. By contrast, spectral luminescence ratios show a different long term pattern with significant increases since approximately 1980 (Fig. 2.9b). For the MAS1 core the long-term trends in G/B and Ba/Ca ratios correlate well, indicating a modern increase in humic acid and sediment runoff, respectively, in northeast Madagascar (Fig. 2.9c; Fig. 2.7). As a corollary, G is negatively correlated with Ba/Ca and positively correlated with density (Fig. 2.7). Correlations of MAS1 and MAS3 annual average G/B are statistically significant ($R = 0.62$, $p < 0.001$, $n = 102$) and higher than G ($R = 44$, $p < 0.001$, $n = 102$), again testifying that G/B identifies an environmental signal of regional significance.

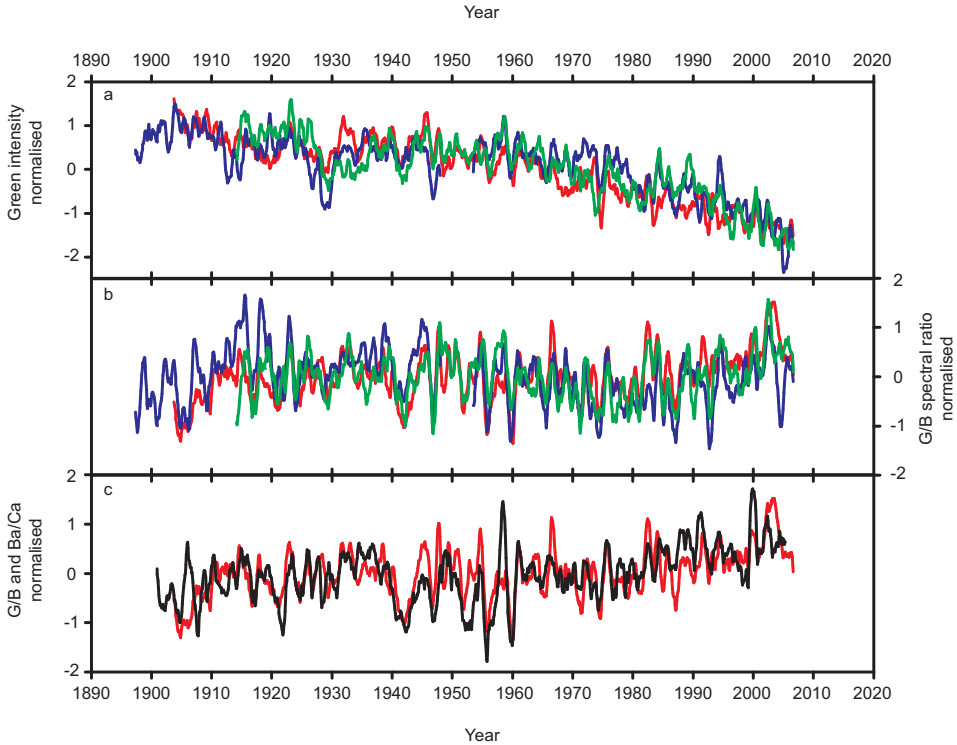


Figure 2.9. Luminescence intensities are shown in the green spectrum (G) for the three cores MAS1 (red), MAS3 (blue) and ANDRA (green). An observed decline from approximately 1950 is, followed by a further sharp decline from 1980 till present (a). G/B spectral luminescence ratios reveal an observed increase since 1980 (b). A long-term comparison of G/B (red) and Ba/Ca (black) is shown for the core MAS1 (c). G/B ratios and Ba/Ca show a good match (see Fig. 7 for correlations) for long-term trends and inter-annual variability. All data were normalised and smoothed using a 21-month filter.

To validate the G/B ratio in coral MAS1, results are compared against precipitation data from the nearest weather station (WMO code 67095) in Tamatave (18.15°S, 49.37°E) which yields the most continuous rainfall time series available for northeast Madagascar for the period 1889 to 1985 (<http://www.ncdc.noaa.gov/oa/climate/ghcn-monthly/>). MAS1 is used since this coral is influenced by the largest watershed. Annual means were computed for September to August (water year) rainfall and G/B ratios (Fig. 2.10). As a tracer of humic acid runoff, G/B ratios track the interannual and decadal variability in Tamatave rainfall, which have a statistically significant correlation ($R = 0.30$, $p = 0.01$, $n = 74$; Fig. 2.10). No significant correlation was observed between G and rainfall ($R = 0.003$, $p = 0.98$, $n = 74$; Fig. 2.10), further testifying that G/B ratios are a true measure of humic acid runoff and not overprinted by coral density effects.

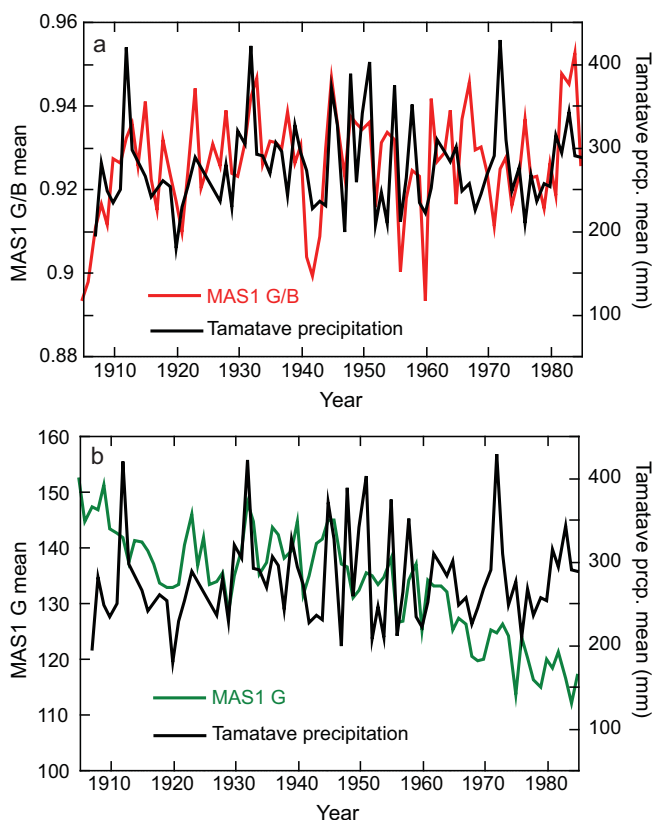


Figure 2.10. A comparison of annual mean G/B (a) and G (b) with precipitation data from Tamatave; the most continuous rainfall time series for northeast Madagascar (WMO code 67095; 18.15°S, 49.37°E) covering the period 1905 to 1985 (data available at <http://www.ncdc.noaa.gov/oa/climate/ghcn-monthly/>). Annual means were calculated by averaging 'water year' monthly values, September to August. The correlation between MAS1 G/B and rainfall (a) is statistically significant ($R = 0.30$, $p = 0.01$, $n = 74$). There is no significant correlation between MAS1 G and rainfall ($R = 0.01$, $p = 0.98$, $n = 74$; b).

Discussion

The coral skeleton is a complex structure reflecting seasonal and long-term changes in growth. The principle component of the aragonite skeleton is CaCO_3 , and therefore quantification of geochemical proxies has been achieved by normalising the tracer element to calcium e.g. Sr/Ca, Ba/Ca (Alibert et al., 2003; McCulloch et al., 2003). Our results show that spectral luminescence ratios (G/B ratios) offer a quantified signal of humic acid incorporation (Isdale, 1984; Isdale et al., 1998; Matthews et al., 1996; Susic et al., 1991; Susic and Boto, 1989; Wild et al., 2000) when normalised against density (Barnes and Taylor, 2001a, Barnes and Taylor, 2001b, Barnes and Taylor, 2005). The coral aragonite and humic acids it incorporates are both luminescent and have emissions in the green-blue domain (Matthews et al., 1996; Nyberg, 2002; Ramseyer et al., 1997; Sierra et al., 2005; Wild et al., 2000). As humic acid emissions have slightly longer wavelengths than aragonite (Ramseyer et al., 1997), dull and bright luminescent intensity bands in coral skeletons have often been referred to as blue and yellow-green bands respectively (Matthews et al., 1996; Wild et al., 2000).

SLS separates the humic acid signal from the density signal by normalising two grouped intensity values in the green and the blue domain, rather than extracting the humic acid wavelength emission from the skeleton using traditional fluorescence spectroscopy (Matthews et al., 1996; Wild et al., 2000). Although part of the humic acid signal will reside in the blue domain and part of the aragonite signal in the green (and vice versa), it is the relative increase of one compared to the other that reflects compositional changes. Indeed, Wild et al. (2000) divided the spectral emission matrix of a bright band by a dull band and found enhanced bright band emissions at longer wavelengths in ratios between 0.9 and 1.25, a range replicated by the G/B ratio. Following up from Wild et al. (2000), compositional changes are quantified by SLS thus providing a means to reconstruct humic acid runoff at a linear resolution of 71.4 μm . The G/B ratio therefore renders a normalised humic acid signal equivalent to a humic acid/aragonite ratio, which is comparable to the geochemical trace element/Ca proxies. Spectral ratios provide more accurate measurements than luminescence intensities for identifying changes in humic acid runoff/erosion within tropical marine environments by normalising for the effects of skeletal density and architecture.

The majority of techniques employed to reconstruct humic acid runoff from coral luminescence have previously focused on intensities alone (Barnes and Taylor, 2001a; Boto and Isdale, 1985; Isdale et al., 1998; Matthews et al., 1996; Wild et al., 2000). Corals produce high and low annual density bands; consequently conventional luminescence intensity measurements result in an indirect density measurement as proven by SLS (Fig. 2.7). High concentrations of humic acids locked into a low density (g/cm^3) section of coral skeleton would result in a weak luminescence intensity signal, as the area measured is significantly porous. In this situation both the green and blue intensities will be low while the G/B ratio will be relatively high, given the high proportion of humic acids locked within the aragonite. This may explain the occurrence of ‘anomalous barium peaks’ in coral records i.e. that are not matched by a similar peak in luminescence intensities (Sinclair, 2005). Indeed for a similar anomaly found in our Madagascar cores for the year 2000, spectral ratios now identify that the ‘anomalous barium spike’ was caused by an extreme runoff event, rather than caused by any of the multiple biological mechanisms inferred by Sinclair (2005). It coincides with the landfall of Tropical Cyclone Hudah, which caused massive destruction in and around Antongil Bay, and catastrophic sediment and humic acid runoff (Birkinshaw and Randrianjanahary, 2007). Consequently spectral ratios rather than luminescence intensities should be taken to reconstruct humic acid runoff. Luminescence intensity profiles remain important however for the construction of age models by counting bands down-core and connecting corresponding marker points (Hendy et al., 2003). Cores possessing individual luminescence intensity traits are likely created by localised intra- and inter-colony variability in density (Felis et al., 2003; Suzuki et al., 2005). Spectral ratios remove this inter-colony variability in density, reflecting predominantly the regional humic acid runoff.

In tropical catchments influencing the Great Barrier Reef, seasonal variability in rainfall was shown to control river flow (Finlayson and McMahon, 1988; Furnas and Mitchell, 2001). For Madagascar, river discharge time series are extremely scarce hindering further calibration of coral luminescence other than by rainfall data from the nearest weather station Tamatave. The MAS1 time series shows a statistically significant correlation between G/B ratios and Tamatave rainfall for September to August annual means (Fig. 2.10). The

coral G/B time series tracks the interannual to decadal variability in Tamatave rainfall rather well and adds confidence to our results. The relatively low correlation coefficient ($R = 0.30$, $p = 0.01$, $n = 74$) most probably results from Tamatave rainfall not precisely replicating the local rainfall variability of the Antainambalana river catchment influencing coral MAS1. However, the green luminescence intensity shows no correlation with rainfall testifying that spectral ratios are the more reliable proxy for river flow carrying soil derived humic acids. Hydrological modelling of river discharge including gridded rainfall products and land-use change data are still required to calibrate spectral ratios for reconstructing river discharge.

Corals far from terrestrial inputs exhibit dull luminescent bands resulting from the high and low density aragonite structure (Barnes and Taylor, 2001a; Barnes and Taylor, 2005). Skeletal pores can amplify or quench luminescence intensities (Barnes and Taylor, 2001a). Indeed, by removing the architecture through crushing left little variance in the baseline signal of aragonite (Fig. 2.8). Since corals devoid of terrestrial inputs only carry a single luminophore (aragonite), internal light reflections caused by the complex skeletal architecture create fluctuating G/B signals, rather than the uniform response from humic acid runoff. Estuarine corals affected by humic acids possess two luminophores normalised by applying G/B spectral ratios. Internal reflections therefore cause both the humic acid and aragonite G/B signal to shift in proportion to one another, but do not affect the significant correlation between G/B and Ba/Ca.

As density also affects luminescence intensity, long-term declining luminescence trends are likely a result of common declining coral densities (De'ath et al., 2009). Since the 1950s, luminescence intensity and density both declined in all the Madagascar cores and correlations are statistically significant as exemplified for the coral core MAS1. Spectral luminescence ratios combined with long-term Ba/Ca now confirm the role of density by revealing similar trends, resolving the question as to what causes the marked decline in luminescence intensities shown by some coral luminescence records (Cobb et al., 2008; Isdale et al., 1998; Lough et al., 2010) e.g. 14 out of 20 coral cores sampled from inshore reefs from the Great Barrier Reef display a significant declining luminescence intensity trend (Lough et al., 2010).

In conclusion, declining density trends are responsible for the marked decrease in absolute luminescence intensities rather than humic acid runoff. Indeed, Barnes and Taylor (2005) found that chemical reduction of skeletal density caused a decline in luminescence intensities. Declining luminescence trends have likely affected the interpretation of past erosion records. Nyberg et al. (2007) show multiple cores with declining luminescence intensity trends, which they relate to a decreasing trend in hurricane activity. The findings presented here suggest that such declining trends may alternatively reflect declining coral densities, perhaps in response to the same cause.

Wild et al. (2000) highlighted the importance of comparing neighbouring bright and dull bands to normalise for varying background luminescence which we now relate to changing aragonite density. A method designed to account for the declining luminescence trends subtracts annual luminescence minimum intensity from the maximum intensity to calculate the annual range (Lough et al., 2010). All luminescence intensity records from NE Madagascar show declining trends, but when spectral ratios are applied they reveal that soil derived humic acid runoff increased as opposed to decreased. This could be related to either increases in precipitation or land-use activity both promoting soil erosion and extraction of humic acids from the watershed (Fig. 2.9). Based on this new understanding of coral luminescence, spectral luminescence ratios are proposed as a novel robust proxy for humic acid runoff as recorded by inshore corals, improving on the uncertainties of climate interpretation as addressed by Cobb et al. (2008). In summary, (1) both humic acids and aragonite density determine luminescence intensities in corals; and (2) that normalisation is required for their deconvolution in order to reconstruct river runoff accurately.

Soil erosion is a major problem in developing countries, with a number of amplifying factors such as land development, cyclone impact and increased seasonal rainfall patterns associated with the monsoon. Coral reefs are presently in a vulnerable state, with increasing sedimentation rates reducing photosynthetic activity of their endosymbiotic algae (Anthony and Connolly, 2004). Accurate long term records of erosion can identify changing rates over time, which coupled with other proxies will assist in identifying potential causes, whether climatic (rainfall) or anthropogenic (land-use change).

Spectral luminescence ratios of massive corals can provide such records for tropical marine catchments, identifying where and when runoff is changing. As humic acids are not significantly affected by biological activity within the marine system, high resolution spectral luminescence ratios provide a reliable proxy for humic acid runoff related to changes in hinterland precipitation and soil erosion. On a local scale, multiple coral core records should identify locations most influenced by changing runoff and erosion into inshore reef systems e.g. by deforestation. Prior to any future development plans to specific regions, SLS may be considered to assess potential environmental impacts. SLS offers a rapid continuous and cost-effective monitor of river discharge, providing valuable information that will assist in reef conservation efforts and understanding past climate change.

Supplementary Information

Research Area and Climate Setting

Antongil Bay is located in the NE of Madagascar, covering an area of 2800 km², with a mean depth of 41.5 m and a coastline of 270 km extending 80 km inland (Ersts and Rosenbaum, 2003). Two protected forest areas are found in the vicinity of the bay, the Makira Forest and the Masoala Peninsula National Park (Birkinshaw and Randrianjanahary, 2007). One of the largest rivers draining into Antongil Bay is the Antainambalana, running through the Makira Forest Area from a source 1450 m above sea level (Goodman and Ganzhorn, 2004). Its watershed covers an estimated 4000 km² (estimated with: <http://www.acme.com/planimeter>) and the river mouth is located in the city of Maroansetra (Fig. 2.3). The MAS1 and MAS3 coral cores were collected next to the island Nosy Mangabe, ca. 7 km from the river mouth (Fig. 2.3). The ANDRA coral core was collected 30 km from MAS1/3 on the east side of the bay, ca. 7 km from the Ambanizana river mouth (Fig. 2.3). The Ambanizana has a much smaller watershed (ca. 160 km²) and runs southwest towards Antongil Bay through a mountainous region with dense forest cover. IFAHO is situated ca. 4.5 km from the mouth of the river Anaovandran (watershed: ca. 180 km²) outside of Antongil Bay (Fig. 2.3). The river originates from the same mountains as the Ambanizana, but flows eastwards away from Antongil Bay. For the last ca. 11 km it flows through a plain before entering the ocean.

One coral core was obtained off the island of St Marie (E 49°, S 17°; Northeast Madagascar; Fig. 2.3). This coral site experiences fully oceanic conditions devoid of terrestrial influences.

The climate in Madagascar can be divided into a August-December cold-dry season and a January-July warm-wet season. Air temperatures peak in December and January and are lowest between July and September (Kremen, 2003). Highest rainfall occurs between January and March, while lowest rainfall occurs between September and November (Kremen, 2003). Highest runoff occurs between February and April, one to two months after peak rainfall (Kremen, 2003).

Summary of Previous Methods Employed

Pioneered by Isdale (1984), a UV source used for excitation together with a spectrophotometer, were first employed to measure light emissions via an optic fibre. Although a UV light still remains popular, a wide variety of other sources have since been used, such as a nitrogen laser (Milne and Swart, 1994), a mercury arc lamp (Isdale et al., 1998) and a quartz-halogen lamp (Barnes et al., 2003). Other techniques employed to retrieve luminescence information from corals include light filters (Boto and Isdale, 1985; Matthews et al., 1996; Isdale et al., 1998; Wild et al., 2000; Barnes and Taylor, 2001), visual categorisation or photography of coral slabs exposed to UV light (Scoffin et al., 1989; Lough et al., 2002; Lough, 2007) and image-analysis of grey scale intensity profiles (Sinclair and McCulloch, 2004; Sinclair, 2005). A more detailed summary of the various techniques employed are described in Barnes et al. (2003).

Spectral Luminescence Scanning Methodology

UV Light Source

The standard light source of the Avaatech core-scanner was replaced by two long-wave UV-A tubes in the 350 - 450 nm range (FPL36BLB, SANKYO DENKI). The bulbs were switched on at least 15 minutes prior to measurements in order to stabilise output. One high frequency electronic ballast (45 KHz) was connected to the UV light source to avoid 50 Hz flickering associated with

the mains frequency. Both UV tubes were fitted into a specifically designed black holder to eliminate the back scatter of reflected light. A 5 mm narrow slit in the middle of the UV-tube holder allows the camera lens located above to acquire line-scan images, capturing the emitted light from the underlying sample (Fig. 2.1). When the scan is initiated the light source and camera progress down the sample slab as a single unit while constantly scanning multiple lines, resulting in a continuous core image. A 450 nm light cut-off filter is optionally placed beneath the camera lens to eliminate reflected light from the UV source and record luminescence intensities in the blue domain.

Camera Sensor

Luminescence emission is recorded by the Jai CV-L105 3 CCD RGB Line Scan Camera. Incoming light passing through the lens is split into three wavelength ranges (Red, Green and Blue) by a Dichroic RGB beam splitter prism, and recorded by separate sensors (Fig. 2.1). Each sensor has 2048 x 1 pixels and the alignment between the three sensors is +/- 1 pixel. The distance between the light source, the sample slab surface and the sensors is kept constant to ensure that incident and detected intensities can be standardised. As the camera moves over the slab it continuously collects a single cross-core line image of 2048 x 1 pixels for each spectral range. The distance between the camera and the slab will determine the area scanned and thus the resolution of the image. The current setup gives a spatial resolution of 140 pixels per cm, each pixel therefore yielding a linear resolution of 71.4 μm . Three data points are produced for each individual pixel in the R, G and B range. Depending on the intensity of luminescence for specific carbonate materials, the appropriate camera settings are chosen (exposure time and lens aperture). Increasing the exposure time enhances the intensity, and thus the sensitivity for samples with low luminescence. In order not to over-saturate the coral carbonate signal, an exposure time of 40 ms was used, generating optimal intensities. The aperture size is adjusted to gain maximum light intensity without saturating the signal as recorded by the camera. The maximum core length that can be measured in one continuous scan is 150 cm, and full scans are routinely completed within an hour. As long as the exposure time and aperture width of the camera setup remains the same, line-scanning provides fast, non-destructive quantified data that allows for matching and comparing carbonates with little sampling effort.

Data and Standardisation

The specifically designed software (Avaatech) enables linear transects to be manually drawn from the luminescence image to retrieve intensity profiles for any specified area and direction (Fig. 2.2). Once the areas of interest are identified, transects are created up to 150 cm in length and 15 cm in width, however usually limited to shorter transects depending on sample size, changes in the direction of growth axes or breaks and/or visual discrepancies in the sample. Connecting transects is achieved by transferring quantified intensity data into a separate program used for data management. Multiple transects can be created for any length, in any direction, at any required width from just a single scan taking up to one hour. A customised platform for positioning the sample slabs was built from a non-luminescent black plastic (polymethyl metacrylate - PMMA). Uranyl glass with homogenous luminescent properties is mounted on the platform and used as a standard reference for all intensity measurements. Line transects drawn through the entire length of the standard material using the image and software will identify any drift in either the light source or camera recording. Comparing relative intensities of all spectra to previous scans indicates spectral shifts in the standard. Subsequently the resulting sample intensities are corrected for any drift to allow direct inter-comparisons between cores to be made over time.

Method Summary

- Quantitative photoluminescence data is produced with a linear resolution of 71.4 μm (pixel length); compatible for coupling with other high resolution analysis e.g. LA-ICP-MS, ion-microprobe.
- Such a resolution is ideal for calibration purposes, identifying short-term (flood/cyclones) events that will remain unresolved by existing methods.
- Plotting transects adjacent to previous sampling tracks is a major advantage of the technique, useful for combining datasets and keeping scales consistent.
- The RGB scanning system obtains data from the Red and Green spectra without filters, and the Blue with the use of a 450 nm filter.
- Spectral ratios indicate changes in the amount of soil organics incorporated in carbonate skeletons and/or changes in mineralogy.

- High quality normalised photoluminescence images are obtained using a line-scan camera, creating digital archives.
- Establishing a number of physical properties by visual assessment is useful in selecting the optimum elemental sampling track line, e.g., growth axes, compositional changes, physical discrepancies, relative intensities.
- Cross comparison of carbonates is possible as long as preparation methods are consistent.
- Scans take no more than 1 hour per 1.5 m to produce the photoluminescence image.
- Once an image is produced, photoluminescence images can be re-sampled without the need for re-scanning.
- Software allows any transects to be manually selected from the image along or across growth axes for any length in any direction, for any width, for multiple transects in a single sample, from a single scan.
- Widths of transects created can be optimised. Long term trends may require averaging of pixels, ridding of sub-millimeter variability.
- For long-term temporal paleoclimate analysis, it may be appropriate to widen transects on the UV image, averaging the cross-core pixels perpendicular to the skeletal growth axis. This provides a smoothed time series record by eliminating cross-core sub-millimetre variability, while retaining a down-core linear resolution of 71.4 μm (Fig. S2.4).
- The exposure time can be optimised to the specific photoluminescence intensity yield of the carbonate, i.e., low intensity requires a high exposure time.

Supplementary Figures

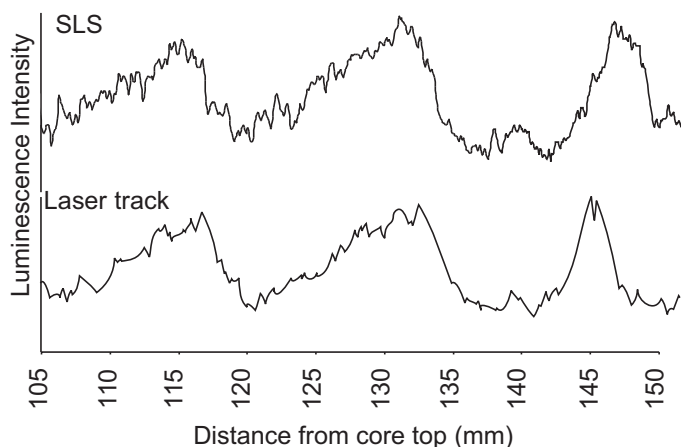


Figure S2.1. Comparison of luminescence intensities between the SLS technique (above), and the argon-ion laser technique (below) measured on the same coral section. The slight offset in timing of the intensity changes between methods was caused by difficulties in defining a fixed transect using the argon-ion laser technique.

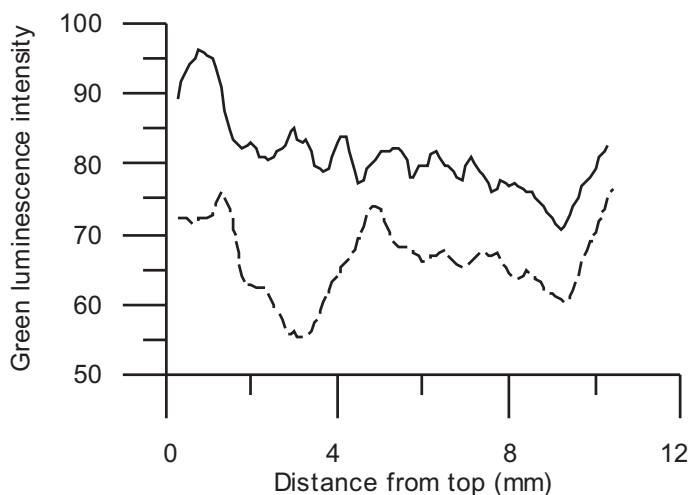


Figure S2.2. Comparison of luminescence intensities measured in the green domain for a coral top measuring 11 mm before (dashed) and after (solid) treatment with sodium hypochlorite. The coral section represents approximately 1 year of growth.

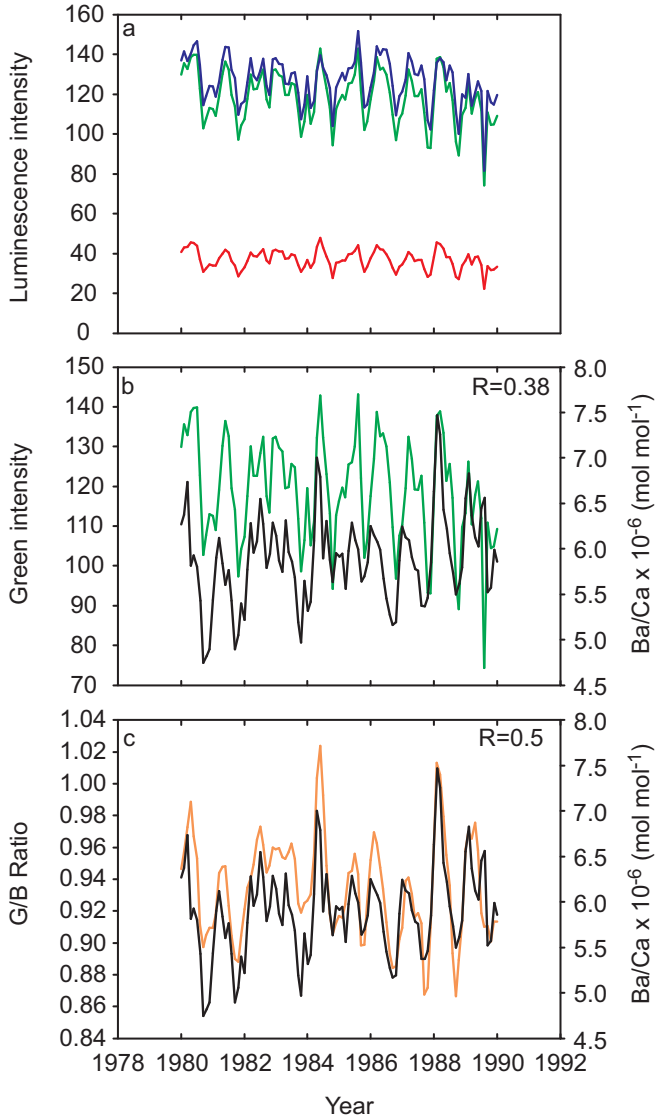


Figure S2.3. The photoluminescence emissions of the MAS1 core between the years 1980 and 1990 (a) for all three emission spectra R (red) G (green) and B (blue); (b) the G (green) plotted against Ba/Ca (black); and (c) the G/B ratio (orange) plotted against Ba/Ca (black). The correlation coefficient value R is given for testing the relationship of G against Ba/Ca (b) and G/B against Ba/Ca; and is shown in the top right corner of the corresponding plot. Correlations of Ba/Ca with G/B are significantly higher, with an improved correlation ($R=0.5$, $p<0.001$, $n=132$) compared to G alone ($R=0.38$, $p<0.001$, $n=132$).

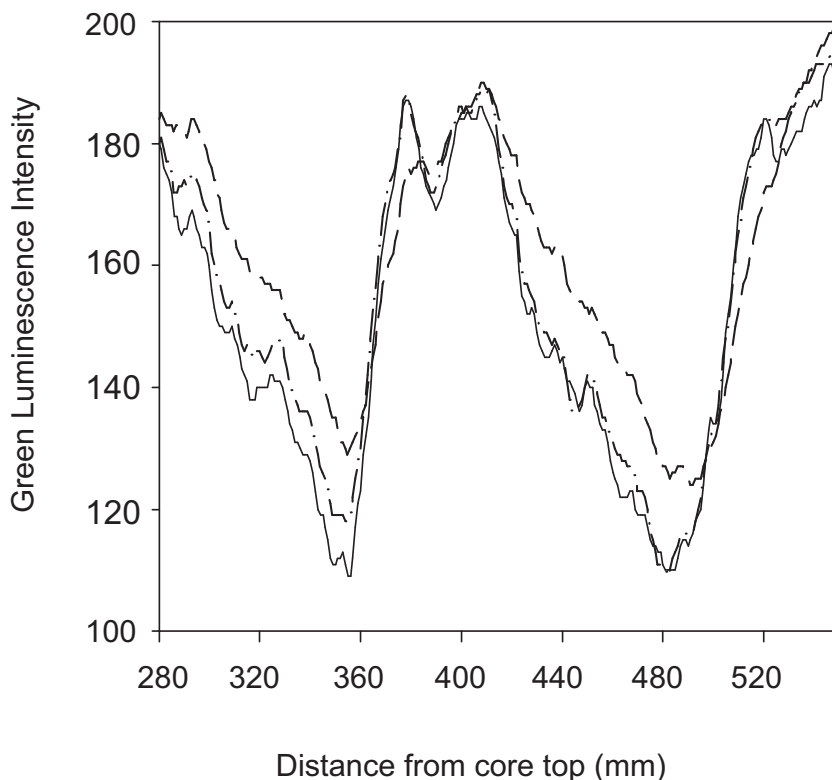


Figure S2.4. Measured luminescence intensities of three equally long transects with widths of 0.25 mm (solid), 0.5 mm (dotted) and 1 mm (dashed). The width of transect determines the number of pixels averaged perpendicular to the growth direction, with the number of pixels parallel to the growth axis remaining constant.

Acknowledgments: This work was supported as part of the SINDOCOM and EKP grant under the Dutch NWO program ‘Climate Variability’, grant 854.00034/035, WOTRO 07.55.2004.028, and Australian Research Council Centre of Excellence in Coral Reef Studies. We thank all involved in the development of the UV core-scanner, especially Aad Vaars and Sjerry van der Gaast of Avaatech, as well as Rineke Gieles and Thomas Richter from the Marine Geology department at NIOZ, and Stephanie Verbeek from Vrije Universiteit Amsterdam, as well as Edwin Keijzer and Herman Boekel from the Engineering department at NIOZ. We thank the Wildlife Conservation Society (WCS) Madagascar, especially Bemahafaly Randriamanantsoa, Heriliala Randriamahazo and the WCS/ANGAP team in Maroantsetra, for support in fieldwork logistics and in the organisation of the research permits. We like to thank CAF/CORE Madagascar for granting the CITES permit. We finally would like to thank the reviewers and Janice Lough for their professional and scientific advice which greatly improved the manuscript.

References

- Alibert, C., Kinsley, L., Fallon, S., McCulloch, M., Berkelmans, R., McAllister, F., 2003. Source of trace element variability in Great Barrier Reef corals affected by Burdekin flood plumes. *Geochimica et Cosmochimica Acta* 67, 231–246.
- Anthony, K.R.N., Connolly, S.R., 2004. Environmental limits to growth: physiological niche boundaries of corals along turbidity-light gradients. *Oecologia* 141, 373–384.
- Barnes, D.J., Taylor, R.B., 2001a. On the nature and causes of luminescent lines and bands in coral skeletons. *Coral Reefs* 19, 221–230.
- Barnes, D.J., Taylor, R.B., 2001b. Natural and artificial luminescence in a skeletal slice of *Porites*. *Coral Reefs* 19, 270–270.
- Barnes, D.J., Taylor, R.B., 2005. On the nature and causes of luminescent lines and bands in coral skeletons: II. Contribution of skeletal crystals. *Journal of Experimental Marine Biology and Ecology* 322, 135–142.
- Barnes, D.J., Taylor, R.B., Lough, J.M., 2003. Measurement of luminescence in coral skeletons. *Journal of Experimental Marine Biology and Ecology* 295, 91–106.
- Birkinshaw, C., Randrianjanahary, M., 2007. The Effects of Cyclone Hudah on the Forest of Masoala Peninsula, Madagascar. *Madagascar Conservation & Development* 2, 17–20.
- Boiseau, M., Juillet-Leclerc, A., 1997. H₂O₂ treatment of recent coral aragonite: oxygen and carbon isotopic implications. *Chemical Geology* 143, 171–180.
- Boto, K., Isdale, P., 1985. Fluorescent bands in massive corals result from terrestrial fulvic-acid inputs to nearshore zone. *Nature* 315, 396–397.
- Carricart-Ganivet, J.P., Lough, J.M., Barnes, D.J., 2007. Growth and luminescence characteristics in skeletons of massive *Porites* from a depth gradient in the central Great Barrier Reef. *Journal of Experimental Marine Biology and Ecology* 351, 27–36.
- Cobb, K., Cole, J., Lough, J., Tudhope, S., 2008. Annually-banded corals as climate proxies. ‘White Paper’ for PAGES meeting (Trieste), 9–11 June 2008, <http://www.pages-igbp.org/cgi-bin/WebObjects/products.woa/wa/product?id=326>
- Corrège, T., 2006. Sea surface temperature and salinity reconstructions from coral geochemical tracers. *Palaeogeography Palaeoclimatology Palaeoecology* 232, 408–428.
- De’ath, G., Lough, J.M., Fabricius, K.E., 2009. Declining Coral Calcification on the Great Barrier Reef. *Science* 323, 116–119.
- Dewar, R.E., Wallis, J.R., 1999. Geographical patterning of interannual rainfall variability in the tropics and near tropics: An L-moments approach. *Journal of Climate* 12, 3457–66.
- Dewar, R.E., Richard, A.F., 2007. Evolution in the hypervariable environment of Madagascar. *PNAS* 104, 13723–27.
- Ersts, P.J., Rosenbaum, H.C., 2003. Habitat preference reflects social organization of humpback whales (*Megaptera novaeangliae*) on a wintering ground. *Journal of Zoology* 260, 337–345.
- Fallon, S.J., McCulloch, M.T., Woesik, R.v., Sinclair, D.J., 1999. Corals at their latitudinal

- limits: laser ablation trace element systematics in *Porites* from Shirigai Bay, Japan. *Earth and Planetary Science Letters* 172, 221-238.
- Fallon, S.J., White, J.C., McCulloch, M.T., 2002. *Porites* corals as recorders of mining and environmental impacts: Misima Island, Papua New Guinea. *Geochimica et Cosmochimica Acta* 66, 45-62.
- Felis, T., Patzold, J., Loya, Y., 2003. Mean oxygen-isotope signatures in *Porites* spp. corals: inter-colony variability and correction for extension-rate effects. *Coral Reefs* 22, 328-336.
- Felis, T., Pätzold, J., 2003. In: *Marine Science Frontiers for Europe* eds. Wefer, G., Lamy, F., Mantoura, F., 11-27 (Springer, Berlin, Heidelberg, New York, Tokyo).
- Finlayson, B.L., McMahon, T.A., 1988. Australia v. the world: A comparative analysis of streamflow characteristics, in *Fluvial Geomorphology of Australia*, edited by Warner RF, Academic, San Diego, Calif 17-40.
- Fleitmann, D., Dunbar, R.B., McCulloch, M.T., Mudelsee, M., Vuille, M., McClanahan, T.R., Cole, J.E., Eggins, S., 2007. East African soil erosion recorded in a 300 year old coral colony from Kenya. *Geophysical Research Letters* 34, doi:10.1029/2006GL028525.
- Furnas, M., Mitchell, A., 2001. Runoff of terrestrial sediment and nutrients into the Great Barrier Reef, in *Oceanographic Processes of Coral Reefs: Physical and Biological Links in the Great Barrier Reef*, edited by Wolanski, E., CRC Press, Boca Raton Fla 37-51.
- Goodman, S.M., Ganzhorn, J.U., 2004. Biogeography of lemurs in the humid forests of Madagascar: the role of elevational distribution and rivers. *Journal of Biogeography* 31, 47-55.
- Grottoli, A.G., Rodrigues, L.J., Matthews, K.A., Palardy, J.E., Gibb, O.T., 2005. Pre-treatment effects on coral skeletal $\delta^{13}\text{C}$ and $\delta^{18}\text{O}$. *Chemical Geology* 221, 225-242.
- Grottoli, A.G., Eakin, C.M., 2007. A review of modern coral $\delta^{18}\text{O}$ and $\Delta^{14}\text{C}$ proxy records. *Earth-Science Reviews* 81, 67-91.
- Grove, C.A., Nagtegaal, R., Scheufen, T., Koster, B., Zinke, J., Brummer, G-J.A., 2009. Luminescence banding in tropical coral skeletons quantified using novel whole-core microscanning. *Geochimica et Cosmochimica Acta* 73, A470.
- Helmle, K.P., Kohler, K.E., Dodge, R.E., 2002. Relative Optical Densitometry and The Coral X-radiograph Densitometry System: CoralXDS. Presented Poster, International Society of Reef Studies, 2002. European Meeting. Cambridge, England. Sept. 4-7.
- Hendy, E.J., Gagan, M.K., Lough, J.M., 2003. Chronological control of coral records using luminescent lines and evidence for non-stationary ENSO teleconnections in northeast Australia. *The Holocene* 13, 187-199.
- Isdale, P. 1984. Fluorescent bands in massive corals record centuries of coastal rainfall. *Nature* 310, 578-579.
- Isdale, P.J., Stewart, B.J., Tickle, K.S., Lough, J.M., 1998. Palaeohydrological variation in a tropical river catchment: a reconstruction using fluorescent bands in corals of the Great Barrier Reef, Australia. *Holocene* 8, 1-8.
- Jansen, J.H.F., van der Gaast, S.J., Koster, B., Vaars, A.J., 1998. CORTEX, a shipboard XRF-scanner for element analyses in split sediment cores. *Marine Geology* 151, 143-153.
- Jones, P.D., Briffa, K.R., Osborn, T.J., Lough, J.M., Ommen, T.d.v., Vinther, B.M.,

- Lutterbacher, J., Wahl, E.R., Zwiers, F.W., Mann, M.E., Schmidt, G.A., Ammann, C.M., Buckley, B.M., Cobb, K.M., Esper, J., Goose, H., Graham, N., Jansen, E., Kiefer, T., Kull, C., Kuettel, M., Mosley-Thompson, E., Overpeck, J.T., Riedwyl, N., Schulz, M., Tudhope, A.W., Villalba, R., Wanner, H., Wolff, E., Xoplaki, E., 2009. High-resolution palaeoclimatology of the last millennium: a review of current status and future prospects. *The Holocene* 19, 3-49.
- Kremen, C., 2003. The natural history of Madagascar: The Masoala Peninsula. University of Chicago Press, 1459-66.
- Lough, J.M., 2010. Measured coral luminescence as a freshwater proxy: comparison with visual indices and a potential age artefact. *Coral Reefs* 30, 169-182.
- Lough, J.M., 2007. Tropical river flow and rainfall reconstructions from coral luminescence: Great Barrier Reef, Australia. *Paleoceanography* 22, doi:10.1029/2006PA001377.
- Lough, J.M., 2004. A strategy to improve the contribution of coral data to high-resolution paleoclimatology. *Palaeogeography Palaeoclimatology Palaeoecology* 204, 115-143.
- Lough, J.M., Barnes, D.J., Mcallister, F.A., 2002. Luminescent lines in corals from the Great Barrier Reef provide spatial and temporal records of reefs affected by land runoff. *Coral Reefs* 21, 333-343.
- Macrae, C.M., Wilson, N.C., 2008. Luminescence database I-Minerals and materials. *Microscopy Microanalysis* 14, 184-204.
- Matthews, B.J.H., Jones, A.C., Theodorou, N.K., Tudhope, A.W., 1996. Excitation-emission-matrix fluorescence spectroscopy applied to humic acid bands in coral reefs. *Marine Chemistry* 55, 317-332.
- McCulloch, M.T., Gagan, M.K., Mortimer, G.E., Chivas, A.R., Isdale, P.J., 1994. High resolution Sr/Ca and $\delta^{18}\text{O}$ coral record from the Great Barrier Reef, Australia, and the 1982-83 El Niño. *Geochimica et Cosmochimica Acta* 58, 2747-2754.
- McCulloch, M., Fallon, S., Wyndham, T., Hendy, E., Lough, J., Barnes, D., 2003. Coral record of increased sediment flux to the inner Great Barrier Reef since European settlement. *Nature* 421, 727-730.
- Milne, P.J., Swart, K.P., 1994. Fibre-optic-based sensing of banded luminescence in corals. *Applied Spectroscopy* 48, 1282-1284.
- Nyberg, J., 2002. Luminescence intensity in coral skeletons from Mona Island in the Caribbean Sea and its link to precipitation and wind speed. *Philosophical Transactions of the Royal Society of London Series A* 360, 749-766.
- Nyberg, J., Malmgren, B.A., Winter, A., Jury, M.R., Kilbourne, K.H., Quinn, T., 2007. Low Atlantic hurricane activity in the 1970s and 1980s compared to the past 270 years. *Nature* 447, 698-701.
- Richter, T.O., van der Gaast, S., Koster, B., Vaars, A., Gieles, R., de Stigter, H.C., de Haas, H., van Weering, T.C.E., 2006. The Avaatech XRF Core Scanner: technical description and applications to NE Atlantic sediments. *Geological Society, London, Special Publications* 267, 39-50.
- Ramseyer, K., Miano, T.M., Dorazio, V., Wildberger, A., Wagner, T., Geister, J., 1997. Nature and origin of organic matter in carbonates from speleothems, marine cements and coral skeletons. *Organic Geochemistry* 26, 361-378.
- Scoffin, T.P., Tudhope, A.W., Brown, B.E., 1989. Fluorescent and skeletal density banding in

- Porites lutea* from Papua New-Guinea and Indonesia. *Coral Reefs* 7, 169-178.
- Sierra, M.M.D., Giovanela, M., Parlanti, E., Soriano-Sierra, E.J., 2005. Fluorescence fingerprint of fulvic and humic acids from varied origins as viewed by single-scan and excitation/emission matrix techniques. *Chemosphere* 58, 715-733.
- Sinclair, D.J., 2005. Non-river flood barium signals in the skeletons of corals from coastal Queensland, Australia. *Earth and Planetary Science Letters* 237, 354-369.
- Sinclair, D.J., Kinsley, L.P.J., Mcculloch, M.T., 1998. High resolution analysis of trace elements in corals by laser ablation ICP-MS. *Geochimica et Cosmochimica Acta* 62, 1889-1901.
- Sinclair, D.J., Mcculloch, M.T., 2004. Corals record low mobile barium concentrations in the Burdekin River during the 1974 flood: evidence for limited Ba supply to rivers? *Palaeogeography Palaeoclimatology Palaeoecology* 214, 155-174.
- Susic, M., Boto, K., Isdale, P., 1991. Fluorescent humic-acid bands in coral skeletons originate from terrestrial runoff. *Marine Chemistry* 33, 91-104.
- Susic, M., Boto, K.G., 1989. High-performance liquid-chromatographic determination of humic-acid in environmental-samples at the nanogram level using fluorescence detection. *Journal of Chromatography* 482, 175-187.
- Suzuki, A., Hibino, K., Iwase, A., Kawahata, H., 2005. Intercolony variability of skeletal oxygen and carbon isotope signatures of cultured *Porites* corals: Temperature-controlled experiments. *Geochimica et Cosmochimica Acta* 69, 4453-4462.
- Watanabe, T., Minagawa, M., Oba, T., Winter, A., 2001. Pretreatment of coral aragonite for Mg and Sr analysis: Implications for coral thermometers. *Geochemical Journal* 35, 265-269.
- Wild, F.J., Jones, A.C., Tudhope, A.W., 2000. Investigation of luminescent banding in solid coral: the contribution of phosphorescence. *Coral Reefs* 19, 132-140.

Chapter 3

Spatial linkages between coral proxies of terrestrial runoff across a large embayment in Madagascar

Craig A. Grove, Jens Zinke, Tim Scheufen, Joseph Maina, Eric Epping,
Wim Boer, Bemahafaly Randriamanantsoa and Geert-Jan A. Brummer

Based on the publication in Biogeosciences Discussions, 9, 3099-3144,
doi:10.5194/bgd-9-3099-2012 (2012)

Abstract

Coral cores provide vital climate reconstructions for site-specific temporal variability in river flow and sediment load. Yet, their ability to record spatial differences across multiple catchments is relatively unknown. Here, we investigate spatial linkages between four coral proxies of terrestrial runoff and their relationships between sites. Coral cores were drilled in and around Antongil Bay, the largest bay in Madagascar, and individually analysed for fifteen years of continuous luminescence (G/B), Ba/Ca, $\delta^{18}\text{O}_{\text{sw}}$ and $\delta^{13}\text{C}$ data. Each coral core was drilled close to individual river mouths (≤ 7 km), and proxy data was compared to modelled river discharge and sediment runoff data for the three corresponding catchments. A reasonable agreement between terrestrial runoff proxies with modelled river discharge and sediment yield was observed. Some inconsistencies between proxy and modelled data we relate to proxy behaviour, watershed size and local environmental physiochemical parameters. In general, the further a coral resided from its river source, the weaker the proxy relationship was with modelled data and other corals, due to mixing gradients and currents. Nevertheless, we demonstrate that two coral Ba/Ca and luminescence (G/B) records influenced by the same watershed are reproducible. Furthermore, a strong Ba/Ca relationship was observed between two cores from distant watersheds, with baseline averages in agreement with modelled sediment runoff data. As humic acids behave conservatively in the water column, luminescence (G/B) data gave the highest regional correlations between cores, and most coherence with site specific modelled discharge. No statistical relationship was observed between cores in terms of interannual $\delta^{18}\text{O}_{\text{sw}}$ and $\delta^{13}\text{C}$, meaning corals were recording a localised signal at their respective sites. Comparing proxy baseline averages and mean seasonal cycles provided a good overview of the runoff dynamics of the bay system.

Introduction

Anthropogenic and climate-induced changes in sediment load entering the coastal realm are of great concern for the sustainability of tropical marine and terrestrial environments (McClanahan and Obura, 1997; McCulloch et al., 2003; Payet and Obura, 2004; Rogers, 1990). Deforestation often leaves soils susceptible to erosion (Agarwal et al., 2005; Green and Sussman, 1990)

thus altering the amount and characteristics of both sediment and leached dissolved components delivered to the coastal ocean (Warrick and Rubin, 2007). Madagascar is an iconic example of the extreme environmental impacts human deforestation and habitat destruction has on soil runoff and land degradation (Green and Sussman, 1990; Harper et al., 2007). It is now estimated that only 10-15% of the original forests remain since extensive deforestation began in the mid 20th century (Green and Sussman, 1990; Harper et al., 2007). Forest protection and management can help stabilise soils within catchment areas, yet requires continuous records of site specific land-use changes, erosion and weather patterns to differentiate between vulnerable and stable areas.

In Madagascar, weather station data are scarce (Dewar and Richard, 2007; Dewar and Wallis, 1999) and satellite derived rainfall data around coastal regions with high cloud cover are often unreliable (Quartly et al., 2007). Previous research efforts in Madagascar have focussed on terrestrial environments, yet an assessment of the status of the coastal marine ecosystems in relation to climatic and anthropogenic stressors is lacking (Goodman and Benstead, 2003; Kremen, 2003). Proxy climate and environmental records preserved in annually-banded massive corals, such as *Porites* spp., can significantly augment the instrumental data that are often too short to identify change in many tropical regions. These massive corals can grow for centuries at relatively fast rates (1 - 2 cm year⁻¹), incorporating trace elements (TE) into the aragonite skeleton according to their relative concentrations in ambient sea water during calcification (Alibert et al., 2003; Jones et al., 2009; Jupiter et al., 2008; Lewis et al., 2007; McCulloch et al., 2003). Such properties make massive corals ideal archives of localised environmental change (e.g. river discharge, sediment load). The down-core analyses of coral proxies in long coral cores can provide information on site-specific temporal variability in river flow and sediment loads influencing corals. Such information can potentially assist in the management of watersheds in Madagascar where instrumental data on water characteristics are lacking. However, the reliability of coral proxies is still debated as cores from the same region can show varying signals (Jones et al., 2009; Lewis et al., 2011; Pfeiffer et al., 2009).

Barium (Ba) is dissolved in the river catchment area and adsorbed to suspended sediments (clay minerals), which are then transported to coastal waters via rivers. As salinities increase, Ba desorbs from the suspended sediment due to the higher ionic strength of seawater. As Ba is diluted by seawater it is thought to follow a conservative mixing pattern (Sinclair and McCulloch, 2004), and thus Ba acts as a tracer for riverine sediment input to the coastal ocean. Accordingly, sediment discharge is reconstructed using Ba/Ca ratios (Alibert et al., 2003; Fleitmann et al., 2007; McCulloch et al., 2003; Sinclair and McCulloch, 2004). However, as estuarine processes, such as phytoplankton uptake and resuspension, can lead to a non-conservative behaviour of Ba (Coffey et al., 1997; Hanor and Chan, 1977), sediment discharge reconstructions can be affected (Sinclair, 2005). Therefore, in some circumstances skeletal Ba/Ca levels may not be directly related to sediment discharge.

Luminescence of the coral skeleton is used as a tracer of temporal variability in river flow. First described by Isdale (1984), the intensity of luminescent lines in corals was thought to be caused by the skeletal incorporation of humic acids (HA) derived from hinterland soils. Subsequent reports indicated that luminescence may also result from changing skeletal densities (Barnes and Taylor, 2001; Barnes and Taylor, 2005). More recently, spectral luminescence scanning (SLS) has shown that both processes contribute to luminescence and that humic acids can be normalised for the effects of changing skeletal density to provide an indicator of humic acid runoff (Grove et al., 2010). As the luminescent emission signal of HA is slightly longer than aragonite, taking the Green/Blue (G/B) ratio gives an estimate of the amount of HA relative to the skeletal density (Grove et al., 2010). SLS resolves density effects associated with luminescence intensities, such as declining trends in intensity with coral age (Jones et al., 2009; Lough, 2011a; Lough, 2011b).

Coral skeletal $\delta^{18}\text{O}$ is a function of both SST and salinity. Calculating the difference between coralline $\delta^{18}\text{O}$ and the sea surface temperature proxy Sr/Ca provides a salinity proxy, $\delta^{18}\text{O}_{\text{seawater}} - (\delta^{18}\text{O}_{\text{sw}})$ (McCulloch et al., 1994; McCulloch et al., 2003; Sinclair and McCulloch, 2004). Indeed, here we propose to couple $\delta^{18}\text{O}$ and Sr/Ca following the method of Ren et al. (2002)

to reconstruct $\delta^{18}\text{O}$ of seawater ($\delta^{18}\text{O}_{\text{sw}}$). Potentially, $\delta^{18}\text{O}_{\text{sw}}$ can identify the coral sites experiencing the lowest and highest salinities. This in turn can enhance our interpretation of the other runoff proxies by factoring in mixing processes.

Coral skeletal $\delta^{13}\text{C}$ is confounded by many vital effects making it difficult to interpret (Grottoli, 2002; Grottoli and Wellington, 1999; Reynaud et al., 2002; Reynaud-Vaganay et al., 2001; Swart et al., 1996). However, there are a number of links to runoff processes, including the $\delta^{13}\text{C}$ composition of DIC and reduction of light associated with river plumes. The DIC of riverine waters is typically more isotopically depleted than seawater $\delta^{13}\text{C}$, caused by the decay of strongly depleted terrestrial vegetation (von Fischer and Tieszen, 1995; Marin-Spiotta et al., 2008; Moyer, 2008; Moyer and Grottoli, 2011). The input of riverine DIC to the coastal ocean will therefore cause depletions in the $\delta^{13}\text{C}$ of ambient seawater DIC and coral skeletons. A reduction in incident light levels may also play a role in determining the skeletal $\delta^{13}\text{C}$ variability (Grottoli, 2002; Grottoli and Wellington, 1999). As sediment and humic acid concentrations increase with runoff, turbidity reduces the incident light reaching benthic communities, including the corals (Larsen and Web, 2009). During photosynthesis the endosymbiotic algae (*Symbiodinium* sp.) preferentially utilize ^{12}C for biomass production, leaving the carbon pool, used by the coral for calcification, enriched in ^{13}C (Reynaud et al., 2002; Reynaud-Vaganay et al., 2001; Swart et al., 1996; Weil et al., 1981). Reduced photosynthesis will reduce the depletion of ^{12}C in the carbon pool and thus the skeletal material will have a lighter $\delta^{13}\text{C}$, yielding an inverse relationship with increasing runoff.

In this study, we collected four coral cores from *Porites* colonies across three watersheds surrounding Antongil Bay in eastern Madagascar. Here, we first examine the reproducibility of the common river runoff proxies Ba/Ca and Luminescence (G/B) at the largest watershed. Secondly, we examine the relationships of four coral proxies indicating river flow, sediment load, salinity and turbidity/DIC (luminescence (G/B), Ba/Ca, $\delta^{18}\text{O}_{\text{sw}}$, $\delta^{13}\text{C}$) for three coral cores located in the same region, yet associated with three separate river systems. We test whether individual proxies reflect a regional river runoff signal, a localised signal or a combination of both. As the temporal

variation of river discharge recorded by corals is a function of the distance from a river source (salinity gradient) and the flow direction, as well as the source input, comparing rivers using corals from different reefs is challenging (Carricart-Ganivet et al., 2007; Jupiter et al., 2008; King et al., 2001; Lough et al., 2002; Prouty et al., 2010). To test how representative proxies are of their corresponding river watersheds, we combine coral proxies and compare results with modeled river discharge and sediment yields.

Materials and Methods

Research Area and Climate Setting

Antongil Bay is located in the NE of Madagascar (Fig. 3.1) covering an area of 2800 km², with a mean depth of 41.5 m and a coastline of 270 km extending 80 km inland (Ersts and Rosenbaum, 2003). Almost all populated areas are located in the northern and western coastal regions of the bay, including the largest urban areas of Maroantsetra and Mananara. Two protected forest areas are found in the vicinity of the bay, the Makira Forest and the Masoala Peninsula National Park. The Makira Forest extends over 4600 km² north of Maroantsetra, and together with the Masoala Peninsula National Park forms one of the largest continuous rain-forest areas remaining in Madagascar (Birkinshaw and Randrianjanahary, 2007). Since the introduction of the National Park there has been a significant reduction in the rate of deforestation, yet it still remains a constant threat to the marine and terrestrial environments (Harper et al., 2007).

One of the largest rivers draining into Antongil Bay is the Antainambalana, running through the Makira Forest Area from a source 1450 m above sea level (Goodman and Ganzhorn, 2004). Its watershed covers an estimated 4000 km² and the river mouth is located in the city of Maroantsetra (Fig. 3.1; Table 3.1). The coral cores MAS1 and MAS3 were collected next to the island Nosy Mangabe, ca. 7 km from the river mouth, on a fringing reef slope and reef flat, respectively, at 4m water depth (Fig. 3.1; Table 3.1). The ANDRA coral core was collected 30 km from MAS1 from the fringing reef slope on the east side of the bay, ca. 7 km from the Ambanizana river mouth, at 4m water depth (Fig. 3.1; Table 3.1). The Ambanizana has a much smaller watershed (ca. 160

km²) and runs southwest towards Antongil Bay through a mountainous region with dense forest cover. Both the Ambanizana and the Antainambalana drain a hinterland that mainly consists of granitic soils (Collins, 2006; Kremen et al., 1999). The IFAHO coral is situated ca. 4.5 km from the mouth of the river Anaovandran (watershed: ca. 180 km²) outside of Antongil Bay (Fig. 3.1; Table 3.1). The river originates from the same mountains as the Ambanizana, but flows eastwards away from Antongil Bay. For the last ca. 11 km it runs through a plain before entering the ocean (Windley et al., 1994 and references therein). The Anaovandran drains a hinterland that consists of granitic soils at high elevations and basaltic rocks that cover the lower elevation partly deforested sedimentary plain (Collins, 2006; Douglas, 1967; Kremen et al., 1999). The IFAHO coral core was collected from the back reef of a fringing reef where direct influence of the open ocean is restricted. All three sampling sites are in the vicinity of marine protected areas.

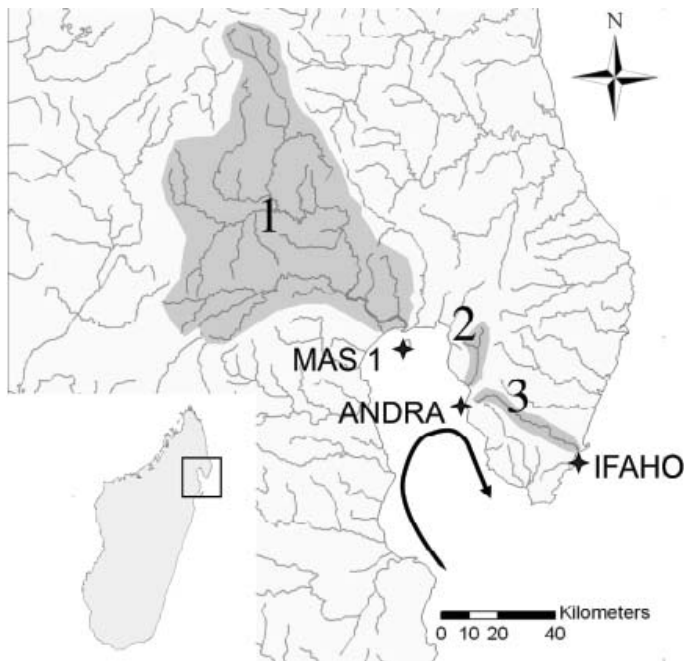


Figure 3.1. Map of Antongil Bay in NE Madagascar showing the three coral sites (stars) and closest rivers with respective watersheds (grey shaded areas). Rivers are marked by the numbers 1 (MAS1, Antainambalana River), 2 (ANDRA, Ambanizana River) and 3 (IFAHO, Anaovandran River). The bay circulation is marked by an arrow indicating a clockwise direction. Please note, MAS3 is located close to MAS1.

The climate in Madagascar can be divided into a August-December cold-dry season and a January-July warm-wet season (Fig. 3.2). Air temperatures peak in December and January and are lowest between July and September (Kremen, 2003). The sea surface temperature (SST) peaks between December and April, reaching maximum average temperatures of 28.5°C (Fig. 3.2). Highest rainfall occurs between January and March, while lowest rainfall occurs between September and November (Xie and Arkin, 1996). Average rainfall levels reach 300 mm/month during the wet season (January to March) and 50 mm/month in the dry season. Average peak river discharge occurs between January and April. River discharge decreases but continues until September, reaching lows in October and November (Fig. 3.2).

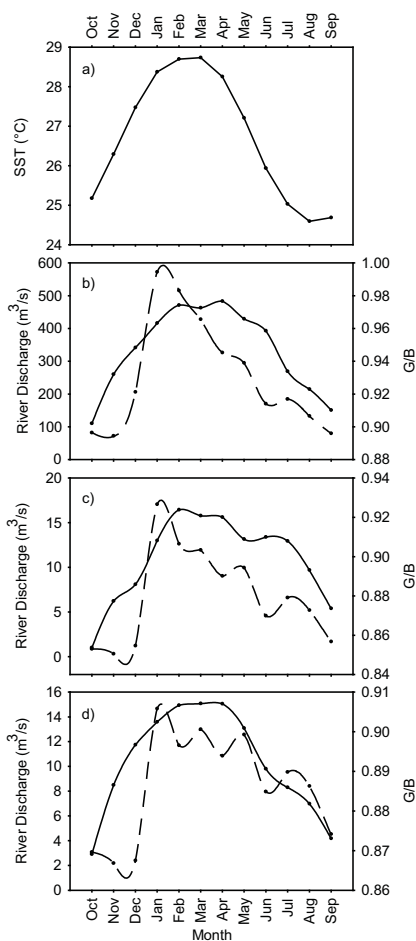


Figure 3.2. Average seasonal cycle of SST (a) (ERSST; Smith et al. 2008) for Antongil Bay (52°E, 16°S) calculated by averaging every month over a 15 year period (1991 – 2005). Similarly, over the same 15 year period the average seasonal G/B (solid line) and modelled river discharge data (dashed line) are calculated for the corals (a) MAS1, (b) ANDRA and (c) IFAHO and their closest respective rivers (a) the Antainambalana River, (b) the Ambanizana River and (c) the Anaovandran River.

Coral Sampling

Coral cores were drilled from massive colonies of *Porites* spp. at depths between 4 – 6 m at different locations in and around Antongil Bay, NE Madagascar (Fig. 3.1 and Table 3.1) during March and April 2007. A commercially available pneumatic drill (Rodcraft 4500) was used to extract 4 cm diameter cores along the central growth axis of the colony. In contrast to the results of Matson (2011), drill holes were not plugged as algal growth was observed on the concrete plugs from earlier drilling campaigns. Drill holes closed by natural coral growth within 2 years when left. Cores were sectioned lengthwise into 7 mm thick slabs, rinsed several times with demineralised water, blown with compressed air to remove any surficial particles and dried for more than 24 hours in a laminar flow hood. Annual density bands were visualised by X-radiograph-positive prints, and the growth axis of the coral slab was defined as the line perpendicular to these bands. The average growth rate of all four coral cores was approximately $13 \pm 2 \text{ mm y}^{-1}$ (Grove et al., 2010 and Table 3.1). With a diamond coated drill, subsamples were taken every 1 mm parallel to the growth axis, equivalent to approximately monthly resolution. All coral slabs were cleaned with sodium hypochlorite (NaOCl, 10-13% reactive chloride; Sigma-Aldrich Company) for 24 hours, after subsampling for geochemistry, to remove residual organics that might quench luminescence.

Coral Core	Location	Distance to closest river source (km)	Average Growth Rate (mm/yr)	Core length (cm)
MAS1	S 15°30,566 E 49°45,437	7 Antainambalana	11.8	121
MAS3	S 15°30,578 E 49°45,456	7 Antainambalana	11.1	143
ANDRA	S 15°41,17 E 49°57,419	7 Ambanizana	12.7	120
IFAHO	S 15°51,968 E 50°18,73	4.5 Anaovandran	14.1	38

Table 3.1. Coral cores with GPS co-ordinates, growth rates, total core length, distance and name to the closest river source.

Coral Luminescence

SLS was performed, as described by Grove et al. (2010), on bleached coral slabs using a line-scan camera fitted with a Dichroic beam splitter prism, separating light emission intensities into three spectral ranges; blue (B), green (G) and red (R). The four coral cores used for this study were also analysed in the study of Grove et al. (2010) to test the SLS technique. Digital core images were analysed with the Line Scan Software Version 1.6 (Avaatech), providing RGB intensity values for individual pixels of 71 μm in length. Since the spectral emissions of humic acids are slightly longer than aragonite, spectral G/B ratios reflect the changing humic acid/aragonite ratios within the coral skeleton (Grove et al., 2010). Indeed, results indicated a significant correlation on monthly and mean annual time scales between G/B and Ba/Ca (measured using LA-ICP-MS) for the coral core MAS1, and for G/B between cores MAS1, MAS3 and ANDRA (Grove et al. 2010). The G/B datasets for the four corals applied in this study all begin in January 1991 and end in December 2005, spanning a total of 15 years.

Coral Geochemistry

Coral Sr/Ca and Ba/Ca were analysed for MAS1, ANDRA and IFAHO by high resolution Inductively Coupled Plasma Mass Spectrometry (HR-ICP-MS; Thermo Scientific Element-2) equipped with a double spray chamber and Teflon microflow nebulizer. Ba/Ca ratios were quantified using the ICP-MS intensity ratio calibration method of Rosenthal et al. (1999). Accuracy of Sr/Ca and Ba/Ca was confirmed by an inter-laboratory comparison with Cambridge University (Fallet et al., 2009). The analytical internal precision was <0.1% relative standard deviation (RSD) for Sr/Ca, and <0.5% RSD for Ba/Ca.

Laser Ablation Inductively Coupled Mass Spectrometry (LA-ICP-MS) analytical methods were identical to those reported in Jupiter et al (2008). The coral slabs of cores MAS1 and MAS3 were mounted on a stage containing standards and analysed using a Varian 820 inductively coupled mass spectrometer. The resultant data were normalised to ^{43}Ca using a Varian Laser Scanning analysis software program developed at the Australian National

University (ANU) Research School of Earth Sciences (by L. Kinsley). Data were first smoothed using a 10 point running mean to reduce the influence of outliers, followed by a 10 point mean to reduce data volume. Further details on the methodology are available in Jupiter et al. (2008). The Ba/Ca (LA-ICP-MS) datasets for the two corals MAS1 and MAS3 begin in January 1991 and end in December 2005, spanning a total of 15 years.

To measure the skeletal $\delta^{18}\text{O}$ and $\delta^{13}\text{C}$, approximately 80 μg of coral powder was reacted with H_3PO_4 in an automated carbonate reaction device (Kiel IV) connected to a Finnigan MAT 253 mass spectrometer at the Royal Netherlands Institute for Sea Research (NIOZ). For the NBS19 carbonate standard we obtained values of $-2.21 \pm 0.08\text{‰}$ and $1.96 \pm 0.037\text{‰}$ for $\delta^{18}\text{O}$ and $\delta^{13}\text{C}$, respectively, relative to the Vienna PeeDee Belemnite (V-PDB) standard. Solution ICP-MS Ba/Ca, Sr/Ca and stable isotope datasets for the three corals MAS1, ANDRA and IFAHO all begin in January 1991 and end in December 2005, spanning a total of 15 years.

To calculate $\delta^{18}\text{O}_{\text{seawater}}$ ($\delta^{18}\text{O}_{\text{sw}}$), we follow the method of Ren et al. (2002). The method assumes that coral Sr/Ca is solely a function of SST and that coral $\delta^{18}\text{O}$ is a function of both SST and $\delta^{18}\text{O}_{\text{sw}}$. This method separates the effects of $\delta^{18}\text{O}_{\text{sw}}$ from SST by breaking the instantaneous changes of coral $\delta^{18}\text{O}$ into separate contributions by instantaneous SST and $\delta^{18}\text{O}$ changes, respectively. We use a $\delta^{18}\text{O}_{\text{coral}}$ -SST relationship of $-0.2\text{‰}/^\circ\text{C}$ (Juilliet-Leclerc and Schmidt, 2001) and the Sr/Ca-SST relationship of $-0.06 \text{ mmol/mol}/^\circ\text{C}$ (Corrège, 2006) to calculate the instantaneous changes in SST.

Hydrological Modelling

Due to a lack of hydrological data for Madagascar, we simulated river discharge and sediment yield in Antongil Bay regional watersheds using a grid-based spatial water balance model. We used STREAM (Spatial Tools for River basins, Environment and Analysis of Management options), a distributed hydrological model, to simulate monthly river discharge (Aerts et al., 1999; Aerts and Bouwer, 2002). STREAM simulates the water balance for each grid (50 km resolution) using a limited number of parameters, including spatial-temporal precipitation and temperature trends, elevation, land-cover

and soil water storage capacity specific to Madagascar (Aerts and Bouwer, 2002). The STREAM model has been successfully applied in various climate and hydrological studies (e.g. Bouwer et al., 2006; Winsemius et al., 2006), which have shown that a monthly time step is sufficient for detecting decadal, inter-annual and seasonal hydrological cycles. Here, we extracted the average seasonal cycle in river discharge for the three rivers studied and the average yearly river discharge per catchment (Maina et al., 2012).

Sediment yield per unit area was computed using the Non-Point Source Pollution and Erosion Comparison Tool (N-SPECT) developed by the National Oceanic and Atmospheric Administration (NOAA) (<http://www.csc.noaa.gov/digitalcoast/tools/nspect/index.html>). N-SPECT combines data on elevation, slope, soils, precipitation, and land cover to derive estimates of runoff, erosion, and pollutant sources (nitrogen, phosphorous, and suspended solids) from across the landscape, as well as estimates of sediment and pollutant accumulation in stream and river networks. Erosion rates and sediment loads were calculated using the Revised Universal Soil Loss Equation (RUSLE) and Modified Universal Soil Loss Equation (MUSLE) (Wischmeier and Smith, 1978). N-SPECT provides annual mean (January – December) estimates of sediment yield per unit area in mt/year at a 50 km resolution. Here, we extracted the average yearly river sediment yield per catchment (Maina et al., 2012).

Coral Age Model Construction

Coral chronologies were based on the seasonal cycle of Ba/Ca and G/B ratios. Luminescence in corals has previously been used to cross date core records (Grove et al., 2010; Hendy et al., 2003) and assist in establishing a chronology for growth and geochemical tracers (Cole et al., 2000; Fleitmann et al., 2007; Smithers and Woodroffe, 2001). In Antongil Bay, the driest month on average in a given year is October (Kremen, 2003). Consequently Ba/Ca and G/B minima were assigned to October (Fig. 3.2), creating consistent age models for all cores. All years were then interpolated linearly between the October anchor points using AnalySeries 2.0 (Paillard et al., 1996). This resulted in a time scale of monthly resolution with 12 equidistant data points.

The mean seasonal cycle of Ba/Ca, G/B, $\delta^{18}\text{O}_{\text{sw}}$ and $\delta^{13}\text{C}$ for each core were constructed by calculating the monthly mean over the 15 year record length. Comparing the mean seasonal cycle of G/B with the mean seasonal cycle of modelled river discharge for each of the three individual watersheds indicates that there is good agreement between the two data in terms of temporal alignment (Fig. 3.2). This gives us confidence in our age model for each of the coral core records.

Seawater Analyses

We established the local salinity- $\delta^{18}\text{O}$ relationship from a set of water samples to subsequently reconstruct salinity from coral skeletal $\delta^{18}\text{O}_{\text{sw}}$, as derived from coupled coral Sr/Ca and $\delta^{18}\text{O}$ measurements (Ren et al., 2002). We obtained the seawater $\delta^{18}\text{O}$ and salinity for seven water samples collected in October 2008, representing the dry season, and a further sample taken in March 2007, capturing the wet season signal. The seven samples were collected along an inshore-offshore gradient between the mouth of the river Antainambalana and the MAS1 coral. The salinity of each water sample, taken in pre-cleaned 1 litre HDPE bottles, was measured with a hand-held probe (Vernier) and a fraction was stored in air-tight 100 ml glass bottles. All water samples were subsequently poisoned with HgCl_2 to prevent biological activity. Samples were then analysed for $\delta^{18}\text{O}$ on a Thermo Finnigan Delta+ mass spectrometer equipped with a GASBENCH-II preparation device at the VU Amsterdam. A 0.5 - 1ml water sample was injected through the septum cap of a 10 ml exetainer vial filled with a mixture of He and 0.2% CO_2 to equilibrate with the oxygen in the headspace CO_2 for 24 hours at 22°C. Subsequently, the headspace mixture is transported by a He carrier flow (dehydrated using NAFION tubing) for analysis of CO_2 in the mass spectrometer after gas separation in a GC column. Values are reported as $\delta^{18}\text{O}$ vs. V-SMOW with a long-term reproducibility better than 0.1‰ (1SD) for a routinely analysed lab water standard.

Results

The results section begins with a comparison of Ba/Ca and G/B variability between cores from a single site to assess proxy reproducibility. Next, we compare the variability of four proxies at three different locations to assess regional similarities. This section also includes a detailed description of the seasonal cycles and baseline averages of individual proxies. At the end of the results section we present hydrological model data for river discharge and sediment yield, to test how well corals directly record river runoff for the three rivers influencing our corals.

Proxy	MAS1 vs. MAS3	MAS1 vs. ANDRA	MAS1 vs. IFAHO	ANDRA vs. IFAHO
G/B	0.74 (P < 0.001)*	0.67 (P < 0.001)*	0.66 (P < 0.001) *	0.56 (P < 0.001)*
Ba/Ca	0.71 (P < 0.001)*	0.071 (P = 0.35)	0.49 (P < 0.001) *	0.095 (P = 0.21)
$\delta^{18}\text{O}_{\text{sw}}$	-	0.12 (P = 0.11)	0.17 (P = 0.022) *	0.046 (P = 0.54)
$\delta^{13}\text{C}$	-	0.0052 (P = 0.94)	0.097 (P = 0.19)	0.052 (P = 0.49)

Proxy	MAS1 vs. MAS3	MAS1 vs. ANDRA	MAS1 vs. IFAHO	ANDRA vs. IFAHO
G/B	0.67 (P = 0.007)*	0.69 (P = 0.005)*	0.50 (P = 0.056)	0.63 (P = 0.013)*
Ba/Ca	0.88 (P < 0.001)*	0.37 (P = 0.17)	0.66 (P = 0.008)*	0.27 (P = 0.32)
$\delta^{18}\text{O}_{\text{sw}}$	-	0.28 (P = 0.32)	0.41 (P = 0.13)	0.014 (P = 0.96)
$\delta^{13}\text{C}$	-	0.12 (P = 0.68)	0.15 (P = 0.60)	0.32 (P = 0.25)

Table 3.2. Correlation coefficients of seasonal (upper) and annual average (lower) coral proxy data between the three coral sites MAS1, ANDRA and IFAHO, and LA-ICP-MS data for MAS1 and MAS3. Significance levels are given in parentheses, and correlation coefficients, which are below the significance level of 0.05, are marked with a star (*). The annual average proxy values were calculated by averaging the months January to December for which the highest between core correlations were found. We did not average the wet year months (i.e. October to September) as comparisons with modelled data would have been limited.

Seasonal and interannual variability of Ba/Ca and G/B between cores associated with the Antainambalana watershed

For the common period of 1991 to 2005, interannual variations in Ba/Ca and G/B, for the cores MAS1 and MAS3, were compared in order to test their reproducibility (Table 3.2). For Ba/Ca, we measured both cores with LA-ICP-MS (LA-) and replicated MAS1 with solution ICP-MS on a monthly resolution. The mean Ba/Ca between cores and techniques differed, with MAS3 having the lowest baseline of $5.51 \pm 0.71 \mu\text{mol/mol}$. The mean

Ba/Ca measured by LA- and solution ICP-MS for MAS1 were 6.05 ± 0.75 $\mu\text{mol/mol}$ and 6.75 ± 0.78 $\mu\text{mol/mol}$, respectively, with standard deviations (1σ) overlapping (Table 3.3). The interannual variations between cores were highly reproducible and statistically significant ($>95\%$), with annual mean MAS1 and MAS3 LA-ICP-MS Ba/Ca sharing 78% of the variance (Fig. 3.3). MAS1 LA- and solution ICP-MS data shared 52% of the variance.

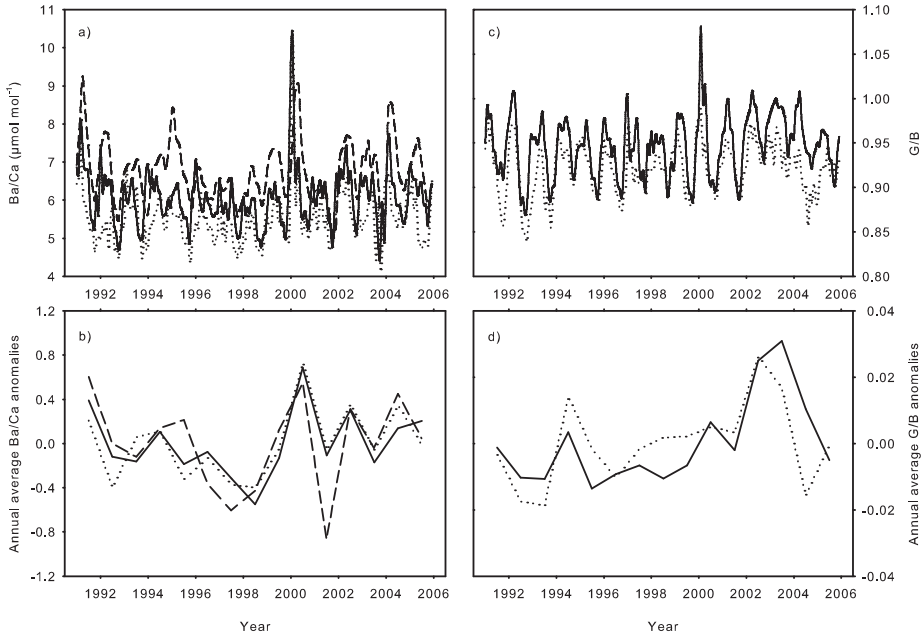


Figure 3.3. The three monthly Ba/Ca (left) profiles and two G/B (right) profiles between January 1991 and December 2005, signifying proxy reproducibility in both seasonality and interannual variability. The three Ba/Ca profiles (a and b) include LA- MAS1 (solid), LA-MAS3 (dotted) and solution ICP-MS MAS1 (dashed). The two G/B profiles (c and d) include MAS1 (solid) and MAS3 (dotted). Absolute values are shown for Ba/Ca and G/B in the upper plots (a and c, respectively), and annual anomalies for both Ba/Ca and G/B are shown in the lower plots (b and d, respectively).

The interannual variations in G/B profiles for MAS1 and MAS3 for the period 1991 to 2005 were also reproducible (Fig. 3.3; Table 3.2). Seasonally, the two cores shared 90% of the variance, and on annual means 45%; all statistically significant at the 95% level. The mean G/B between MAS1 (0.95 ± 0.03) and MAS3 (0.92 ± 0.03) differed, yet their standard deviations overlapped (Table 3.3). Similar to Ba/Ca, MAS3 showed the lowest baseline

level in G/B. We therefore note that both Ba/Ca and G/B are reproducible between cores from the largest watershed in Antongil Bay.

MAS1	Mean	SD	Range	Max	Min
G/B	0.95	0.03	0.21	1.08	0.87
Ba/Ca ($\mu\text{mol mol}^{-1}$) – HR-ICP-MS	6.75	0.78	4.20	9.26	5.06
Ba/Ca ($\mu\text{mol mol}^{-1}$) – LA-ICP-MS	6.05	0.75	5.56	10.06	4.50
$\delta^{18}\text{O}_{\text{sw}}$ (‰)	-0.50	0.40	1.79	0.26	-1.53
Reconstructed salinity (psu)	25.54	2.93	13.25	31.17	17.92
$\delta^{13}\text{C}$ (‰)	-3.01	0.58	2.83	-1.89	-4.72

MAS3	Mean	SD	Range	Max	Min
G/B	0.92	0.03	0.15	0.98	0.84
Ba/Ca ($\mu\text{mol mol}^{-1}$) – LA-ICP-MS	5.51	0.71	5.69	9.88	4.19

ANDRA	Mean	SD	Range	Max	Min
G/B	0.90	0.03	0.16	0.98	0.82
Ba/Ca ($\mu\text{mol mol}^{-1}$) – HR-ICP-MS	3.80	0.58	3.61	6.38	2.71
$\delta^{18}\text{O}_{\text{sw}}$ (‰)	0.17	0.28	1.53	0.82	-0.72
Reconstructed salinity (psu)	30.55	2.07	11.37	35.33	23.96
$\delta^{13}\text{C}$ (‰)	-3.33	0.65	2.76	-2.01	-4.77

IFAHO	Mean	SD	Range	Max	Min
G/B	0.89	0.018	0.09	0.94	0.85
Ba/Ca ($\mu\text{mol mol}^{-1}$) – HR-ICP-MS	5.42	0.28	1.39	6.21	4.81
$\delta^{18}\text{O}_{\text{sw}}$ (‰)	-0.27	0.20	1.07	0.21	-0.86
Reconstructed salinity (psu)	27.26	1.50	7.91	30.80	22.89
$\delta^{13}\text{C}$ (‰)	-2.83	0.45	2.79	-2.09	-4.88

Table 3.3. Statistical description of coral proxy data for MAS1 (upper), MAS3 (middle upper), ANDRA (middle lower) and IFAHO (lower). The mean, standard deviation (SD), range, maximum value (Max) and minimum value (Min) were calculated from the monthly interpolated data spanning January 1991 till December 2005 (15 years). The proxy data include G/B, Ba/Ca (two methods), $\delta^{18}\text{O}_{\text{sw}}$, $\delta^{13}\text{C}$ and reconstructed salinity based on the $\delta^{18}\text{O}_{\text{sw}}$ (Fig. 3.7).

Seasonal and interannual variability of four river runoff proxies associated with three individual watersheds

Here, we compare G/B profiles and geochemical data for three coral cores associated with three individual watersheds across Antongil Bay. Geochemical data was measured on splits of the same powdered coral samples representing approximately 1 month of growth for individual cores. The three cores, MAS1, ANDRA and IFAHO, showed strong seasonal cycles in the

monthly G/B time series for the 15 year period studied, from January 1991 to December 2005 (Fig. 3.4). Similarly, strong seasonal cycles were observed in the monthly Ba/Ca time series of MAS1 and IFAHO, yet the seasonal cycles of ANDRA were not as clearly defined (Fig. 3.4). The $\delta^{18}\text{O}_{\text{sw}}$ and $\delta^{13}\text{C}$ seasonal cycles of MAS1 were both strong and well defined (Figs. S3.1 and S3.2). However, in ANDRA and IFAHO the $\delta^{18}\text{O}_{\text{sw}}$ and $\delta^{13}\text{C}$ seasonal cycles were less defined yet showed strong variability (Figs. S3.1 and S3.2).

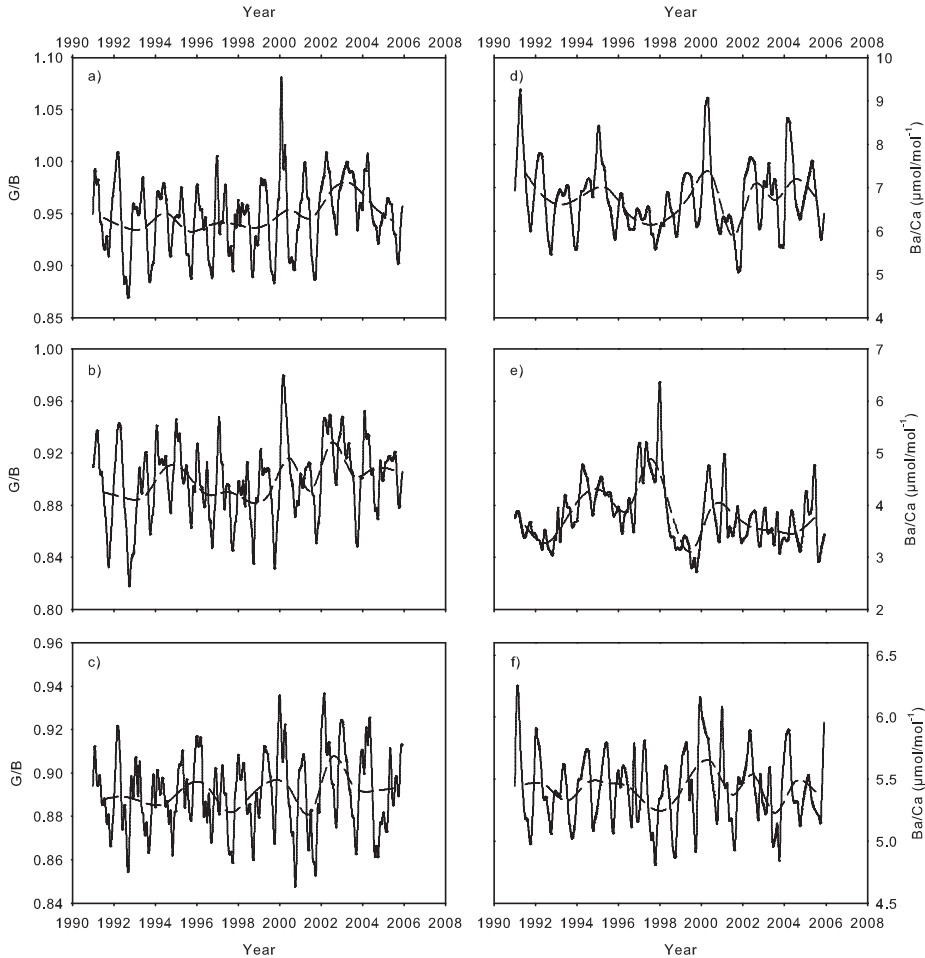


Figure 3.4. Monthly G/B (a, b and c) and Ba/Ca (d, e and f) time-series over the 15 year period between 1991 and 2005 for the three corals MAS1 (a and d), ANDRA (b and e) and IFAHO (c and f). The annual average (dashed line) G/B (a, b and c) and Ba/Ca (d, e and f) values were calculated by averaging the months January to December for each of the 15 years.

For annual averages, luminescence (G/B) showed the highest spatial correlations between the three cores/regions for the 15 year period out of all proxies studied ($n = 15$). ANDRA luminescence was statistically correlated with both MAS1 ($R = 0.69$; $P = 0.005$) and IFAHO ($R = 0.63$; $P = 0.013$) (Table 3.2). The relationship between MAS1 and IFAHO luminescence was strong ($R = 0.50$; $P = 0.056$), yet, just outside of the significance level ($P > 0.05$). This relationship was significant, however, when considering the seasonal data (Table 3.2).

Conversely, the strongest and only statistically significant annual average Ba/Ca relationship was between cores MAS1 and IFAHO ($R = 0.66$; $P = 0.008$) (Table 3.2). ANDRA Ba/Ca showed a weaker relationship with both MAS1 ($R = 0.37$; $P = 0.17$) and IFAHO ($R = 0.27$; $P = 0.32$), which were not significant (Table 3.2).

The strongest relationship between average annual $\delta^{18}\text{O}_{\text{sw}}$ values was again between MAS1 and IFAHO ($R = 0.41$; $P = 0.13$), yet not significant (Table 3.2). This relationship was significant, however, when considering the seasonal data (Table 3.2). The correlation coefficients of ANDRA $\delta^{18}\text{O}_{\text{sw}}$ with MAS1 and IFAHO $\delta^{18}\text{O}_{\text{sw}}$ were lower and not significant (Table 3.2).

The strongest relationship between average annual $\delta^{13}\text{C}$ values was between ANDRA and IFAHO ($R = 0.32$; $P = 0.25$), yet not significant (Table 3.2). The correlation coefficients of MAS1 $\delta^{13}\text{C}$ with ANDRA and IFAHO $\delta^{13}\text{C}$ were both lower and also not significant (Table 3.2).

Luminescence (G/B) seasonal cycles and baseline averages

Comparing the 15 year time series of all three G/B records revealed differences in baseline values and signal amplitudes (Fig. 3.5a). MAS1 G/B had the highest mean value and standard deviation (0.95 ± 0.034) compared to ANDRA (0.90 ± 0.029) and IFAHO (0.89 ± 0.018) (Table 3.3). Moreover, ANDRA and IFAHO had similar mean values. However, the signal amplitude of ANDRA was far greater than IFAHO (Fig. 3.5a). During the dry season ANDRA G/B was below IFAHO G/B, yet during the wet season ANDRA G/B was higher. This is further highlighted by the mean seasonal cycles of

G/B for the three cores (Fig. 3.6). Here, it becomes clear that the MAS1 G/B signal was far higher than both the ANDRA and IFAHO G/B signals for the entire calendar year, while the ANDRA G/B signal overtakes the IFAHO G/B signal during the wet season. Standard deviations indicate the variability of each site over the 15 year period (Fig. 3.6), with MAS1 G/B overlapping ANDRA (not IFAHO) only in four out of twelve calendar months. Three of those four months were in the dry season.

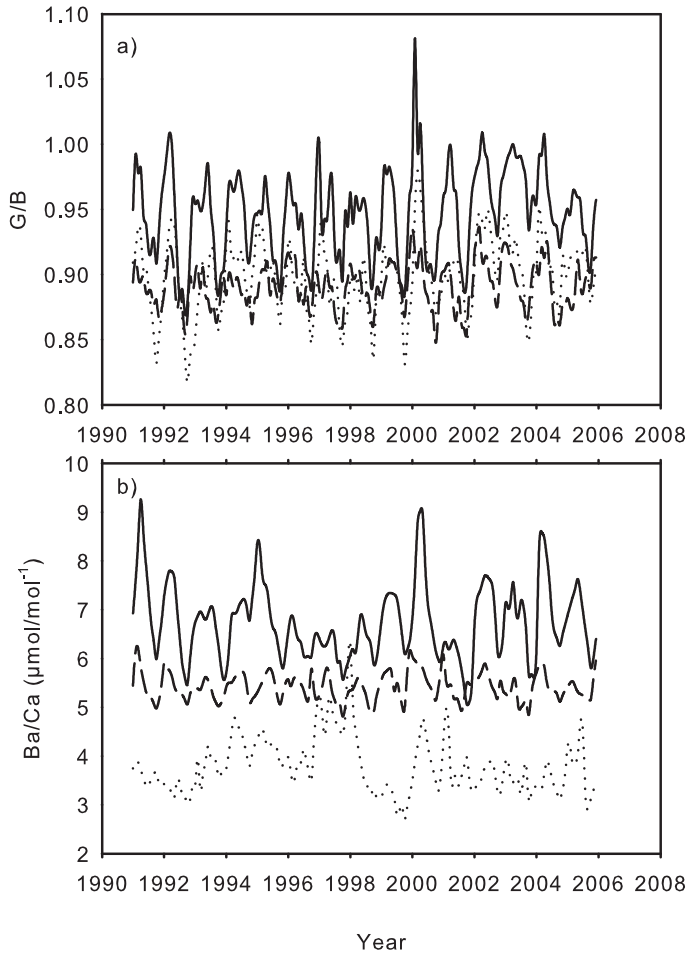


Figure 3.5. Cross-core comparison of monthly G/B (a) and Ba/Ca (b) absolute values for the complete 15 year time-series of the three cores MAS1 (solid), ANDRA (dotted) and IFAHO (dashed).

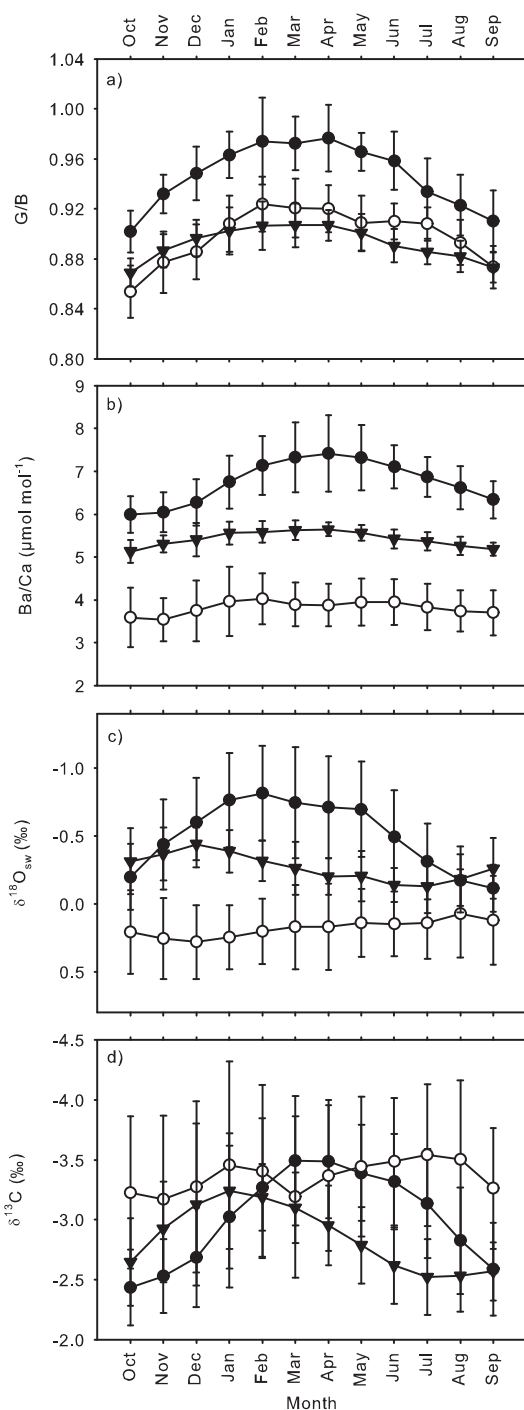


Figure 3.6. Monthly averaged G/B (a), Ba/Ca (b), $\delta^{18}\text{O}_{\text{sw}}$ (c) and $\delta^{13}\text{C}$ for MAS1 (solid circles), ANDRA (open circles) and IFAHO (triangles), indicating the average seasonal cycles. Monthly averages were calculated for the 15 year period spanning January 1991 till December 2005. The standard deviations for individual months are given as error bars. The $\delta^{18}\text{O}_{\text{sw}}$ and $\delta^{13}\text{C}$ are given relative to V-PDB.

Ba/Ca seasonal cycles and baseline averages

The most noticeable contrast between the G/B and Ba/Ca time series was in their respective baseline averages (Fig. 3.5b). Although the MAS1 Ba/Ca mean value ($6.75 \pm 0.78 \mu\text{mol/mol}$) was highest of the three records, similar to the results of G/B, a significant difference between the mean Ba/Ca values of ANDRA and IFAHO was observed (Fig. 3.5b and Table 3.3). The mean IFAHO Ba/Ca value ($5.42 \pm 0.28 \mu\text{mol/mol}$) was significantly higher than ANDRA ($3.80 \pm 0.58 \mu\text{mol/mol}$), despite the higher range and variability of ANDRA (Table 3.3). This contrast in results is further emphasised when comparing the mean seasonal cycles of the three Ba/Ca records (Fig. 3.6). Only in November and December was there an overlap in standard deviations between MAS1 and IFAHO (Fig. 3.6). All ANDRA monthly Ba/Ca values were significantly below the Ba/Ca values of IFAHO. Further, a small decrease was observed in the Ba/Ca signal of ANDRA, which occurred between February and May (during the wet season). This was not the case for MAS1 or IFAHO (Fig. 3.6).

$\delta^{18}\text{O}_{\text{sw}}$ seasonal cycles and baseline averages

Measuring the salinity and $\delta^{18}\text{O}$ of seawater samples, we established a regional regression equation and applied it to transform coral derived $\delta^{18}\text{O}_{\text{sw}}$ values into reconstructed salinities (Fig. 3.7). The core with the most negative mean $\delta^{18}\text{O}_{\text{sw}}$ value ($-0.50 \pm 0.39 \text{‰}$) was MAS1 (Table 3.2). When converting the skeletal $\delta^{18}\text{O}_{\text{sw}}$ signal, the mean reconstructed salinity of MAS1 equated to $25.54 \pm 2.93 \text{ psu}$ (Table 3.3). IFAHO had a mean $\delta^{18}\text{O}_{\text{sw}}$ value of $-0.27 \pm 0.20 \text{‰}$, which equated to a mean reconstructed salinity of $27.26 \pm 1.50 \text{ psu}$ (Table 3.3). The most positive mean $\delta^{18}\text{O}_{\text{sw}}$ value was ANDRA ($0.17 \pm 0.28 \text{‰}$), equating to the highest mean reconstructed salinity of $30.55 \pm 2.07 \text{ psu}$ (Table 3.3). The standard deviations given for the mean $\delta^{18}\text{O}_{\text{sw}}$ seasonal cycles of MAS1 and IFAHO overlap in every month with the exception of February (Fig. 3.6). Both showed a mean seasonal $\delta^{18}\text{O}_{\text{sw}}$ cycle decreasing during the wet season and increasing during the dry season (albeit IFAHO values start to increase earlier than MAS1) (Fig. 3.6). However, this is not the case for ANDRA, which showed a reverse mean seasonal cycle whereby $\delta^{18}\text{O}_{\text{sw}}$ values increased during the wet season and decreased during the dry

season (Fig. 3.6). Moreover, during the months November to February there was no overlap of standard deviations between IFAHO and ANDRA as the $\delta^{18}\text{O}_{\text{sw}}$ values of IFAHO were significantly more negative than ANDRA (Fig. 3.6).

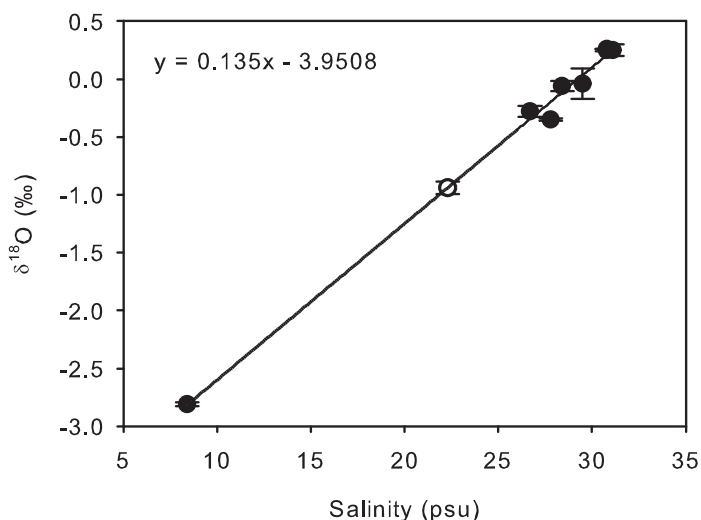


Figure 3.7. Calibration of the $\delta^{18}\text{O}$ of water samples with salinity measurements used to reconstruct salinity from coral $\delta^{18}\text{O}_{\text{sw}}$. All data points are given as averages of two samples taken during the dry season (solid circles) and wet season (open circle). The standard deviation is given as error bars.

$\delta^{13}\text{C}$ seasonal cycles and baseline averages

Core ANDRA gave the most negative mean $\delta^{13}\text{C}$ signal, being -3.33 ± 0.65 ‰ (Table 3.3). The core with the most positive mean $\delta^{13}\text{C}$ signal was IFAHO (-2.83 ± 0.45 ‰), whereas MAS1 measured -3.01 ± 0.58 ‰ (Table 3.3). All cores showed high variability over the 15 year period (Table 3.3). Moreover, the monthly standard deviations given for the $\delta^{13}\text{C}$ mean seasonal cycles indicate that individual $\delta^{13}\text{C}$ baseline values were statistically similar over the 15 years (Fig. 3.6 and Table 3.3). Further, the mean seasonal cycles were inconsistent between cores as both IFAHO and MAS1 showed a depleted $\delta^{13}\text{C}$ signal during the wet season and an enrichment during the dry season (albeit IFAHO again enriched earlier than MAS1), whereas, ANDRA showed a bimodal cycle (Fig. 3.6).

Hydrological model data

River discharge

The river with the highest modelled discharge was the Antainambalana, associated with coral MAS1, which had a mean discharge rate of $255.42 \pm 91.79 \text{ m}^3 \text{ s}^{-1}$ (Table 3.4). The rivers Ambanizana and Anaovandran, associated with corals ANDRA and IFAHO, respectively, had a statistically similar modelled discharge rate, however, of significantly lower magnitude to the river Antainambalana (Table 3.4). Nevertheless, the mean discharge rate of the Anaovandran ($8.22 \pm 4.74 \text{ m}^3 \text{ s}^{-1}$) was slightly higher than the Ambanizana ($6.76 \pm 3.95 \text{ m}^3 \text{ s}^{-1}$). This order of relative discharge rate between the three rivers was similar to the proxy results of G/B (Fig. 3.6).

River discharge ($\text{m}^3 \text{ s}^{-1}$)	Mean	SD	Range	Max	Min
Antainambalana	255.42	91.79	435.37	528.79	93.42
Ambanizana	6.76	3.95	18.55	19.43	0.88
Anaovandran	8.22	4.74	21.79	23.42	1.63

Sediment runoff (kg yr^{-1})	Mean	SD	Range	Max	Min
Antainambalana	1.10×10^9	0.39×10^9	1.36×10^9	2.03×10^9	6.78×10^8
Ambanizana	1.72×10^8	9.73×10^7	3.35×10^8	3.88×10^8	5.35×10^7
Anaovandran	9.31×10^6	4.57×10^6	1.76×10^7	2.24×10^7	4.83×10^6

Table 3.4. Statistical description of modelled river discharge (upper) and sediment yield (lower) data for the three river catchments Antainambalana, Ambanizana and Anaovandran; the closest rivers to corals MAS1, ANDRA and IFAHO, respectively. The mean, standard deviation (SD), range, maximum value (Max) and minimum value (Min) are calculated from the mean annual data spanning 15 years (1991 – 2005).

Sediment runoff

The river with the highest modelled sediment runoff was the Antainambalana associated with coral MAS1, which also recorded the highest Ba/Ca values (Fig. 3.6b and Table 3.4). However, unlike the modelled discharge data, there was a significant difference between the modelled sediment runoff of the two other rivers (Table 3.4). The modelled sediment runoff for the river Ambanizana, associated with coral ANDRA was significantly higher

than for the river Anaovandran, associated with the coral IFAHO (Table 3.4). The relative order of sediment runoff rates between the rivers ANDRA and IFAHO is opposite to those of the Ba/Ca results, as ANDRA Ba/Ca values were lowest (Fig. 3.6b).

Discussion

Reproducibility of Ba/Ca and G/B between cores from the same watershed

We demonstrate that two coral cores from the same watershed in Antongil Bay share a significant amount of interannual variation in both Ba/Ca and G/B (Fig. 3.3). This indicates that both of these terrestrial runoff proxies respond to a common environmental signal. These results are in agreement with previous analyses, in which G/B signals were compared between the coral cores MAS1 and MAS3 (Grove et al., 2010). Grove et al. (2010) used 100 years of G/B data, which revealed an even higher correlation than for the 15 year period considered here. A comparison of Ba/Ca and G/B was only performed for core MAS1, which showed a significant correlation for annual mean values (Grove et al., 2010).

Here, we replicated Ba/Ca for a second core (MAS3) and can confirm that interannual variations for this particular watershed are reproducible (Fig. 3.3). This agrees with similar studies from adjacent watersheds in the Great Barrier Reef (GBR), where Ba/Ca profiles showed significant correlations between cores (Alibert et al., 2003). Slight offsets in mean Ba/Ca and G/B signals between MAS1 and MAS3 are most likely related to different hydrodynamic regimes of flood plume currents between the reef slope (MAS1) and reef flat (MAS3) sites along the Nosy Mangabe island fringing reef. Similar small-scale differences in terrestrial runoff proxies have been observed for GBR catchments related to ‘island wake’ effects (Jupiter et al., 2008; Lewis et al., 2011).

The differences in absolute values observed between LA- Ba/Ca and solution ICP-MS Ba/Ca in MAS1 are likely related to 1) time averaging in monthly milled samples compared to sub-weekly LA- data and/or 2) differences between standards used to correct absolute values in Ba/Ca

between measurement techniques (Fig. 3.3). However, the relative changes in Ba/Ca do share 52% of the variability between different techniques and the main sediment runoff spikes were reproducible, i.e. years 1991, 2000.

Spatial linkages between coral proxies of terrestrial runoff across Antongil Bay

Proxy validation is a common problem in coral palaeoclimatology, as long-term *in situ* data are rarely available (Jones et al., 2009). Lower resolution data are often applied as a substitute to calibrate proxies, i.e. satellite and model data (Corrège, 2006; Quartly et al., 2007; Reynolds et al., 2002). In this study, luminescence was the only proxy to show a near significant relationship between all three corals. Therefore, for the majority of proxies, localised differences were likely more dominant than the regional climate signal expressed in the values. To best understand these differences between river signals at individual corals and at their respective river mouths we compared our proxy data with hydrological model data. Although not ideal, the model data give a good indication of both sediment yield and river discharge for the three watersheds studied.

A strong relationship was observed between annual average G/B of the three coral cores MAS1, ANDRA and IFAHO, suggesting that corals are recording a regional signal likely reflecting HA runoff. This argument is further strengthened when considering the modelled discharge data. Core MAS1 and the river Antainambalana (associated with MAS1) showed highest G/B values and modelled discharge, respectively, compared to the other two cores/rivers. Moreover, corals ANDRA and IFAHO showed statistically similar baseline averages in G/B, again replicated by the modelled discharge data. As HA runoff is linked to river discharge (Grove et al., 2010; Lough, 2011a), this likely explains the patterns observed in our corals. The only contrast between the two datasets was that ANDRA G/B peaked above IFAHO G/B during the wet season. Discharge data suggests otherwise, whereby the mean, range, maximum and minimum river discharge of Ambanizana, associated with coral ANDRA, are all less than the Anaovandran, associated with the coral IFAHO. However, at this stage, we cannot exclude the possibility that the recorded discharge signal by the coral may also be influenced by adjacent

ivers. Further, in contrast to the large watershed of the Antainambalana, the rivers influencing ANDRA and IFAHO have much smaller watersheds, which increases uncertainties in modelled discharge due to the relatively large model grid size (50 km).

When considering both the $\delta^{18}\text{O}_{\text{sw}}$ baseline averages and mean seasonal cycles, it becomes clear that strong hydrographic differences exist between the three coral sites. Coral MAS1 recorded the freshest waters, comparable to the modelled discharge rates for the Antainambalana. However, the reconstructed salinity signal at ANDRA indicated most saline conditions as well as a slightly reversed mean seasonal water cycle (Fig. 3.6c). As both the river Ambanizana and Anaovandran, associated with ANDRA and IFAHO respectively, have similar watershed sizes and modelled discharge rates, the $\delta^{18}\text{O}_{\text{sw}}$ baseline averages and seasonal cycles were expected to be similar. Such inconsistencies are likely a result of a difference between the distances from the river mouth to the coral.

Coral ANDRA is located 7 km from the Ambanizana river mouth, compared to IFAHO, which lies 4.5 km from the Anaovandran. The river signal at ANDRA is therefore likely to have been diluted by seawater via conservative mixing more than the signal at IFAHO, giving it a higher recorded salinity. Alternatively, the higher salinity signal at ANDRA may be linked to currents. As coral ANDRA is located further from the river mouth than IFAHO, it is increasingly likely that currents may channel the freshwater signal, associated with the river Ambanizana, away from the coral head. Nevertheless, according to proxy data, coral ANDRA receives no freshwater signal during the warm/wet season, and furthermore, has a slight increase in salinity. This may be related to the $\delta^{18}\text{O}$ hydrological balance (evaporation) of the water body influencing ANDRA at this time.

Comparing the Ba/Ca signals between cores and with modelled sediment runoff data, augments the argument that coral ANDRA is not influenced by runoff from the river Ambanizana. Coral MAS1 showed the highest recorded levels of Ba/Ca compared to the other two corals, which is in agreement with the modelled data, as the river Antainambalana had the highest modelled sediment runoff. As the Ba/Ca annual averages of

MAS1 and IFAHO are statistically correlated, they seem to be recording a regional sediment runoff signal (Alibert et al., 2003; Fleitmann et al., 2007; McCulloch et al., 2003; Sinclair and McCulloch, 2004). Coral IFAHO showed a significantly lower mean Ba/Ca signal. This signifies that the source input at the river Anaovandran is considerably lower than the river Antainambalana, which is again in agreement with modelled sediment runoff data.

Model data for the river Ambanizana, associated with coral ANDRA, indicates that sediment runoff is far higher than that of the river Anaovandran, associated with IFAHO. ANDRA resides a further 2.5 km from its river source than IFAHO, therefore any river signal from the Ambanizana would be diluted/mixed by seawater for an extra 2.5 km. However, given the significantly higher modelled sediment runoff for the Ambanizana, it is expected that ANDRA Ba/Ca would still be higher or similar to IFAHO. This is not the case, as the Ba/Ca signal in ANDRA is significantly less than IFAHO. Given that the annual average Ba/Ca results of ANDRA do not correlate with either MAS1 or IFAHO, it is therefore likely that 1) skeletal Ba/Ca variability is linked to a different source other than sediment runoff, and/or 2) skeletal Ba/Ca variability is derived from the largest watershed and its Ba/Ca signature is well mixed and diminished before arriving at the coral site.

Previous studies have also found no relationship between Ba/Ca and river discharge across a water quality gradient (Jupiter et al., 2008; Lewis et al., 2011; Prouty et al., 2010). Again, in contrast to the large watershed of the Antainambalana, the rivers influencing ANDRA and IFAHO have much smaller watersheds, which increases uncertainties in modelled sediment yield due to the large model grid size. Furthermore, the model data indicate the sediment yield at the river mouth whereas the corals record the ambient Ba/Ca signals (not sediment) at the reef site along a water quality gradient (Lewis et al., 2011).

The low Ba/Ca values and high reconstructed salinities of ANDRA provide further evidence that the river Ambanizana is not (or only marginally) influencing the coral site. Yet, the high G/B values indicate that a runoff signal does exist during the wet season. Indeed, the strongest annual average G/B relationship observed between cores was between coral MAS1 and ANDRA.

Therefore, it is more likely that the HA signal reaching coral ANDRA is not from the river Ambanizana, but from the river Antainambalana, associated with MAS1. This is plausible given the clockwise direction of the currents within the bay (Fig. 3.1) and the conservative mixing nature of HA (Bowers and Brett, 2008). Unlike HA, barium behaves non-conservatively in estuaries, as it is influenced by processes such as phytoplankton cycling (Coffey et al., 1997; Hanor and Chan, 1977; Sinclair, 2005). Therefore, the riverine Ba signal associated with MAS1 may well have diminished by the time it reached coral ANDRA. Further, the salinity signal ($\delta^{18}\text{O}_{\text{sw}}$) from the Antainambalana may have been lost due to mixing of different water masses (Fig. 3.7). However, as HA are conservative and are only associated with terrestrial inputs, they are duly transported to and recorded by coral ANDRA.

The skeletal $\delta^{13}\text{C}$ signals of all three cores showed similar baseline averages and high standard deviations, making it difficult to statistically differentiate between signals. Nevertheless, the mean seasonal cycles of MAS1 and IFAHO showed a depletion during the wet season. This likely reflects either a depleted $\delta^{13}\text{C}$ signal of DIC associated with the river plume (von Fischer and Tieszen, 1995; Marin-Spiotta et al., 2008; Moyer, 2008; Moyer and Grottoli, 2011; Swart et al., 1996), or a decrease in photosynthesis reducing the depletion of ^{12}C in the carbon pool (Grottoli, 2002; Grottoli and Wellington, 1999; Reynaud et al., 2002; Reynaud-Vaganay et al., 2001; Swart et al., 1996; Weil et al., 1981). Both would yield an inverse relationship with increasing runoff. As the freshest waters are associated with coral MAS1, this might explain the more depleted $\delta^{13}\text{C}$ values compared to IFAHO.

The $\delta^{13}\text{C}$ signal of coral ANDRA was more depleted than both MAS1 and IFAHO. This is surprising as it was not influenced by discharge directly, and therefore values were expected to be more enriched (von Fischer and Tieszen, 1995; Marin-Spiotta et al., 2008; Moyer, 2008; Moyer and Grottoli, 2011; Swart et al., 1996). Further, the mean seasonal cycle of ANDRA $\delta^{13}\text{C}$ was bimodal, as both $\delta^{13}\text{C}$ enrichment occurred during the peak runoff season as well as the dry season. As ANDRA is not (or only marginally) influenced by runoff, there are likely many other factors contributing to skeletal $\delta^{13}\text{C}$ variability and the baseline average, including ambient seawater productivity. Interestingly, the mean seasonal cycle of Ba/Ca in ANDRA also showed

a decrease in March when $\delta^{13}\text{C}$ enriched slightly (Fig. 3.6). This may be linked to phytoplankton uptake of Ba during peak runoff, when nutrients are plentiful, causing enrichment of $\delta^{13}\text{C}$ due to the preferential uptake of ^{12}C by phytoplankton (Sinclair, 2005 and references therein; Stecher and Kogut, 1999). An increase in primary production causes Ba to be scavenged from the water column due to the active cycling of algal blooms (Sinclair, 2005; Stecher and Kogut, 1999). As the nutrient levels are reduced, decaying algae will increase Ba concentrations within the water column by recycling. Correlating the annual average Ba/Ca values with the annual average $\delta^{13}\text{C}$ values indeed gives an indication that this is the case. Although not statistically significant, ANDRA gave the highest correlation ($R = 0.46$; $P = 0.086$), compared to MAS1 ($R = 0.029$) and IFAHO ($R = 0.13$).

In this study we demonstrate that Ba/Ca and G/B signals from the same watershed are reproducible. However, due to the large distances separating the corals, strong localised signals are observed between cores associated with different watersheds. G/B was the only proxy which showed a regional similarity across the bay, although the relationship between MAS1 and IFAHO was just outside the 5% significance level. A strong relationship was observed in Ba/Ca for MAS1 and IFAHO, yet not with ANDRA. This is likely related to ANDRA residing a further 2.5 km from its associated river mouth compared to IFAHO, despite having a similar sized watershed. No significant regional signal was observed for $\delta^{18}\text{O}_{\text{sw}}$ and $\delta^{13}\text{C}$. The $\delta^{13}\text{C}$ signal was likely overwhelmed by coral vital effects and *in situ* productivity, whereas the $\delta^{18}\text{O}_{\text{sw}}$ signals are likely inconsistent due to site-specific environmental differences in the hydrological balance.

Discrepancies between the proxy results and modelled data indicate that corals are not ideally suited for directly comparing rivers systems. Absolute proxy values give an indication of the ambient concentration surrounding the coral at the time of precipitation, yet not the source input. Prouty et al. (2010) compare Ba/Ca baselines for Hawaiian corals to other published Ba/Ca records from the GBR (McCulloch et al., 2003) and Kenya (Fleitmann et al., 2007), relating differences to river input. This is problematic since the Ba/Ca signal at each site reflects both the distance from the source and the source input. Moreover, mixing gradients (distance), currents, proxy behavior

and vital effects can all influence the precipitated skeletal signal significantly from the moment it leaves the river source. In a recent study, Lewis et al. (2011) provided evidence of the impact small-scale hydrodynamic differences have on skeletal Ba/Ca across the complex hydrography of reefs in the GBR from multiple cores across a water quality gradient. However, by combining runoff proxies and comparing baseline averages and mean seasonal cycles, aided by hydrological model data, a good overview of the runoff products influencing the coral sites was achieved in our study. Moreover, all proxies provide information on the runoff dynamics of the bay system, which will assist both terrestrial and marine management programmes in Madagascar.

Conclusions

Models provide an estimate of discharge and sediment runoff at the mouth of a river, whereas corals record a signal potentially several kilometres away. Subsequently, the riverine signal can be modified by the time it reaches the coral. The distance from the river source is a primary reason why comparing absolute runoff proxy values to differentiate between watersheds is unreliable. The further a coral resides from the river mouth the more the proxy signal is mixed/diluted by seawater. Depending on the behaviour of the proxy, the distance from the river can also have dramatic effects on the recorded signal at the coral. Proxies such as Ba/Ca and $\delta^{13}\text{C}$ are non-conservative mixers, and therefore altered by recycling processes such as phytoplankton uptake. Nevertheless, we find Ba/Ca to be reproducible within the same watershed and also across distant watersheds given there is a close proximity of the coral to a river mouth and/or associated with a large river. Humic acids and the $\delta^{18}\text{O}$ signal mix conservatively in the water column. Indeed, there was a good regional relationship observed between coral G/B signals, making it an ideal proxy for paleoclimate reconstructions and spatial comparisons of corals (not rivers). Yet, the skeletal $\delta^{18}\text{O}_{\text{sw}}$ signal showed little consensus between cores, which was likely due to local differences in the hydrological balance and their vicinity to the river mouths. Other physiochemical parameters such as currents also need to be considered when interpreting proxy results. Even though a coral may reside closer to one river than another, currents can determine which river signal the coral receives. Nevertheless, comparing proxy baseline averages and mean seasonal cycles provides a good overview of the runoff dynamics over a bay system.

Supplementary Information

Supplementary Figures

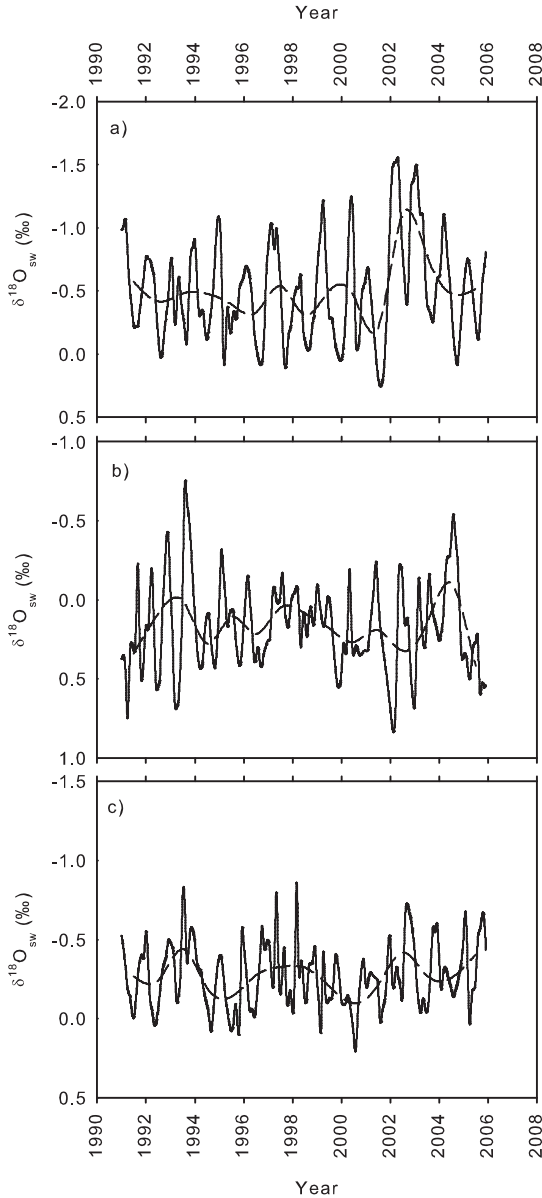


Figure S3.1. The $\delta^{18}\text{O}_{\text{seawater}}$ ($\delta^{18}\text{O}_{\text{sw}}$) of coral cores MAS1 (a), ANDRA (b) and IFAHO (c) calculated by subtracting the thermal component from coral skeletal $\delta^{18}\text{O}$ based on the relative changes in Sr/Ca-SST following Ren et al. (2002). The annual average (dashed line) values were calculated by averaging the months January to December for each of the 15 years.

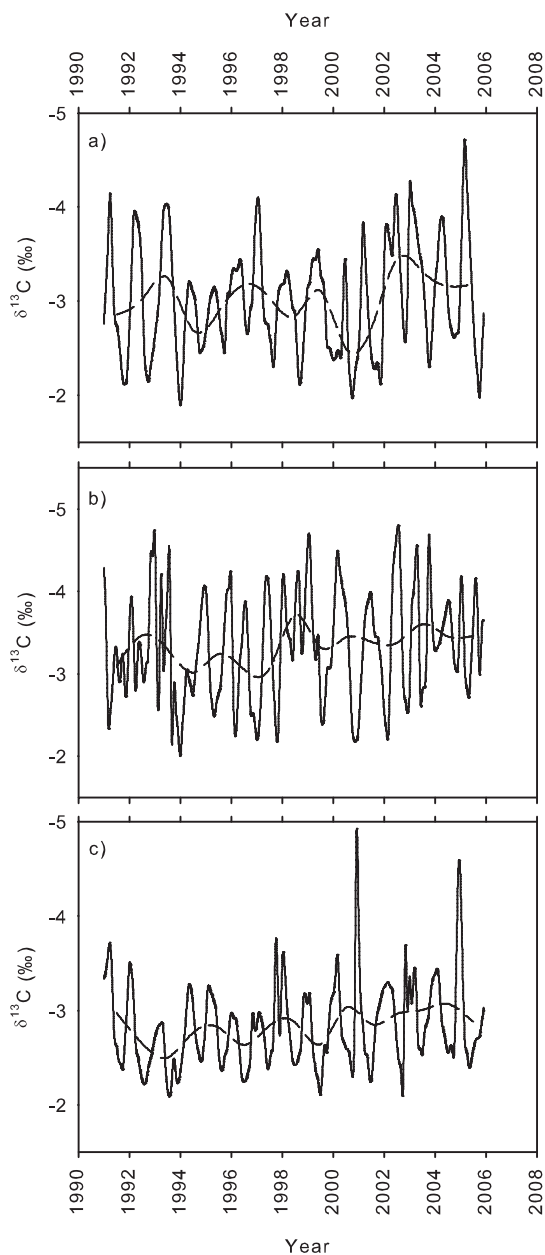


Figure S3.2. The $\delta^{13}\text{C}$ of coral cores MAS1 (a), ANDRA (b) and IFAHO (c) relative to V-PDB. The annual average (dashed line) values were calculated by averaging the months January to December for each of the 15 years.

Acknowledgements: This work was supported as part of the SINDOCOM grant under the Dutch NWO program ‘Climate Variability’, grant 854.00034/035. Additional support comes from the NWO ALW project CLIMATCH, grant 820.01.009, and the Western Indian Ocean Marine Science Association through the Marine Science for Management programme under grant MASMA/CC/2010/02. We thank the Wildlife Conservation Society (WCS) Madagascar, especially Heriliala Randriamahazo and the WCS/ANGAP team in Maroantsetra, for their support in fieldwork logistics and in the organisation of the research permits, CAF/CORE Madagascar for granting the CITES permit and ANGAP Madagascar for support of our research activities in the vicinity of the marine and forest nature parks. Furthermore, we would like to thank Bob Koster and Rineke Gieles for continuous development and maintenance of the UV-Core Scanner, and Michiel Kienhuis, Suzanne Verdegaal and Evaline van Weerlee for assisting with stable isotope measurements. We thank Jan Vermaat and Hans de Moel (both VU University Amsterdam) for providing the STREAM model data outputs for Antongil Bay (Madagascar) and for discussions of the sediment yield N-SPECT model results.

References

- Aerts, J.C.J.H., Kriek, M., Schepel, M., 1999. STREAM, spatial tools for river basins and environment and analysis of management options: 'Set up and requirements'. Physics and Chemistry of the Earth, Part B 24, 591-595.
- Aerts, J.C.J.H., Bouwer, L.M., 2002. Calibration and validation for the wider Perfume River Basin in Vietnam. Commissioned report and guided by R. Misdorp RIKZ/ Coastal Zone Management Centre, The Hague, 35-35.
- Agarwal, D.K., Silander, J.A., Gelfand, A.E., Dewar, R.E. and Mickelson, J.G., 2005. Tropical deforestation in Madagascar: analysis using hierarchical spatially explicit, Bayesian regression models. Ecological Modelling 185(1), 105-131.
- Alibert, C., Kinsley, L., Fallon, S.J., McCulloch, M.T., Berkelmans, R. and McAllister, F., 2003. Source of trace element variability in Great Barrier Reef corals affected by the Burdekin flood plumes. Geochimica et Cosmochimica Acta 67(2), 231-246.
- Barnes, D.J. and Taylor, R.B., 2001. On the nature and causes of luminescent lines and bands in coral skeletons. Coral Reefs 19(3), 221-230.
- Barnes, D.J. and Taylor, R.B., 2005. On the nature and causes of luminescent lines and bands in coral skeletons: II. Contribution of skeletal crystals. Journal of Experimental Marine Biology and Ecology 322(2), 135-142.
- Birkinshaw, C. and Randrianjanahary, M., 2007. The Effects of Cyclone Hudah on the Forest of Masoala Peninsula, Madagascar. Madagascar Conservation & Development 2(1), 17-20.
- Bowers, D.G. and Brett, H.L., 2008. The relationship between CDOM and salinity in estuaries: An analytical and graphical solution. Journal of Marine Systems 73(1-2), 1-7.
- Carricart-Ganivet, J.P., Lough, J.M. and Barnes, D.J., 2007. Growth and luminescence characteristics in skeletons of massive *Porites* from a depth gradient in the central Great Barrier Reef. Journal of Experimental Marine Biology and Ecology 351, 27-36.
- Coffey, M., Dehairs, F., Collette, O., Luther, G., Church, T. and Jickells, T., 1997. The behaviour of dissolved barium in estuaries. Estuarine, Coastal and Shelf Science 45(1), 113-121.
- Cole, J.E., Dunbar, R.B., McClanahan, T.R. and Muthiga, N.A., 2000. Tropical Pacific forcing of decadal SST variability in the western Indian Ocean over the past two centuries. Science 287, 617-619.
- Collins, A.S., 2006. Madagascar and the amalgamation of Central Gondwana. Gondwana Research 9, 3-16.
- Corrège, T., 2006. Sea surface temperature and salinity reconstructions from coral geochemical tracers. Palaeogeography, Palaeoclimatology, Palaeoecology 232, 408-428.
- Dewar, R.E. and Richard, A.F., 2007. Evolution in the hypervariable environment of Madagascar. Proceedings of the National Academy of Sciences 104(34), 13723-13727.
- Dewar, R.E. and Wallis, J.R., 1999. Geographical patterning of interannual rainfall variability in the tropics and near tropics: An L-moments approach. Journal of Climate 12(12),

- 3457-3466.
- Douglas, I., 1967. Man, vegetation and the sediment yields of rivers. *Nature* 215, 925-928.
- Ersts, P.J. and Rosenbaum, H.C., 2003. Habitat preference reflects social organization of humpback whales (*Megaptera novaeangliae*) on a wintering ground. *Journal of Zoology* 260(4), 337-345.
- Fallet, U., Boer, W., van Assen, C., Greaves, M. and Brummer, G.-J.A., 2009. A novel application of wet oxidation to retrieve carbonates from large organic-rich samples for ocean-climate research. *Geochemistry, Geophysics, Geosystems* 10, Q08004, doi:10.1029/2009GC002573.
- von Fischer, J.C. and Tieszen, L.L., 1995. Carbon isotope characterization of vegetation and soil organic matter in Subtropical forests in Luquillo, Puerto Rico. *Biotropica* 27, 138-148.
- Fleitmann, D., Dunbar, R.B., McCulloch, M.T., Mudelsee, M., Vuille, M., McClanahan, T.R., Cole, J.E. and Eggins, S., 2007. East African soil erosion recorded in a 300 year old coral colony from Kenya. *Geophysical Research Letters* 34(4). doi:10.1029/2006GL028525.
- Goodman, S.M. and Benstead, J.P., 2003. *The natural history of Madagascar*. University of Chicago Press. Chicago and London. pp. 1701.
- Goodman, S.M. and Ganzhorn, J.U., 2004. Biogeography of lemurs in the humid forests of Madagascar: the role of elevational distribution and rivers. *Journal of Biogeography* 31(1), 47-55.
- Green, G.M. and Sussman, R.W., 1990. Deforestation history of the eastern rain forests of Madagascar from satellite images. *Science* 248(4952), 212-215.
- Grottoli, A.G., 2002. Effect of light and brine shrimp on skeletal $\delta^{13}\text{C}$ in the Hawaiian coral *Porites compressa*: A tank experiment. *Geochimica et Cosmochimica Acta* 66(11), 1955-1967.
- Grottoli, A.G. and Wellington, G.M., 1999. Effect of light and zooplankton on skeletal $\delta^{13}\text{C}$ values in the eastern Pacific corals *Pavona clavus* and *Pavona gigantea*. *Coral Reefs* 18, 29-41.
- Grove, C.A., Nagtegaal, R., Zinke, J., Scheufen, T., Koster, B., Kasper, S., McCulloch, M., van den Berg, G. and Brummer, G.-J.A., 2010. River runoff reconstructions from novel spectral luminescence scanning of massive coral skeletons. *Coral Reefs* 29, 579-591.
- Hanor, J.S. and Chan, L.H., 1977. Non-Conservative behaviour of barium during mixing of Mississippi River and Gulf of Mexico waters. *Earth and Planetary Science Letters* 37(2), 242-250.
- Harper, G.J., Steininger, M.K., Tucker, C.J., Juhn, D., and Hawkins, F., 2007. Fifty years of deforestation and forest fragmentation in Madagascar. *Environmental Conservation* 34(4), 325-333.
- Hendy, E.J., Gagan, M.K. and Lough, J.M., 2003. Chronological control of coral records using luminescent lines and evidence for non-stationary ENSO teleconnections in northeast Australia. *The Holocene* 13, 187-199.
- Isdale, P., 1984. Fluorescent bands in massive corals record centuries of coastal rainfall. *Nature* 310(5978), 578-579.

- Jones, P.D., Briffa, K.R., Osborn, T.J., Lough, J.M., van Ommen, T.D., Vinther, B.M., Luterbacher, J., Wahl, E.R., Zwiers, F.W., Mann, M.E., Schmidt, G.A., Ammann, C.M., Buckley, B.M., Cobb, K.M., Esper, J., Goose, H., Graham, N., Jansen, E., Kiefer, T., Kull, C., Kuttel, M., Mosley-Thompson, E., Overpeck, J.T., Riedwyl, N., Schulz, M., Tudhope, A.W., Villalba, R., Wanner, H., Wolff, E. and Xoplaki, E., 2009. High-resolution paleoclimatology of the last millennium: a review of current status and future prospects. *The Holocene* 19, 3-49.
- Juillet-Leclerc, A. and Schmidt, G., 2001. A calibration of the oxygen isotope paleothermometer of coral aragonite from *Porites*. *Geophysical Research Letters* 28, 4135-4138.
- Jupiter, S., Roff, G., Marion, G., Henderson, M., Schrameyer, V., McCulloch, M. and Hoegh-Guldberg, O., 2008. Linkages between coral assemblages and coral proxies of terrestrial exposure along a cross-shelf gradient on the southern Great Barrier Reef. *Coral Reefs* 27, 887-903.
- King, B., McAllister, F., Wolanski, E., Done, T. and Spagnol, S., 2001. River plume dynamics in the central Great Barrier Reef. In: Wolanski, E. (eds.) *Oceanographic Processes of Coral Reefs - Physical and biological links in the Great Barrier Reef*, CRC Press, Boca Raton, Florida, 145-159.
- Kremen, C., 2003. The Masoala Peninsula, in: *The natural history of Madagascar*. Univ. of Chicago Press. Chicago and London. pp. 1459-1466.
- Kremen, C., Razafimahatratra, V., Guillery, R.P., Rakotomalala, J., Weiss, A. and Ratsisompatrarivo, J.S., 1999. Designing the Masoala National Park in Madagascar based on biological and socioeconomic data. *Conservation Biology* 13(5), 1055-1068.
- Larsen, M.C. and Webb, R.M.T., 2009. Potential Effects of Runoff, Fluvial Sediment, and Nutrient Discharges on the Coral Reefs of Puerto Rico. *Journal of Coastal Research* 25(1), 189-208.
- Lewis, S.E., Brodie, J.E., McCulloch, M.T., Mallela, J., Jupiter, S.D., Williams, H.S., Lough, J.M., Matson, E.G., 2011. An assessment of an environmental gradient using coral geochemical records, Whitsunday Islands, Great Barrier Reef, Australia. *Marine Pollution Bulletin*, doi:10.1016/j.marpolbul.2011.09.030.
- Lewis, S.L., Shields, G.A., Kamber, B.S., Lough, J.M., 2007. A multi-trace element coral record of land-use changes in the Burdekin River catchment, NE Australia. *Palaeogeography Palaeoclimatology Palaeoecology* 246, 471-487.
- Lough, J.M., 2011a. Great Barrier Reef coral luminescence reveals rainfall variability over northeastern Australia since the 17th century. *Paleoceanography* 26, PA2201, doi:10.1029/2010PA002050.
- Lough, J.M., 2011b. Measured coral luminescence as a freshwater proxy: comparison with visual indices and a potential age artifact. *Coral Reefs* 30, 169-182.
- Lough, J.M., Barnes, D.J. and Mcallister, F.A., 2002. Luminescent lines in corals from the Great Barrier Reef provide spatial and temporal records of reefs affected by land runoff. *Coral Reefs* 21, 333-343.
- Maina, J., de Moel, H., Vermaat, J., Bruggemann, H.J., Guillaume, M.M.M., Grove, C.A., Madin, J.S., Mertz-Kraus, R., Zinke, J., 2012. Linking coral river runoff proxies with climate variability, hydrology and land-use in Madagascar catchments, *Marine Pollution Bulletin* (submitted).

- Marin-Spiotta, E., Swanston, C.W., Torn, M.S., Silver, W.L. and Burton, S.D., 2008. Chemical and mineral control of soil carbon turnover in abandoned tropical pastures. *Geoderma* 143, 49-62.
- Matson, E.G., 2011. Core plugs. *Encyclopedia of Modern Coral Reefs*. Hopley, D., Springer: 294-296.
- McClanahan, T.R., 2007. Testing for correspondence between coral reef invertebrate diversity and marine park designation on the Masoala Peninsula of eastern Madagascar. *Aquatic Conservation* 17(4), 409-419.
- McClanahan, T.R. and Obura, D., 1997. Sedimentation effects on shallow coral communities in Kenya. *Journal of Experimental Marine Biology and Ecology* 209(1-2), 103-122.
- McCulloch, M.T., Gagan, M.K., Mortimer, G.E., Chivas, A.R. and Isdale, P.J.A., 1994. A high-resolution Sr/Ca and $\delta^{18}\text{O}$ coral record from the Great Barrier Reef, Australia, and the 1982-1983 El Nino. *Geochimica et Cosmochimica Acta* 58, 2747-2754.
- McCulloch, M.T., Fallon, S., Wyndham, T., Hendy, E.J., Lough, J.M. and Barnes D.J., 2003. Coral record of increased sediment flux to the inner Great Barrier Reef since European settlement. *Nature* 421(6924), 727-30.
- Milliman, J.D. and Syvitski, J.P.M., 1992. Geomorphic tectonic control of sediment discharge to the ocean – The importance of small mountainous rivers. *Journal of Geology* 100(5), 525-44.
- Moyer, R.P., 2008. Carbon isotopes ($\delta^{13}\text{C}$ & $\Delta^{14}\text{C}$) and trace elements (Ba, Mn, Y) in small mountainous rivers and coastal coral skeletons in Puerto Rico. Ph. D. thesis, The Ohio State Univ.
- Moyer, R.P., Grottoli, A.G., 2011. Coral skeletal carbon isotopes ($\delta^{13}\text{C}$ and ΔC) record the delivery of terrestrial carbon to the coastal waters of Puerto Rico. *Coral Reefs* 30, 791-802.
- Paillard, D., Labeyrie, L. and Yiou, P., 1996. Macintosh program performs time series analysis. *Eos Transactions AGU* 77, 379-379.
- Payet, R. and Obura, D.O., 2004. The negative impacts of human activities in the Eastern African region: An international waters perspective. *Ambio* 33(1-2), 24-33.
- Pfeiffer, M., Dullo, W.C., Zinke, J., Garbe-Schönberg, D., 2009. Three monthly coral Sr/Ca records from the Chagos Archipelago covering the period of 1950-1995 A.D.: reproducibility and implications for quantitative reconstructions of sea surface temperature variations *International Journal of Earth Sciences* 98, 53-66, doi:10.007/s00531-008-0326-z.
- Prouty, N.G., Field, M.E., Stock, J.D., Jupiter, S.D. and McCulloch, M., 2010. Coral Ba/Ca records of sediment input to the fringing reef of the southshore of Moloka'i, Hawai'i over the last several decades. *Marine Pollution Bulletin* 60(10), 1822-1835.
- Quartly, G.D., Kyte, E.A., Srokosz, M.A. and Tsimplis, M.N., 2007. An intercomparison of global oceanic precipitation climatologies. *Journal of Geophysical Research* 112, D10121, doi:10.1029/2006JD007810.
- Ren, L., Linsley, B.K., Wellington, G.M., Schrag, D.P. and Hoegh-guldberg, O., 2002. Deconvolving the $\delta^{18}\text{O}$ seawater component from subseasonal coral $\delta^{18}\text{O}$ and Sr/Ca at Rarotonga in the southwestern subtropical Pacific for the period 1726 to 1997. *Geochimica et Cosmochimica Acta* 67(9), 1609-1621.

- Reynaud, S., Ferrier-Pages, C., Sambrotto, R., Juillet-Leclerc, A., Jaubert, J. and Gattuso, J.P., 2002. Effect of feeding on the carbon and oxygen isotopic composition in the tissues and skeleton of the zooxanthellate coral *Stylophora pistillata*. *Marine Ecology Progress Series* 238, 81-89.
- Reynaud-Vaganay, S., Juillet-Leclerc, A., Jaubert, J. and Gattuso, J.P., 2001. Effect of light on skeletal $\delta^{13}\text{C}$ and $\delta^{18}\text{O}$, and interaction with photosynthesis, respiration and calcification in two zooxanthellate scleractinian corals. *Palaeogeography, Palaeoclimatology, Palaeoecology* 175, 393-404.
- Reynolds, R.W., Rayner, N.A., Smith, T.M., Stokes, D.C. and Wang, W., 2002. An improved *in situ* and satellite SST analysis for climate. *Journal of Climate*. 15, 1609-1625.
- Rogers, C.S., 1990. Responses of coral reefs and reef organisms to sedimentation. *Marine Ecology Progress Series* 62(1-2), 185-202.
- Rosenthal, Y., Field, M.P. and Sherrell, R.M., 1999. Precise determination of element/calcium ratios in calcareous samples using sector field inductively coupled plasma mass spectrometry. *Analytical Chemistry* 71(15), 3248-3253.
- Sinclair, D.J., 2005. Non-river flood barium signals in the skeletons of corals from coastal Queensland, Australia. *Earth and Planetary Science Letters* 237, 354-369.
- Sinclair, D.J. and McCulloch, M.T., 2004. Corals record low mobile barium concentrations in the Burdekin River during the 1974 flood: evidence for limited Ba supply to rivers? *Palaeogeography, Palaeoclimatology, Palaeoecology* 214(1-2), 155-174.
- Smith, T.M., Reynolds, R.W., Peterson, T.C. and Lawrimore, J., 2008. Improvements to NOAA's historical merged land-ocean surface temperature analysis (1880-2006). *Journal of Climate* 21(10), 2283-2296.
- Smithers, S.G. and Woodroffe, C.D., 2001. Coral microatolls and 20th century sea level in the eastern Indian Ocean. *Earth and Planetary Science Letters* 191, 173-184.
- Stecher, H.A. and Kogut, M.B., 1999. Rapid barium removal in the Delaware estuary. *Geochimica et Cosmochimica Acta* 63, 1003-1012.
- Swart, P.K., Leder, J.J., Szmant, A.M., and Dodge, R.E., 1996. The origin of variations in the isotopic record of scleractinian corals .2. Carbon. *Geochimica et Cosmochimica Acta* 60, 2871-2885.
- Warrick, J.A. and Rubin, D.M., 2007. Suspended-sediment rating curve response to urbanization and wildfire, Santa Ana River, California. *Journal of Geophysical Research* 112, F02018, doi:10.1029/2006JF000662.
- Weil, S.M., Buddemeier, R.W., Smith, S.V. and Kroopnick, P.M., 1981. The stable isotopic composition of coral skeletons – Control by environmental variables. *Geochimica et Cosmochimica Acta* 45, 1147-1153.
- Windley, B.F., Razafiniparany, A., Razakamanana, T. and Ackermann, D., 1994. Tectonic framework of the Precambrian of Madagascar and its Gondwana connections – a review and reappraisal. *Geologische Rundschau* 83, 642-659.
- Winsemius, H.C., Savenije, H.H.G., Gerrits, A.M.J., Zapreeva, E.A., Klees, R., 2006. Comparison of two model approaches in the Zambezi river basin with regard to model reliability and identifiability. *Hydrology and Earth System Sciences* 10, 339–352.
- Wischmeier, W.H., Smith, D.D., 1978. Predicting rainfall erosion losses - a guide to conservation planning. U.S. Department of Agriculture, Washington D.C., AH-537.

Xie, P.P. and Arkin, P.A., 1996, Analyses of global monthly precipitation using gauge observations, satellite estimates, and numerical model predictions. *Journal of Climate*. 9(4), 840-858.

Chapter 4

Madagascar corals reveal Pacific multidecadal modulation of rainfall since 1708

Craig A. Grove, Jens Zinke, Frank Peeters, Wonsun Park,
Tim Scheufen, Sebastian Kasper, Bemahafaly Randriamanantsoa,
Malcolm T. McCulloch and Geert-Jan A. Brummer

Based on the publication in *Climate of the Past Discussions*, 8, 787-817,
doi:10.5194/cpd-8-787-2012 (2012)

Abstract

The Pacific Ocean modulates Australian and North American rainfall variability on multidecadal timescales, in concert with the Pacific Decadal Oscillation (PDO). It has been suggested that Pacific decadal variability may also influence Indian Ocean surface temperature and rainfall in a far-field response, similar to the El Niño Southern Oscillation (ENSO) on interannual timescales. However, instrumental records of rainfall are too short and too sparse to confidently assess such multidecadal climatic teleconnections. Here, we present four climate archives spanning the past 300 years from giant Madagascar corals. We decouple 20th century human deforestation effects from rainfall induced soil erosion using spectral luminescence scanning and geochemistry. The corals provide the first evidence for Pacific decadal modulation of rainfall over the western Indian Ocean. We find that positive PDO phases are associated with increased Indian Ocean temperatures and rainfall in eastern Madagascar, while precipitation in southern Africa and eastern Australia declines. Consequently, the negative PDO phase that started in 1998 should lead to reduced rainfall over eastern Madagascar and increased precipitation in southern Africa and eastern Australia. We conclude that the PDO has important implications for future multidecadal variability of African rainfall, where water resource management is increasingly important under the warming climate.

Introduction

Tropical Indian Ocean warming in the 20th century has accelerated since the late 1970's affecting rainfall patterns and intensity across much of the western Indian Ocean and adjacent landmasses of eastern and southern Africa (Funk et al., 2008; Richard et al., 2000). Warming of the south-central Indian Ocean (0-15°S, 60-90°E) is thought to reduce the moisture flux towards sub-Saharan Africa promoting droughts in austral summer and fall (Funk et al., 2008; Goddard and Graham, 1999; Hoerling et al., 2006; Richard et al., 2000). As eastern and southern Africa heavily depends on regular rainfall for food production and ecosystem sustainability (Fleitmann et al., 2007), the uncertainty in the rainfall response to accelerated warming of the Indian Ocean is a serious socioeconomic issue of global importance (Funk et al., 2008). However, to fully assess this response it is necessary to identify the

long-term natural rainfall patterns, yet currently we lack an understanding of the major drivers of natural decadal rainfall variability in the Indian Ocean and what the regional synergy is with global warming (Cane, 2010).

There is some evidence indicating that multidecadal South African rainfall is associated with ENSO-like interdecadal variability, due to the shifting tropical temperature troughs in response to large-scale changes in Indo-Pacific SST and sea level pressure (Reason and Rouault, 2002). Since rainfall patterns are sensitive to sea surface temperature (SST) change, which includes both natural internal variability and anthropogenic forcing, here we investigate natural multidecadal modulation of Indian Ocean rainfall in response to multidecadal SST variability. Massive corals such as *Porites* sp. generate precisely dated century-long, highly resolved and continuous proxy records of changing land-ocean interactions (Fleitmann et al., 2007; Lough, 2007; McCulloch et al., 2003). Here we present 300 years of monthly resolved proxy records of soil erosion from four giant *Porites* sp. colonies growing in two coastal marine catchments of eastern Madagascar (Fig. 4.1).

The PDO is a major internal mode of ocean-atmosphere variability (Mantua et al., 1997). Positive PDO phases are characterised by low SST in the central midlatitude Pacific and warm anomalies along the northern and eastern margins, and south of 30°N. The PDO is remotely forced from the Tropics in part (Schneider and Cornuelle, 2005), and responsible for strong multidecadal (50 – 70 years) (Minobe, 1997) and interdecadal Pacific oscillations in SST (IPO; 17 – 28 years) (Meehl and Hu, 2006). It is considered the leading mode of North Pacific SST defined by instrumental data for the past 120 years (Mantua et al., 1997), and recognised in extended proxy time series, e.g. tree ring records of rainfall in NE Asia (D'Arrigo and Wilson, 2006). Moreover, mounting evidence indicates that the PDO has teleconnections extending over thousands of kilometers to the Indian Ocean (Cole et al., 2000; Crueger et al., 2009). The positive PDO phase corresponds to warm Indian Ocean SST anomalies (Deser et al., 2004), thought to exceed anomalies associated with ENSO (Krishnan and Sugi, 2003), particularly in the southwestern Indian Ocean (Fig. 4.2a) (Meehl and Hu, 2006). While it is evident that changing rainfall patterns over Australia respond to the PDO (Arblaster et al., 2002), links to rainfall in southeastern Africa and the western Indian Ocean have only been suggested (Deser et al., 2004; Zinke et al., 2008).

Materials and Methods

Coral Sampling and Analysis

Three corals MAS1, MAS3 and ANDRA were drilled in March 2007 from Antongil Bay, NE Madagascar, dating back to 1904, 1880 and 1914 respectively (Fig. 4.1) (Grove et al., 2010). The core MASB (S 15°30,566; E 49°45,437) was drilled in October 2008, dating back to 1708. Three of the corals used for this study, MAS1, MAS3 and MASB are influenced by a major river draining into the Bay, named Antainambalana (Fig. 4.1). Its source lies 1450 m above sea level and its watershed covers an estimated 4000 km². As well as being influenced by the Antainambalana, a third coral ANDRA is located 30 km south of MAS1/3/B, and is influenced by a much smaller river called the Ambanizana, which has a watershed of 160 km² (Fig. 4.1).

The average growth rate of the three short coral cores was approximately 12 mm y⁻¹. Growth laminae were visualized by X-radiograph-positive prints, and the growth axis of the coral slab was defined as the line normal to these laminae. All cores were sectioned into 7 mm slabs, cleaned with sodium hypochlorite (NaOCl, 10-13% reactive chloride; Sigma-Aldrich Company) for 24 hours to remove residual organics that would quench luminescence, and subsequently scanned under UV-light to measure continuous spectral luminescence ratios (G/B). Luminescence in banded corals is indicative of past humic acid runoff from river discharge (Barnes and Taylor, 2005; Isdale, 1984; Grove et al., 2010; Lough et al., 2002). Indeed, correlations of MAS1 G/B and regional rainfall are statistically significant (Grove et al., 2010). Luminescence images of the MAS3 core revealed dark stains, likely organics, in the older sections of the core which could not be removed by bleaching, therefore as a precaution luminescence data ends in 1930.

Laser-Ablation Inductively Coupled Plasma Mass Spectrometry (Laser-Ablation ICP-MS) profiles were taken to analyse the trace element ratios of Sr/Ca, Ba/Ca and Mn/Ca at 40 µm intervals on the coral cores MAS1 and MAS3 at ANU Canberra (Fallon et al., 2002; Sinclair et al., 1998). Profiles cover the entire age of MAS1 (1906 - 2006) and since 1935 for MAS3 (1935

- 2006). We use Sr/Ca ratios as indicators of SST (Alibert and McCulloch, 1997; Corrège, 2006), whereas suspended sediment runoff is reconstructed using Ba/Ca ratios (Alibert and McCulloch, 1997; McCulloch et al., 2003; Sinclair and McCulloch, 2004). Ba/Ca in the coral cores analysed here showed a high temporal correlation with spectral luminescence ratios (Grove et al., 2010). Mn/Ca is used as an indicator of ash fallout from slash and burn deforestation (Abram et al., 2003; Lewis et al., 2007). As luminescence and Laser-Ablation data have a sub-weekly resolution, interpolation to a monthly time-series provides a high level of accuracy.

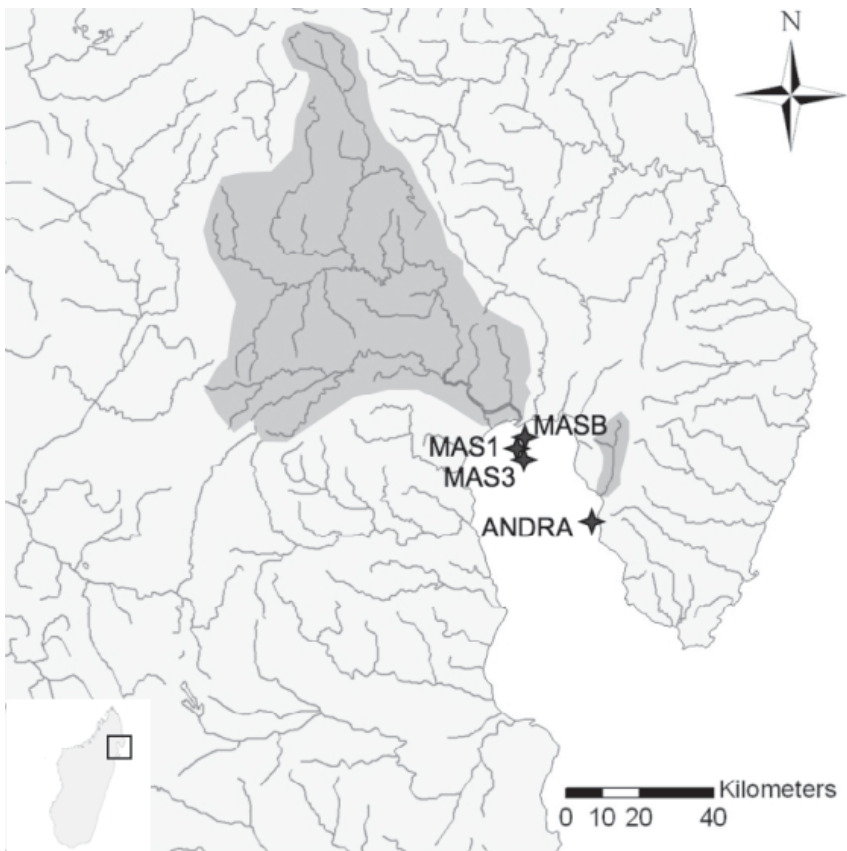


Figure 4.1. Map of the region where cores MAS1, MAS3, MASB and ANDRA were drilled. Coral locations (stars) and their corresponding rivers and watersheds (grey shaded areas) are marked accordingly in Antongil Bay. The largest river is the Antainambalana, influencing MAS1, MAS3 and MASB; the river influencing ANDRA is the Ambanizana, flowing south westward into the bay.

Research Area and Climate Setting

Coral cores were taken from Antongil Bay in NE Madagascar, which is surrounded by one of the country's largest remaining rainforests (Birkinshaw and Randrianjanahary, 2007). Air temperature and rainfall in Antongil Bay was monitored for the period 1992 to 1996 (Kremen, 2003). Antongil Bay is characterised by an August-December cold-dry season and a January-July warm-wet season. Air temperatures peak in December and January and are lowest between July and September. Highest rainfall occurs between January and April, while lowest rainfall occurs between September and November (Kremen, 2003; Jury et al., 1995). The annual average precipitation at Andranobe (coral site ANDRA) was 6049 mm (1 SD = 979 mm) between 1992 and 1996. Highest river discharge occurs between February and April, one to two months after peak rainfall (Gerten et al., 2008). Runoff decreases but continues until September then reaches lows in October and November.

Results and Discussion

We measured soil-derived humic acids in the coral skeletons by spectral luminescence scanning (Green/Blue ratio; G/B) to determine seasonally resolved runoff resulting from hinterland rainfall (Grove et al., 2010). Our longest coral G/B record dating from 1708 to 2008 (MASB; Fig. 4.1) was compared to the NE Asia tree ring based PDO reconstruction (D'Arrigo and Wilson, 2006) to investigate multidecadal variability in rainfall (Fig. 4.2a, grey box), since the instrumental PDO index (Mantua et al., 1997) only dates back to 1880. Both climate records show near identical changes in amplitude and timing for over two centuries (Fig. 4.2c) then diverge after the 1920's. Cross spectral (Fig. 4.3) and wavelet coherence analysis (Fig. 4.4) of the PDO tree ring index and MASB G/B confirm the clear relationship between rainfall and the PDO on multidecadal time scales since at least 1708 and until the 1920's (Appendix A). Coherent temporal changes in signal amplitudes and timing between both records show that positive phases of the PDO correspond to positive rainfall anomalies (Fig. 4.2c).

To further investigate post 1920 PDO modulation of eastern Madagascar soil runoff, we also analysed the G/B records of additional

corals in combination with high resolution geochemistry. We used Laser-Ablation ICP-MS to determine coral Ba/Ca as a proxy of past sediment runoff (Fleitmann et al., 2007; McCulloch et al., 2003), Sr/Ca as a robust proxy for SST (Abram et al., 2003; Zinke et al., 2008) and Mn/Ca as an indicator for ash fallout from slash and burn deforestation (Abram et al., 2003; Lewis et al., 2007). Together, they allowed us to decouple the three major components influencing eastern Madagascar soil runoff; i.e. human land-use changes and natural decadal climate variability interacting with Indian Ocean warming. Long-term changes in runoff appear in the 10-year running mean of both G/B and Ba/Ca in each coral (MAS1, Fig. 4.5a, c; MAS3, Fig. 4.5d, f). Most pronounced is the continuous increase in humic acid runoff since the mid-1970s and sediment runoff from the mid-1950s, towards a maximum in recent years in concert with rising south central Indian Ocean SST (Fig. 4.5). Also, the longest continuous precipitation record from Madagascar (Antananarivo) is in agreement with our Ba/Ca and SST records, whereby rainfall increased from the mid-1950s until the record ends in 1987 (Fig. 4.5b, e). Consequently, increasing rainfall (runoff) over the catchment area appears tightly coupled to rising SST (Fig. 4.5).

The reduced coherence between humic acid runoff and Indian Ocean SST in the mid-20th century suggests that other factors are involved in large-scale erosion. Discrepancies between 1945-1955 and 1966-1980 occur in both cores whereby G/B increases while temperature decreases (1940-1960) or remains stable (1960-1980). These periods are also marked by enhanced coral Mn/Ca above the seasonal background (Figs. 4.5 and S4.1; Appendix B), as found in response to ash fallout from wild fires (Abram et al., 2003; Lewis et al., 2007). Indeed, the pronounced increase in Mn/Ca testifies to the well documented intense slash-and-burn deforestation for upland rice cultivation between 1950 and 1980 (Green and Sussman, 1990; Harper et al., 2007), associated with the economic collapse of Madagascar and the return to subsistence agriculture. Segmentation analysis (Webster, 1973; Webster, 1979) of the coral composite G/B record (MAS1, MAS3 and ANDRA) highlights these mid-20th century human deforestation periods (Figs. S4.3 and S4.4; Appendix C; Supplementary Material).

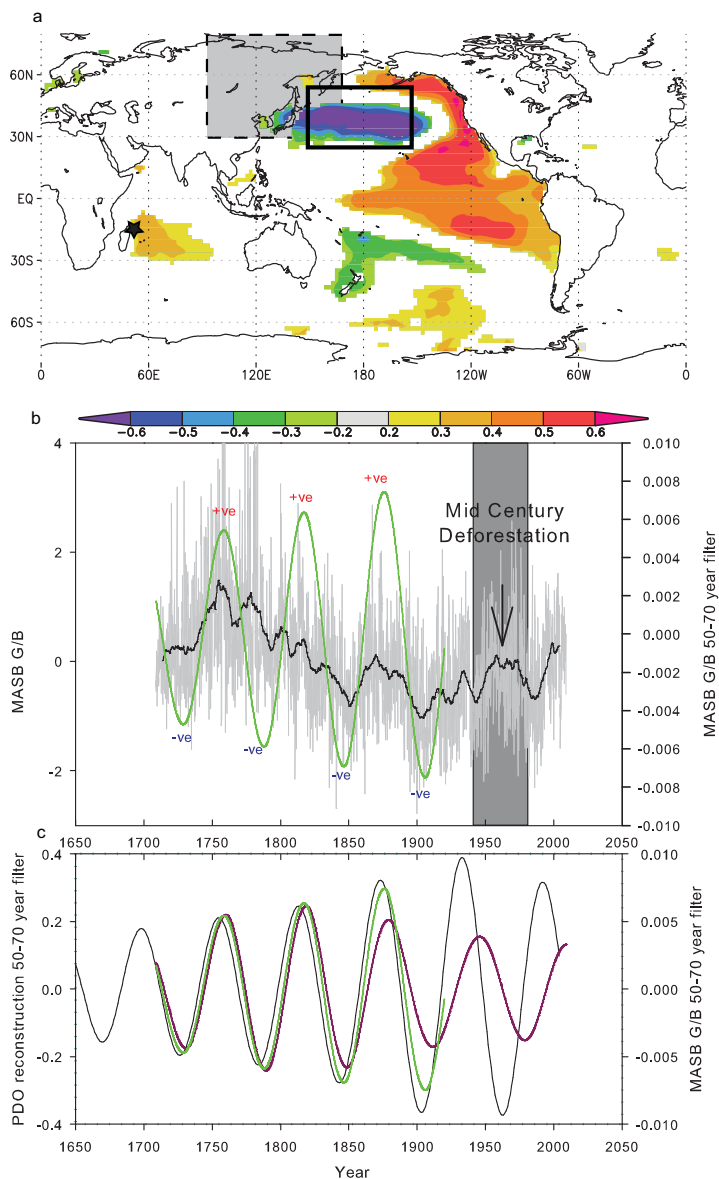


Figure 4.2. Typical positive PDO phase (a) indicated by global SST anomalies. Yearly (Jan – Dec) global SST (ERSSTv.3) correlate with the PDO index (Mantua et al., 1997), with positive and negative anomalies at >90% significance level indicated by colours. The black outlined box on the map (a) shows the strong negative anomalies of the central north Pacific during a positive PDO phase. The grey shaded box (a) indicates the region used to compile the NE Asian 500 year reconstructed tree ring PDO index (D’Arrigo and Wilson, 2006). Monthly MASB G/B (grey line) and the 10 year running mean (black line) are shown (b) together with

the 50 – 70 year band-pass filtered (0.017000 ± 0.002800) data up to 1920 (green). Peaks and troughs (b) represent multidecadal positive (red) and negative (blue) runoff anomalies. The same 50 – 70 year band pass filter (c) is also applied to the tree ring based PDO reconstruction (black), MASB G/B 1708 – 2008 (purple) and MASB G/B 1708 – 1920 (green). Both the tree ring based PDO reconstruction and the MASB G/B 1708 – 1920 are coherent (c), therefore positive PDO phases are associated with positive runoff anomalies. When considering the total MASB G/B time series (1708 – 2008), the relationship with the reconstructed PDO index breaks down post 1920.

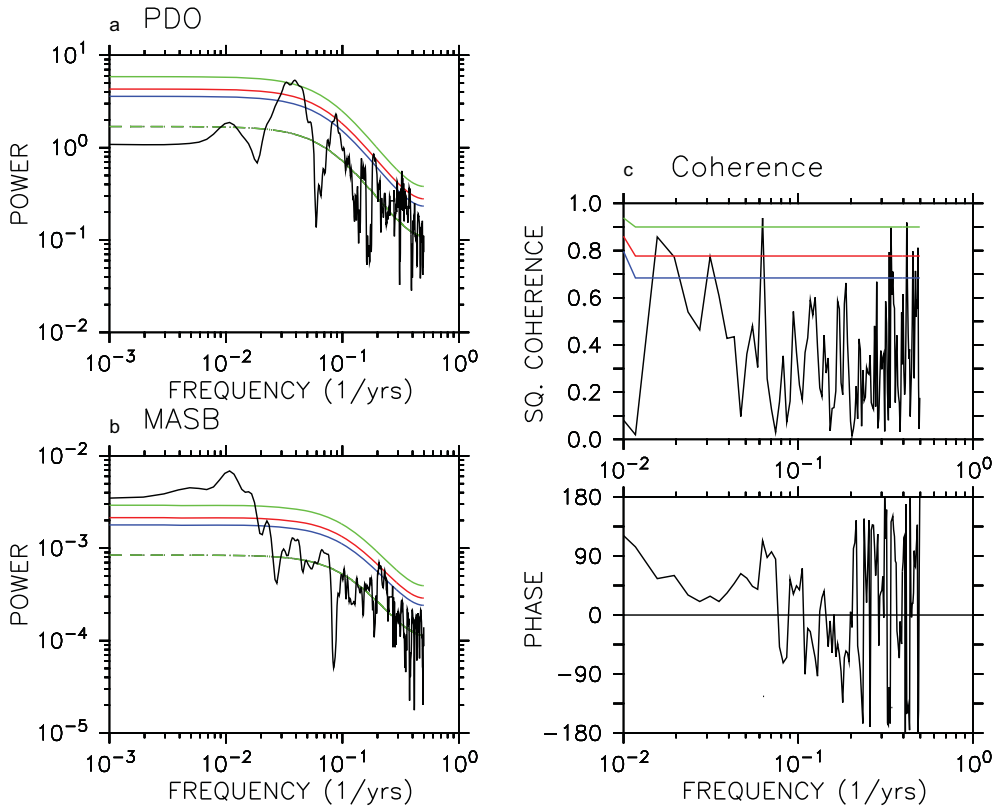


Figure 4.3. Spectrum of (a) the tree ring based PDO reconstruction (D’Arrigo and Wilson, 2006) and (b) MASB. Annual mean data are used for the analysis during 1708-1920 when two data sets are commonly available. Confidence levels are indicated with green (99%), red (95%), blue (90%) and green dashed (median) lines, respectively. Coherence and phase lag of the two annual datasets (c) are shown. Positive phase lag represents the lead of the PDO. Data are detrended prior to the analysis.

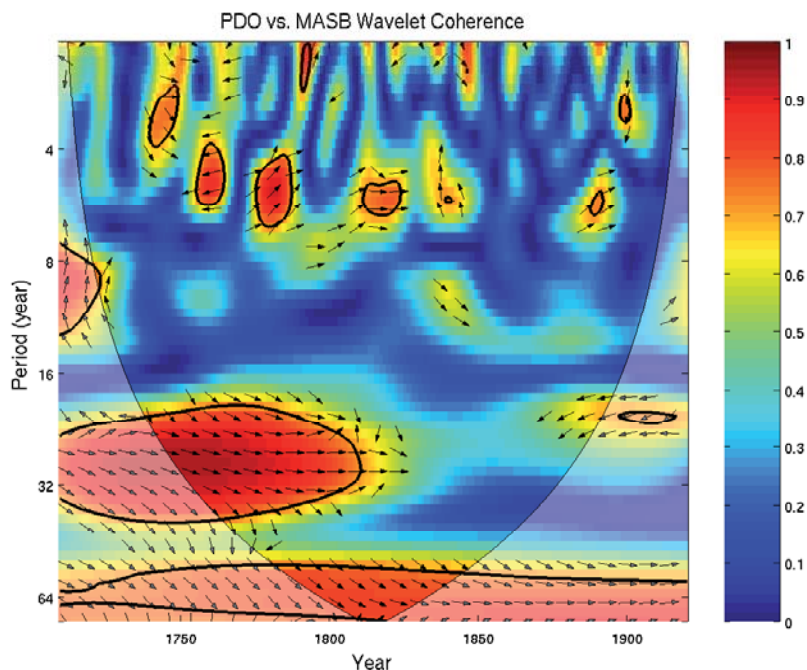


Figure 4.4. Cross wavelet coherence analysis with the tree ring based PDO reconstruction (D'Arrigo and Wilson, 2006) and MASB G/B indices, as used in Figure 4.3. The 5% significance level against red noise is shown as a thick contour. Phases are indicated as arrows, where directing right represents an in phase, and a clockwise direction indicates a lead of the PDO.

The coupling between increasing runoff and central Indian Ocean warming is evident after the prominent climate shift around 1976/77 when both global mean temperatures and rainfall strongly increased (Fig. 4.5) (Meehl et al., 2009). As Mn is also associated with seasonal soil runoff through erosion (Lewis et al., 2007), we observe similar increasing linear trends in the G/B and Mn/Ca ratios in response to Indian Ocean warming (Fig. S4.1; Appendix B). As G/B is a direct indicator of soil erosion and not rainfall, we removed the deforestation effect from the record prior to spectral analysis and filtering of the MAS1 time series by subtracting the normalised record of Mn/Ca from the normalised G/B record (Figs. 4.6 and S4.1; Appendix B). This also removed the long-term erosion trend, resulting in a G/B-Mn/Ca record that is reflecting the natural rainfall variability, now increasing from the mid-1950s in agreement with the SST and Ba/Ca data (Figs. 4.5 and 4.6).

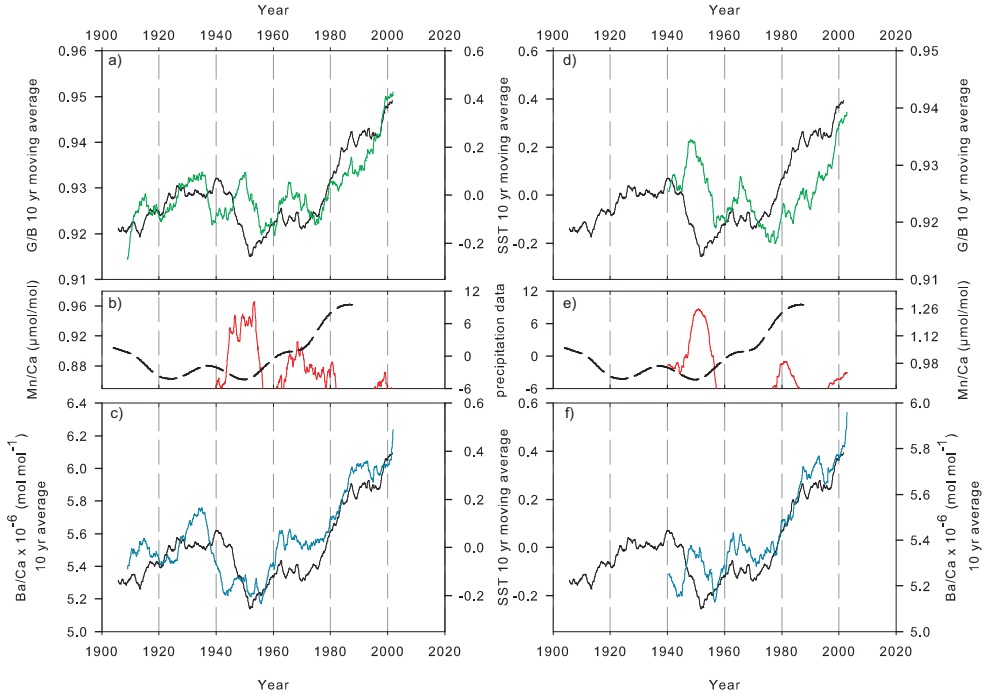


Figure 4.5. A 10-year running mean of MAS1 and MAS3 coral G/B (green) compared to the SST anomaly (ERSSTv.3) for the southern central Indian Ocean 5-20°S, 60-90°E (black) since 1904 (a, d), the coral Mn/Ca (red solid; $\mu\text{mol/mol}$) (b, e), and the Ba/Ca (blue) (c, f). Note that multi-decadal oscillations in G/B and Ba/Ca show high coherence with SST. Higher Mn/Ca ratios identify periods of slash and burn deforestation that overprint the climatic control of humic acid runoff. Differences observed between Ba/Ca and G/B is linked to watershed composition. A 120 month low pass filter of Antananarivo precipitation anomalies (18.80°S, 47.50°E, 1276m, WMO station code: 67083 ANTANANARIVO/IVATO) is shown (black dashed; b, e), indicating increasing rainfall conditions. Note that this precipitation record ends in 1987 due to recent data gaps.

Spectral analysis of the monthly instrumental PDO index (1880-present) (Mantua et al., 1997) and coral G/B-Mn/Ca show strong power in the multidecadal band (Fig. S4.2), in agreement with the pre-1920 frequency analysis of MASB G/B and the tree ring based PDO index (Figs. 4.3 and 4.4). The tight temporal relationship with the PDO index shows that a positive (negative) phase is associated with wet (dry) conditions (Fig. 4.6). Interestingly, G/B-Mn/Ca correlates with typical positive PDO-like conditions in global SSTs, coupled with a positive correlation with south central Indian

Ocean SST (Fig. 4.6). Also, in the Sr/Ca temperature proxy record of MAS1, a positive PDO phase is associated with a warm SST anomaly (Fig. 4.7), pointing to a typical response to Pacific decadal forcing found in Indian Ocean SST (Cole et al., 2000; Crueger et al., 2009; Deser et al., 2004; Krishnan and Sugi, 2003). The temporal alignment of all records (Sr/Ca, Ba/Ca, G/B-Mn/Ca) with the PDO (Fig. 4.7) therefore argue for Pacific modulation of Madagascar rainfall on multidecadal timescales for at least the past 300 years.

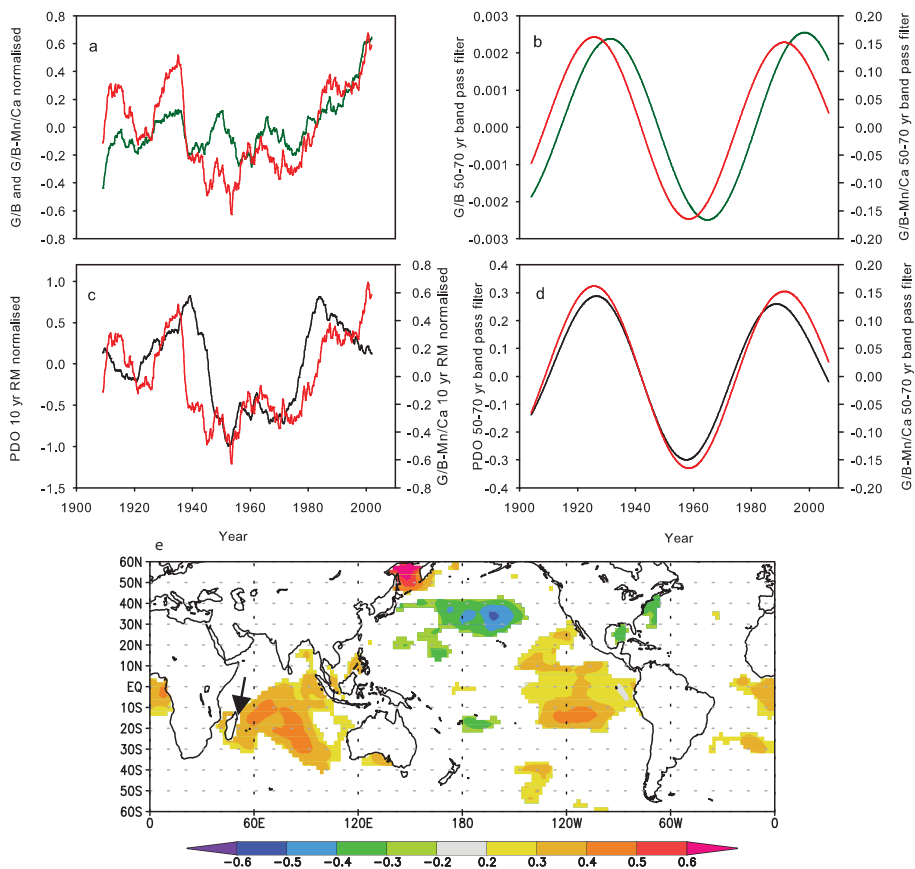


Figure 4.6. The 10 year running means (a, c) and 50 – 70 year band pass filter (b, d; 0.017000 ± 0.002800) of normalised MAS1 G/B (green), normalised MAS1 G/B-Mn/Ca (red) and the PDO (black). Note, with the removal of Mn/Ca from the G/B record, runoff is now in phase with the PDO. The spatial correlation of global SST (ERSSTv.3) with (e) the 360-month low pass filter of normalised MAS1 G/B-Mn/Ca is shown, indicating PDO-like spatial SST patterns (Fig. 4.2a). Only correlations above 90% significance level are shown. Correlations were computed at <http://climexp.knmi.nl/>. An arrow points the region where all coral cores were drilled in NE Madagascar.

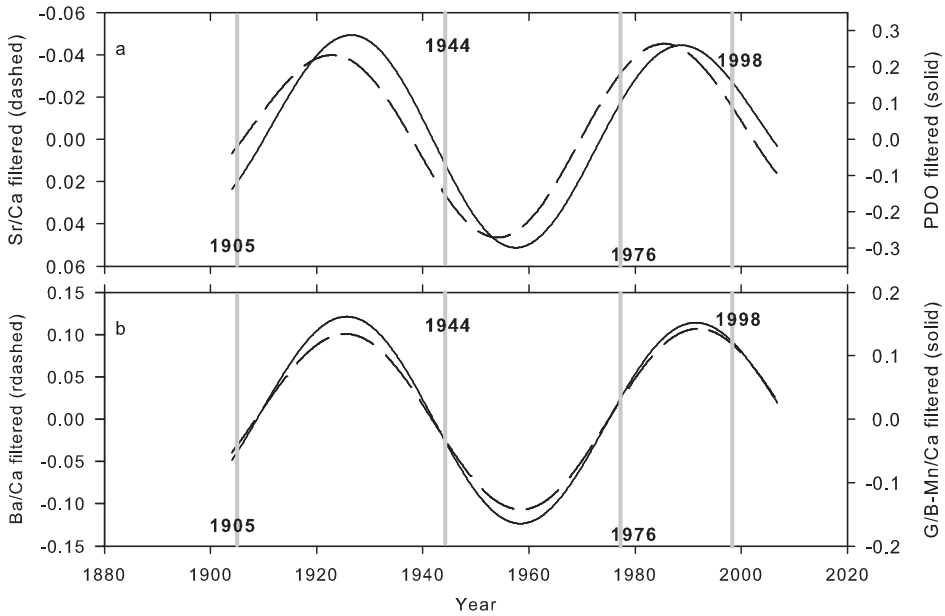


Figure 4.7. A 50 – 70 year band pass filter (0.017000 ± 0.002800) applied to (a) the MAS1 Sr/Ca data (dashed) and the Mantua PDO index (solid); and (b) MAS1 Ba/Ca (dashed) and MAS1 G/B-Mn/Ca (solid). The grey bars represent the transition years of different phase changes of the PDO.

Madagascar is an iconic example of the extreme environmental impacts human deforestation and habitat destruction has on soil runoff and land degradation (Green and Sussman, 1990; Harper et al., 2007). Human activity is also reported for two 200-300 year erosion records from Kenya that show a simultaneous major shift in base level runoff at 1906 ± 3 years and 1908 ± 5 years (Fleitmann et al., 2007). This 1908 shift in soil erosion was attributed predominantly to a change from traditional subsistence agriculture to intensive European land-use practices introduced by the British settlers. Yet, the Kenya coral records also indicate accelerated soil erosion between the late 1940s and early 1950s and in the late 1970s following periods of intense drought which occur simultaneously with shifts in our Madagascar coral records. These multidecadal runoff changes co-occur with the 1905, 1947 and 1976 shifts in the PDO, also suggesting a Pacific modulation of Kenyan soil erosion by rainfall.

The PDO/river runoff relationship in Great Barrier Reef corals and east Australia river gauges is opposite to that in Madagascar, as the negative PDO phase (i.e. 1947 to 1976) is linked with higher river discharge, and vice versa, for the positive PDO phase (Lough, 2007; McGowan et al., 2009). Correlating precipitation with the principle component time series of the IPO (Meehl and Hu, 2006), and the PDO (Felis et al., 2010) shows a negative response over eastern Australia and southern Africa, and a positive response in eastern Madagascar and eastern Africa (Fig. S4.5; Appendix D). Since Indian Ocean SST is sensitive to the PDO (Krishnan and Sugi, 2003) and rainfall is linked to SST (Goddard and Graham, 1999), runoff variability is ultimately controlled by Pacific Ocean multidecadal variability. During the positive PDO phase, higher mean SST is responsible for enhanced atmospheric convection over the Indian Ocean, which in turn drives anomalous subsidence over southern Africa and eastern Australia (Goddard and Graham, 1999; Hoerling et al., 2006; Lough, 2007; McGowan et al., 2009; Richard et al., 2000).

Long term coral data provide the first evidence that southwest Indian Ocean rainfall is linked to the PDO on multidecadal time scales. Consequently, for the upcoming decades rainfall in eastern Madagascar should decrease as the PDO is currently in a transition from a positive to a negative phase. Elsewhere, PDO teleconnected regions with weaker rains in recent decades should experience more precipitation, i.e. in eastern Australia and southern Africa. However, it remains a major milestone in future research to unravel if and when projected anthropogenic warming of the Indian Ocean (Forster et al., 2007) will dominate rainfall over the inherent multidecadal component. Our data illustrate this interplay as an acceleration of rainfall and erosion following the prominent 1976/77 climate shift (Meehl et al., 2009), which is related to both anthropogenic and multidecadal forcing. The widespread operation of Pacific multi-decadal modulation recognised here provides new constraints for future rainfall patterns on human timescales that will assist in water management, soil conservation and biodiversity programmes throughout the tropical Indo-Pacific.

Appendix A

Coherence and wavelet analysis

We compared the long time series of the PDO and MASB directly without using an agent (CIO SST). Annual mean data of the PDO reconstruction (D'Arrigo and Wilson, 2006) and MASB for the period 1708-1920 were used for coherence analysis. The reconstructed PDO (D'Arrigo and Wilson, 2006) and MASB show significant power at decadal, interdecadal and centennial time scales (Figs. 4.3a,b). Strong coherence between the PDO and MASB is found at multidecadal (60 yr) and bidecadal (15-30 yr) frequencies, with the PDO slightly leading MASB (Fig. 4.3c). Further, wavelet coherence analysis (Grinsted et al., 2004) with the same time series supports strong coherence between the PDO and MASB on interannual, bidecadal (20 -30 yr) and multidecadal bands (Fig. 4.4).

Appendix B

Coral Mn/Ca

The MAS1 Mn/Ca record is in and out of phase with the MAS1 G/B time-series on seasonal timescales (Fig. S4.1). This indicates that high Mn concentrations, associated with slash and burn deforestation, are likely flushed into Antongil Bay during both the wet and dry seasons. Both the G/B and Mn/Ca have similar runoff trends as shown by their linear equations (Fig. S4.1). This indicates that a fraction of Mn is flushed into the bay associated with the soils or sediment, not just ash fallout (Lewis et al., 2007). This fraction is, however, far weaker in concentration than that associated with ash fallout (Abram et al., 2003). By subtracting the normalised Mn/Ca record from the normalised G/B record, we remove the deforestation effect, as well as the long-term runoff trend (Fig. S4.1), leaving a G/B-Mn/Ca record that shows the natural runoff variability (Figs. 4.6 and S4.2). This method is conceptually similar to removing the thermal component of coral skeletal $\delta^{18}\text{O}$ by subtracting Sr/Ca, leaving the salinity component $\delta^{18}\text{O}_{\text{sw}}$ (Ren et al., 2002).

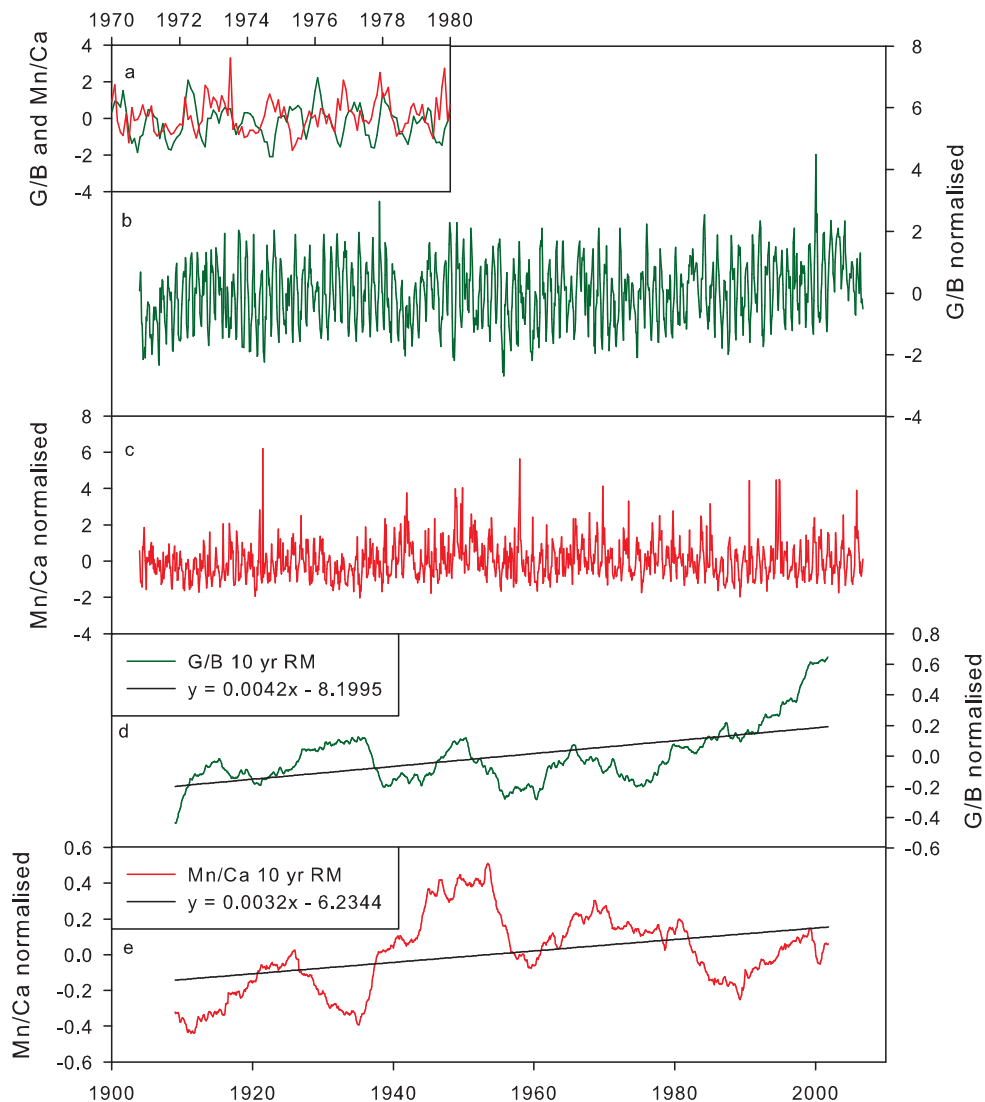


Figure S4.1. The seasonal alignment of (a) the MAS1 coral G/B record with Mn/Ca values for the years 1970 – 1980. The complete time-series of normalised (b) G/B and (c) Mn/Ca is shown in green and red, respectively. The 10 year running means of (d) G/B and (e) Mn/Ca are shown together with linear trends (black line). The regression equations of each line are given in the top left hand corner of each plot. Note that the trend lines have a similar slope.

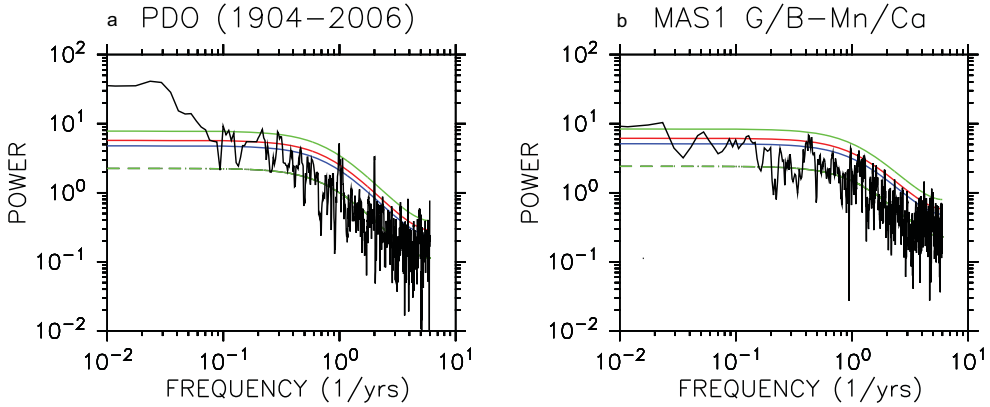


Figure S4.2. Spectrum of (a) the PDO index (Mantua et al., 1997) and (b) MAS1 G/B-Mn/Ca. Monthly anomaly data from January 1904 to October 2006 are used, whereby the monthly climatology of 1971-2000 is removed. Detrended data are standardised prior to spectral analysis. Confidence levels are indicated with green (99%), red (95%), blue (90%) and green dashed (median) lines, respectively.

Appendix C

Record segmentation analysis

Record segmentation analysis of the coral composite G/B record, which includes MAS1, MAS3 and ANDRA (Fig. 4.1), identify years within the G/B time series that correspond to phase changes in the PDO, south central Indian Ocean SST and periods of major deforestation (Figs. S4.3 and S4.4; Supplementary Material). Two major shifts are detected in the PDO time series: in 1944 and 1976. The timing of these major shifts is in agreement with PDO multi-decadal changes as described in previous studies (Minobe, 1997; Mantua et al., 1997). The 1944 shift of the PDO is associated with a shift in our composite G/B record (Fig. S4.3); however, SST data shows a highly significant transition 2 years later in 1946 (Fig. S4.4). This is most likely an artefact created by the sampling bias in observational data for this period (Gedalof et al., 2002). At the second major shift in the PDO in 1976, the south central Indian Ocean SST shows a prolonged transition from 1976 to 1982, whereas the G/B records a sharper transition in 1982 (Fig. S4.3). This difference in the timing of the transition is likely a perturbation created by the 1970s deforestation period. The transitions in G/B associated with the

years surrounding 1955 - 58 and 1970 (Figs. S4.3 and S4.4) are assigned to the enhanced deforestation marked by the highly pronounced Mn/Ca peaks (Fig. 4.2; Fig. S4.1). As the record segmentation method uses 2 x 10 year windows, the 1970's deforestation period influences the timing of the defined G/B transition (1982) in relation to the 1976 PDO shift.

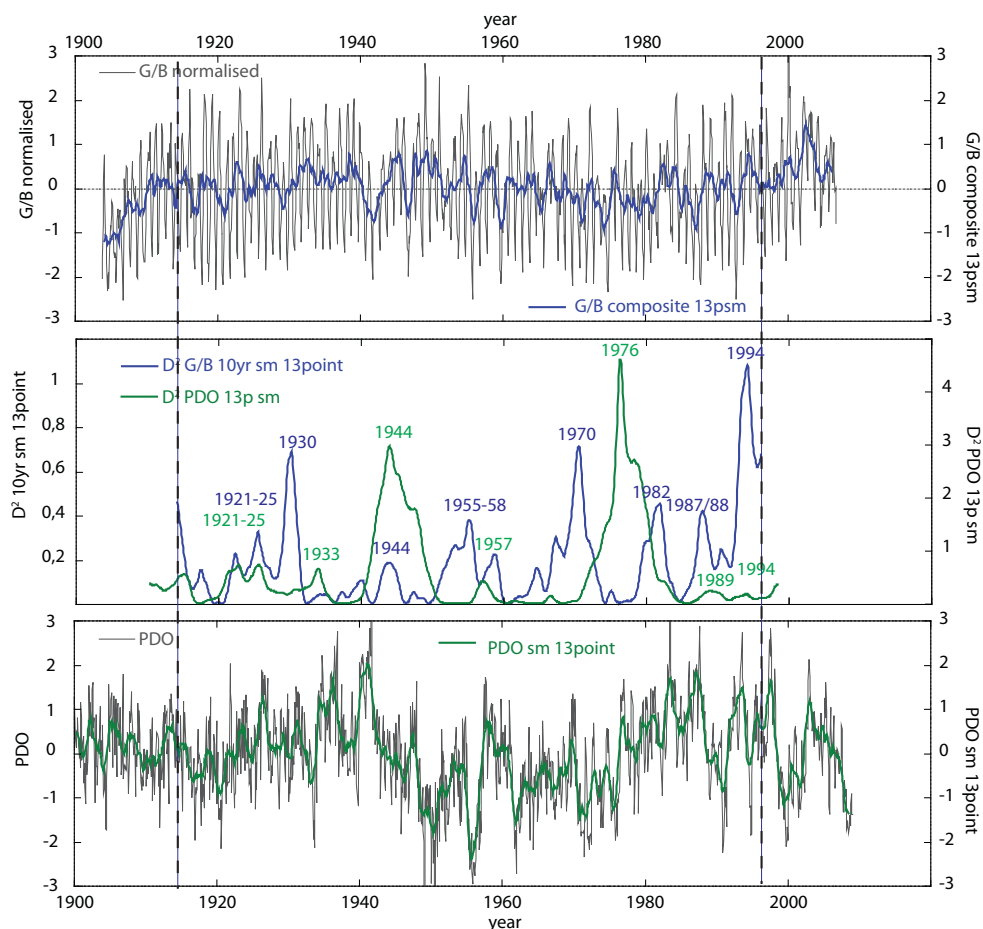


Figure S4.3. Record segmentation of the PDO vs. 3 core composite G/B (MAS1, MAS3 and ANDRA). The top panel shows the raw G/B record with a 13 point smoothing superimposed. Middle Panel shows the change points which are above the 95% significance level. Major change points are indicated by years (green = PDO; blue = G/B). Lower panel shows the raw PDO time series with a 13 point smoothing superimposed. The vertical dashed line marks the start and end point for reliable interpretation of the record segmentation analysis taking into account that the first and last 10 years cannot be used for interpretation.

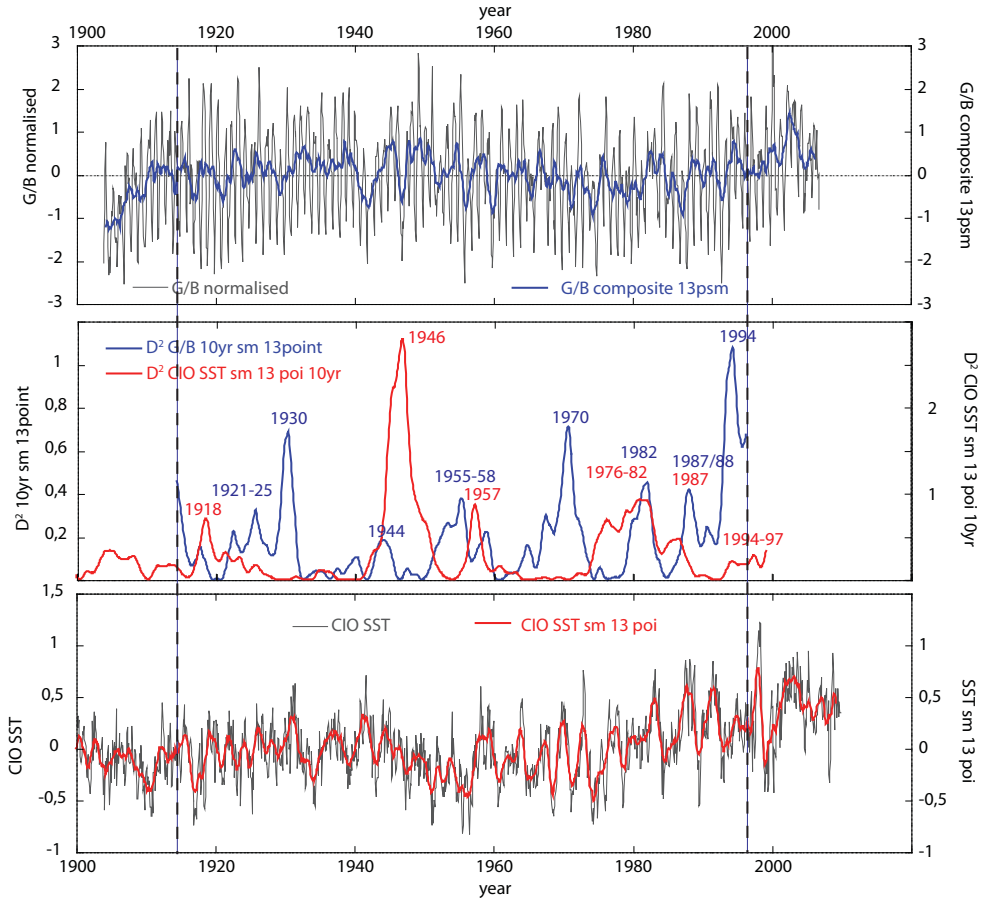


Figure S4.4. Record segmentation of the south CIO ERSST (Smith et al., 2008) vs. 3 core composite G/B (MAS1, MAS3 and ANDRA). The top panel shows the raw G/B record with a 13 point smoothing superimposed. Middle Panel shows the change points which are above the 95% significance level. Major change points are indicated by years (red = CIO SST; blue = G/B). Lower panel shows the raw CIO SST time series with a 13 point smoothing superimposed. The vertical dashed line marks the start and end point for reliable interpretation of the record segmentation analysis taking into account that the first and last 10 years cannot be used for interpretation.

Significant shifts (2 x 10-year window) in the G/B also occurred in 1921 - 25, 1930, 1944, 1955 - 1958, 1970, 1982, 1987 - 1988 and recently in 1994 (Figs. S4.3 and S4.4). Other than the two major shifts in the PDO (Gedalof et al., 2002; Mantua et al., 1997) at 1944 and 1976 (1982), significant transitions at 1921 - 25, 1930 - 1933, 1957, 1989 and 1994 also co-occur with G/B (Fig.

S4.3). The south CIO SST shows transitions in 1918, 1946, 1957, 1976 - 1982, 1987 and 1994 - 1997 (Fig. S4.4). Minor shifts in the PDO are associated with the interdecadal frequency mode (Interdecadal Pacific Oscillation/IPO), which are also recorded in the G/B and the south CIO SST at 1921 - 1925, 1930 - 1933, 1955 - 1958, 1987 - 1989 and 1994 (Figs. S4.3 and S4.4). The 1994 shift most likely marks the start of a transition to a negative PDO phase on multi-decadal time scales (Verdon and Franks, 2006). The deforestation period in the 1950's overlaps with one of the interdecadal changes in the PDO and south CIO SST.

Appendix D

Spatial correlation of the PDO with rainfall

A spatial correlation of the PDO and global rainfall supports our results, with a negative correlation shown in southern Africa, eastern Australia (Lough, 2007; McGowan et al., 2009) and the northern Rocky Mountains (St. Jacques et al., 2010), as well as a positive correlation in Madagascar (Fig. S4.5). These results are replicated by the spatial correlation pattern of the IPO (Meehl and Hu, 2006) and PDO (Felis et al., 2010) with precipitation.

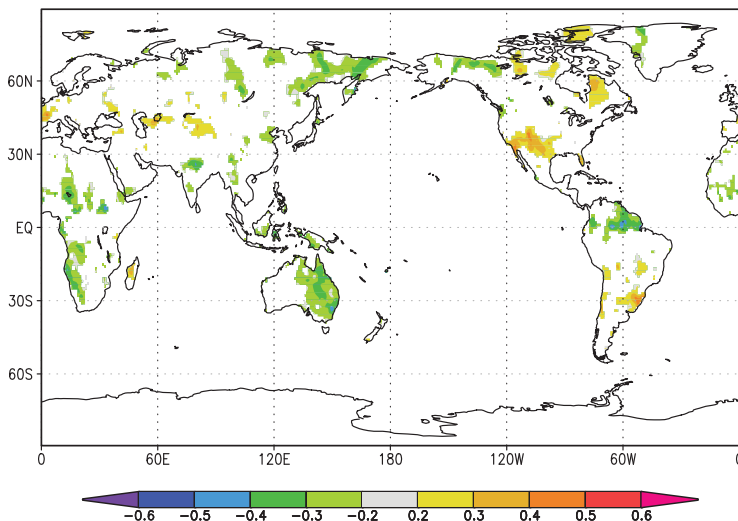


Figure S4.5. Spatial correlation of mean annual averages (May to April) of the Pacific Decadal Oscillation (PDO) (Mantua et al., 1997) with global annually averaged (May to April) rainfall data produced by the Climate Research Unit (CRU) at the University of East

Anglia (CRU TS3) (Mitchell and Jones, 2005). Colour shading represents confidence of 90% and greater. Red shading indicates positive correlations and green negative correlations. Note the positive correlation of rainfall with the PDO over Madagascar and negative correlation over Eastern Australia and the Northern Rocky Mountains. Correlations were computed at <http://climexp.knmi.nl/>.

Supplementary Information

Records Segmentation methodology: Appendix C

The G/B time series used for record segmentation analysis was created by normalising the three short coral G/B records (MAS1, MAS3, ANDRA) and taking an average, therefore creating a single composite record. To detect shifts in the G/B composite, PDO index and SST time series, we applied a segmentation analysis. Webster (1979) aims to divide a given time series into relatively (statistically) homogeneous segments (Webster, 1979). In order to do so, a window, split about its midpoint, is moved along the sequence, from one end to the other, while at each position in the record the two halves are statistically compared by calculating the D^2 statistic, i.e. the Mahalanobis distance. In the next step, the D^2 statistic is plotted as ordinate against the window midpoint position, thereby indicating division points in the time series as local maxima. Following Webster (1979), we chose a window size of 20 years, hence comprising two half windows of each 10 years, allowing us to detect points of maximum change at decadal time scales (Webster, 1979). Given our record has a monthly time resolution, $10 \times 12 = 120$ points comprise the half window size. This means that at every point in the time series we compare the statistics of 120 point backward to the statistics of a window of 120 points forward. We apply the segmentation analysis predominantly to detect points at which a major transition takes place in the G/B, PDO and SST time series. Although the 95% significance of the D^2 statistic is reached at a level of $D^2 = 0.05$, it is important to note that not the absolute value but rather the local maxima should be considered as the transitions or change point in the time series. It is important to keep in mind that, given the window size of 2×10 years, we are not able to interpret change points in the first and the last 10 years of the time series.

Acknowledgements: This work was supported as part of the SINDOCOM grant under the Dutch NWO program ‘Climate Variability’, grant 854.00034/035. Additional support comes from the NWO ALW project CLIMATCH, grant 820.01.009, and the Western Indian Ocean Marine Science Association through the Marine Science for Management programme under grant MASMA/CC/2010/02. We thank the Wildlife Conservation Society (WCS) Madagascar, especially Heriliala Randriamahazo and the WCS/ANGAP team in Maroantsetra, for their support in fieldwork logistics and in the organisation of the research permits. We would also like to thank CAF/CORE Madagascar for granting the CITES permit and ANGAP Madagascar for support of our research activities in the vicinity of the marine and forest nature parks. Furthermore we would like to thank Bob Koster and Rineke Gieles for their continuous development and maintenance of the XRF-Core Scanner, and Rik Tjallingii and Thomas Richter for their fruitful discussions concerning the manuscript. We are grateful to the ARC Centre of Excellence in Coral Reef Studies and ANU Research School of Earth Sciences for support of the Laser-Ablation analysis.

References

- Abram, N.J., Gagan, M.K., McCulloch, M.T., Chappell, J. and Hantoro, W.S., 2003. Coral reef death during the 1997 Indian Ocean Dipole linked to Indonesian wildfires. *Science* 301, 952-955.
- Alibert, C., McCulloch, M.T., 1997. Strontium/calcium ratios in modern *Porites* corals from the Great Barrier Reef as a proxy for sea surface temperature: calibration of the thermometer and monitoring of ENSO. *Paleoceanography* 12, 345-363.
- Arblaster, J.M., Meehl, G.A. and Moore, A., 2002. Interdecadal modulation of Australian rainfall. *Climate Dynamics* 18, 519-531.
- Barnes, D.J., Taylor, R.B., 2005. On the nature and causes of luminescent lines and bands in coral skeletons: II. Contribution of skeletal crystals. *Journal of Experimental Marine Biology and Ecology* 322, 135-142.
- Birkinshaw, C., Randrianjanahary, M., 2007. The effects of Cyclone Hudah on the forest of Masoala Peninsula, Madagascar. *Madagascar Conservation & Development* 2(1), 17-20.
- Cane, M.A., 2010. Decadal predictions in demand. *Nature Geoscience* 3, 231-232.
- Cole, J.E., Dunbar, R.B., McClanahan, T.R. Muthiga, N.A., 2000. Tropical Pacific forcing of decadal SST variability in the Western Indian Ocean over the past two centuries. *Science* 287, 617-619.
- Corrège, T., 2006. Sea surface temperature and salinity reconstructions from coral geochemical tracers. *Palaeogeography Palaeoclimatology Palaeoecology* 232, 408-428.
- Crueger, T., Zinke, J. Pfeiffer, M., 2009. Patterns of Pacific decadal variability recorded by Indian Ocean corals. *International Journal of Earth Sciences* 98, 41-52.
- D'Arrigo, R. Wilson, R., 2006. On the Asian expression of the PDO. *International Journal of Climatology* 26, 1607-1617.
- Deser, C., Phillips, A.S. Hurrell, J.W., 2004. Pacific Interdecadal climate variability: linkages between the tropics and the North Pacific during boreal winter since 1900. *Journal of Climate* 17, 3109-3124.
- Fallon, S.J., White, J.C., McCulloch, M.T., 2002. *Porites* corals as recorders of mining and environmental impacts: Misima Island, Papua New Guinea. *Geochimica et Cosmochimica Acta* 66, 45-62.
- Felis, T., Suzuki, A., Kuhnert, H., Rimbu, N. Kawahata, H., 2010. Pacific Decadal Oscillation documented in a coral record of North Pacific winter temperature since 1873. *Geophysical Research Letters* 37, L14605, doi:10.1029/2010GL043572.
- Fleitmann, D., Dunbar, R.B, McCulloch, M.T., Mudelsee, M., Vuille, M., McClanahan, T.R., Cole, J.E., Eggins, S., 2007. East African soil erosion recorded in a 300 year old coral colony from Kenya. *Geophysical Research Letters* 34, L04401, doi:10.1029/2006GL028525.
- Forster, P. *et al.*, 2007. Changes in Atmospheric Constituents and in Radiative Forcing, Ch. 2 *Climate Change 2007: The Physical Science Basis. Contribution of Working Group I to the Fourth Assessment Report of the Intergovernmental Panel on Climate Change*, eds. Solomon, S. *et al.* Cambridge Univ. Press, Cambridge, UK.

- Funk, C., Dettinger, M.D., Michaelsen, J.C., Verdin, J.P., Brown, M.E., Barlow, M., Hoell, A., 2008. Warming of the Indian Ocean threatens eastern and southern African food security but could be mitigated by agricultural development. *Proceedings of the National Academy of Sciences USA* 105, 11081-11086.
- Gedalof, Z., Mantua, N.J., Peterson, D.L., 2002. A multi-century perspective of variability in the Pacific Decadal Oscillation: new insights from tree rings and coral. *Geophysical Research Letters* 29, doi:10.1029/2002GL015824.
- Gerten, D., Rost, S., von Bloh, W., Lucht, W., 2008. Causes of change in 20th century global river discharge. *Geophysical Research Letters* 35, L20405, doi:10.1029/2008GL035258.
- Goddard, L. Graham, N.E., 1999. Importance of the Indian Ocean for simulating rainfall anomalies over eastern and southern Africa. *Journal of Geophysical Research* 104, 19099-19116.
- Green, G.M. Sussman, R.W., 1990 Deforestation history of the eastern rain forests of Madagascar from satellite images. *Science* 248(4952), 212-215.
- Grinsted, A., Moore, J.C., Jevrejeva, S., 2004. Application of the cross wavelet transform and wavelet coherence to geophysical time series. *Nonlinear Processes in Geophysics* 11, 561-566.
- Grove, C.A. Nagtegaal R., Zinke, J., Scheufen, T. Koster, B., Kasper, S., McCulloch, M.T., van den Bergh, Brummer, G-J.A., 2010. River runoff reconstructions from novel spectral luminescence scanning of massive coral skeletons. *Coral Reefs* 29(3), 579-591.
- Harper, G.J., Steininger, M.K., Tucker, C.J., Juhn, D., Hawkins, F., 2007. Fifty years of deforestation and forest fragmentation in Madagascar. *Environmental Conservation* 34(4), 325-33.
- Hoerling, M., Hurrell, J., Eischaid, J., Phillips, A., 2006. Detection and attribution of 20th century northern and southern African rainfall change. *Journal of Climate* 19, 3989-4008.
- Isdale, P., 1984. Fluorescent bands in massive corals record centuries of coastal rainfall. *Nature* 310, 578-579.
- Jury, M.R., Parker, B.A., Raholijao, N., Nassor, A., 1995. Variability of summer rainfall over Madagascar: Climate determinants at interannual scales. *International Journal of Climatology* 15, 1323-1332.
- Kremen, C., 2003. The natural history of Madagascar: The Masoala Peninsula. Edited by Goodman, S.M., and Benstead, J.P., University of Chicago Press, Chicago, 1459-66.
- Krishnan, P. Sugi, M., 2003. Pacific decadal Oscillation and variability of the Indian summer monsoon rainfall. *Climate Dynamics* 21, 233-242.
- Lewis, S.L., Shields, G.A., Kamber, B.S., Lough, J.M., 2007. A multi-trace element coral record of land-use changes in the Burdekin River catchment, NE Australia. *Palaeogeography Palaeoclimatology Palaeoecology* 246, 471-487.
- Lough, J.M., 2007. Tropical river flow and rainfall reconstructions from coral luminescence: Great Barrier Reef, Australia. *Paleoceanography* 22, PA2218, doi:10.1029/2006PA001377.
- Lough, J.M., Barnes, D.J., Mcallister, F.A., 2002. Luminescent lines in corals from the Great Barrier Reef provide spatial and temporal records of reefs affected by land runoff.

- Coral Reefs 21, 333-343.
- Mantua, N.J., Hare, S.R., Zhang, Y., Wallace, J.M., Francis, R.C., 1997. A Pacific interdecadal climate oscillation with impacts on salmon production. *Bulletin of the American Meteorological Society* 78, 1069-1079.
- McCulloch, M.T., Fallon, S., Wyndham, T., Hendy, E., Lough, J., Barnes, D., 2003. Coral record of increased sediment flux to the inner Great Barrier Reef since European settlement. *Nature* 421(6924), 727-730.
- McGowan, H.A., Marx, S.K., Denholm, J., Soderholm, J., Kamber, B.S., 2009. Reconstructing annual inflows to the headwater catchments of the Murray River, Australia, using the Pacific Decadal Oscillation. *Geophysical Research Letters* 36, L06707, doi:10.1029/2008GL037049.
- Meehl, G.A., Hu, A., 2006. Megadroughts in the Indian Monsoon Region and Southwest North America and a mechanism for associated Multidecadal Pacific Sea Surface Temperature Anomalies. *Journal of Climate* 19, 1605-1623.
- Meehl, G.A., Hu, A., Santer, B.D., 2009. The mid-1970s climate shift in the Pacific and the relative roles of forced versus inherent decadal variability. *Journal of Climate* 22, 780-792.
- Minobe, S., 1997. A 50–70 year climatic oscillation over the North Pacific and North America. *Geophysical Research Letters* 24(6), 683–686, doi:10.1029/97GL00504.
- Mitchell, T.D., Jones, P.D., 2005. An improved method of constructing a database of monthly climate observations and associated high-resolution grids. *International Journal of Climatology* 25, 693-712, doi:10.1002/joc.1181.
- Reason, C.J.C., Rouault, M., 2002. ENSO-like decadal variability and South African rainfall. *Geophysical Research Letters* 29(13), 1638-1641, doi:10.1029/2002GL014663.
- Ren, L., Linsley, B.K., Wellington, G.M., Schrag, D.P., Hoegh-guldberg, O., 2002. Deconvolving the $\delta^{18}\text{O}$ seawater component from subseasonal coral $\delta^{18}\text{O}$ and Sr/Ca at Rarotonga in the southwestern subtropical Pacific for the period 1726 to 1997. *Geochimica et Cosmochimica Acta* 67(9), 1609-1621.
- Richard, Y., Trzaska, S., Roucou, P., Rouault, M., 2000. Modification of the southern African rainfall variability/ENSO relationship since the late 1960's. *Climate Dynamics* 16, 883-895.
- Schneider, N., Cornuelle, B.D., 2005. The Forcing of the Pacific Decadal Oscillation. *Journal of Climate* 18, 4355–4373.
- Sinclair, D.J., Kinsley, L.P.J., McCulloch, M.T., 1998. High resolution analysis of trace elements in corals by laser ablation ICP-MS. *Geochimica et Cosmochimica Acta* 62, 1889-1901.
- Sinclair, D.J., McCulloch, M.T., 2004. Corals record low mobile barium concentrations in the Burdekin River during the 1974 flood: evidence for limited Ba supply to rivers? *Palaeogeography Palaeoclimatology Palaeoecology* 214, 155-174.
- Smith, T.M., Reynolds, R.W., Peterson, T.C., Lawrimore, J., 2008. Improvements to NOAA's Historical Merged Land-Ocean Surface Temperature Analysis (1880-2006). *Journal of Climate* 21, 2283-2296.
- St. Jacques, J.-M., Sauchyn, D.J., Zhao, Y., 2010. Northern Rocky Mountain streamflow records: Global warming trends, human impacts or natural variability? *Geophysical*

Chapter 4

- Research Letters 37, L06407, doi:10.1029/2009GL042045.
- Verdon, D.C., Franks S.W., 2006. Long-term behaviour of ENSO: Interactions with the PDO over the past 400 years inferred from paleoclimate records. *Geophysical Research Letters* 33, L06712, doi:10.1029/2005GL025052.
- Webster, R., 1973. Automatic Soil-Boundary Location from Transect Data. *Mathematical Geology* 5(1), 27-37.
- Webster, R., 1979. Divide: A FORTRAN IV program for segmenting multivariate one-dimensional spatial series. *Computers and Geosciences* 6, 61-68.
- Zinke, J., Pfeiffer, M., Timm, O., Dullo, W-C., Kroon, D., Thomassin, B.A., 2008. Mayotte coral reveals hydrological changes in the western Indian Ocean between 1881 and 1994. *Geophysical Research Letters* 35, L23707, doi:10.1029/2008GL035634.

Chapter 5

Opposing Sr/Ca response to reef scale sea surface temperature in Eastern Madagascar corals: implications for tropical paleothermometry

Craig A. Grove, Sebastian Kasper, Jens Zinke, Miriam Pfeiffer,
Dieter Garbe-Schönberg and Geert-Jan A. Brummer

Abstract

Massive corals offer continuous records of climate locked within their skeleton, with the most commonly applied paleo-thermometer being Sr/Ca. Recently, however, problems with Sr/Ca thermometry indicate that the intrinsic variance of single-core Sr/Ca time series differs from core to core. Here, we compare the Sr/Ca records and growth parameters of two *Porites lutea* colonies sampled 0.72 km apart, with two gridded SST datasets, ERSST and HadISST, off NE Madagascar. Specifically, we address the seasonal and interannual variability as well as trend differences between records over the same 43 year period. The two gridded SST datasets showed strong seasonality and weak positive ENSO anomalies on a slow 43-year warming trend at slightly different rates. Both the coral Sr/Ca records showed the same clear seasonality and similar amplitudes in SST. However, on interannual timescales they displayed diverging 43-year Sr/Ca trends and opposite responses to weak ENSO anomalies. Moreover, their growth response also differed as one coral showed increasing extension/calcification rates and Sr/Ca ratios (cooling) over the 43 years, while the other coral showed decreasing extension/calcification rates and Sr/Ca ratios (warming). Further, during positive ENSO events the calcification rates of the two corals were negatively correlated, while skeletal density anomalies were opposite. Possible explanations to why these corals are so different may be related to SST variability itself. The growth response of individual corals to rising SST seems to be opposite, which in turn may be related to biological factors, such as zooxanthellae genetic types. Consequently, coral growth responses likely explain much of the inter-colony Sr/Ca variability.

Introduction

Massive corals, such as *Porites* spp., can grow for centuries while residing in a fixed position, continuously building an aragonite (CaCO_3) skeleton at a rate between 0.5 - 2 cm yr^{-1} . As the coral precipitates its skeleton, a number of minor and trace elements are incorporated at different concentrations relative to Ca in relation to changing physiochemical parameters (Felis and Pätzold, 2003). The Sr/Ca ratio of the coral aragonite seems to be the most robust paleo-thermometer, whereby a negative relationship exists with SST,

i.e. as temperatures increase, less Sr is incorporated into the aragonite lattice relative to Ca (Alibert and McCulloch, 1997; DeLong et al., 2007). Since Sr has a long oceanic residence time, heterogeneity in skeletal Sr/Ca is assumed to mainly reflect SST variability. Therefore, down-core sampling of massive corals yields an *in situ* SST time-series in which the resolution is only limited by the coral growth rate. A compilation of Sr/Ca-SST calibrations for *Porites* spp. revealed a mean Sr/Ca relationship with SST of $-0.061 \text{ mmol/mol per } 1^\circ\text{C}$ increase (Corrège, 2006).

Despite many successful Sr/Ca-based SST reconstructions, skeletal Sr/Ca heterogeneity has been found to not only reflect temperature variability. Micro-analytical studies have shown the distribution of Sr to be highly heterogeneous at the micrometer scale, corresponding to skeletal components and ultra-structure (Allison, 1996; Cohen et al., 2002). Consequently, sampling along intersects of the corralite bundles (valleys) should be avoided where Sr/Ca are relatively high (Alibert and McCulloch, 1997; DeLong et al., 2007; Hart and Cohen, 1996). Other biological factors, or ‘vital effects’, are also thought to influence Sr concentrations in the skeleton. Changing extension rate and density of the corals, associated with calcification processes (vital effect), have been shown to correlate with Sr/Ca (Alibert and McCulloch, 1997; Allison, 1996; Allison et al., 2001; Cohen and Gaetani, 2010; Ferrier-Pages et al., 2002; Sinclair et al., 2005; de Villiers et al., 1994). Complicating the relationship further, some studies have found that temperature itself is influencing growth parameters such as coral extension rates (Lough and Barnes, 2000; Storz and Gischler, 2011). This in turn may indirectly influence the Sr/Ca signal.

Recently published coral Sr/Ca records covering the past hundreds of years indicate specific problems with the Sr/Ca thermometer, particularly on decadal to secular time scales (e.g., Linsley et al., 2004, Linsley et al., 2006; Quinn et al. 2006). Pfeiffer et al. (2009) showed that the intrinsic variance of the single-core Sr/Ca time series differs from core to core, limiting their use for absolute estimates of past temperature variations. This inter-colony variability seems linked to vital effects. Averaging the multiple-core data improves the correlation with instrumental temperature and allows more accurate estimates of interannual temperature variations (0.35°C or better; Pfeiffer et al., 2009).

Here, we assess the reproducibility of SST reconstructions from two northeast Madagascar coral Sr/Ca records, located 0.72 km apart. We argue that single core Sr/Ca reconstructions are modulated by changes in the colony growth response to temperature, which may overwhelm the actual SST signal in the skeleton (Cohen and Gaetani, 2010; Gaetani et al., 2011). To test this we examine the inter-colony skeletal Sr/Ca variability and trends of two corals over the same 43 year period, and compare our results with growth parameters and gridded SST for the region.

Historical SST data

The assessment of site specific reef environments to temperature change is largely based on the analyses of long-term gridded instrumental SST data (e.g. McClanahan et al. 2009). As this form of data averages large areas ($1^{\circ}\times 1^{\circ}$ or $2^{\circ}\times 2^{\circ}$) with few *in situ* measurements, reef scale interannual (ENSO) variability and long-term SST trends may be underestimated. Indeed, our study site in northeast Madagascar has little or no historical *in situ* SST observations (ICOADS SST data; Woodruff et al., 2005), making it difficult to assess the validity of skeletal Sr/Ca as a reef scale paleothermometer. Nevertheless, we use two gridded SST datasets to evaluate relative regional trends and interannual variability, and compare with coral Sr/Ca-based SST variability.

Historical SST data collected primarily by ships-of-opportunity has been summarised in the comprehensive ocean atmosphere data set (ICOADS) to produce monthly averages on a $2^{\circ}\times 2^{\circ}$ grid basis (Woodruff et al., 2005). In the grid that includes the island of St. Marie (northeast Madagascar) the data are extremely sparse (<http://climexp.knmi.nl>). We therefore extracted SST from the extended reconstructed SST (ERSST) version 3 (Smith and Reynolds, 2004), also based on ICOADS data, which uses sophisticated statistical methods to reconstruct SST in time of sparse data. From ERSST, we extracted data in the $2^{\circ}\times 2^{\circ}$ grid centred at $49\text{--}50^{\circ}\text{E}$, $17\text{--}18^{\circ}\text{S}$. Over the period 1963 to 2006, the ERSST data averaged 26.31°C ($\pm 1.60^{\circ}\text{C}$), with an average annual range of 5.61°C (Table 5.1).

Variable	ERSST v.3b2 SST 49°-50°E, 17°-18°S	HadISST 49°-50°E, 17°-18°S
Mean	26.31	26.48
Standard Error	0.07	0.07
Median	26.24	26.68
Mode	28.16	28.03
Standard Deviation	1.60	1.58
Sample Variance	2.56	2.50
Kurtosis	-1.44	-1.41
Skewness	-0.09	-0.19
Range	5.61	5.62
Minimum	23.29	23.56
Maximum	28.90	29.18
Sum	13601.54	13690.47
Count	517.00	517.00
SST rise (°C yr ⁻¹)	0.010	0.002

Table 5.1. Statistical comparison of ERSST and HadISST for the same study site (49°-50°E – 17°-18°S) based on monthly replicated 100 × 100 km data for the years between 1963 and 2006.

In addition to ERSST, we used Met Office Hadley Centre’s sea ice and sea surface temperature (HadISST) data for the grid 49-50°E, 17-18°S (Rayner et al., 2003). HadISST temperatures are reconstructed using a two-stage reduced-space optimal interpolation procedure, followed by superposition of quality-improved gridded observations onto the reconstructions to restore local detail. Since January 1982, SST time series for HadISST use the optimal interpolation SST (OISST), version 2 (Reynolds et al., 2002) that includes continuous time series of satellite-based SST measurements. Over the period 1963 to 2006, the HadISST data averaged 26.48°C ($\pm 1.58^\circ\text{C}$), with an average annual range of 5.62°C (Table 5.1).

For the entire time series ERSST and HadISST show only slight statistical differences, with the exception of a two fold difference in the skewness of the data (Table 5.1). Consequently, the 43-year trend from 1963 to 2006 in ERSST and HadISST differs, being 0.010°C year⁻¹ and 0.002°C year⁻¹, respectively (Table 5.1). Nevertheless, we assume some degree of warming has occurred in the region over the 43-year period, and will test whether our corals record this warming in their skeletal Sr/Ca records.

During a positive El Niño-Southern Oscillation (ENSO) event the southwest Indian Ocean, including our study site, experiences small positive SST anomalies during the mature ENSO phase between January - March (JFM; Fig. S5.1, Schott et al., 2009). The twelve El Niño events (defined by the Oceanic Niño Index/ONI; www.cpc.ncep.noaa.gov) that occurred between the period 1963 – 2006 (1966, 1969, 1973, 1977, 1983, 1987, 1988, 1992, 1995, 1998, 2003, 2005) lead to minor, variable warming around the St. Marie region of 0.22°C ($\pm 0.23^{\circ}\text{C}$) and 0.25°C ($\pm 0.23^{\circ}\text{C}$), calculated over a 3-month average from January to March according to ERSST and HadISST, respectively ($\text{JFM}_{\text{ENSO}} - \text{JFM}_{\text{tot}}$; Table S5.1). The magnitude of these SST anomalies is small, and therefore lie within the range of observational errors (Annamalei et al., 1999), potentially resulting in a poor signal-to-noise ratio of Indian Ocean grid SST.

Materials and Methods

Coral Sampling

In March 2007, coral cores STM2 and STM4 were drilled from two separate massive dome-shaped colonies of *Porites lutea* on the eastern side of St. Marie, an island off the East coast of Madagascar facing the open SW Indian Ocean (Fig. 5.1). Colony STM4 measured 4.5 m in height and 3.5 m in diameter, while colony STM2 was 1.8 m in height with a diameter of 1.8 m. A commercially available pneumatic drill (Rodcraft 4500) was used to extract 4 cm diameter cores along the central growth axis of the colony. The apexes of the colonies were situated 1.0 m and 0.5 m below the water surface at low tide for STM2 and STM4, respectively (Table 5.2). Colonies were located 0.72 km from each other, both experiencing clear oceanic waters as there was full exchange with the open ocean (Fig. 5.1; Table 5.2). The total length of cores STM2 and STM4 were 180 cm and 365 cm, respectively.

Coral cores were sectioned lengthwise into equal 7 mm thick slabs, rinsed several times with demineralised water, blown with compressed air to remove any surficial particles and dried for more than 24 hours in a laminar flow hood. Annual bands were visualised by X-radiograph-positive prints and luminescence imagery (Grove et al., 2010; Hendy and Gagan, 2003). As there

is no humic acid input from terrestrial sources, the intensity of luminescence is considered to be a product of density only (Barnes and Taylor, 2005; Grove et al., 2010). Visualising the growth axis of the coral slab meant we could define the sampling track perpendicular to the bands (Fig. S5.2 and S5.3). Unfortunately, it was difficult to distinguish between the individual corallite bundles of STM4, therefore the sampling track may be slightly offset to the optimal growth axis for the years before 1978 (Fig. S5.3). Using a diamond coated drill of 1.1 mm in diameter, subsamples for Sr/Ca analysis were taken every 1 mm parallel to the growth axis, equivalent to an approximate monthly resolution. Both datasets cover the same 43 year period of 1963 to 2006. The annual extension rates (cm yr^{-1}) were calculated by measuring the distance (cm) between Sr/Ca maxima. Coral densities (g/cm^3) were calculated by analysing digital X-rays using the program CoralXDS (Carricart-Ganivet et al., 2007; Helmle et al., 2002, 2011), and calcification rate ($\text{g/cm}^2 \text{ yr}^{-1}$) by multiplying density with extension rate.

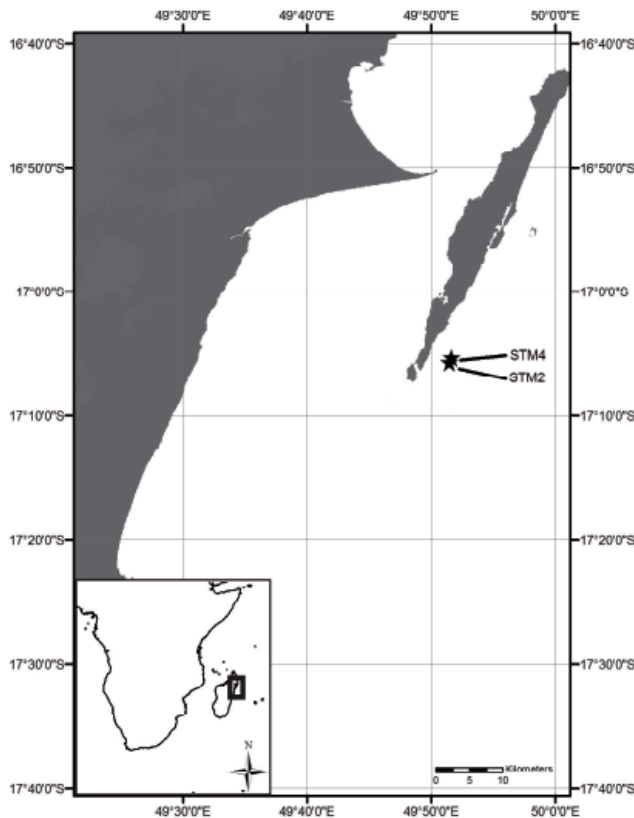


Figure 5.1. Location of coral cores STM2 and STM4 (stars) off the eastern coast of St. Marie, NE Madagascar (bottom left). The coral cores are located 0.72 km apart.

Core name	GPS position	Species	Water depth (m)	Mean growth rate cm year ⁻¹	Mean density g/cm ³	Mean Calcification rate g/cm ² year ⁻¹
STM2	S17°05,685	<i>Porites</i>	1.0	1.42	0.86	1.21
	E49°51,483	<i>lutea</i>		(±0.22)	(±0.13)	(±0.24)
STM4	S17°05,322	<i>Porites</i>	0.5	1.79	0.65	1.15
	E49°51,632	<i>lutea</i>		(±0.35)	(±0.03)	(±0.21)

Table 5.2. Coral core names listed together with their GPS co-ordinates, depths at low tide, and mean rates of extension, calcification and densities over the same 43 year period.

Analytical procedures

Skeletal Sr/Ca sub-samples were measured by inductively coupled plasma optical emission spectrometry (ICP-OES) using a simultaneous, radially viewing instrument (Ciros side-on plasma (SOP), SPECTRO Analytical Instruments GmbH, Kleve, Germany) at the University of Kiel. Respective element emission signals were simultaneously collected, following a combination of the techniques described by Schrag (1999) and de Villiers et al. (2002). The sample solution was prepared by dissolving approximately 0.5 mg of coral powder in 1.00 ml ultrapure HNO₃ 2%. The working solution was prepared by serial dilutions of the sample solution with HNO₃ 2% to a Ca concentration of ca. 8 ppm. Standard solution was prepared by diluting 1.00 ml of the stock solution (0.52 grams of homogenized coral powder from an in-house standard in 250 ml HNO₃ 2%) with 2.00 ml ultrapure HNO₃ 2%. The Sr and Ca lines used for this measurement were 407 and 317 nm, respectively. Analytical precision on Sr/Ca determinations was 0.15% RSD or 0.01 mmol/mol (1 σ). The average Sr/Ca measured for the JCp_1 standard (Inoue et al., 2004) was 8.57 mmol/mol, with a RSD of 0.09 %.

Coral chronology

The coral chronologies were developed based on the seasonal cycle of Sr/Ca (Fig. 5.2). We assigned the coldest month (either August or September) to the highest measured Sr/Ca ratio in any given year, according to both HadISST and ERSST. We then interpolated linearly between these anchor points to obtain age assignments for all other Sr/Ca measurements. In a second step, the Sr/Ca data was interpolated to 12 equidistant points per year

to obtain monthly time series using AnalySeries 2.0 (Paillard et al., 1996). This approach creates a non-cumulative time scale error of 1 - 2 month in any given year due to interannual differences in the exact timing of peak SST. The monthly resolved age-model for density was created by aligning the X-ray density profile with the Sr/Ca based age-model.

Results

Single and composite Sr/Ca records

Both STM2 and STM4 show strong seasonal cycles in the monthly Sr/Ca time series (Fig. 5.2). Also, STM_{composite} shows clear seasonality in monthly Sr/Ca with a mean value of 8.868 mmol/mol (Fig. 5.2). The STM_{composite} is the arithmetic mean of STM2 and STM4, which have statistically different 43-year means ($>1\sigma$) at 8.771 mmol/mol and 8.965 mmol/mol, respectively (Fig. 5.2). The standard deviations (1σ) around the means of STM2 and STM_{composite} were the same at 0.085 mmol/mol, whereas STM4 is slightly higher at 0.095 mmol/mol (Fig. 5.2).

Regressions of monthly Sr/Ca with gridded SST all gave very high correlation coefficients ($r^2 = 0.710 - 0.820$) enhanced by the seasonal cycles inflating relationships; and even more so for the maximum and minimum (max – min) Sr/Ca values regressed against the coldest and warmest months in SST ($r^2 = 0.909 - 0.956$; Table 5.3). For both cores and the composite, the monthly and max – min slope relationship to a 1°C increase in ERSST and HadISST ranged between $-0.064 \text{ mmol/mol } ^\circ\text{C}^{-1}$ and $-0.045 \text{ mmol/mol } ^\circ\text{C}^{-1}$ (Table 5.3). These values are close to that of a recent compilation of Sr/Ca-SST calibrations (Corrège, 2006).

The annual means of the three Sr/Ca records, STM2, STM4 and STM_{composite}, were calculated by averaging the Sr/Ca values for all months from September through to August, the two coldest months of the calendar year. The standard deviations for the annual means for STM2, STM4 and STM_{composite} were 0.029 mmol/mol, 0.028 mmol/mol and 0.020 mmol/mol, respectively (Fig. 5.2). The correlation coefficient of the annual mean Sr/Ca for STM2 regressed against STM4 was not significant: $r^2 = 0.02$, $n = 43$, $p = 0.9$.

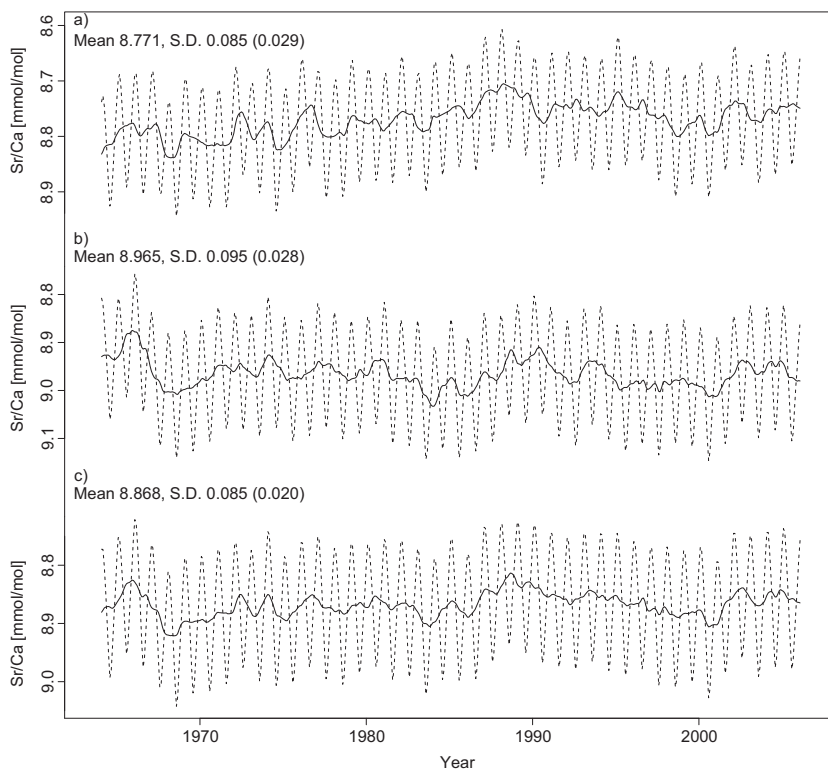


Figure 5.2. Monthly interpolated Sr/Ca time series (dotted line) and 12 month moving average (solid line) of coral cores STM2 (a), STM4 (b) and the STM_{composite} (c). Means and standard deviation of monthly (annual mean) time series are indicated above left of the corresponding core record.

Linear regressions of the coral annual means against either ERSST or HadISST annual means (September - August) resulted in very low correlation coefficients with consistently negative slopes (Table 5.3). Only STM2 regressed against ERSST returned a correlation coefficient that was significant at the 95% confidence level, being $r^2 = 0.19$, $p < 0.005$ (Table 5.3). Its slope of -0.056 mmol/mol/ $^{\circ}\text{C}$ is within the range of published relationships (Corrège, 2006; Table. 5.3). Removal of the anomalous warm years pre-1972 slightly improved correlations for STM4 with ERSST (not HadISST) ($r^2 = 0.1$, $p < 0.07$), and its slope of -0.044 mmol/mol/ $^{\circ}\text{C}$ falls within the lower range of published relationships (Corrège, 2006). However, detrending annual mean Sr/Ca and gridded data did not improve regressions for either STM2 or STM4. Further, the significant correlation of STM2 with gridded ERSST data is lost after detrending.

(a) Monthly	Regression equation	r^2	P	σ
STM4	Sr/Ca = $-0.051(\pm 0.001)$ * SST + $10.304(\pm 0.036)$	0.732	$< 2.2 \times 10^{-16}$	0.05
	Sr/Ca = $-0.052(\pm 0.001)$ * SST + $10.338(\pm 0.036)$	0.741	$< 2.2 \times 10^{-16}$	0.05
STM2	Sr/Ca = $-0.045(\pm 0.001)$ * SST + $9.951(\pm 0.032)$	0.721	$< 2.2 \times 10^{-16}$	0.04
	Sr/Ca = $-0.045(\pm 0.001)$ * SST + $9.963(\pm 0.048)$	0.710	$< 2.2 \times 10^{-16}$	0.05
STM _{composite}	Sr/Ca = $-0.048(\pm 0.001)$ * SST + $10.127(\pm 0.026)$	0.820	$< 2.2 \times 10^{-16}$	0.04
	Sr/Ca = $-0.048(\pm 0.001)$ * SST + $10.151(\pm 0.027)$	0.819	$< 2.2 \times 10^{-16}$	0.04
(b) Annual mean	Regression equation	r^2	P	σ
STM4	Sr/Ca = $-0.013(\pm 0.019)$ * SST + $8.624(\pm 0.509)$	0.011	0.506	0.03
	Sr/Ca = $-0.002(\pm 0.021)$ * SST + $9.020(\pm 0.036)$	0.0002	0.923	0.03
STM2	Sr/Ca = $-0.056(\pm 0.018)$ * SST + $10.245(\pm 0.474)$	0.191	0.003	0.03
	Sr/Ca = $-0.030(\pm 0.021)$ * SST + $9.555(\pm 0.567)$	0.045	0.174	0.03
STM _{composite}	Sr/Ca = $-0.022(\pm 0.013)$ * SST + $9.434(\pm 0.353)$	0.059	0.116	0.02
	Sr/Ca = $-0.016(\pm 0.015)$ * SST + $9.287(\pm 0.395)$	0.027	0.295	0.02
(c) Max-min	Regression equation	r^2	P	σ
STM4	Sr/Ca = $-0.064(\pm 0.002)$ * SST + $10.640(\pm 0.057)$	0.909	$< 2.2 \times 10^{-16}$	0.04
	Sr/Ca = $-0.064(\pm 0.002)$ * SST + $10.664(\pm 0.055)$	0.919	$< 2.2 \times 10^{-16}$	0.04
STM2	Sr/Ca = $-0.055(\pm 0.002)$ * SST + $10.204(\pm 0.046)$	0.920	$< 2.2 \times 10^{-16}$	0.04
	Sr/Ca = $-0.055(\pm 0.002)$ * SST + $10.211(\pm 0.048)$	0.912	$< 2.2 \times 10^{-16}$	0.04
STM _{composite}	Sr/Ca = $-0.057(\pm 0.001)$ * SST + $10.379(\pm 0.035)$	0.956	$< 2.2 \times 10^{-16}$	0.03
	Sr/Ca = $-0.058(\pm 0.001)$ * SST + $10.392(\pm 0.035)$	0.956	$< 2.2 \times 10^{-16}$	0.03

Table 5.3. Linear regression equations, correlation coefficients and significance levels of monthly (a), annual mean (b) and max – min Sr/Ca with both ERSST (grey) and HadISST (white) for STM2, STM4 and STM_{composite}. The ERSST and HadISST data is from the region 49°-50°E, 17°-18°S for the years between 1963 and 2006. The residual standard errors are given as σ .

Trend Estimates

Coral Sr/Ca was converted to relative temperature units using the relationship of -0.06 mmol/mol per 1°C warming (Corrège, 2006). All 43-year SST trends were different, with ERSST showing a warming of $0.010^{\circ}\text{C yr}^{-1}$ ($+0.430^{\circ}\text{C}$ trend), HadISST a slight warming of $0.002^{\circ}\text{C yr}^{-1}$ ($+0.086^{\circ}\text{C}$ trend), STM2 a strong warming of $0.023^{\circ}\text{C yr}^{-1}$ ($+0.989^{\circ}\text{C}$ trend) and STM4 a cooling of $0.010^{\circ}\text{C yr}^{-1}$ (-0.430°C trend) (Fig. 5.3). Despite diverging trends in STM2 and STM4, both showed similar standard deviations of 0.483°C and 0.469°C , respectively, about twice that of ERSST (0.226°C) and HadISST (0.206°C). The annual mean of the $\text{STM}_{\text{composite}}$ had a standard deviation of 0.333°C , less than STM2 and STM4 yet higher than ERSST and HadISST (Fig. 5.4). The $\text{STM}_{\text{composite}}$ had a warming trend of $0.007^{\circ}\text{C yr}^{-1}$ ($+0.301^{\circ}\text{C}$ trend), which lies between the trends of the two gridded SST time-series (Fig. 5.4; Fig. 5.5a). Figure 5.5a indicates the large discrepancies between the five trends, of which $\text{STM}_{\text{composite}}$ is shown to be outside both the error bars of STM2 and STM4. Direct comparison of the annual means of $\text{STM}_{\text{composite}}$ with the gridded SST data shows higher residuals ($>1\sigma$) in the earlier period, that decrease towards present day (Fig. 5.4). Further, for the years (2000, 2001, and 2006) with a large number of SST observations (ICOADS; Fig. 5.4c) the differences between residuals were closer to zero.

ENSO years

According to ERSST and HadISST, the average SST anomaly for 12 ENSO years calculated over a 3-month average from January to March lead to warming of 0.22°C ($\pm 0.23^{\circ}\text{C}$) and 0.25°C ($\pm 0.23^{\circ}\text{C}$), respectively. Subtracting the mean JFM_{ENSO} Sr/Ca from the mean JFM Sr/Ca provides an estimate of the Sr/Ca ENSO anomaly at the reef scale. ENSO anomalies were therefore calculated by subtracting the mean JFM_{ENSO} SST (Sr/Ca) from the mean JFM_{tot} SST (Sr/Ca). STM2 had a negative Sr/Ca anomaly of -0.014 mmol/mol (± 0.037 mmol/mol), whereas STM4 had a positive anomaly of 0.009 mmol/mol (± 0.029 mmol/mol; Table 5.4a). Coral Sr/Ca was then converted to temperature units using the relationship of -0.06 mmol/mol per 1°C warming (Corrège, 2006), which result in an SST anomaly of 0.23°C ($\pm 0.61^{\circ}\text{C}$) and -0.14°C ($\pm 0.49^{\circ}\text{C}$) for STM2 and STM4, respectively (Fig. 5.5b; Table S5.1). Consequently, the $\text{STM}_{\text{composite}}$ Sr/Ca anomaly was only

-0.003 mmol/mol (± 0.024 mmol/mol; Table 5.4a), which equates to a mean warming of 0.04°C ($\pm 0.40^{\circ}\text{C}$) (Fig. 5.5b; Table S5.1). The Sr/Ca difference between the STM4 and STM2 anomaly was negative at -0.005 mmol/mol (STM4-STM2), equating to a positive SST anomaly of 0.08°C .

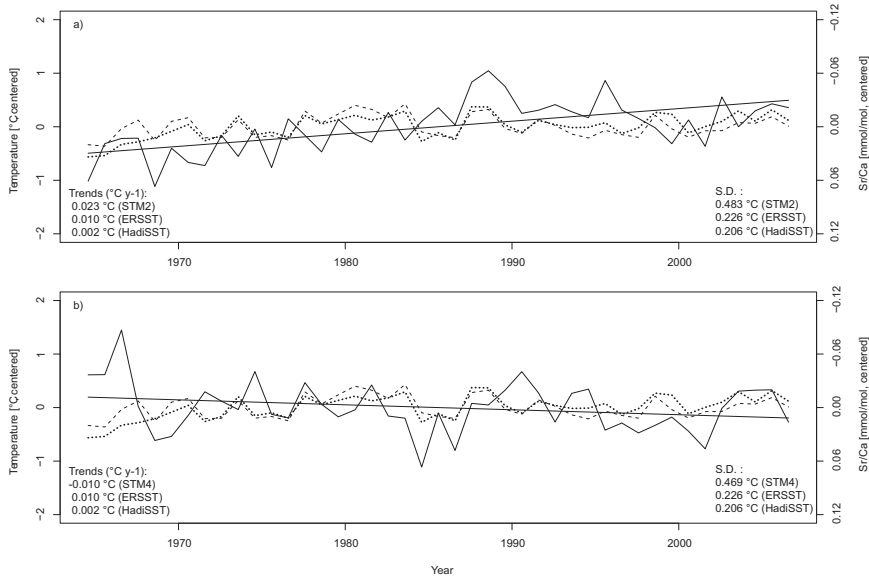


Figure 5.3. Annual mean Sr/Ca time series (solid line) of (a) STM2 and (b) STM4, together with the annual mean ERSST (dotted line) and HadISST (dashed line) time series. Sr/Ca has been scaled so that -0.06 mmol/mol corresponds to a warming of 1°C (Corrège, 2006). The standard deviation and trends of all time series are given in the bottom right and left of each record, respectively. Linear trends are shown as a straight black line.

(a) Sr/Ca	JFM _{ENSO} mmol/mol	JFM _{tot} mmol/mol	ENSO anomaly
STM2	8.671 (± 0.037)	8.685 (± 0.034)	-0.014 (± 0.037)
STM4	8.868 (± 0.029)	8.859 (± 0.031)	+0.009 (± 0.029)
STM _{composite}	8.769 (± 0.024)	8.772 (± 0.025)	-0.003 (± 0.024)
(b) Density	JFM _{ENSO}	JFM _{tot}	Density anomaly
STM2	0.874 (± 0.121)	0.858 (± 0.121)	+0.016 (± 0.121)
STM4	0.638 (± 0.028)	0.643 (± 0.034)	-0.005 (± 0.028)

Table 5.4. ENSO event Sr/Ca ratios (a) for STM2, STM4 and STM_{composite}. Anomalies were calculated by subtracting the mean Sr/Ca value for January to March (JFM) from the mean JFM Sr/Ca for the 12 ENSO years (1966, 1969, 1973, 1977, 1983, 1987, 1988, 1992, 1995, 1998, 2003, 2005) between 1963 – 2006. It should be noted that the total difference between the ENSO anomaly of STM2 and STM4 equates to -0.005 mmol/mol. The JFM skeletal densities and anomalies (b) for STM2 and STM4 were calculated similar to Sr/Ca data.

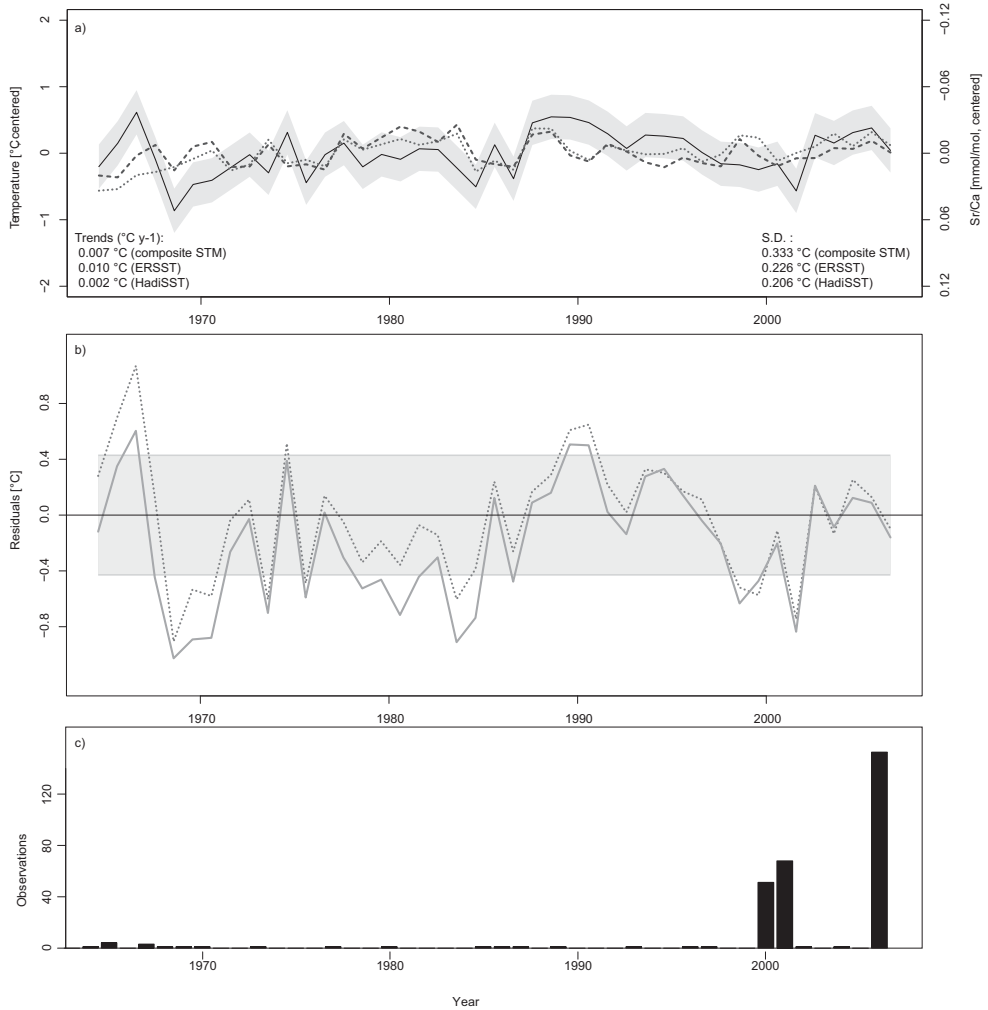


Figure 5.4. Time series of (a) annual mean composite Sr/Ca ($STM_{\text{composite}}$; solid line), ERSST (dotted line) and HadISST (dashed line), with trends and standard deviation (1σ) bottom right and left, respectively. Composite Sr/Ca is the arithmetic mean of STM2 and STM4, with ± 1 SD shaded. Temperature residuals (b) of ERSST (dotted line) and HadISST (dashed line) are shown in relation to $STM_{\text{composite}}$, with ± 1 SD shaded. Sr/Ca has been scaled so that -0.06 mmol/mol corresponds to 1°C . The number of observations (c), according to ICOADS, is shown for the 43 years used for this study.

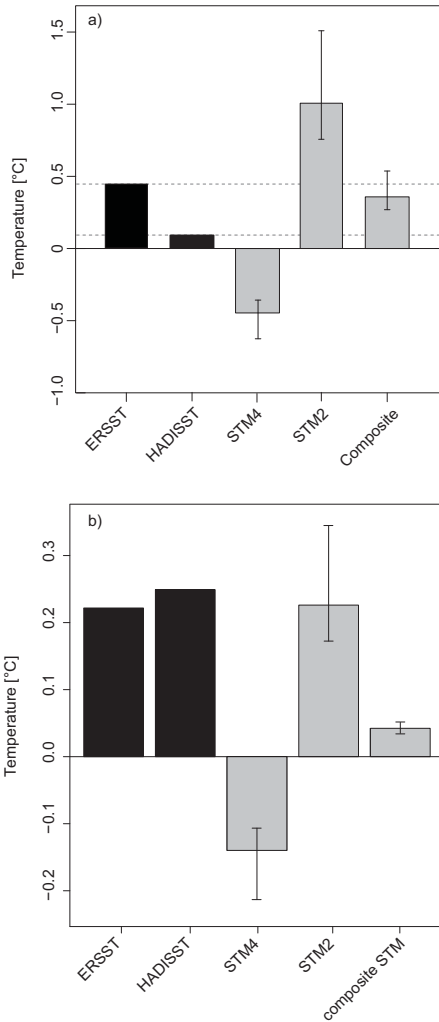


Figure 5.5. The mean temperature change (a) and average ENSO anomalies for 12 positive ENSO years (b) over the 43 year period used in this study (1963 – 2006) for ERSST and HadISST (black bars), and STM2, STM4 and STM_{composite} (grey bars). ENSO anomalies were calculated by subtracting the mean JFM_{ENSO} SST (Sr/Ca) from the mean JFM_{tot} SST (Sr/Ca). Coral Sr/Ca was converted to temperature units using $-0.06 \text{ mmol/mol/}^{\circ}\text{C}$ (Corrège, 2006). Error bars on Sr/Ca-temperatures are computed using the range of published slopes -0.04 and $-0.08 \text{ mmol/mol/}^{\circ}\text{C}$, respectively (Corrège, 2006).

Growth parameters

Annual coral extension rates showed diverging trends over the 43 years (Table 5.2), with STM2 declining by $-0.007 \text{ cm yr}^{-1}$ and STM4 increasing by $+0.018 \text{ cm yr}^{-1}$ (Fig. 5.6 and 5.7). Neither corals showed a significant change during the 12 ENSO years compared to the 43 year mean in annual extension rates. The average ENSO year extension rate for STM2 was 1.41 cm yr^{-1} ($\pm 0.19 \text{ cm yr}^{-1}$) and 1.75 cm yr^{-1} ($\pm 0.35 \text{ cm yr}^{-1}$) for STM4.

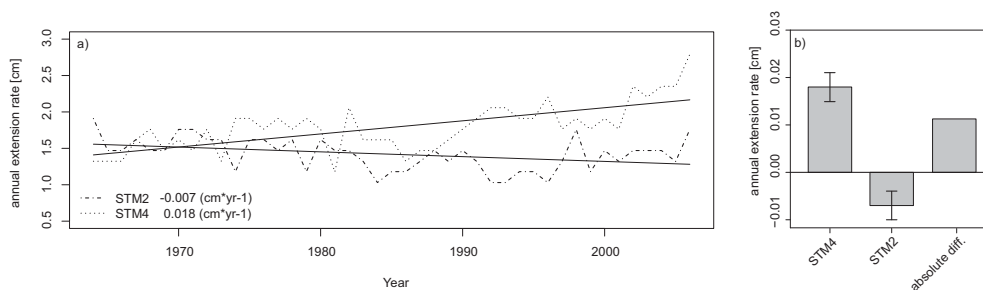


Figure 5.6. The mean annual extension rates (a) over the 43 year period (1963 – 2006) for STM2 (stippled line) and STM4 (dotted line), are shown together with linear trends (straight black lines). The extension rate trend is also indicated (bottom left for both records) and shown graphically for STM2 and STM4 (b), together with the trend difference (STM4-STM2). Error bars indicate the slope standard error.

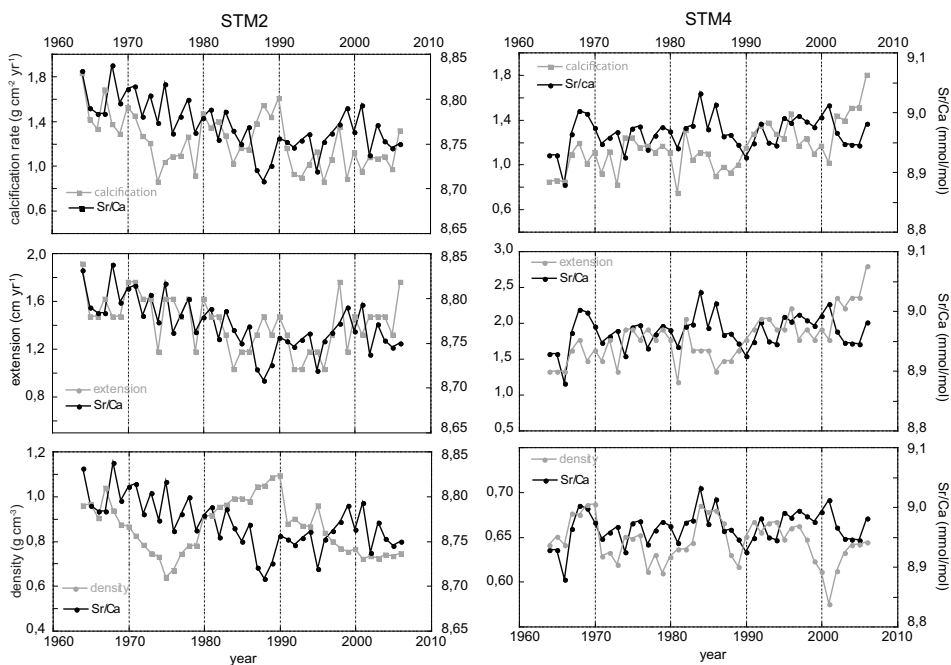


Figure 5.7. Time series of annual mean coral Sr/Ca ratios compared to calcification rate (top), extension rate (middle) and density (bottom) for STM2 (left) and STM4 (right). Note the opposite long-term trends in calcification and extension rate between the two corals.

Coral density of STM2 and STM4 showed no linear trend over the 43 years, despite considerable interannual and decadal variability (Fig. 5.8). Subtracting the mean density for JFM from the mean density in the 12

JFM ENSO years revealed the ENSO density anomaly. The average density anomaly for each core during a positive ENSO year was different, with STM2 being positive and STM4 negative, yet the differences were statistically not significant (Table 5.4b; Fig. 5.7).

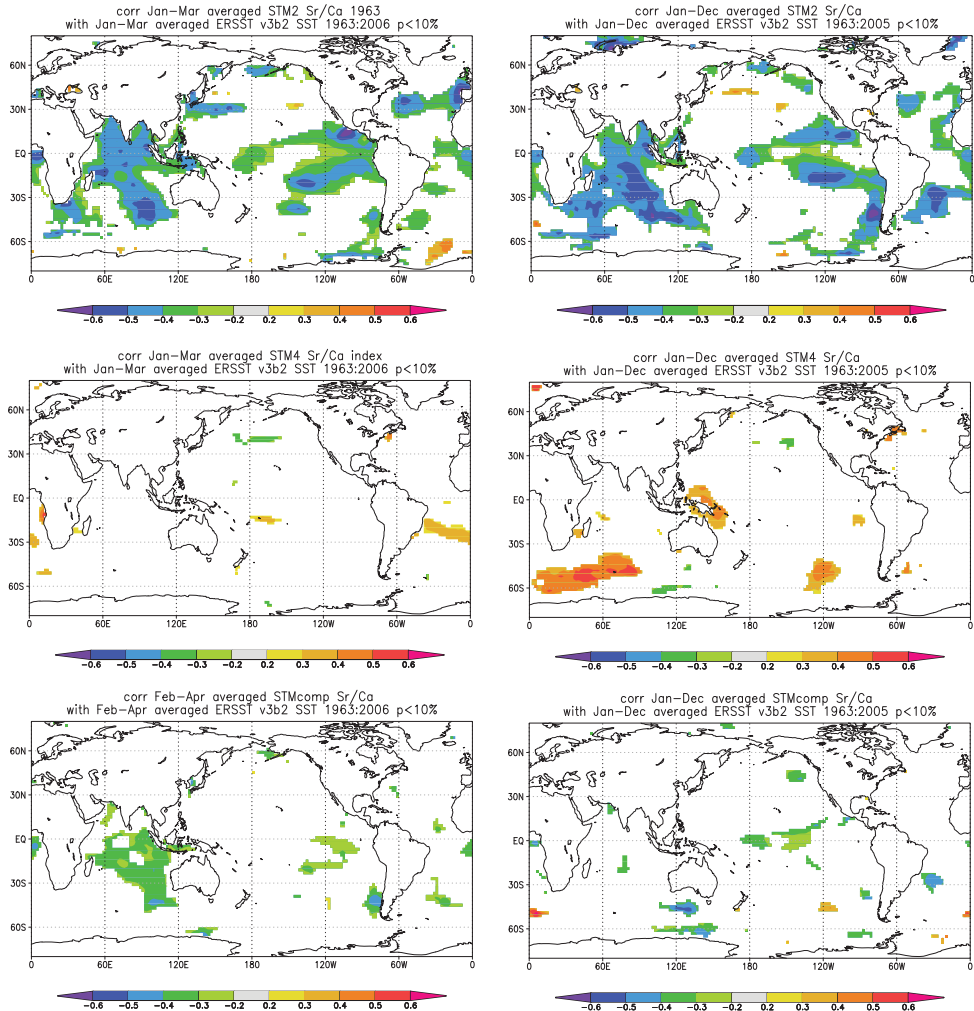


Figure 5.8. Spatial correlation of coral Sr/Ca with global SST for January to March or February to April period (left), together with the annual means (right). Correlations are shown for STM2 (top), STM4 (middle) and STM_{composite} (bottom), computed using the years 1963 to 2006. Only correlations significant above the 90% level are coloured. Correlations were computed at <http://climexp.knmi.nl/>.

Calcification rates declined over the 43 year period for coral STM2 while they increased for STM4 (Fig. 5.7). On interannual time scales, calcification rates were negatively correlated with Sr/Ca values in both corals, particularly since 1983 (Fig. 5.7). Annual calcification rates of STM2 and STM4 were negatively correlated ($r^2 = 0.2$, $p < 0.1$). A highly significant negative correlation ($r^2 = 0.54$; $p < 0.001$) between ENSO-year calcification rates was also observed between the two corals (Fig. 5.7; Fig. S5.4).

Discussion

Various studies have found inconsistencies between long-term Sr/Ca records from coral colonies sampled close to one another (Cahyarini et al., 2008; Cahyarini et al., 2011; Pfeiffer et al., 2009). These differences are often attributed to local SST or environmental stress (DeLong et al., 2007; Linsley et al., 2004; Marshall and McCulloch, 2002). However, in cases where the relationship between coral Sr/Ca records cannot solely be explained by localised SST discrepancies, vital effects are considered the main contributor to inter-colony Sr/Ca variability (Allison et al., 2001; Allison and Finch, 2004; Cohen and Gaetani, 2010; Cohen et al., 2001; Cohen et al., 2002; DeLong et al., 2011; Gaetani et al., 2011; Sinclair et al., 2005, 2006). Here, two coral colonies sampled 0.72 km apart showed similar seasonal amplitudes in Sr/Ca, yet had different baseline averages, opposite long-term trends and displayed diverging interannual responses to ENSO anomalies.

Coral Sr/Ca and instrument records

When considering the relationship of Sr/Ca with gridded SST data, results indicate that coral STM2 was recording annual and interannual SST variability more than STM4. Further, with respect to the annual mean regressions, the weak Sr/Ca-SST relationship of STM4 caused the composite record not to improve correlations with instrumental data, but to reduce them. When considering the annual means, only STM2 showed a statistically significant Sr/Ca relationship with gridded data (i.e. ERSST). However, the significant correlation of annual mean ERSST and STM2 Sr/Ca was lost when both datasets were detrended. This suggests that the Sr/Ca-SST relationship was largely related to the long-term warming trend rather than interannual variability.

The slope of the regression between annual mean STM2 Sr/Ca and ERSST was $-0.056 \text{ mmol/mol/}^{\circ}\text{C}$, close to the mean published Sr/Ca-SST response of $-0.06 \text{ mmol/mol/}^{\circ}\text{C}$ (Corrège, 2006). Regressing the maximum and minimum Sr/Ca monthly values with the minimum and maximum monthly ERSST and HadISST values improved the relationship for all three coral records. As with the monthly regressions, this is due to the seasonal cycle inflating the relationship between the two parameters. It is worth noting that the max – min slope for STM2 was only slightly different from the annual mean regression with ERSST ($-0.055 \text{ mmol/mol/}^{\circ}\text{C}$ compared to $-0.056 \text{ mmol/mol/}^{\circ}\text{C}$). However, such values are lower than the expected Sr/Ca-SST relationship from abiogenic precipitation of aragonite ($-0.038 \text{ mmol/mol/}^{\circ}\text{C}$) (Cohen and Gaetani, 2010; Gaetani and Cohen, 2006; Gaetani and Cohen, 2011). Consequently, biogenic partitioning has likely influenced STM2 and STM4. To equally assess Sr/Ca trends and interannual anomalies of both corals, we applied the mean published Sr/Ca-SST relationship of $-0.06 \text{ mmol/mol/}^{\circ}\text{C}$ (Corrège, 2006). This value falls between the calculated max - min regressions of Sr/Ca with gridded data, with slopes of $-0.055 \text{ mmol/mol/}^{\circ}\text{C}$ and $-0.064 \text{ mmol/mol/}^{\circ}\text{C}$ for STM2 and STM4, respectively.

Long- term SST trends

ERSST and HadISST displayed different rates of warming over the 43 year period, with ERSST increasing by $0.010 \text{ }^{\circ}\text{C yr}^{-1}$ and HadISST by $0.002 \text{ }^{\circ}\text{C yr}^{-1}$. These differences are likely a result of the few observational data (ICOADS) available for the region, resulting in a weak consensus. Only the annual mean Sr/Ca record of STM2 is significantly correlated with ERSST and not HadISST, albeit weakly. Corals STM2 and STM4 displayed diverging trends over the 43 year period studied, with STM2 warming (negative Sr/Ca trend) by $0.023 \text{ }^{\circ}\text{C yr}^{-1}$ and STM4 cooling (positive Sr/Ca trend) by $0.010 \text{ }^{\circ}\text{C yr}^{-1}$. Interestingly, the extension rates of both corals also differed, with STM2 showing a declining extension rate over the 43 years, and STM4 an increasing extension rate (Fig. 5.6). Further, the extension rate increase of STM4 was far greater ($+0.018 \text{ cm yr}^{-1}$) than the decrease in extension rate of STM2 ($-0.007 \text{ cm yr}^{-1}$; Fig. 5.6). Assuming SST has increased over the 43 year period, it is likely that the two corals have responded differently to warming, causing STM2 to grow slower and STM4 to grow faster.

Differences in the extension rates (i.e. vital effect) of the two corals may have influenced the skeletal Sr/Ca composition, causing diverging trends. According to Cohen and Gaetani (2010), as the rate of aragonite crystal growth increases so does Sr/Ca. Given the increasing extension rate of STM4, this might account for the increase in skeletal Sr/Ca, resulting in an apparent cooling trend. Similarly, STM2 displayed a decreasing Sr/Ca trend giving an apparent warming trend; therefore as its extension rate also decreased, the observed Sr/Ca trend is most likely enhanced (towards more negative values).

As the extension rate increase of STM4 is far greater than the extension rate decrease of STM2 ($+0.011 \text{ cm yr}^{-1}$; Fig. 5.6), the difference between Sr/Ca trends should have been positive rather than negative (-0.039 mmol/mol over 43 years), assuming no temperature control. However, as the difference between Sr/Ca trends was negative, a warming trend has likely influenced both corals in agreement with the gridded SST data.

Differences between the Sr/Ca regression slopes of corals with SST are related to both the reliability of instrumental data and vital effect strength. As the difference in extension rates between our cores indicate that STM4 increased at a faster rate than STM2 decreased, we assume that the vital effect influence on the STM4 Sr/Ca trend was greater than STM2. This may explain why there was no relationship observed between annual mean SST and STM4 Sr/Ca.

In order to constrain the extent to which the declining extension rate (vital effect) of STM2 has enhanced its Sr/Ca trend, we can estimate a range in which SST has increased using the lower limit of other published slopes ($-0.08 \text{ mmol/mol/}^{\circ}\text{C}$) to take the maximum vital effects into consideration (assuming the $-0.038 \text{ mmol/mol/}^{\circ}\text{C}$ slope of abiogenic aragonite precipitation represents no vital effects). As a result, the SST increase would equate to a lower limit of $+0.75^{\circ}\text{C}$, which is higher than both satellite datasets ($+0.43^{\circ}\text{C}$ and $+0.09^{\circ}\text{C}$ for ERSST and HadISST, respectively). For an upper limit, we use the regressed slope of the annual mean Sr/Ca relationship with ERSST ($-0.056 \text{ mmol/mol/}^{\circ}\text{C}$), which would equate to a rise of $+1.07^{\circ}\text{C}$. This would suggest that SST off northeast Madagascar has risen by $0.75^{\circ}\text{C} - 1.07^{\circ}\text{C}$ between 1963 and 2006. This value is significantly higher than the HadISST

trend of $+0.09^{\circ}\text{C}$, which McClanahan et al. (2009) used for satellite based coral mortality or ecological extinction prediction models (Hoegh-Guldberg, 1999; Hughes et al., 2003; Sheppard, 2003). An explanation as to why these warming trends are so different might be related to corals recording a local signal and HadISST recording a more regional signal. However, given we have no long-term *in situ* data we cannot verify this.

For the coral Sr/Ca composite record ($\text{STM}_{\text{composite}}$), the calculated 43-year trend of $+0.30^{\circ}\text{C}$ (range of $0.23 - 0.32^{\circ}\text{C}$ using slopes of -0.08 and -0.056 mmol/mol/ $^{\circ}\text{C}$) lies between the ERSST and HadISST trends, yet closer to that of ERSST. Further, the standard deviation of $\text{STM}_{\text{composite}}$ was closer to that of HadISST and ERSST, compared to STM2 and STM4. This is most likely caused by the elimination of opposing trends between the two corals, meaning future studies dealing with Sr/Ca based SST reconstructions should be cautious when compiling composite records. If we assume that gridded data reflects the true SST trend at the reef scale, averaging of the two coral records indeed improves the long-term trend estimates, as suggested by Pfeiffer et al. (2009). However, we cannot rule out that gridded SST underestimates long-term trends at the reef scale, particularly given the rather large disagreement between ERSST and HadISST and the lack of *in situ* data available over the 43 year period. We must therefore treat the composite record with caution and suggest a coincidental similarity with gridded SST data in terms the long-term trend. Nevertheless, what is most significant from our results is that our two coral Sr/Ca records from the same location displayed opposite trends.

ENSO years

There were twelve recorded positive ENSO events over the 43 year period studied here (www.cpc.ncep.noaa.gov). Both ERSST and HadISST showed similar positive JFM anomalies that indicated an average warming of 0.22°C and 0.25°C , respectively, yet varied considerably for individual ENSO years (Table S5.1). For the same twelve ENSO years, the STM2 Sr/Ca anomalies (negative Sr/Ca) were in agreement with the gridded SST products and displayed positive temperature anomalies of similar magnitude, whereas STM4 displayed negative temperature anomalies, and $\text{STM}_{\text{composite}}$ only slightly positive (Table S5.1). Similar to the gridded data, Sr/Ca-based

SST anomalies for individual years varied considerably. Standard deviations indicate that ENSO year JFM averages between the cores are statistically the same as the gridded SST anomalies (Table S5.1). Nevertheless, the assessment of individual positive ENSO events revealed that only STM2 showed reasonable agreement with instrumental SST data, compared to STM4 and STM_{composite} (Tab. S5.1).

Interestingly, calcification rates in STM2 and STM4 were opposite in their response to individual positive ENSO events (Fig. S5.4). This also suggests a different growth response to ENSO SST anomalies, which may have modulated the coral Sr/Ca composition of either coral. According to Cohen and Gaetani (2010) and Gaetani et al. (2011), Rayleigh fractionation may cause Sr/Ca depletion as the mass of aragonite precipitated per ‘batch of calcifying fluid’ increases. As there is an anomalous negative mean skeletal density and calcification response recorded by coral STM4 during a positive ENSO event, such Rayleigh fractionation would account for the anomalously higher mean skeletal Sr/Ca signal (Table 5.4). Similarly, as the mean density and calcification anomaly for STM2 is positive during a positive ENSO event, this would cause a negative mean Sr/Ca signal. In both cases, the mean Sr/Ca anomalies for corals STM2 and STM4 follow this pattern, suggesting densities and/or calcification rates may have modulated the skeletal Sr/Ca signal.

In order to constrain how much coral calcification has enhanced the STM2 ENSO anomalies, we can use the lower limit of other published slopes (-0.08 mmol/mol/°C) to take the maximum vital effects into consideration. As a result, the SST anomaly would then equate approximately to an average increase of $+0.17^{\circ}\text{C}$, which is lower than what both satellite datasets show ($+0.22^{\circ}\text{C}$ and $+0.25^{\circ}\text{C}$ for ERSST and HadISST, respectively). For an upper limit, we use the regressed slope of the annual mean Sr/Ca relationship with ERSST (-0.056 mmol/mol/°C), which would equate to an average positive anomaly of $+0.25^{\circ}\text{C}$. This would suggest that positive ENSO events lead to an average SST increase of $0.17^{\circ}\text{C} - 0.25^{\circ}\text{C}$ off northeast Madagascar for the 12 ENSO years studied. However, given the large standard deviations involved, there was likely much variability between ENSO years, which was similarly observed in the gridded SST data.

To individually test the reliability of our three coral Sr/Ca records (STM2, STM4, STM_{composite}) we correlated each record with global SST to assess large-scale climate teleconnection patterns such as ENSO (Fig. 5.8). Indeed, coral STM2 reveals the spatial correlation pattern typical for Indo-Pacific SST teleconnections, whereas STM_{composite} shows a weaker correlation and STM4 no correlation. This suggests that STM2 is a more reliable time series to assess large-scale teleconnections related to past ENSO variability than both STM4 and STM_{composite}.

Normalising vital effects

Skeletal Sr/Ca is modulated by changes in colony growth as well as SST variability. However, if the growth related vital effects on Sr/Ca are accounted for, coral skeletal archives can potentially assist in quantifying past changes of both short and long term SST. Multiple regressions go some way to achieving this (Goodkin et al., 2005, 2007). More recently, however, Cohen and Gaetani (2010) and Gaetani and Cohen (2011) suggest multiple trace elements need to be taken into consideration in order to retrieve the SST signal, rather than a single trace element to calcium ratio i.e. Sr/Ca, Mg/Ca, Ba/Ca. As SST-proxies are incorporated into the skeleton at different rates related to growth parameters, as well as SST, taking their relationship into consideration may refine paleothermometry by normalising the skeletal influence (Sinclair et al., 2006). The relationship between individual trace element/Ca ratios is extrapolated using a series of equations, providing an SST-proxy composite record, which can potentially provide robust coral-based SST reconstructions.

Inter-colony Sr/Ca variability: Potential causes

Our results show that corals react differently to external forcing in terms of extension rate, density and calcification (Helmle et al., 2011), which likely modulates the skeletal Sr/Ca composition. More specifically, *Porites* spp. have been shown to be particularly sensitive to thermal stress in terms of calcification (Carricart-Ganivet et al., 2012). Corals STM2 and STM4 are good examples of how two colonies of the same species located less than 1 km apart can show opposite Sr/Ca trends and anomalies. Warming SST

trends of the SW Indian Ocean are accompanied by an increasing extension rate of STM4 and a decrease in extension rate of STM2. This observation suggests high variability in coral growth between individual colonies in subtropical reef locations paired with relatively high SST seasonal cycles ($>5^{\circ}\text{C}$). Consequently, interannual SST variations are of minor amplitude in comparison to seasonal changes. This in turn will complicate the coral based-SST reconstructions, especially interannual variability, due to vital effects likely increasing with increasing SST and growth variability. The recent 30 years have seen high rates of warming which can potentially enhance physiological stress for corals undermining the corals ability to faithfully record SST from its geochemistry. This assumption needs to be further tested at sites with reliable *in situ* SST observations.

As STM2 and STM4 were both drilled from the same coral species, *Porites lutea*, differences in growth responses may have been affected by the presence of distinct zooxanthellae genetic types within the coral host. It has been reported that some corals can shuffle or switch symbiont types in response to thermal stress events (Berkelmans and van Oppen, 2006), and that this may represent a means of adaptation to environmental change. Furthermore, distinct symbiont genotypes are known to differ in their photosynthetic contribution to the coral host (Loram et al., 2007), and calcification is thought to be a 'photosynthesis driven' process (Colombo-Pallotta et al., 2010). For instance, corals with the more heat tolerant symbiont type D are shown to grow considerably slower (up to 38%) than corals with type C2 (Jones and Berkelmans, 2010). Cohen et al. (2002) proposed that algal symbionts affect the accuracy of the Sr/Ca thermometer in tropical coral species. Increased water temperature and increased symbiont activity are both thought to cause a simultaneous decrease in the Sr incorporation into the skeleton. This process is more dominant during summer calcification when symbiont activity is highest.

Assuming the local physio-chemical conditions were similar given the close proximity of the two corals and full seawater exchange with the open ocean, other potential variables that may have influenced inter-colony Sr/Ca variability include 1) depth and 2) sampling off the optimal growth axis. Depth, and in turn light intensity, may have influenced the growth response of

coral STM4, as its apex was located 0.5 m higher than STM2, and therefore closer to the warmer wave-dominated surface. Increased extension rates are indeed linked to warmer SSTs and/or more optimal light levels (Lough and Barnes, 2000; Reynaud et al., 2007); however, this does not explain the declining extension rates observed in STM2 under warming temperatures. Also, it is unclear whether depth would cause the corals to respond differently to warmer ENSO years in terms of calcification. Sampling off the optimal growth axis of STM4, pre-1978, may have caused more positive Sr/Ca values, although the Sr/Ca-growth relationship remained similar both pre- and post-1978.

Conclusions

Coral vital effects modulate the precipitation of skeletal Sr/Ca, which can in turn affect its relationship with SST. Altering extension/calcification rates and densities in response to SST variability may overwhelm the Sr/Ca signal and in extreme circumstances produce opposing results. Here, we find two corals of the same species in the same environment with diverging growth responses to SST; yet, the influence of vital effects on Sr/Ca are consistent between corals. Increasing extension/calcification rates in STM4, over the 43 year period, were coupled with increasing Sr/Ca ratios, while decreasing extension/calcification rates in STM2 were coupled with decreasing Sr/Ca ratios. During individual positive ENSO events, calcification rates in STM4 and STM2 were negatively correlated, which may have modulated the Sr/Ca signals. It is therefore important to measure multiple cores to fully assess vital effects and their impact on Sr/Ca. Pooling records together can increase the reliability of reconstructions, however, in extreme circumstances, such as this, the coral composite record can be less reliable when two corals display such opposite signals. Whether zooxanthellae genetic types and/or local physiochemical environmental differences are the cause for Sr/Ca discrepancies between corals, measuring growth parameters will assist in identifying and constraining them.

Supplementary Information

Supplementary Figures

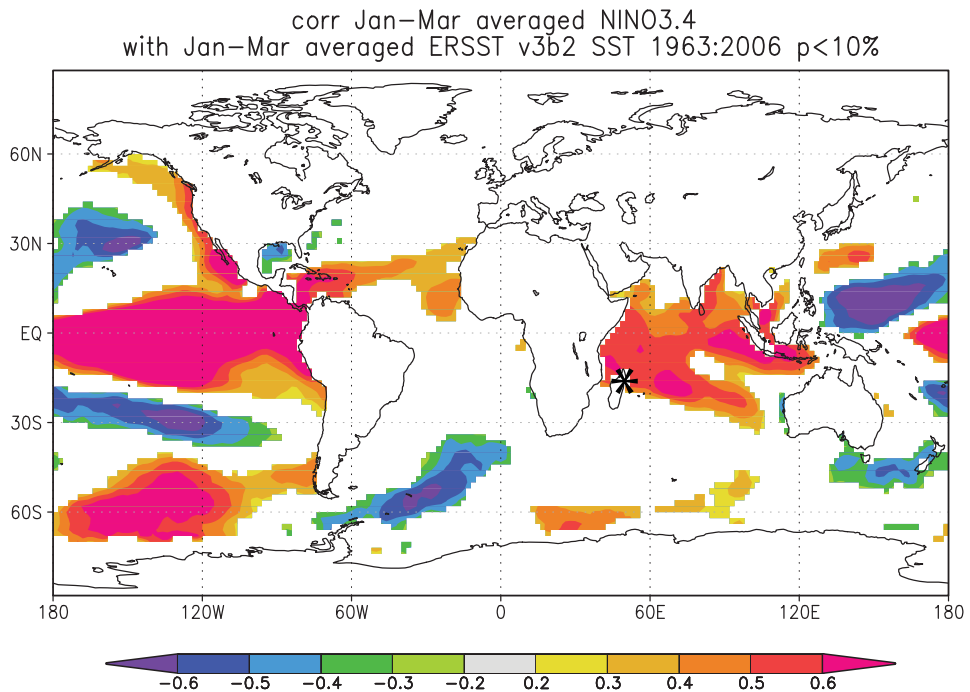


Figure S5.1. Spatial correlation of the Niño 3.4 index with global SST (ERSSTv.3) for the period January to March. Correlations are computed using the years 1963 to 2006. Only correlations significant above the 90% level are coloured. Our research area is marked by a star (*) on the map, which is significantly influenced by interannual variability associated with ENSO. Correlations were computed at <http://climexp.knmi.nl/>.

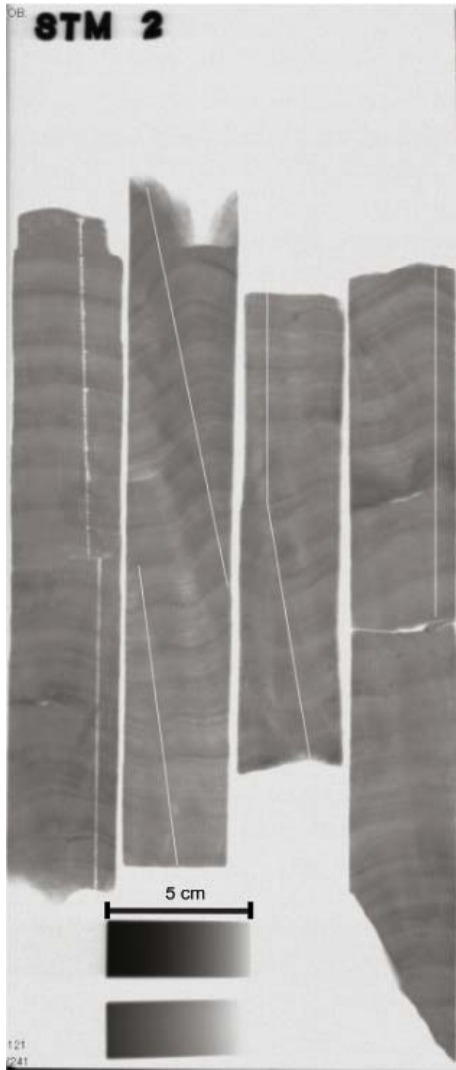


Figure S5.2. X-Ray of STM2 core pieces, with the geochemical sampling transect marked in white.

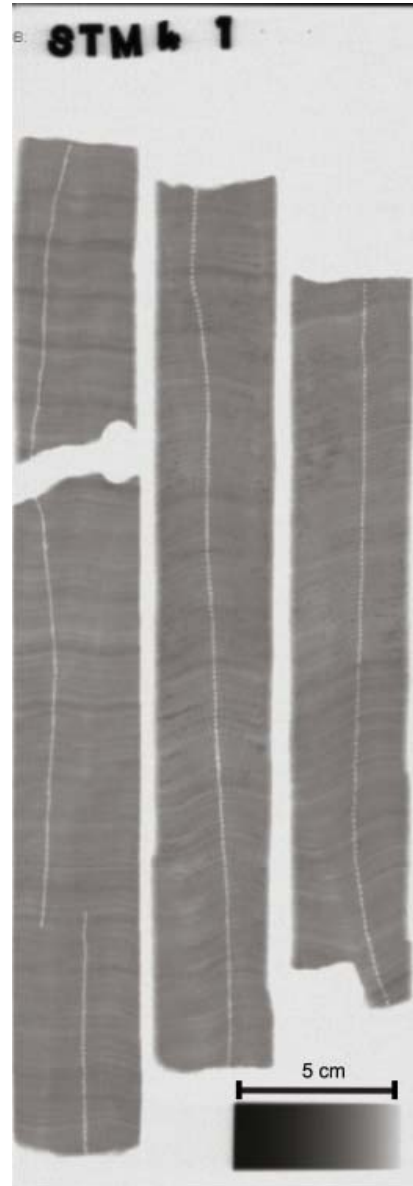


Figure S5.3. X-Rays of STM4 core pieces, with the geochemical sampling transect marked in white.

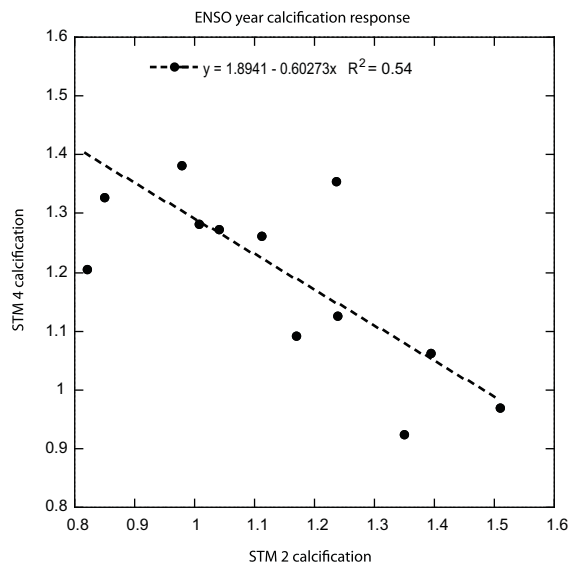


Figure. S5.4. Linear regression of ENSO-year calcification rates between corals STM2 and STM4. Note the significant negative correlation indicating opposing responses.

Supplementary Table

Positive ENSO Year	ERSST anomaly (°C)	HadISST anomaly (°C)	STM2 anomaly (°C)	STM4 anomaly (°C)	STM _{composite} anomaly (°C)
1966	-0.24	-0.04	-0.21	1.03	0.41
1969	0.03	0.14	-0.22	-0.75	-0.48
1973	0.14	-0.06	-1.04	-0.75	-0.89
1977	0.07	0.33	0.11	-0.04	0.04
1983	0.24	0.48	0.29	-0.08	-0.18
1987	0.42	0.24	0.89	-0.32	0.28
1988	0.54	0.48	0.68	-0.53	0.08
1992	0.05	0.19	0.14	0.10	0.12
1995	0.12	-0.05	1.08	-0.23	0.42
1998	0.46	0.55	0.66	-0.43	0.11
2003	0.35	0.20	0.77	0.21	0.49
2005	0.42	0.51	0.20	0.07	0.14
Mean	0.22	0.25	0.23	-0.14	0.04
SD	0.23	0.23	0.61	0.49	0.40

Table S5.1. Mean SST anomalies for ERSST, HadISST, STM2, STM4 and STM_{composite} for positive ENSO events. Coral Sr/Ca was converted to temperature units assuming that -0.06 mmol/mol corresponds to a warming of 1°C. Anomalies were calculated by subtracting the mean Sr/Ca value for JFM 1977 from the mean JFM Sr/Ca for the 12 ENSO years between 1963 – 2006 (1966, 1969, 1973, 1977, 1983, 1987, 1988, 1992, 1995, 1998, 2003, 2005).

Acknowledgements: This work was supported as part of the SINDOCOM grant under the Dutch NWO program ‘Climate Variability’, grant 854.00034/035. Additional support comes from the NWO ALW project CLIMATCH, grant 820.01.009, and the Western Indian Ocean Marine Science Association through the Marine Science for Management programme under grant MASMA/CC/2010/02. We thank Karin Kissling for her assistance with the ICP-OES measurements at the University of Kiel, and Bob Koster and Rineke Gieles for their help with the UV-Core Scanner. Furthermore, we thank CAF/CORE Madagascar for granting the CITES permit, Bert Hoeksema from Naturalis for identifying the species of the corals, and Lars Reuning (RWTH Aachen, Germany) and Delphine Dissard (UWA Perth) for fruitful discussions while writing this manuscript.

References

- Alibert, C., McCulloch, M.T., 1997. Strontium/calcium ratios in modern *Porites* corals from the Great Barrier Reef as a proxy for sea surface temperature: calibration of the thermometer and monitoring of ENSO. *Paleoceanography* 12, 345-363.
- Allison, N., Tudhope, A.W., Fallick, A.E., 1996. Factors influencing the stable carbon and oxygen isotopic composition of *Porites lutea* coral skeletons from Phuket, South Thailand. *Coral Reefs* 15, 43-57.
- Allison, N., Finch, A.A., Sutton, S.R., Newville, M., 2001. Strontium heterogeneity and speciation in coral aragonite: implications for the strontium paleothermometer. *Geochimica Cosmochimica Acta* 65, 2669-2676.
- Allison, N., Finch, A.A., 2004. High-resolution Sr/Ca records in modern *Porites lobata* corals: Effects of skeletal extension rate and architecture. *Geochemistry Geophysics Geosystems* 5, doi:10.1029/2004GC000696
- Annamalai, H., Slingo, J.M., Sperber, K.R., Hodges, K., 1999. The mean evolution and variability of the Asian summer monsoon: comparison of the ECMWF and NCEP/NCAR reanalysis. *Monthly Weather Review* 127, 1157-1186.
- Barnes, D.J., Taylor, R.B., 2005. On the nature and causes of luminescent lines and bands in coral skeletons: II. Contribution of skeletal crystals. *Journal of Experimental Marine Biology and Ecology* 322(2), 135-42.
- Berkelmans, R., van Oppen, M.J.H., 2006. The role of zooxanthellae in the thermal tolerance of corals: a 'nugget of hope' for coral reefs in an era of climate change. *Proceedings of the Royal Society B* 273, 2305-2312.
- Cahyarini, S.Y., Pfeiffer, M., Dullo, W.-C., 2008. Improving SST reconstructions from coral Sr/Ca records: multiple corals from Tahiti (French Polynesia). *International Journal of Earth Sciences*, doi:10.1007/s00531-008008-00302-00532.
- Cahyarini, S.Y., Pfeiffer, M., Dullo, W.C., Zinke, J., Hetzinger, S., Kasper, S., Grove, C., Garbe-Schonberg, D., 2011. Comment on "A snapshot of climate variability at Tahiti at 9.5 ka using a fossil coral from IODP Expedition 310" by Kristine L. DeLong, Terrence M. Quinn, Chuan-Chou Shen, and Ke Lin. *Geochemistry Geophysics Geosystems* 12.
- Carricart-Ganivet, J.P., Cabanillas-Terán, N., Cruz-Ortega, I., Blanchon, P., 2012. Sensitivity of Calcification to Thermal Stress Varies among Genera of Massive Reef-Building Corals. *PLoS ONE* 7(3), e32859, doi:10.1371/journal.pone.0032859.
- Carricart-Ganivet, J.P., Lough, J.M., Barnes, D.J., 2007. Growth and luminescence characteristics in skeletons of massive *Porites* from a depth gradient in the central Great Barrier Reef. *Journal of Experimental Marine Biology and Ecology* 351, 27-36.
- Cohen, A.L., Layne, G.D., Hart, S.R., Lobel, P.S., 2001. Kinetic controls of skeletal Sr/Ca in a symbiotic coral: implications for the paleotemperature proxy. *Paleoceanography* 16, 20-26.
- Cohen, A.L., Owens, K.E., Layne, G.D., Shimizu, N., 2002. The effect of algal symbionts on the accuracy of Sr/Ca paleotemperatures from coral. *Science* 296, 331-333.
- Cohen, A.L., Gaetani, G.A., 2010. Ion partitioning and the geochemistry of coral skeletons:

- solving the mystery of the vital effect. *EMU Notes in Mineralogy* 11, 377-397.
- Colombo-Pallotta, M.F., Rodríguez-Román, A., Iglesias-Prieto, R., 2010. Calcification in bleached and unbleached *Montastraea faveolata*: evaluating the role of oxygen and glycerol. *Coral Reefs* 29(4), 899-907.
- Corrège, T., 2006. Sea surface temperature and salinity reconstructions from coral geochemical tracers. *Palaeogeogr. Palaeoclimatol. Palaeoecol.* 232, 408-428.
- DeLong, K.L., Quinn, T.M., Taylor, F.W., 2007. Reconstructing twentieth-century sea surface temperature variability in the southwest Pacific: A replication study using multiple coral Sr/Ca records from New Caledonia. *Paleoceanography* 22.
- DeLong, K.L., Flannery, J., Maupin, C.R., Poore R.Z., Quinn T.M., 2011. A coral Sr/Ca calibration and replication study of two massive corals from the Gulf of Mexico. *Palaeogeography, Palaeoclimatology, Palaeoecology*, doi:10.1016/j.palaeo.2011.05.005.
- Felis, T., Pätzold, J., 2003. Climate records from corals. In: *Marine Science Frontiers for Europe*, eds. Wefer, G., Lamy, F., Mantoura, F., Springer, Berlin, Heidelberg, New York, Tokyo, 11-27.
- Ferrier-Pages, C., Boisson, F., Allemand, D., Tambutte, E., 2002. Kinetics of strontium uptake in the scleractinian coral *Stylophora pistillata*. *Marine Ecology-Progress Series* 245, 93-100.
- Gaetani, G.A., Cohen, A.L., 2006. Element partitioning during precipitation of aragonite from seawater: A framework for understanding paleoproxies. *Geochimica et Cosmochimica Acta* 70, 4617-4634.
- Gaetani, G.A., Cohen, A.L., Wang, Z., Crusius, J., 2011. Rayleigh-based, multi-element coral thermometry: a biomineralization approach to developing climate proxies. *Geochimica et Cosmochimica Acta* 75, 1920-1932.
- Goodkin, N.F., Hughen, K.A., Cohen, A.L., Smith, S.R., 2005. Record of Little Ice Age sea surface temperatures at Bermuda using a growth-dependent calibration of coral Sr/Ca. *Paleoceanography* 20, doi:10.1029/2005pa001140.
- Goodkin, N.F., Hughen, K.A., Cohen, A.L., 2007. A multicoral calibration method to approximate a universal equation relating Sr/Ca and growth rate to sea surface temperature. *Paleoceanography* 22, doi:10.1029/2006pa001312.
- Grove, C.A., Nagtegaal, R., Zinke, J., Scheufen, T., Koster, B., Kasper, S., McCulloch, M., van den Berg, G., Brummer G.-J.A., 2010. River runoff reconstructions from novel spectral luminescence scanning of massive coral skeletons. *Coral Reefs* 29, 579-591.
- Hart, S.R., Cohen, A.L., 1996. An ion probe study of annual cycles of Sr/Ca and other trace elements in corals. *Geochimica et Cosmochimica Acta* 60, 3075-3084.
- Helmle, K.P., Kohler, K.E., Dodge, R.E., 2002. Relative Optical Densitometry and The Coral X-radiograph Densitometry System: CoralXDS. Presented Poster, Int. Soc. Reef Studies 2002 European Meeting. Cambridge, England. Sept. 4-7.
- Helmle, K.P., Dodge, R.E., Swart, P.K., Gledhill, D.K., Eakin, C.M., 2011. Growth rates of Florida corals from 1937 to 1996 and their response to climate change. *Nature Communications* 2, doi: 0.1038/ncomms1222.
- Hendy, E.J., Gagan, M.K., 2003. Chronological control of coral records using luminescent lines and evidence for non-stationary ENSO teleconnections in northeast Australia.

- The Holocene 13, 187-199.
- Hoegh-Guldberg, O., 1999. Climate change, coral bleaching and the future of the world's coral reefs. *Marine and Freshwater Research* 50, 839–866.
- Hughes, T.P., Baird, A.H., Bellwood, D.R., Card, M., Connolly, S.R., Folke, C., Grosberg, R., Hoegh-Guldberg, O., Jackson, J.B.C., Kleypas, J., Lough, J.M., Marshall, P., Nystrom, M., Palumbi, S.R., Pandolfi, J.M., Rosen, B., Roughgarden, J., 2003. Climate Change. Human Impacts, and the Resilience of Coral Reefs. *Science* 301, 929–933.
- Inoue, M., Nohara, M., Okai, T., Suzuki, A., Kawahata, H., 2004. Concentrations of Trace Elements in Carbonate Reference Materials Coral JCp-1 and Giant Clam JCT-1 by Inductively Coupled Plasma-Mass Spectrometry. *Geostandards and Geoanalytical Research* 411-416.
- Jones, A., Berkelmans, R., 2010. Potential costs of acclimatization to a warmer climate: growth of a reef coral with heat tolerant vs. sensitive symbiont types. *Plos One* 5, doi:10.1371/journal.pone.0010437.t005.
- Linsley, B.K., Wellington, G.M., Schrag, D.P., Ren, L., Salinger, M.J., Tudhope, A.W., 2004. Geochemical evidence from corals for changes in the amplitude and spatia; pattern of South pacific interdecadal climate variability over the last 300 years. *Climate Dynamics* 22, 1-11.
- Linsley, B.K., Kaplan, A., Gouriou, Y., Salinger, J., deMenocal, P.B., Wellington, G. M., Howe, S.S., 2006. Tracking the extent of the South Pacific Convergence Zone since the early 1600s. *Geochemistry, Geophysics, Geosystems* 7, doi:10.1029/2005GC00115.
- Loram, J.E., Trapido-Rosenthal, H.G., Douglas, A.E., 2007. Functional significance of genetically different symbiotic algae *Symbiodinium* in a coral reef symbiosis. *Molecular Ecology* 16, 4849–4857, doi:10.1111/j.1365-294X.2007.03491.x.
- Lough, J.M., Barnes, D.J., 2000. Environmental controls on growth of the massive coral *Porites*. *Journal of Experimental Marine Biology and Ecology* 245, 225-243.
- Marshall, J.F., McCulloch, M.T., 2002. An assessment of the Sr/Ca ratio in shallow water hermatypic corals as a proxy for sea surface temperature. *Geochimica et Cosmochimica Acta* 66, 3263-3280.
- McClanahan, T.R., Ateweberhan, M., Omukoto, J., Pearson, L., 2009. Recent seawater temperature histories, status, and predictions for Madagascar's coral reefs. *Marine Ecology Progress Series* 380, 117-128.
- Paillard, D., Labeyrie, L., Yiou, P., 1996. Macintosh program performs time series analysis. *Eos Transactions AGU* 77, 379.
- Pfeiffer, M., Dullo, W.-C., Zinke, J., Garbe-Schönberg, D., 2009. Three monthly coral Sr/Ca records from the Chagos Archipelago covering the period of 1950-1995 A.D.: reproducibility and implications for quantitative reconstructions of sea surface temperature variations. *International Journal of Earth Sciences* 98, doi:10.007/s00531-008-0326-z.
- Quinn, T.M., Taylor, F.W., Crowley, T.J., 2006. Coral-based climate variability in the Western Pacific Warm Pool since 1867. *Journal of Geophysical Research* 111.
- Rayner, N.A., Parker, D.E., Horton, E.B., Folland, C.K., Alexander, L.V., Rowell, D.P., Kent, E.C., Kaplan, A., 2003. Global analyses of sea surface temperature, sea ice, and night marine air temperature since the late nineteenth century. *Journal of Geophysical*

- Research 108, doi:10.1029/2002JD002670.
- Reynaud, S., Ferrier-Pages, C., Meibom, A., Mostefaoui, S., Mortlock, R., Fairbanks, R., Allemand, D., 2007. Light and temperature effects on Sr/Ca and Mg/Ca ratios in the scleractinian coral *Acropora* sp. *Geochimica et Cosmochimica Acta* 71, 354-362.
- Reynolds, R.W., Rayner, N.A., Smith, T.M., Stokes, D.C., Wang, W.Q., 2002. An improved *in situ* and satellite SST analysis for climate. *Journal of Climate* 15, 1609-1625.
- Schott, F.A., Xie, S.-P., McCreary Jr., J.P., 2009. Indian Ocean circulation and climate variability. *Reviews of Geophysics* 47, RG1002, 1-46.
- Schrag, D., 1999. Rapid analysis of high-precision Sr/Ca ratios in corals and other marine carbonates. *Paleoceanography* 14(2), 97-102.
- Sinclair, D.J., 2005. Correlated trace element "vital effects" in tropical corals: A new geochemical tool for probing biomineralization. *Geochimica et Cosmochimica Acta* 69, 3265-3284.
- Sinclair, D.J., Williams, B., Risk, M., 2006. A biological origin for climate signals in corals - Trace element "vital effects" are ubiquitous in Scleractinian coral skeletons. *Geophysical Research Letters* 33, doi:10.1029/2006GL027183.
- Sheppard, C., 2003. Predicted recurrences of mass coral mortality in the Indian Ocean. *Nature* 425, 294-297.
- Smith, T.M., Reynolds, R.W., 2004. Improved Extended Reconstruction of SST (1854-1997). *Journal of Climate* 17, 2466-2477.
- Storz, D., Gischler, E., 2011. Coral extension rates in the NW Indian Ocean I: reconstruction of 20th century SST variability and monsoon current strength. *Geo-Marine Letters* 31, 141-154.
- de Villiers, S., Shen, G.T., Nelson, B.K., 1994. The Sr/Ca-temperature relationship in coralline aragonite: Influence of variability in (Sr/Ca)seawater and skeletal growth parameters. *Geochimica et Cosmochimica Acta* 58, 197-208.
- de Villiers, S., Greaves, M., Elderfield, H., 2002. An intensity ratio calibration method for the accurate determination of Mg/Ca and Sr/Ca of marine carbonates by ICP-AES. *Geochemistry Geophysics Geosystems* 3(1), 1001.
- Woodruff, S.D., Diaz, H.F., Worley, S.J., Reynolds, R.W., Lubker, S.J., 2005. Early ship observational data and ICOADS. *Climatic Change*, 73, 169-194.

Chapter 6

Synthesis

Proxy Development

Proxy interpretation

Corals provide a wealth of climatic information locked within their skeleton. However, difficulties exist in extracting these climate signals to maximise their full potential in reconstructing past environmental conditions (Cohen et al., 2002; Reynaud et al., 2007; Sinclair, 2005; Sinclair et al., 2006). Coral skeletons are complicated structures, precipitated at different rates associated with an environmentally induced biological response (Helmle et al., 2011; Lough and Barnes, 1997, Lough and Barnes, 2000; Storz and Gischler, 2011). This indirectly influences the precipitation of the skeleton and subsequently the incorporation of geochemical signals through growth rate variability, affecting their ability to accurately reconstruct the past (Cohen and Gaetani, 2010; Meibom et al., 2006; Sinclair et al., 2006). Recent research has shown that the skeletal architecture has also hampered luminescence-based reconstructions, due the fluorescent properties of the coral aragonite (Grove et al., 2010; Lough, 2010). Unlocking the climatic signal from the coral skeleton is the most challenging task modern coral paleoclimate scientists currently face. This thesis goes some way to addressing these problems, however, specifically in the case of paleothermometry there remains a huge task in front of us.

Altering extension rates and densities in response to SST variability can result in a Sr/Ca signal not necessarily related to temperature (Allison and Finch, 2004; Felis et al., 2003; de Villiers et al., 1994). We found two eastern Madagascar corals of the same species sampled in the same environment that displayed opposing growth responses to SST. The resulting vital effects were so overwhelming that reconstructed temperature changes of one coral were opposite to that of the likely temperature signal (Chapter 5). Increasing extension rates over time led to increasing Sr/Ca values, with decreasing rates resulting in lower Sr/Ca signals. Similarly, during positive ENSO events, Sr/Ca values increased (cooling) in response to a negative density anomaly, with a positive density anomaly resulting in a decreased Sr/Ca signal (warming).

As the eastern Madagascar coral Sr/Ca records presented here differ from a number of other studies claiming no Sr/Ca growth effects (Alibert and

McCulloch, 1997; Inoue et al., 2007; Marshall and McCulloch, 2002; Shen et al., 1996), we cannot rule out the possibility that STM4 is simply an anomaly, and therefore the majority of other corals previously sampled are recording SST more accurately. However, if this were true and no growth effects exist, correlations between coral Sr/Ca records and SST would be far greater than the ones currently reported (Corrège, 2006). Given the poor correlations of our Sr/Ca records with SST and opposite trends and anomalies, our results are in agreement with de Villiers (1994, 1995) and Goodkin (2005, 2007), who also found that vital effects indeed have a significant influence on the coral Sr/Ca, and need to be considered in order to reconstruct SST more accurately.

Previous research has found that pooling records together can increase the reliability of reconstructions (Cahyarini et al., 2008; Pfeiffer et al., 2009). However, in extreme circumstances where two corals display opposite signals, such as the data presented here, the coral composite record can actually be less reliable (Chapter 5). For reasons such as this, there is a greater need to sample more than one coral from a single site, and couple Sr/Ca results together with growth parameter measurements. Unless more than one coral is analysed from the same location it will remain difficult to assess whether or not a single coral has been overwhelmed by growth patterns. Measuring more than a single coral record, however, is not the complete solution in identifying growth related Sr/Ca variability. In circumstances where two corals from the same region both respond consistently to SST variability in terms of growth, the influence on Sr/Ca will likely be masked. Such a scenario would yield either an overestimation or underestimation of reconstructed SST depending on whether the growth response is positive or negative e.g. STM2.

We suggest that all coral Sr/Ca records should be assumed to have been influenced by growth, and future developments in coral-based SST reconstructions should focus on removing this effect. Nevertheless, until two corals from the same location are shown to display opposing growth patterns and similar Sr/Ca trends and anomalies, the debate on whether or not coral growth influences coral skeletal Sr/Ca will continue. To this date, however, assuming our results are correct, there still remains an issue in fully removing the influence of vital effects, which would in turn further increase the reliability of coral-based SST reconstructions.

Overcoming proxy issues

Previous attempts to correct Sr/Ca for growth effects have been made using a multiple regression approach (Goodkin, 2005; 2007). Further, pioneering research by Cohen and Gaetani (2010) and Gaetani and Cohen (2011) have suggested that in order to extract the SST signal from the skeletal geochemistry, a number of elements related to SST need to be taken into consideration, rather than a single proxy element to calcium ratio i.e. Sr/Ca, Mg/Ca, Ba/Ca. As SST-proxies are incorporated into the skeleton at different rates related to growth parameters, as well as SST, taking their relationship into consideration may reveal the real SST signal, by normalising the skeletal influence. This relationship between individual trace element/Ca ratios can then be extrapolated using a series of equations, providing an SST-proxy composite record, which can potentially provide more reliable coral-based SST reconstructions (Cohen and Gaetani, 2010; Gaetani et al., 2011).

Although initial signs of an SST-proxy composite record are promising, the basis for the model is theoretical and many unknowns remain to be solved. A substantial amount of research is therefore required to adequately normalise the coral skeletal influence (vital effect), separating the effects of growth related trace element partitioning into the coral carbonate. If achieved, however, there is great potential for future coral-based SST reconstructions. For example, the research on coral skeletal luminescence demonstrates how skeletal normalisation can drastically improve climatic reconstructions (Grove et al., 2010). By effectively normalising the skeleton using spectral luminescence scanning (SLS), the key humic acid signal is optically extracted from the background coral aragonite signal, which is used to analyse past runoff changes, linked to rainfall (Grove et al., 2010).

Previous to this research, luminescence-based reconstructions were hampered as there was much debate as to what were the underlying causes of coral skeletal luminescence; similar to the current issues we now face in terms of geochemical proxies i.e. Sr/Ca. Variability in emission intensities were first thought to be caused by the incorporation of luminescent humic acids and soil-derived organic compounds introduced by seasonal river runoff (Isdale, 1984; Isdale et al., 1998; Matthews et al., 1996; Susic and Boto, 1989; Wild

et al., 2000). Later, a changing coral density and architecture was proposed as the cause since massive corals form a skeleton of luminescent aragonite (MacRae and Wilson, 2008), and banded luminescence is also found in corals from oceanic environments, devoid of terrestrial inputs (Barnes and Taylor, 2001, 2005). Taking both these theories into consideration, we hypothesised and proved that both factors were responsible for the luminescent signal in corals, and deconvolution of the two fractions was required to accurately reconstruct runoff. The resulting spectral luminescence ratio (Green/Blue; G/B) eliminated the skeletal luminescence signal, which has likely influenced a number of previous climate reconstructions.

Much progress in river runoff reconstructions has been made through the application of spectral luminescence scanning. Nevertheless, a few problems still exist with the technique which we will continue to address. Firstly, for a number of coral cores, resistant organic substances are associated with the coral skeleton that cannot be fully removed by bleaching. These organics have a detrimental affect on the measured fluorescent properties of the skeleton. In such cases, a more vigorous oxidising reagent is required to remove these organics, yet without influencing the skeletal geochemistry. Although we cannot remove these substances currently, we have the advantage of visualising them, as the image generated by SLS acts as an optical map. This enables us to avoid such organic discrepancies by drawing transects on the image that do not overlap the affected skeletal areas. Secondly, there is now a growing desire to apply the SLS technique to coral cores taken from the Great Barrier Reef (or an equivalent region), where river discharge data are highly resolved and abundant (Lough, 2011). Previously, we have only been able to correlate with precipitation data far from the study site in Madagascar (although significant). Therefore, one of the problems associated with working in regions such as Madagascar is the lack of instrument data available to calibrate the method. One could argue, however, that applying such a technique to a region with little data available is one of the primary reasons why we need paleoclimate reconstructions. Still, a highly resolved calibration would serve a purpose to increase confidence in the luminescence proxy.

Calcification: Implications for proxies

As the coral precipitates its aragonite skeleton, it regulates the transport of trace elements through its tissue layers by a number of active transport mechanisms, in turn regulating the pH at the calcifying site (Allemand et al., 2004; Furla et al., 2000; Ingalls et al., 2003). Although debated, it is also likely that the coral passively allows seawater to cross the tissue layer (Allemand et al., 2004). It is this passive mechanism that must be responsible for the humic acids to pass through the tissue layers and subsequently get incorporated into the skeleton as it is precipitated. As humic acids are not actively regulated at the coral calcifying site, nor affected by fractionation processes associated with calcification, the G/B signal should give a clear indication of humic acids in the water column at the time of precipitation, linked to river runoff. However, unlike humic acids, geochemical temperature proxies (i.e. Sr/Ca, Mg/Ca, B/Ca) are likely affected by both active transport and fractionation processes, therefore single trace element/Ca ratio analysis can be influenced by growth (Sinclair, 2005). Again, the development of a multi-elemental composite record that can remove the growth related skeletal influence on the geochemistry is crucial in taking coral-based paleothermometry to the next level (Cohen and Gaetani, 2010; Gaetani et al., 2011).

All coral-based proxies, and perhaps others i.e. foraminifera-based and/or bivalve-based, need to take calcification and the skeletal structure into consideration to ensure accurate reconstructions. It is important to stress that in many cases climate is reconstructed from a living organism; therefore collaborations with biologists are important. For certain regions, previously reported luminescence intensities and Sr/Ca coral records have indicated improbable trends in runoff and temperature, respectively. These results are likely down to long-term trends in skeletal growth parameters (linked to environmental change, e.g. SST trends, variability and extremes) overprinting the environmental signal. Proxy development and a better understanding of calcification, is therefore fundamental to increasing the accuracy of climate reconstructions. Moreover, robust proxy records are crucial to assess the extent climate change is modulated by natural oscillations and the modern human imprint.

Rainfall anomalies over Madagascar

The PDO and anthropogenic warming

Applying the spectral G/B ratio to our Madagascar coral records, specifically the long 300 year record (MASB), we were able to identify a climatic link to the northern Pacific Ocean. The Pacific Decadal Oscillation (PDO) has a frequency of 50-70 years, switching from a positive to a negative phase (Mantua et al., 1997). A positive PDO phase forces sea surface temperatures (SST) in the Indian Ocean to rise via a series of ocean-atmosphere teleconnections (Schneider and Cornuelle, 2005). Our research provides the first evidence of a link between the PDO and Madagascar rainfall, whereby a positive PDO phase has a positive influence on rainfall. The increase in SST, associated with positive PDO phases, is therefore likely responsible for anomalously high rainfall conditions over the region. Similarly, a negative PDO phase causes anomalously low Indian Ocean SST and reduced rainfall over NE Madagascar.

Understanding the relationship between sea surface temperatures and rainfall is fundamental to climate predictions (Neelin et al., 2003). A strong coupling between G/B and Indian Ocean SST provides further evidence that SST and rainfall over Madagascar are linked. Both show an accelerated increase since 1976 when global climate shifted to a new baseline level. This so-called 1976-shift was identified as a change in the SST base-level state of the Pacific basin, which had an impact on all other ocean basins (Meehl et al., 2009). One of the primary reasons why the 1976 shift was so strong was that both the PDO phase and anthropogenic greenhouse forcing acted in the same positive direction (Meehl et al., 2009). However, post 1976 warming was not uniform in its magnitude across the Indian Ocean basin (Deser et al., 2010; Xie et al., 2010). As spatial heterogeneity in Indian Ocean SST controls the spatial pattern of rainfall over the Indian Ocean and adjacent land masses, maximum convection and rainfall is shown to shift towards the region with the maximum SST anomaly (Neelin et al., 2003; Xie et al., 2010). This region of maximum anomalous SST, associated with anthropogenic warming, is located in the western Indian Ocean (Williams and Funk, 2011). A coupled positive PDO and anthropogenic warming could therefore explain

the increased convection over northeast Madagascar through rapidly rising Indian Ocean SST, which would therefore increase atmospheric moisture content, triggering more rainfall. Nevertheless, at this point it is unclear what the impact land-use change may have influenced the post-1976 accelerated G/B signal.

It was difficult to distinguish between the combined decadal forcing and global warming effect on G/B from the local anthropogenic land use changes post-1950. The PDO signal was masked by the strong mid-20th century deforestation in Madagascar, which will have contributed in some level to the accelerated humic acid and sediment runoff traced by or corals. We made a first attempt to isolate the ‘natural’ decadal climate forcing of the PDO from that caused by deforestation through the application of multiple proxies (i.e. Mn/Ca) (Chapter 4). By separating the deforestation influence from our coral records (G/B-Mn/Ca) it is clear that the increasing trend had indeed been inflated. Future research therefore needs to apply hydrological models that take into account the best available temporal land use and population change patterns in combination with our coral data to better quantify the role of climate versus anthropogenic forcing in regulating Madagascar river runoff.

ENSO impact on rainfall

The impact of the El Niño Southern Oscillation (ENSO) is felt globally (Cane, 2005). During positive ENSO events (El Niño), SST in the Indian Ocean rises significantly, and cools during negative ENSO events (La Niña). In general, during a positive ENSO event, rainfall over southern Africa declines (Richard et al., 2000), whereas over eastern Africa it increases during the short rains (October – December; OND) and decreases in the long rains (March – May; MAM) (Funk et al., 2008; Williams and Funk, 2011). This means that during Madagascar’s wet season (January – April; JFMA), a positive ENSO event will have a negative impact on rainfall over both southern and eastern Africa. Preliminary results have shown that during austral summer the PDO causes positive rainfall anomalies over eastern Africa and a negative anomaly over southern Africa (Chapter 4). It is therefore likely that different spatial Indian Ocean SST patterns, associated with ENSO and the PDO, cause regional differences in the rainfall response. Spectral analysis of the

composite G/B record from NE Madagascar, dating back to 1914, indicates a significant frequency band of 2 - 7 years, which is coherent with the Niño 3.4 index (Fig. 6.1). This suggests that rainfall over NE Madagascar is indeed influenced by ENSO, yet the direction of the response is not yet revealed.

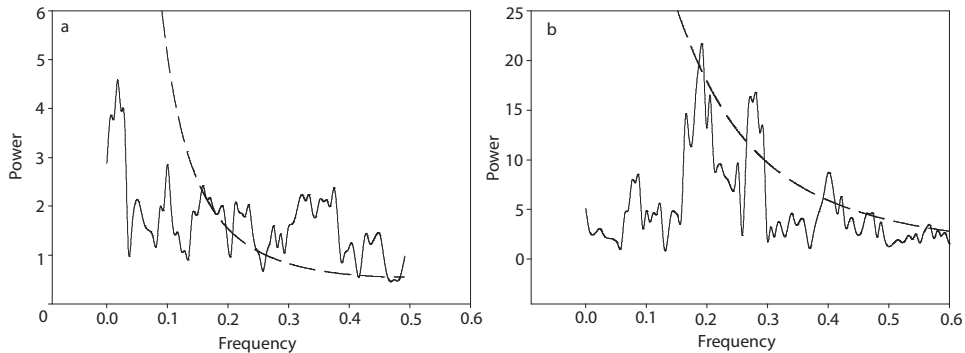


Figure 6.1. MTM of G/B composite (MAS1 and ANDRA) (a) and the Niño 3.4 index (b). Both spectra have a 2 - 7 year component within their records, signifying that G/B is linked to ENSO. The dashed lines represent the 99% significance level.

Applying the multi-taper method (MTM; Fig. 6.1) to both the G/Bcomp and Niño 3.4 records identifies a significant peak within the 2 - 7 year frequency at 5.17 years (frequency of 0.1933). Both the reconstructed component frequencies are identical; however, when they are plotted against one another it is apparent that there is little coherence between them in terms of timing and amplitude (Fig. 6.2). Moreover, it is not clear whether El Niño or La Niña is responsible for anomalously high rainfall conditions, although it seems that in general La Niña conditions were associated with increased river runoff (and thus rainfall) pre-1976.

In order to further examine the impact of ENSO on Madagascar rainfall, the two time-series were examined using a cross-wavelet coherence analysis method. Again, there seems to be little or no coherence between the two datasets post-1976, nor for the period between 1940 and 1950 (Fig. 6.3). Nevertheless, even when the two time-series are coherent there is little consistency between phases. This again suggests that a complicated relationship exists between rainfall and ENSO between 1914 and present.

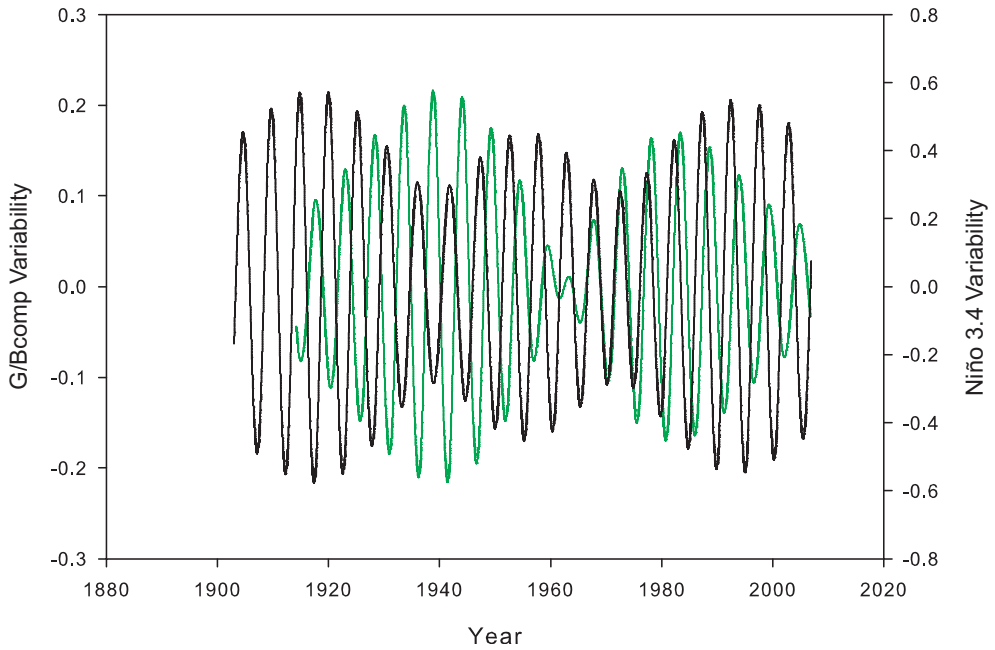


Figure 6.2. The significant reconstructed components of G/Bcomp (green) and the Niño 3.4 index (black). Both components are equal at 0.1933 (5.17 years), as identified by the MTM. There is little coherence between the two in terms of either timing or amplitude.

Since the 1976 climate shift there may have been a breakdown in the relationship between ENSO and rainfall over Madagascar, as indicated by cross wavelet coherence analysis. To further investigate this, the Niño 3.4 time series was split into two datasets, a pre 1976 and a post 1976 index. By doing so, any relationship breakdown would become clearer. The limited coherence observed between the previous reconstructed components of the two complete time series may have deviated from one another because of such a relationship breakdown (5.17 years; Figs 6.1 and 6.2). We therefore repeated the MTM method for both the Niño 3.4 datasets (a pre 1976 and a post 1976), and compared the reconstructed component of each with the G/Bcomp (Figs 6.4 and 6.5).

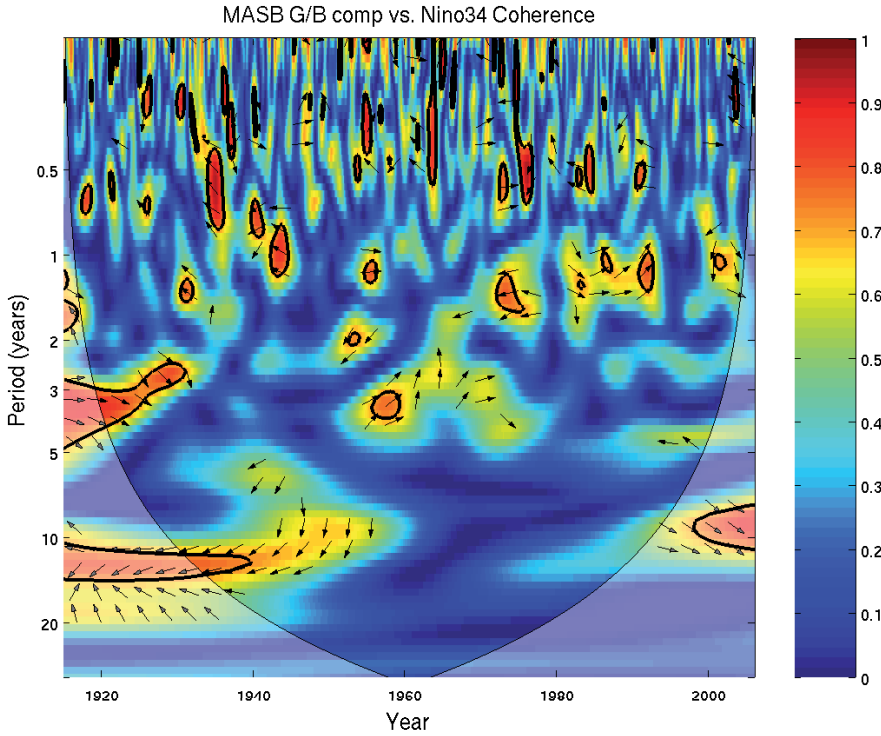


Figure 6.3. Cross wavelet coherence analysis of G/Bcomp and the Niño 3.4 index. The 5% significance level against red noise is shown as a thick contour. Phases are indicated as arrows.

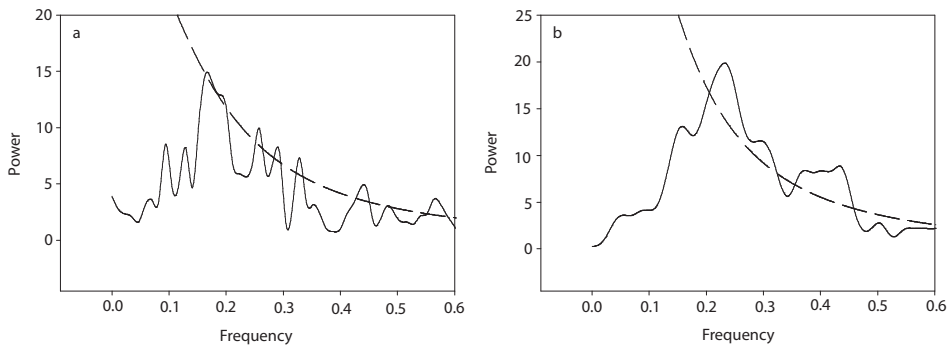


Figure 6.4. MTM of the Niño 3.4 index pre 1976 (a) and the Niño 3.4 index post 1976 (b). Both spectra have a 2 - 7 year component within their records. The dashed lines represent the 95% significance level.

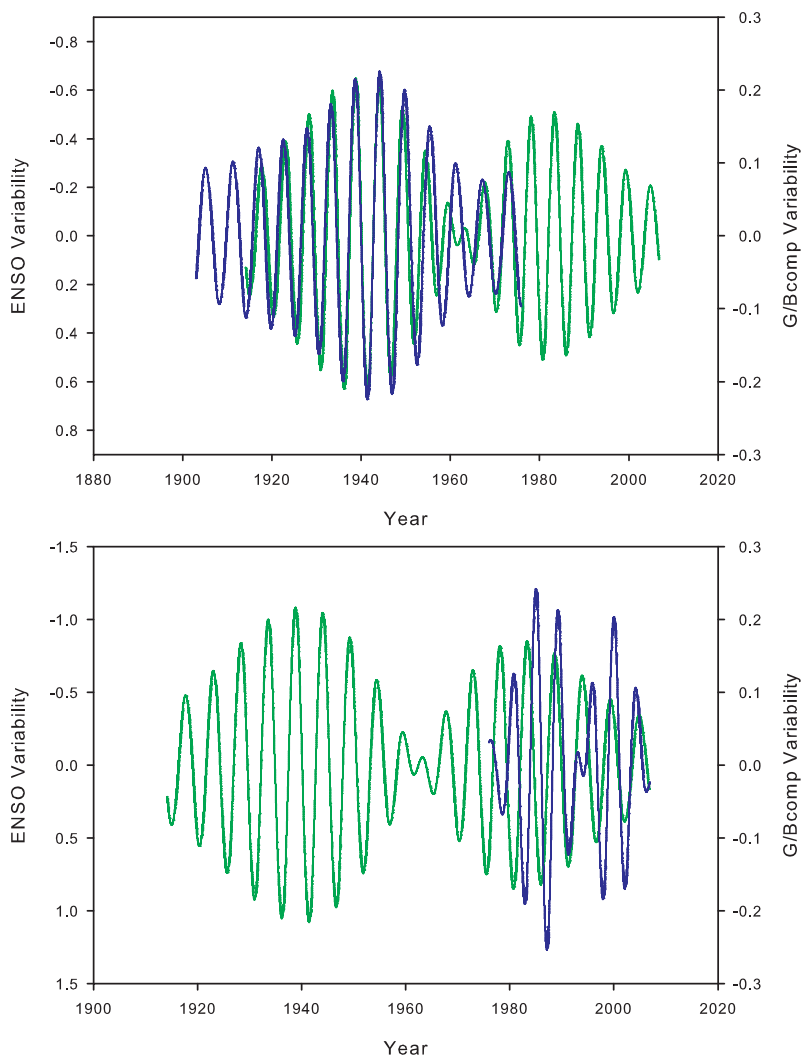


Figure 6.5. The significant reconstructed components of G/Bcomp (green) and the Niño 3.4 index (blue) pre 1976 (a) and post 1976 (b). The G/Bcomp component is 0.1933 (5.17 years), as identified by the MTM, whereas the reconstructed components for Niño 3.4 pre 1976 and post 1976 are 0.1757 (5.69 years) and 0.2343 (4.27 years), respectively. The G/Bcomp and Niño 3.4 index pre 1976 show great coherency in both amplitude and timing, where La Niña conditions are in line with anomalously high G/B. Note, that the x-axes have been reversed for the Niño 3.4 index, indicating the relationship between La Niña and G/B. There is no clear relationship between G/Bcomp and the Niño 3.4 index post 1976.

In both the pre and post 1976 Niño 3.4 datasets, a significant frequency was identified within the 2 -7 year band (Fig. 6.4). However, both frequencies were slightly different to the complete time series, as the most significant frequency for the pre 1976 dataset was longer at 5.69 years (frequency of 0.1757), and the post 1976 band shorter at 4.27 years (frequency of 0.2343). This result is expected as ENSO activity has indeed increased over the past 30 years (Cane, 2005; Nicholls, 2008). We then compared the reconstructed ENSO components of the pre and post 1976 Niño 3.4 index with the reconstructed ENSO component of the G/B time series (Fig. 6.5). Results indicate that before 1976 there seems to be a strong link between La Niña and positive rainfall anomalies over NE Madagascar, however, post 1976 this link breaks down. Further, there seems to be no link to ENSO post 1976, as rainfall anomalies occurred both in and out of phase (Fig. 6.5).

Differences between ENSO and PDO related rainfall

Comparing the reconstructed components of ENSO and G/B identified two important results. Firstly, that La Niña conditions have likely caused increasing rainfall anomalies over NE Madagascar; and secondly that the relationship between ENSO and rainfall breaks down post 1976. These results are unexpected as La Niña-like conditions cause Indian Ocean SST to fall, therefore opposite in the response observed for the PDO and anthropogenic warming, where increasing Indian Ocean SST causes positive rainfall anomalies. These results suggest that SST is not the sole forcing mechanism responsible for rainfall anomalies over the Indian Ocean, and another physical mechanism related to SST must be considered.

The strongest SST anomalies associated with ENSO are in the tropical Pacific Ocean, and for the PDO in the temperate northern Pacific Ocean (Fig. 6.6). Differences exist therefore in the teleconnected global SST anomalies associated with each climate oscillation, as the position of maximum anomalous SST likely determines the position of the convection cells and hence the winds (Fig. 6.6). It is the changes in wind strength and direction which will further determine the cooling or warming of regions around the world (Cane, 2005). These knock-on effects are known as teleconnections, and will influence precipitation. ENSO variability is responsible for strong SST anomalies in the eastern tropical Pacific, southwest temperate Pacific

and the tropical and southern Atlantic Ocean (Cane, 2005), whereas the PDO has little or no impact on these regions (Fig. 6.6) (Mantua et al., 1997). Both oscillations, however, have a significant impact on Indian Ocean SST, whereby positive phases are associated with positive SST anomalies (Fig. 6.6); yet according to coral G/B records, rainfall anomalies are opposite.

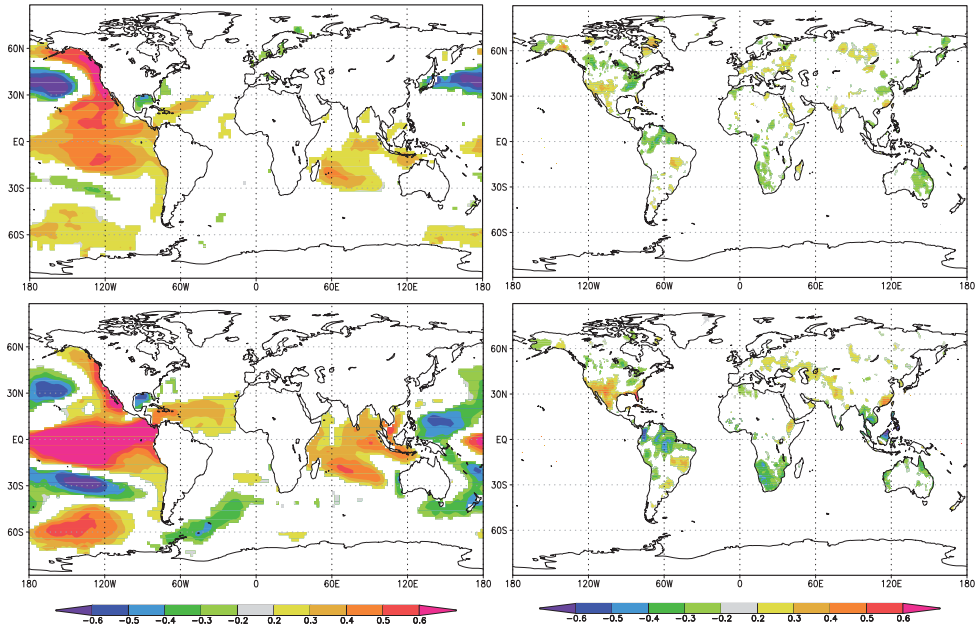


Figure 6.6. The spatial correlation of global SST (ERSSTv.3; left) and precipitation (CRU TS3.1; right) with the PDO index (upper panels) and the Niño 3.4 index (lower panels) for Madagascar wet season (JFMA). Note the position of the strongest SST anomaly for both the PDO and ENSO in the Indian Ocean.

SST-dipoles are often responsible for rainfall variability over the southwest Indian Ocean region. Southern Africa rainfall is thought to be modulated by an SST gradient in the subtropics between southern Madagascar and western Australia (Behera and Yamagata, 2001; Reason, 2002). When the southern Madagascar pole is warm, southern African rainfall increases. Similarly a north-south dipole exists off the eastern coast of Madagascar, which also influences rainfall (Kay and Washington, 2008; Washington and Preston, 2006). Again, when the southern tip of Madagascar is warm, there is increased rainfall over southern Africa. Interestingly, however, when the

northern pole warms in the Mascarene region, there is a positive rainfall anomaly in northern Madagascar (Kay and Washington, 2008; Washington and Preston, 2006). It seems therefore that the northeast Madagascar region is particularly sensitive to SST variability in the Mascarene region.

The most striking difference between the austral summer (JFMA) Indian Ocean SST anomalies for the PDO and ENSO is the positioning of maximum anomalous SST (Fig. 6.6). According to ERSST data, during a positive ENSO event the most significant increase in SST is in the south-central Indian Ocean (15-30S; 70-90E), whereas the maximum PDO anomaly is in the south-west Indian Ocean (Mascarene region; 15-30S; 50-70E; Fig. 6.6). It is likely that this difference in the positioning of the maximum SST anomaly is responsible for the opposite rainfall anomalies. During a positive PDO phase the maximum anomaly is situated just off the eastern coast of Madagascar (south-west Indian Ocean; Mascarene region). This causes anomalously high convection over the region, likely explaining the positive rainfall anomalies during a positive PDO phase. Moreover, as the maximum SST anomaly associated with positive ENSO events is in the south-central Indian Ocean, it is probable that in this region both convection and rainfall are anomalously high (Chowdary and Gnanaseelan, 2007). Further, the increase in south-central Indian Ocean SST during austral summer, associated with positive ENSO events, has likely shifted the convection cell from west to east, therefore reducing rainfall over NE Madagascar as well as eastern and southern Africa. During negative ENSO events there is a reversal of the system, generating stronger easterly winds bringing in more moisture to NE Madagascar, southern Africa and eastern Africa (long rains). This ENSO related west to east shift in convection (positive ENSO) is similar to the central tropical Pacific Ocean, where the Walker circulation shifts in the same direction (Cane, 2005; McPhaden et al., 2006).

Results suggest that the opposite rainfall anomalies associated with different climate oscillations are linked to the positioning of maximum anomalous SST. However, post 1976 there is a breakdown observed between ENSO and NE Madagascar rainfall, with no consistency between phases and rainfall anomalies. As the positioning of the SST anomaly seems to be crucial in determining the rainfall response, there has likely been a shift in the Indian Ocean convection cells since the global climate shift of 1976. Indeed, there

is an apparent difference between observed warming of the south-central and south-western Indian Ocean between 1900 and 2009 (Fig. 6.7). According to Williams and Funk (2011), since 1900, SST in the south-west Indian Ocean has increased at a faster rate than the south-central Indian Ocean for the months MAMJ (March – June). It is probable therefore that a combination of these spatial heterogeneous patterns of anthropogenic warming with ENSO events has caused a complex precipitation relationship over northeast Madagascar.

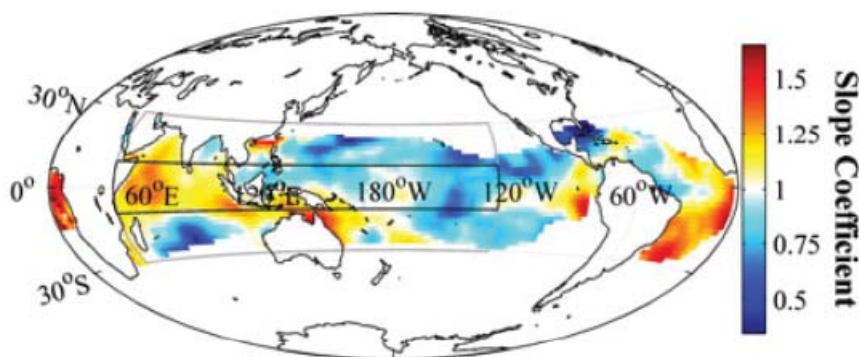


Figure 6.7. Change in March–June SST (NOAA extended reanalysis) versus change in global mean March–June surface temperature (GISS dataset). Slope coefficients are 7-years running mean SSTs regressed on 7-years running mean global temperature from 1900 to 2009. A slope of 1 indicates SST warming at the same pace as the global mean. From Williams and Funk, (2011).

During a positive ENSO event (post 1976), the associated rise in SST over the south-central Indian Ocean may not generate a strong enough SST gradient with the south-western Indian Ocean to shift convection and cause a negative rainfall anomaly. The greater rise in SST over the south-west Indian Ocean, associated with anthropogenic warming, may therefore counteract to some extent the ENSO associated SST rise in the south-central Indian Ocean. If this were the case, it would cause ENSO related rainfall anomalies over NE Madagascar to be inconsistent, which is observed (Fig. 6.5). Since 1976, both positive and negative ENSO events may have caused anomalous convection over NE Madagascar. Subsequently, the strength of ENSO, or a combination with another climate oscillation, may have determined the rainfall response over Madagascar. If anthropogenic warming continues, there may be a complete switch in the ENSO related rainfall response whereby positive ENSO events will cause positive rainfall anomalies.

The Little Ice Age

The Little Ice Age (LIA) was a period of cooling that occurred after the Medieval Warm Period, between 1550 and 1850. There is now mounting evidence that the LIA also affected Africa (Huffman, 1996; Verschuren et al., 2000). However, the precise timing of hydrological change during this period remains unclear, and more specifically, the direction of the observed patterns of climate change appears different between regions, especially in eastern Africa.

Both positive and negative rainfall responses have been inferred from paleoclimate records across Africa. ENSO-like conditions, associated with a southern shift in the ITCZ and Congo Air Boundary, have been suggested as possible explanations to why rainfall changed so dramatically (Brown and Johnson, 2005; Garcin et al., 2007). Lake Naivasha (Verschuren et al., 2000) and Lake Victoria (Stager et al., 2005), located in the equatorial eastern Africa region, both show higher levels and therefore wetter conditions during the LIA. Further south, levels of Lake Masoko (Garcin et al., 2007), Lake Malawi (Owen et al., 1990) and Lake Tanganyika (Cohen et al., 1997) indicated an opposite response whereby dryer conditions prevailed during the LIA. However, this North-South contrast between wet and dry conditions was not consistent for all lake records. Lake levels from Lake Edward (Russell and Johnson, 2005), located west of Lake Victoria and Lake Naivasha, inferred dryer conditions between the 16th and 17th centuries. Past shifts in the position of the Congo Air Boundary (Nicholson, 1996), driven by large scale changes in the Atlantic and Indian Ocean monsoons (associated with the southerly shift in the ITCZ), may have caused these large meridional moisture gradients across equatorial Africa (Russell and Johnson, 2005). Again, such shifts are thought to be associated with positive ENSO-like conditions (Brown and Johnson, 2005; Garcin et al., 2007).

Spectral luminescence results of coral core MASB indicate that a significant rise in runoff occurred pre-1850, during the LIA (Fig. 6.8). These results are in agreement with lake records from the eastern equatorial Africa region, yet opposite to central equatorial and southern Africa region. Positive ENSO-like conditions have been suggested to trigger the rainfall response

during the LIA (Garcin et al., 2007; Russell and Johnson, 2005). As positive ENSO events cause positive rainfall anomalies in eastern Africa (during OND) and negative anomalies in southern Africa (Funk et al., 2008), these results would seem to favor such a hypothesis. However, in NE Madagascar, during a positive ENSO event (1914 - 1976) a negative rainfall anomaly exists; therefore unexpectedly, the spatial link is more in line with southern Africa rather than eastern Africa. This result is in agreement with recent paleodata published from central Indonesia (Oppo et al., 2009). They suggest that during the LIA, wet conditions prevailed, which would contradict suggestions of positive ENSO-like conditions, as Indonesia experiences drought during El Niño (Oppo et al., 2009).

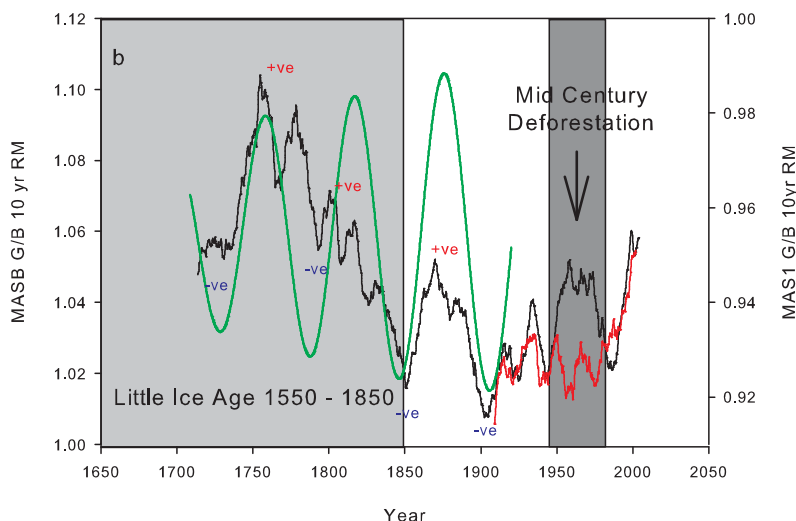


Figure 6.8. The 10 year running mean of coral MASA G/B (black line) and MAS1 G/B (red) are shown together with the 50 – 70 year band-pass filtered MASA G/B data (0.017000 ± 0.002800), up to 1920 (green). The filtered data finishes in 1920 as the influence of the deforestation period in the mid-century (dark grey box) affects the filtering. There is little coherence in MAS1 and MASA G/B between 1940 and 1980 due to localised differences in deforestation. Peaks and troughs in the filtered data represent multidecadal positive (red) and negative (blue) runoff anomalies associated with the PDO. The MASA G/B is high during the period associate with the Little Ice Age (light grey box).

A southerly shift in the ITCZ and the Congo Air Boundary likely defines the wet or dry boundary during the LIA. Southerly excursions of the ITCZ would cause NE Madagascar precipitation to be more coherent with eastern equatorial Africa due to the meridional positioning of the ITCZ (Fig. 1.2). A shift in the ITCZ would in turn generate stronger northeasterly winds bringing in more moisture to the region from the Indian Ocean. Indeed, a strong seasonal monsoon system in the Indian Ocean likely caused the wet response recorded in our Madagascar coral records and the eastern African lake records (Oppo et al., 2009; Tierney et al., 2010).

A shift in the ITCZ and associated strengthening of the Indian Ocean monsoon system likely explains the precipitation anomalies over eastern Africa and NE Madagascar during the LIA. However, central and southern Africa was dryer during this period. This may be related to a weakened western Africa monsoon caused by reduced thermohaline circulation in the Atlantic and lower meridional SST gradients (Saenger et al., 2009; Zhang et al., 2005). This would in turn have an impact on Congo Air Boundary convergence (Tierney et al., 2011), which likely determines the African hydroclimatological gradient during the LIA. As the Indian Ocean is land locked in the north and the Atlantic Ocean is not, perhaps differences in the monsoonal strengths during the LIA are related to the land-ocean SST gradients when the northern hemisphere cooled. A combination of the shifting ITCZ and Congo Air Boundary with the strength of the monsoonal systems likely explains the spatial and temporal precipitation variability during the LIA.

To further investigate the LIA precipitation response, there is a greater need to increase the spatial sampling resolution within the eastern and southern Africa regions. By doing so the boundary between wet and dry regions, associated with the LIA response, can be better defined. These results will help to answer the question whether the position of the ITCZ during the LIA was the primary modulator of rainfall. Future coral drilling is therefore planned for Mozambique, where we hope to further define the wet-dry LIA boundary.

References

- Alibert, C., McCulloch, M.T., 1997. Strontium/calcium ratios in modern *Porites* corals from the Great Barrier Reef as a proxy for sea surface temperature: calibration of the thermometer and monitoring of ENSO. *Paleoceanography* 12, 345-363.
- Allemand, D., Ferrier-Pages, C., Furla, P., Houlbreque, F., Puverel, S., Reynaud, S., Tambutte, E., Tambutte, S., Zoccola, D., 2004. Biomineralisation in reef-building corals: from molecular mechanisms to environmental control. *Comptes Rendus Palevol* 3, 453-467.
- Allison, N., Finch, A.A., 2004. High-resolution Sr/Ca records in modern *Porites lobata* corals: Effects of skeletal extension rate and architecture. *Geochemistry, Geophysics, Geosystems* 5, doi:10.1029/2004GC000696
- Barnes, D.J., Taylor, R.B., 2001. On the nature and causes of luminescent lines and bands in coral skeletons. *Coral Reefs* 19, 221-230.
- Barnes, D.J., Taylor, R.B., 2005. On the nature and causes of luminescence lines and bands in coral skeletons: II. contribution of skeletal crystals. *Journal of Experimental Marine Biology and Ecology* 322, 135-142.
- Behera, S.K., Yamagata, T., 2001. Subtropical SST dipole events in the southern Indian Ocean. *Geophysical Research Letters* 28, 327-330.
- Brown, E.T., Johnson, T.C., 2005. Coherence between tropical East African and South American records of the Little Ice Age. *Geochemistry Geophysics Geosystems* 6.
- Cahyarini, S.Y., Pfeiffer, M., Dullo, W.-C., 2008. Improving SST reconstructions from coral Sr/Ca records: multiple coreals rom Tahiti (French Polynesia). *International Journal of Earth Sciences*, doi:10.007/s00531-00008-00302-00532.
- Cane, M.A., 2005. The evolution of El Niño, past and future. *Earth and Planetary Science Letters* 230, 227-240.
- Chowdary, J.S., Gnanaseelan, C., 2007. Basin-wide warming of the Indian Ocean during El Niño and Indian Ocean dipole years. *International Journal of Climatology*, doi:10.1002/joc.1482.
- Cohen, A.L., Gaetani, G.A., 2010. Ion partitioning and the geochemistry of coral skeletons: solving the mystery of the vital effect. *EMU Notes in Mineralogy* 11, 377-397.
- Cohen, A.L., Owens, K.E., Layne, G.D., Shimizu, N., 2002. The effect of algal symbionts on the accuracy of Sr/Ca paleotemperatures from coral. *Science* 296, 331-333.
- Cohen, A.S., Talbot, M.R., Awramik, S.M., Dettman, D.L., Abell, P., 1997. Lake level and paleoenvironmental history of Lake Tanganyika, Africa, as inferred from late Holocene and modern stromatolites. *Geological Society of America Bulletin* 109, 444-460.
- Corrège, T., 2006. Sea surface temperature and salinity reconstructions from coral geochemical tracers. *Palaeogeography, Palaeoclimatology, Palaeoecology* 232, 408-428.
- Deser, C., Phillips, A.S., Alexander, M.A., 2010. Twentieth century tropical sea surface temperature trends revisited. *Geophysical Research Letters* 37.
- Felis, T., Paetzold, J., Loya, Y., 2003. Mean oxygen-isotope signatures in *Porites* spp. corals: inter-colony variability and correction for extension-rate effects. *Coral Reefs* 22, 328-336.

- Funk, C., Dettinger, M.D., Michaelsen, J.C., Verdin, J.P., Brown, M.E., Barlow, M., Hoell, A., 2008. Warming of the Indian Ocean threatens eastern and southern African food security but could be mitigated by agricultural development. *PNAS* 105, 11081-11086.
- Furla, P., Galgani, I., Durand, I., Allemand, D., 2000. Sources and mechanisms of inorganic carbon transport for coral calcification and photosynthesis. *Journal of Experimental Biology* 203, 3445-3457.
- Gaetani, G.A., Cohen, A.L., Wang, Z., Crusius, J., 2011. Rayleigh-based, multi-element coral thermometry: a biomineralization approach to developing climate proxies. *Geochimica et Cosmochimica Acta* 75, 1920-1932.
- Garcin, Y., Williamson, D., Bergonzini, L., Radakovitch, O., Vincens, A., Buchet, G., Guiot, J., Brewer, S., Mathe, P.E., Majule, A., 2007. Solar and anthropogenic imprints on Lake Masoko (southern Tanzania) during the last 500 years. *Journal of Paleolimnology* 37, 475-490.
- Goodkin, N.F., Hughen, K.A., Cohen, A.L., 2007. A multicoral calibration method to approximate a universal equation relating Sr/Ca and growth rate to sea surface temperature. *Paleoceanography* 22.
- Goodkin, N.F., Hughen, K.A., Cohen, A.L., Smith, S.R., 2005. Record of Little Ice Age sea surface temperatures at Bermuda using a growth-dependent calibration of coral Sr/Ca. *Paleoceanography* 20.
- Grove, C.A., Nagtegaal, R., Zinke, J., Scheufen, T., Koster, B., Kasper, S., McCulloch, M.T., Bergh, G.v.d., Brummer, G.J.A., 2010. River runoff reconstructions from novel spectral luminescence scanning of massive coral skeletons. *Coral Reefs* 29, 579-591.
- Helmle, K.P., Dodge, R.E., Swart, P.K., Gledhill, D.K., Eakin, C.M., 2011. Growth rates of Florida corals from 1937 to 1996 and their response to climate change. *Nature Communications* 2:215, doi:10.1038/ncomms1222.
- Huffman, T.N., 1996. Archaeological evidence for climatic change during the last 2000 years in southern Africa. *Quat. Int.* 33, 55-60.
- Ingalls, A.E., Lee, C., Druffel, E.R.M., 2003. Preservation of organic matter in mound-forming coral skeletons. *Geochimica et Cosmochimica Acta* 67, 2827-2841.
- Inoue, M., Suzuki, A., Nohara, M., Hibino, K., Kawahata, H., 2007. Empirical assessment of coral Sr/Ca and Mg/Ca ratios as climate proxies using colonies grown at different temperatures. *Geophysical Research Letters* 34.
- Isdale, P.J., 1984. Fluorescent bands in massive corals record centuries of coastal rainfall. *Nature* 310, 578-579.
- Isdale, P.J., Stewart, B.J., Tickle, K.S., Lough, J.M., 1998. Palaeohydrological variations in a tropical river catchment: a reconstruction using fluorescent bands in corals of the Great Barrier Reef, Australia. *The Holocene* 8, 1-8.
- Kay, G., Washington, R., 2008. Future southern African rainfall variability related to a southwest Indian Ocean dipole in HadCM3. *Geophysical Research Letters* 35, doi:10.1029/2008GL034180.
- Lough, J., 2011. Great Barrier Reef coral luminescence reveals rainfall variability over northeastern Australia since the 17th century. *Paleoceanography* 26, doi:10.1029/2010PA002050.

- Lough, J.M., 2010. Measured coral luminescence as a freshwater proxy: comparison with visual indices and a potential age artefact. *Coral Reefs*.
- Lough, J.M., Barnes, D.J., 1997. Several centuries of variation in skeletal extension, density and calcification in massive *Porites* colonies from the Great Barrier Reef: A proxy for seawater temperature and a background of variability against which to identify unnatural change. *Journal of Experimental Marine Biology and Ecology* 211, 29-67.
- Lough, J.M., Barnes, D.J., 2000. Environmental controls on growth of the massive coral *Porites*. *Journal of Experimental Marine Biology and Ecology* 245, 225-243.
- MacRae, C.M., Wilson, N.C., 2008. Luminescence database I-Minerals and materials. *Microscopy and Microanalysis* 14, 184-204.
- Mantua, N., Hare, S., Zhang, Y., Wallace, J., Francis, R., 1997. A Pacific interdecadal oscillation with impacts on salmon production. *Bulletin Am. Meteorol. Soc.* 78, 1069-1079.
- Marshall, J.F., McCulloch, M.T., 2002. An assessment of the Sr/Ca ratio in shallow water hermatypic corals as a proxy for sea surface temperature. *Geochimica et Cosmochimica Acta* 66, 3263-3280.
- Matthews, B.J.H., Jones, A.C., Theodorou, N.K., Tudhope, A.W., 1996. Excitation-emission-matrix fluorescence spectroscopy applied to humic acid bands in coral reefs. *Marine Chemistry* 55, 317-332.
- McPhaden, M.J., Zebiak, S.E., Glantz, M.G., 2006. ENSO as an integrating concept in Earth Science. *Science* 314, 1740-1745.
- Meehl, G.A., Hu, A., Santer, B.D., 2009. The mid-1970s climate shift in the Pacific and the relative roles of forced versus inherent decadal variability. *J. Clim.* 22, 780-792.
- Meibom, A., Yurimoto, H., Cuif, J.-P., Domart-Coulon, I., Houlbreque, F., Constantz, B., Dauphin, Y., Tambutte, E., Tambutte, S., Allemand, D., Wooden, J., Dunbar, R.B., 2006. Vital effects in coral skeletal composition display strict three-dimensional control. *Geophysical Research Letters* 33, doi:10.1029/102006GL025968.
- Neelin, J.D., Chou, C., Su, H., 2003. Tropical drought regions in global warming and El Niño teleconnections. *Geophysical Research Letters* 30, doi: 10.1029/2003GL018625.
- Nicholls, N., 2008. Recent trends in the seasonal and temporal behaviour of the El Niño-Southern Oscillation. *Geophysical Research Letters* 35, doi:10.1029/2008GL034499.
- Nicholson, S.E., 1996. A review of climate dynamics and climate variability in eastern Africa. Gordon and Breach Publishers.
- Oppo, D.W., Rosenthal, Y., Linsley, B.K., 2009. 2,000-year-long temperature and hydrology reconstructions from the Indo-Pacific warm pool. *Nature* 460, 1113-1116.
- Owen, R.B., Crossley, R., Johnson, T.C., Tweddle, D., Kornfield, I., Davison, S., Eccles, D.H., Engstrom, D.E., 1990. Major low-levels of Lake Malawi and their implication for speciation rates in cichlid fishes. *Proceedings of the Royal Society of London Series B-Biological Sciences* 240, 519-553.
- Pfeiffer, M., Dullo, W.-C., Zinke, J., Garbe-Schoenberg, D., 2009. Three monthly coral Sr/Ca records from the Chagos Archipelago covering the period of 1950-1995 A.D.: reproducibility and implications for quantitative reconstructions of sea surface temperature variations. *International Journal of Earth Sciences* 98, doi:10.007/s00531-00008-00326-z.

- Reason, C.J.C., 2002. Sensitivity of the southern African circulation to dipole sea-surface temperature patterns in the south Indian Ocean. *International Journal of Climatology* 22, 377-393.
- Reynaud, S., Ferrier-Pages, C., Meibom, A., Mostefaoui, S., Mortlock, R., Fairbanks, R., Allemand, D., 2007. Light and temperature effects on Sr/Ca and Mg/Ca ratios in the scleractinian corals *Acropora* sp. *Geochimica et Cosmochimica Acta* 71, 354-362.
- Richard, Y., Trzaska, S., Roucou, P., Rouault, M., 2000. Modification of the southern African rainfall variability/ENSO relationship since the late 1960's. *Climate Dynamics* 16, 883-895.
- Russell, J.M., Johnson, T.C., 2005. A high-resolution geochemical record from Lake Edward, Uganda Congo and the timing and causes of tropical African drought during the late Holocene. *Quaternary Science Reviews* 24, 1375-1389.
- Saenger, C., Chang, P., Ji, L., Oppo, D.W., Cohen, A.L., 2009. Tropical Atlantic climate response to low-latitude and extratropical sea-surface temperature: A Little Ice Age perspective. *Geophysical Research Letters* 36.
- Schneider, N., Cornuelle, B.D., 2005. The forcing of the Pacific decadal oscillation. *J. Clim.* 18, 4355-4373.
- Shen, C.-C., Lee, T., Chen, C.-Y., Wang, C.-H., Dai, C.-F., Li, L.-A., 1996. The calibration of D (Sr/Ca) versus sea surface temperature relationship for *Porites* corals. *Geochimica et Cosmochimica Acta* 60, 3849-3858.
- Sinclair, D.J., 2005. Correlated trace element "vital effects" in tropical corals: A new geochemical tool for probing biomineralization. *Geochimica et Cosmochimica Acta* 69, 3265-3284.
- Sinclair, D.J., Williams, B., Risk, M., 2006. A biological origin for climate signals in corals - Trace element "vital effects" are ubiquitous in Scleractinian coral skeletons. *Geophysical Research Letters* 33, doi:10.1029/2006GL027183.
- Stager, J.C., Ryves, D., Cumming, B.F., Meeker, L.D., Beer, J., 2005. Solar variability and the levels of Lake Victoria, East Africa, during the last millenium. *Journal of Paleolimnology* 33, 243-251.
- Storz, D., Gischler, E., 2011. Coral extension rates in the NW Indian Ocean I: reconstruction of 20th century SST variability and monsoon current strength. *Geo-Marine Letters* 31, 141-154.
- Susic, M., Boto, K.G., 1989. High-performance liquid-chromatographic determination of humic-acid in environmental-samples at the nanogram level using fluorescence detection. *Journal of Chromatography* 482, 175-187.
- Tierney, J.E., Oppo, D.W., Rosenthal, Y., Russell, J.M., Linsley, B.K., 2010. Coordinated hydrological regimes in the Indo-Pacific region during the past two millennia. *Paleoceanography* 25.
- Tierney, J.E., Russell, J.M., Damste, J.S.S., Huang, Y.S., Verschuren, D., 2011. Late Quaternary behavior of the East African monsoon and the importance of the Congo Air Boundary. *Quaternary Science Reviews* 30, 798-807.
- Verschuren, D., Laird, K.R., Cumming, B.F., 2000. Rainfall and drought in equatorial east Africa during the past 1,100 years. *Nature* 403, 410-414.
- Villiers, S.d., Nelson, B.K., Chivas, A.R., 1995. Biological controls on coral Sr/Ca and $\delta^{18}\text{O}$

- reconstructions of sea surface temperatures. *Science* 269, 1247-1249.
- Villiers, S.d., Shen, G.T., Nelson, B.K., 1994. The Sr/Ca-temperature relationship in coralline aragonite: Influence of variability in (Sr/Ca)seawater and skeletal growth parameters. *Geochimica et Cosmochimica Acta* 58, 197-208.
- Washington, R., Preston, A., 2006. Extreme wet years over southern Africa: Role of Indian Ocean sea surface temperatures. *Journal of Geophysical Research-Atmospheres* 111.
- Wild, F.J., Jones, A.C., Tudhope, A.W., 2000. Investigation of luminescence banding in solid coral: the contribution of phosphorescence. *Coral Reefs* 19, 132-140.
- Williams, A., Funk, C., 2011. A westward extension of the warm pool leads to a westward extension of the Walker circulation, drying eastern Africa. *Climate Dynamics*, 1-19.
- Xie, S.P., Deser, C., Vecchi, G.A., Ma, J., Teng, H.Y., Wittenberg, A.T., 2010. Global Warming Pattern Formation: Sea Surface Temperature and Rainfall. *J. Clim.* 23, 966-986.
- Zhang, P.Q., Yang, S., Kousky, V.E., 2005. South Asian high and Asian-Pacific-American climate teleconnection. *Adv. Atmos. Sci.* 22, 915-923.

Acknowledgements

Acknowledgements

It gives me great joy to finally write this last remaining section of my thesis. These past five years have been like riding a rollercoaster; full of highs and lows. Now I have reached the end of this ride I can look back to all of those that have helped me through it. Particularly, I want to thank my supervisors, Geert-Jan Brummer and Jens Zinke, and my two reliable students, Tim Scheufen and Sebastian Kasper.

I have been lucky enough to have had two supervisors with two very different scientific backgrounds. The specific coral paleoclimate background of Jens and the broad geological knowledge of Geert-Jan have complimented each other perfectly and contributed much wealth to this thesis. Not only have you both been highly professional in your supervision, I think we've also had a few laughs over the years (not to mention the odd adventure). Jens, being trapped on an uninhabited island with you while a cyclone battered down on us was a unique experience. This was where I really got to know you. It was here when you first suggested we should 'stimulate' each other over the upcoming years. So Jens thanks for all of your stimulating! Of course, behind every successful man is a strong 'man'. Andrew, thanks for all the great hospitality you've offered me at your home when I've turned up unannounced. I've really enjoyed your cooking! It has been great to get to know you both and I wish you all the best down under. Geert-Jan, when our boat crashed into the reef and we started to sink, listening to you scream 'leave the samples behind' made me realise that science can never rule your life. On a professional and personal level it has been a pleasure.

To my students Tim and Sebastian; your hard work, commitment and determination during the nine months working with me was commendable. I pushed you both to your limits (maybe breaking points), however, looking back on it now I hope you realise the extent of what you each achieved. I was very lucky to have you both as my students, and very proud that you have both gone on to undertake your own PhDs. Tim, I will never forget how you were continuously running from all the Madagascar girls towards the end of our fieldwork together. I can only imagine what you did to them at the beginning. Nevertheless, we had a blast! Sebastian, I have enjoyed immensely sharing and experiencing the fruits of our different cultures. Music, beer and sausages rule! I have a new-found respect for 'Ze Germans'.

The development of the XRF core scanner was pivotal to this thesis. Thanks go to Rineke Gieles and Bob Koster for their flexibility and continuous support throughout my PhD. Rineke, you always found time for me to access the scanner even on very short notice. Bob, there was never a problem you could not solve. It was a pleasure working with you both.

I would like to thank all the people that offered their support and advice over the past few years. They include Rolf Bak, Frank Peeters, Hubert Vonhof, Marcel Wernard, Anne Cohen, Joseph Maina and Eric Epping. Also, the people that I have met and now work together with; it has been (and hopefully continue to be) a pleasure. They include, Carlos Jimenez, Nicolas Duprey, Wonsun Park, Tsuyoshi Watanabe, Steffen Hertzinger, Chris Perry, Beto Rodriguez-Ramires, Malcolm McCulloch, Bemahafaly Randriamanantsoa, Miriam Pfeiffer, Yuda Cahyarini and Ronan Roche. I also want to thank all of those who were involved in measuring the countless amounts of samples for me, in particular Wim Boer, Dieter Garbe-Schönberg, Paul Mason, Bert Hoeksema, Michiel Kienhuis, Evaline van Weerlee, Philippe Leonide, Lars Reuning and Karin Kissling. This thesis would not have been possible without you.

Most of my fieldwork was conducted in the wonderful country that is Madagascar. I would like to thank the Wildlife Conservation Society (WCS) Madagascar, Conservation International (CI), FRONTIERS and the WCS/ANGAP team in Maroantsetra, for their support in fieldwork logistics and in the organisation of the research permits. I would also like to thank CAF/CORE Madagascar for granting all the CITES permits and ANGAP Madagascar for supporting my research activities in the vicinity of the marine and forest nature parks.

There have also been a number of people that I have worked with over the past few years which have contributed to some extent in the completion of this thesis. To all the Bachelor and Master students of Jens, namely Jasper, Charlotte, Christiane and Laura; it was great to work with you either in the field, lab or library. I'm sorry if you were forced to come to Texel from Amsterdam on a few occasions. Thanks to Thomas Richter and Isla Castaneda for always answering your office door when I would come knocking. I know I asked a lot of stupid questions regarding climate before the last century. I

Acknowledgements

was more an oceanographer rather than a geologist before I started my PhD at NIOZ. Roel, I had a great time with you during your Masters thesis at NIOZ. We conducted some of the craziest experiments together. It was also great getting to know you and Yolande on a personal level. We shared some great times together in Den Helder, Portugal and the UK. Yolande, thanks for all the times you looked after our cats while Julie and I were out of town. You've been great friends.

Judith, Harry, Laura, Anneke, Elda, Dennis, Yvonne, Jan Boon, Louis Peperzak and Marcel Veldhuis, thanks for all of the support you have shown Julie. It was great that she could work at NIOZ while I was continuing with my PhD.

The backing I have received from the NIOZ and the Marine Geology Department particularly has been fantastic. I have thoroughly enjoyed both the social and scientific interactions with all the staff and students past and present. Cees, thanks for all the kindness you have shown me over the years. We have had some wonderful evenings together on Texel (and one in Den Helder). I appreciate all the times you let me stay at your house after football when I could not make the last ferry back to Den Helder. It has been a real delight getting to know you. You are indeed one of a kind! Lukas, I could not have asked for a better office mate. It was great listening to all of the Reggae beats with you on a Friday afternoon. Aneurin, my second office mate, thanks for being so patient with me over the final few months while trying to complete this thesis. Rik, it has been great to work with you recently. It is a pity that when we go out you can only last till 11 pm. We can work on that in the upcoming two years. Ulrike, I have loved our discussions over the years together, and also having someone to vent out my frustrations with regarding my PhD. If it was not for you I may have gone a little insane. Jens Greinert, thanks for your support as the new department head. It may not have been for so long, yet it is much appreciated. And for the rest, Henko, Henk, Furu, Tjeerd, Sharyn, Erica, Catarina, Caroline, Roel, Thomas, Julianne, Jan-Berend, Jeroen, Catarina, Lieke, Nelleke, Martina, Piet and all in the NUTS department, you have been fantastic. Also, the students past and present, namely Felix, Kristina, Catarina, Julia, Peter, Chris and Iris, it was great to have met you all. Gila, Mozambique was quite an experience together with you and Drew. I look forward to working with you in the future.

Outside of the department, many people associated with NIOZ have helped me out in times of need. Peter Vooijs, Hilde Kooijman, Joke Mulder-Starreveld, Jolanda Evers, Nelleke Krijgsman, Hans van Tuinen, Andrea Keijser, Cornelia Poleacov, Roland Mik, Bert Aggenbach and Edward Bonne, thanks for your assistance! It's been great getting to know you all in the process. Also, thanks to Edwin Keijzer, Herman Boekel, Roel Bakker and Johan van Heerwaarden for constructing all the reliable equipment I've needed both in the field and the lab. To all of the cleaners, I've enjoyed all of the gossip up and down the corridors of NIOZ. It was a nice distraction from my work. My Dutch has definitely improved somewhat over the years.

As most of you reading this will know, my passion in life is football. I'd like to thank the Dutch television company for broadcasting virtually every Tottenham Hotspur game over the past four years. If I ever go back to the UK I will for sure be getting a Dutch television connection. Not only have I enjoyed watching the mighty Tottenham Hotspur, I have thoroughly enjoyed playing with the 'not so mighty' NIOZ football team. Win, lose or draw we always celebrated. I have had a real blast with all of you and for that I thank you. Cees, Matthijs, Allert, Pedro and Maarten, I blame you for the lack of sleep on Thursday nights. Also, Luis, Bert, Rob, Adam, Thorsten, Santiago, Yvo, Leon, Jan-Dirk, Lennart, Dave, Eli, Luke, Ingmar, Roeland and Arjen, you played your part! Also, Ingmar, thanks for lunch service with a smile.

Allert, you are a true 'burgerlul' as well as a good friend. I too have just become a burgerlul myself. I look forward to joining in on all of your burgerlul conversations with Maarten and Matthijs next season. However, I will never buy a station wagon! Maarten, you are one of the nicest guys I have ever met. It was fantastic going to the UK with you to see the Spurs at White Hart Lane beating Liverpool 2-1. Also, celebrating Spurs beating Arsenal 5-1 in the cup was a great moment. Matthijs, history repeated itself when we went to White Hart Lane and beat Liverpool 2-1 one year later. I know now never again to feed you insanity hot sauce. At least we got your camera back in the end. Nevertheless, there is one thing for sure which I have appreciated from you more than anything. You have always said it how it is. Thanks for being so brutally honest about my football performances in the past. Oh, by the way my sink is still blocked. Pedro, you have been a great friend to me

Acknowledgements

in times high and low. The six months you spent living with Julie and I was a joy. I will never forget your PhD defence party. Going to the UK, Portugal, Austria, Spain and Morocco with you was a blast. You are a great guy and you bring a lot of joy into many people's lives. However, you will NEVER beat me at a 'head butt'! Kristin, thanks for looking after Pedro. It was great to get to know you in Morocco. Also, thanks for letting me stay at your place during the EGU conference.

Socialising with the football team often involved hanging out with their better halves. To all the WAGS, it has been great to get to know you over the years. Darci, Roos and Tamar, I am sorry for all the times I woke you up in the night as I tried to locate a bed in the dark. Darci, not only have you been a great friend to me, you have been a true friend to Julie. In the UK you would be referred to as a 'top bird'. Roos, thanks for being a secret smoker with me. I enjoyed all our conversations outside the Balken during a sly cigarette. Tamar, you are true legend. Thanks for all the wonderful meals you cooked for me before football games. Also, for unleashing Veerle on me regularly at 6am. Sabine, you are a great supporter of the NIOZ football team and a great friend to Julie and I. It's been a pleasure winding you up over the years. I don't think I've met anyone before with quite so much energy as you have. Nicole, it's been great to have you around, and thanks for being there for Julie. Carine and Thalia, thanks for the good times.

Much of my time at NIOZ was spent drinking coffee the Dutch way at precisely 10am, 12pm and 3pm. Often these coffee breaks were welcoming periods away from staring at a computer screen. However, occasionally they would drag on for longer than expected due the wonderful company. Thanks to Jort, Lesley, Sofia, Francien, Cecile, Claudia, Jord, Veronica, Jasper, Jane, Antje, John, Roland, Kristina, Libby, Ellen, Arjan, Claire, Joost, Angela, David, Jenny, Laura, Luke, Alina, Lisa, Joanna, Petra, Marta, Eli, Lisa, Marcel, Cindy and Paul for inspiring me during the wonderful NIOZ coffee breaks and social events.

As much as Texel appeals to a number of people, it was never for me. Drinking a coffee on the ferry in the morning and a having a beer on the way back to Den Helder was a great way to prep myself for the island and relax

before I returned home. Den Helder is a great place and I've made a lot of friends there of which I have thoroughly enjoyed their company over the past five years. Raquel, Vânia and Filipe, we've had a lot of fun together in the bars, restaurants and at each others houses. Life at the weekends would not have been the same without you. Sílvia, you have been a fantastic friend. I will miss your cooking and your red velvet cake when you are gone. The evening we had spinach curry together with Jeremy and Julie will forever live in my memory. Jeremy, you are quite cool for a yank. Relaxing with you, Pedro and MJ at TOPS/SPOT were always great times. I'm impressed how well you have taken to football (soccer). Although I have started to get to grips with the American version I am nowhere near your level yet. You are a great friend and I look forward to coming to visit you in South Carolina. Come on you Gamecocks!

There was one restaurant particularly that has saved me from curry withdrawal symptoms. Thanks to Ali and his family at the Bombay Palace for their great food and hospitality. Also, thanks to my neighbour Audi and his family for all the great times we had on our balcony. It's quite high up!

Although I have lived in Den Helder for four and a half years, I did spend five months on Texel living in Tubantia. Thanks to Erwin, Roel, Stefan, Sander, Fons, Julia, Rowan, Tim, Frank, Edwin, Nico, Peter Paul, Glenn, Joop and Catalina for all the great times. Catalina, you are a great person and a fantastic friend. I am so happy to have introduced you to the world of whisky. I can't wait to visit both you and Beto down under.

Thanks to all my friends back home in the UK for coming to visit me in the Netherlands. I'm sure it was not too painful for you to visit Amsterdam for the odd weekend. Pete, I'm sorry for not escorting you to the bus stop on Texel at 5 am. Great that you managed to hitch hike to the ferry and make it in time for your flight though. Drew, unfortunately you did not make your flight. That never happened to me in four and a half years. Damo, I've never seen anyone sleep on the stairs of the Dutch trains before. It was a great Queens Day together, except for the last bar we entered. Charlie, we had a blast together at Queens Day the year after. It was a shame your stage fright slowed us up so much. Duncan, I was so impressed with how much bread you

Acknowledgements

could eat in the Pizzeria. I guess there was only one way to move you after that! Grainne, Sarah, Nicola and Kelly, thanks for supporting the guys when they returned. I know they were a little jet lagged.

Mum and Dad, your support over the years has been fantastic. I could not have got here today without you both. Returning home for some home cooking and a trip to the Spurs was a welcoming break from work. I loved every minute of it. Thanks for everything. Steve, Jemma and Heather, it was great to see you all when I came home. Thanks for being there when I needed you. Nan and Nan, thanks for all of your encouragement. It has given me a lot of strength and motivation. Also, thanks to Mick, Di, Joanne, Graham, Kirsty, James, Sarah, Anna, Alex, Louise, Alan, Jane, Jake, Rory, Mick, Sarah and Babs for all of their support over the years. It means a lot to me.

Kreinie, you have given Julie and I incredible support over the past five years. Thanks for everything you've done for us. Hervé, Aline, Agathe and Charlotte, I have thoroughly enjoyed your company both in Holland and in France. It has been great getting to know you all. I'm sorry my French is still so bad. Opa, oma and family, thanks for being so welcoming. I'm sorry my Dutch is still so bad. Barbara, Aniek, Tineke and Martine, we have had some great times together. You are great friends of Julie and now to me. Thanks for all the support you've shown Julie, even when you found out she was moving to Den Helder.

Julie, you are the best thing that has ever happened to me. You have given me everything I have ever needed to succeed, and more enjoyment than I could ever have wished for. I could not have done this without your calming influence and drive. Now we begin a new chapter in our lives together with Lauren. How lucky I am to have you both in my life. Thanks for everything.

Curriculum Vitae

Craig Grove was born on the 19th March 1982 in Irvine, Scotland. In 2004 he graduated with a 2:1 Masters degree in Oceanography from the University of Southampton. Later that year he worked for Othniel shellfish, where he cultivated a number of shellfish species for a global market in Poole harbour. In 2005 he spent 18 months scuba diving around the reefs of Belize as the director of Marine Science for Reef Conservation International. Here, he continuously monitored the coral reef ecosystem and many of the key species which had a commercial or biological significance. During his PhD his focus was reconstructing past climate conditions of the western Indian Ocean using coral core samples, with specific emphasis on global warming and natural climate oscillations, such as ENSO and the PDO.

